Cover art:

A soft X-ray image of the world's highest beta tokamak plasma is superimposed on measured magnetic flux surfaces. The color snapshot of the 11% beta DIII–D plasma is generated with computer-aided tomographic imaging — from a GA–LLNL–ORNL collaboration (Shot 69605 at 1.415 seconds).

U.S. Department of Energy funds were not used
to support color printing for the cover of this report.

GA-A--20790

DE92 010068

DIII–D RESEARCH OPERATIONS

ANNUAL REPORT TO THE U.S. DEPARTMENT OF ENERGY

OCTOBER 1, 1990 THROUGH SEPTEMBER 30, 1991

by
PROJECT STAFF
T.C. SIMONEN and T.E. Evans, Editors

Work prepared under
Department of Energy
Contract DE-AC03-89ER51114

GENERAL ATOMICS PROJECTS 3466/3467/3470/3473
DATE PUBLISHED: MARCH 1992

GENERAL ATOMICS

DISCLAIMER

This report has been reproduced
directly from the best available copy.

Available to DOE and DOE contractors from the
Office of Scientific and Technical Information
P.O. Box 62
Oak Ridge, TN 37831
Prices available from (615) 576-8401,
FTS 626-8401.

Available to the public from the
National Technical Information Service
U.S. Department of Commerce
5285 Port Royal Rd.
Springfield, VA 22161

THE 1991 DIII-D RESEARCH TEAM

General Atomics
San Diego, California, U.S.A.

J. Allen, A. Arnold, C. Baxi, G. Bramson, A. Borshchegovsky,[h] N.H. Brooks, D. Buchenauer,[a] K.H. Burrell, R.W. Callis, G. Campbell, T.N. Carlstrom, W. Cary, V. Chan, S.C. Chiu, M.S. Chu, S. Coda,[b] A. Colleraine, J. Cummings, J. Cuthbertson,[a] J.C. DeBoo, J. DeGrassie, J. DeHaas,[c] M. DiMartino, J. Doane, R. Dominguez, E.J. Doyle,[d] H. Duong,[e] R. Ellis,[c] R. Evanko, J. Evans,[c] T.E. Evans, J.R. Ferron, R.L. Freeman, D. Finkenthal,[g] A. Futch,[c] P. Gohil, A. Gootgeld, K. Greene, C.M. Greenfield, R.J. Groebner, R. Harvey, W. Heidbrink,[e] P. Henline, D.N. Hill,[c] D. Hillis,[f] F. Hinton, T. Hodapp, K. Holtrop, J. Hogan, R. Hong, C.L. Hsieh, G.L. Jackson, R.A. James,[c] S. Janz,[m] T. Jarboe,[p] T. Jensen, R. Jong,[c] H. Kawashima,[i] A.G. Kellman, D. Kellman, R. Khayrutdinov,[l] J. Kim, Y. Kim,[q] C.C. Klepper,[f] T. Kurki-Suonio,[g] R. La Haye, A. Langhorn, L.L. Lao, E.A. Lazarus,[f] R. Lee, A. Leonard, J. Leuer, Y. Lin Liu, S.I. Lippmann, J.M. Lohr, T.C. Luce, J.L. Luxon, M.A. Mahdavi, K. Matsuda, H. Matsumoto,[i] M. Mayberry, J. McChesney, W. McHarg, E. McKee, M. Menon,[f] C.P. Moeller, R. Moyer,[d] A. Nerem, T. Ohkawa, R. O'Neill, I. Opimach,[l] T.H. Osborne, D.O. Overskei, L. Owen,[f] A. Peebles,[d] P.I. Petersen, P. Petrach, T.W. Petrie, C. Petty, R. Phelps, R. Philipona,[d] J. Phillips, R. Pinsker, P.A. Politzer, G.D. Porter,[c] R. Prater, F. Puhn, E. Reis, D. Remsen, M.E. Rensink,[c] C. Rettig,[d] T. Rhodes,[d] M.J. Schaffer, D.P. Schissel, U. Schneider,[n] J.T. Scoville, R.P. Seraydarian, L. Sevier, K. Shoolbred, T.C. Simonen, J. Smith, T. Smith, R.T. Snider, G.M. Staebler, R.D. Stambaugh, H. St. John, R.E. Stockdale, E.J. Strait, P.L. Taylor, T.S. Taylor, D. Thomas, M. Thomas, P. Thurgood, P.K. Trost, V. Trukhin,[h] M. Tupper, S. Turgarinov,[l] A. Turnbull, J. Vanderlann, R. Waltz, J. Watkins,[j] J. Wesley, W.P. West, J. Wight, J. Winter,[k] C. Wong, D. Wroblewski,[c] and A. Zwicker[o]

PERMANENT ADDRESS

(a) Sandia National Laboratories, Livermore, USA
(b) Massachusetts Institute of Technology, USA
(c) Lawrence Livermore National Laboratory, USA
(d) University of California at Los Angeles, USA
(e) University of California at Irvine, USA
(f) Oak Ridge National Laboratory, USA
(g) University of California at Berkeley, USA
(h) Kurchatov Institute, Moscow, USSR
(i) Japan Atomic Energy Research Institute, Japan
(j) Sandia National Laboratories, Albuquerque, USA
(k) Institute of Plasmaphysics KFA, Jülich, Germany
(l) Kurchatov Laboratory, Troitsk, USSR
(m) University of Maryland, USA
(n) Max-Planck Institute, Garching, Germany
(o) John Hopkins University, USA
(p) University of Washington, USA
(q) University of California at San Diego, USA

CORE PHYSICS DIVISION

G. Bramson	M. Chu	R. Fisher	R. La Haye	R. Stockdale	A. Turnbull
H. Brummage	J. DeBoo	J. Greene	L. Lao	E. Strait	R. Waltz
T. Carlstrom	R. Dominguez	C. Greenfield	D. Schissel	T. Taylor	
V. Chan	J. Ferron	C. Hsieh	H. St. John	M. Thomas	

RF PHYSICS & TECHNOLOGY DIVISION

J. Allen	J. Darling	T. Harris	W. Martin	R. Prater	Y. Lin-Liu
R. Brambila	M. Dimartino	R. Harvey	C. Moeller	D. Remsen	
R. Callis	J. Doane	B. Koz	R. O'Neil	M. Roberts	
W. Cary	R. Freeman	J. Lohr	C. Petty	D. Whitaker	
S. Chiu	W. Grosnickle	T. Luce	R. Pinsker	A. Wright	

BOUNDARY PHYSICS & TECHNOLOGY DIVISION

N. Brooks	R. Groebner	J. Kim	T. Osborne	B. Shaw	W.P. West
K. Burrell	F. Hinton	A. Leonard	T. Petrie	J.P. Smith	
L. Cerda	M. Hollerbach	S. Lippmann	M. Schaffer	G. Staebler	
T. Evans	A. Hyatt	M. Mahdavi	R. Seraydarian	R. Stambaugh	
P. Gohil	G. Jackson	J. McChesney	L. Sevier	D. Thomas	

DIII–D OPERATIONS DIVISION

A. Acera	D. Cummings	R. Hong	E. McKee	J. Phillips	G. Stewart
R. Beckwith	J. Cummings	K. Keith	R. McNulty	S. Riggs	T. Suzik
N. Besker	P. Dvorsky	A. Kellman	S. Miller	G. Rolens	E. Taylor
P. Blackmore	D. Estes	D. Kellman	R. Mitra	A. Rouleau	P. Taylor
L. Boaz	R. Evanko	D. Kessler	J. Morse	K. Schaubel	M. Thompson
C. Brown	J. Freeman	N. Kirkpatrick	A. Nerem	J. Schroeder	P. Thurgood
E. Brown	J. Gilgallon	J. Land	M. Nilsen	B. Scoville	M. Tupper
R. Bruce	E. Gonzales	G. Laughon	R. O'Hara	J. Scoville	J. Vanderlaan
J. Busath	A Gootgeld	R. Lee	C. Parker	M. Siltanen	G. Vavrunek
G. Campbell	K. Greene	J. Luxon	D. Patrick	R. Simas	J. Walin
C. Chang	P. Henline	M. Madruga	R. Patterson	T.L. Smith	J. Wight
D. Clow	T. Hodapp	C. Makariou	P. Petersen	R. Snider	K. Williams
R. Coon	K. Holtrop	E. Martinez	P. Petrach	M. Srinivasan	R.D. Williams
R. Cranford	G. Holtz	B. McHarg	R. Phelps	J. Stanton	

FUSION PROGRAM SUPPORT DIVISION

J. Bakalarski	R. Brown	B. Hamilton	E. Miracle	R. Savercool	P. Turner
W. Bamford	J. Creutz	C. Hamilton	D. Murray	K. Shoolbred	L. Walker
W. Bellman	C. Danielson	C. Isherwood	P. Nap	T. Simonen	R. Walker
B. Bowman	D. Forster	W. Jarrett	D. Overskei	M. Stav	R. Wilson
V. Brancaccio	J. Gish	D. MacPherson	C. Riedel	P. Sutherland	

NEW CONCEPTS DIVISION

C. Baxi	M. Conley	R. Junge	J. Pashesnik	K. Redler	G. Webb
R. Bourque	H. Curiel	J. Leuer	V. Pham	E. Reis	J. Wesley
A. Colleraine	R. Gibson	J. McMullen	P. Politzer	K. Stuart	R. Will
J. Cometa	T. Jensen	G. Minet	F. Puhn	S. Visser	C. Wong

Sandia National Laboratories, Livermore, USA

D. Buchenauer J. Cuthbertson

Massachusetts Institute of Technology, USA

S. Coda

Lawrence Livermore National Laboratory, USA

J. DeHaas	D.N. Hill	R. Jong	M.E. Rensink
A. Futch	R.A. James	G.D. Porter	D. Wroblewski

University of California at Los Angeles, USA

E.J. Doyle	A. Peebles	C. Rettig
R. Moyer	R. Philipona	T. Rhodes

University of California at Irvine, USA

H. Duong W. Heidbrink

Oak Ridge National Laboratory, USA

D. Hillis	E.A. Lazarus	L. Owen
C.C. Klepper	M. Menon	

University of California at Berkeley, USA

D. Finkenthal T. Kurki-Suonio

Kurchatov Institute, Moscow, USSR

A. Borshchegovsky V. Trukhin

Japan Atomic Energy Research Institute, Japan

H. Kawashima H. Matsumoto

Sandia National Laboratories, Albuquerque, USA

J. Watkins

Institute of Plasmaphysics KFA, Jülich, Germany

J. Winter

Kurchatov Laboratory, Troitsk, USSR

R. Khayrutdinov I. Opimach S. Turgarinov

University of Maryland, USA

S. Janz

Max-Planck Institute, Garching, Germany

U. Schneider

John Hopkins University, USA

A. Zwicker

University of Washington, USA

T. Jarboe

University of California at San Diego, USA

Y. Kim

TABLE OF CONTENTS

LIST OF FIGURES

LIST OF TABLES

SECTION 1

DIII-D PROGRAM OVERVIEW

1. DIII–D PROGRAM OVERVIEW

1.1. INTRODUCTION

Results obtained from the DIII–D tokamak experiment, which is operated by General Atomics for the United States Department of Energy, are internationally acknowledged as a leading force in development of magnetically confined fusion plasmas physics and technology. Historically innovative solutions to difficult technical problems have contributed to the remarkable success of the DIII–D experiment and led to sustained progress toward the eventual production of fusion energy. This progress is typified by the evolution of the fusion (performance) triple product, *i.e.*, the product of the plasma density, the temperature, and the energy confinement time. During the last ten years, the fusion performance of DIII and DIII–D has doubled every two years reaching 2×10^{20} keV-s/m^3 during this year's experiments in which a new type of very high confinement VH–mode was discovered. This progress is shown in Fig. 1.1-1.

The overall objectives of the DIII–D research program are, to a large extent, driven by the needs of design activities such as the International Thermonuclear Experimental Reactor (ITER) Program with the expectation that the resulting machines will be approximately three times larger than DIII–D with twice the magnetic field and as much as 6-8 times the plasma current. Presently, DIII–D, the largest poloidally diverted tokamak in the United States, is one of the best diagnosed, most flexible, experiments in the world. Many of the experiments carried out during FY91 have contributed to an increase in the machines operational parameters. In addition to approaching plasma conditions which are expected in a fusion reactor, we have developed a clearer understanding of the physical mechanisms which govern the stability and confinement of the plasma. We have also tested advanced boundary layer control techniques and completed an assessment of boronized wall conditions while continuing to make progress on radio frequency heating and current drive. These new capabilities, along with a steadily growing base of experience, have placed the DIII–D program in an excellent position to address issues which will have a critical impact on the direction of national and international fusion research programs.

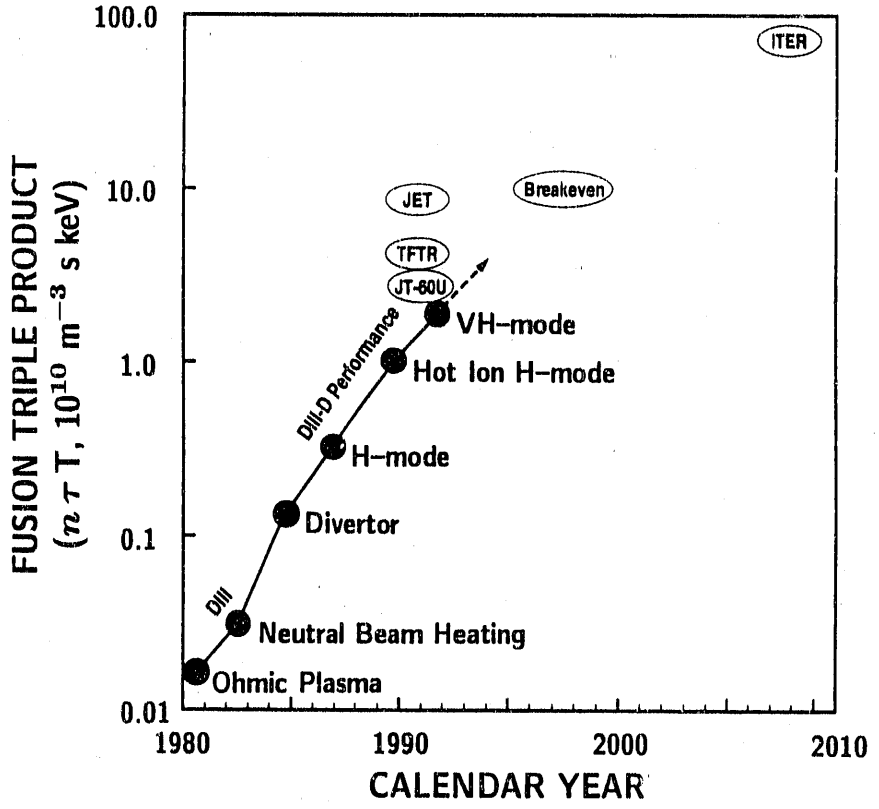

Fig. 1.1-1. The fusion (performance) triple product (i.e., plasma temperature, plasma density, and energy confinement time) has doubled every two years since 1980 in DIII/DIII–D.

Before discussing intermediate term program goals and specific results obtained during FY91, a brief overview of the DIII–D tokamak and its current capabilities is presented. The relative size and layout of the DIII–D experiment is shown in Fig. 1.1-2. This is a view of the machine, slightly offset to the right of center, as seen from a viewpoint several meters above the top of the main torus. One of the three neutral beam injectors interfaced to the machine fills the lower left hand corner of the figure. Several diagnostics, such as the Fast Neutron Fluctuation Measurement System, also appear in the figure. Inside the torus, graphite tiles completely cover the center post and divertor interaction regions located at the top and bottom of the vessel. These tiles are easily identified in the center portion of Fig. 1.1-3 which is a wide angel view looking inside the torus from a horizontal port. A small section of the advanced divertor ring, located around the outer circumference of the vessel floor, is seen in the lower right hand portion of the figure. A cross sectional view of DIII–D, in Fig. 1.1-4, shows a diverted configuration in which the magnetic equilibrium forms a so-called double-null geometry. Several of the major

machine components are also called out in this figure. This equilibrium configuration is only one of many available in DIII–D. Because of this flexibility in selecting the shape and position of the magnetic equilibrium, a relatively broad range of plasma parameters are available for experimentation. On the other hand, limitations in basic machine capabilities result in less operational flexibility and reduce the range of experiments which are possible. A summary of the current machine capabilities is given in Table 1.1-1 along with some proposed systems upgrades which are specifically required for progress toward our intermediate term program goals. Table 1.1-2 lists the key plasma parameters needed for an assessment of fusion performance levels and the largest values achieved for the parameters in DIII–D.

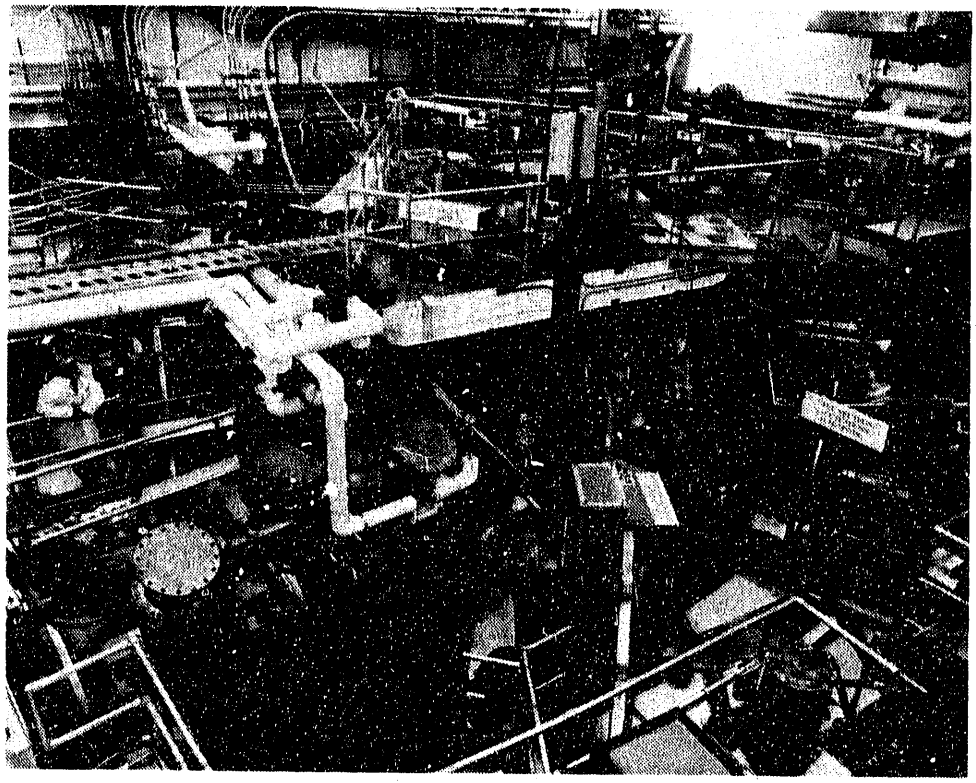

Fig. 1.1-2. View of the DIII–D tokamak.

Sustained progress on DIII–D has, for the most part, resulted from well established programmatic goals which facilitate the integration of complex technical research and development activities into a workable program plan. The current DIII–D Integrated Program Plan is shown in Fig. 1.1-5. The five key program elements (*i.e.*, radio frequency rf physics and technology, core physics, DIII–D operations, boundary physics and technology, and collaborative programs) form a coupled foundation which bridges the current drive program and the divertor program across a converging sequence of steps ultimately

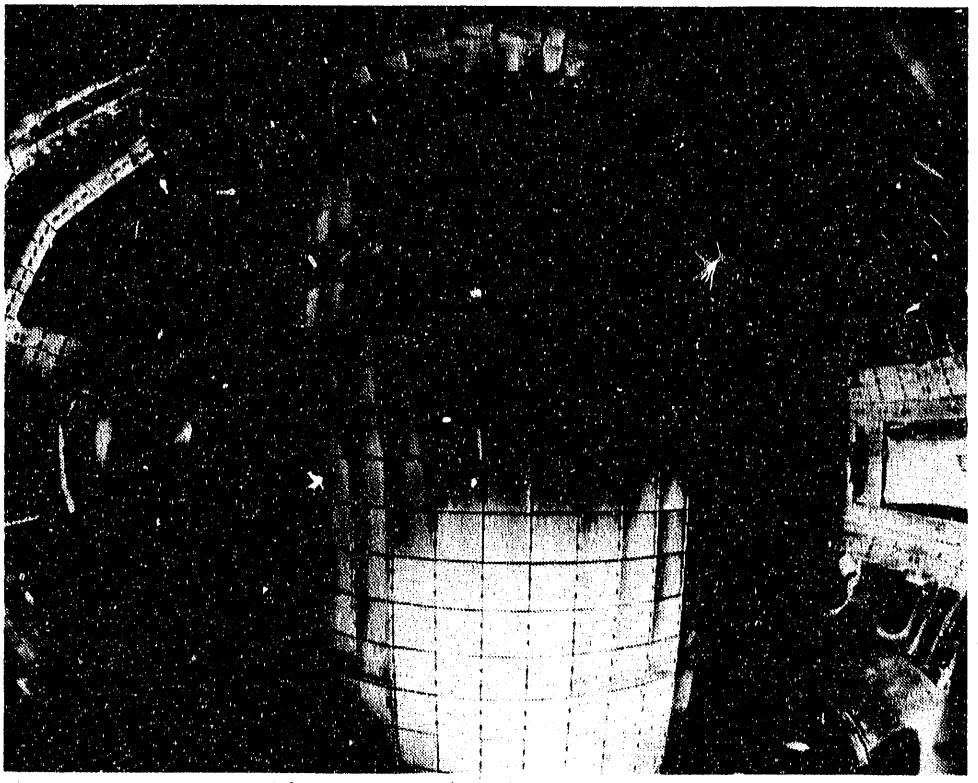

Fig. 1.1-3. Inside view of DIII-D.

resulting in experiments with noninductively driven currents of 2 MA with 5% beta, the ratio of the plasma pressure to the magnetic pressure, and pulse lengths of 10 seconds. Each of the program elements are separately highlighted in individual sections of this report.

With the completion of this Intermediate Term DIII-D Integrated Program Plan we will have made substantial progress toward assessing a minimum level of technology required for the design of a machine such as ITER. The current profile capability that the future rf system offer will enable advanced tokamak concepts to be developed in order to develop an attractive commercial DEMO to follow in the footsteps of ITER. In addition, the hardware implemented and experience gained during this period will provide new DIII-D operational capabilities which are essential for investigating critical issues related to the long pulse (or quasi-steady state) discharge conditions.

1.2. DIII-D PROGRAM SUMMARY

In general, progress in the DIII-D program during FY91 has been exceptional, particularly with respect to new physics results and improved operational capabilities.

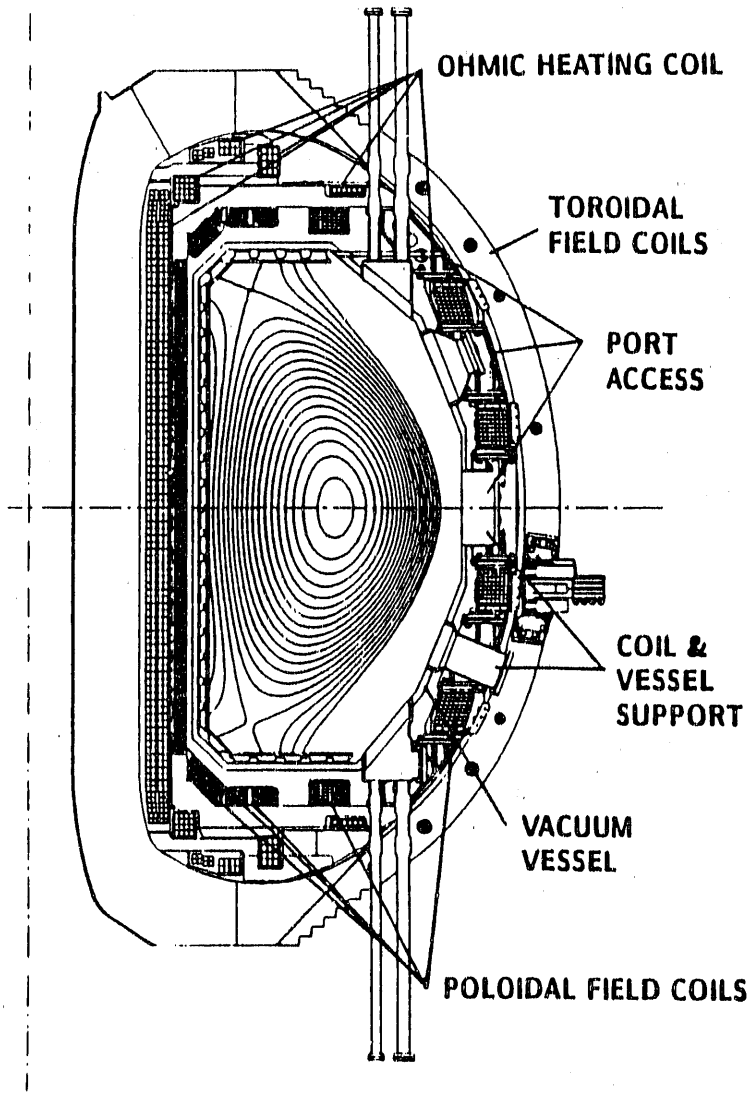

Fig. 1.1-4. Cross section of DIII–D with flux surfaces of a double-null divertor discharge superimposed.

These results, accomplished during 22 weeks of machine operations, were primarily related to work done in the areas of: new improved confinement regimes, electron cyclotron heating and heat pulse propagation, fast wave heating and current drive, toroidal Alfvén eigenmode studies, magnetohydrodynamic stability studies, and biasing experiments with the advanced divertor. Table 1.2-1 highlights some of the key FY91 accomplishments.

TABLE 1.1-1
DIII-D CAPABILITIES

	Present	Proposed Upgrades
Vacuum vessel volume	37 m^3	
Major radius	1.67 m	
Minor radius	0.67 m	
Maximum toroidal field	2.2 T	
Vertical elongation ratio	2.6	
Available OH flux	12 V-sec	
Maximum plasma current	3.0 MA	3.5 MA*
Neutral beam power	20 MW	
RF power (electron)	1.8 MW	10 MW
RF power (ion)	2 MW	8 MW
Current flattop (divertor at 2 MA)	5 s	10 s
Current flattop (divertor at 1 MA)	10 s	60 s

*Divertor operation; 5 MA limiter operation design.

TABLE 1.1-2
DIII-D ACHIEVED PARAMETERS
(NOT SIMULTANEOUS)

$1/aB$	3.3
$\beta_T(0)$	44% (second stability)
$\langle\beta_T\rangle$	11%
β_N	6.0
β_P	5.2
$\epsilon\beta_P$	2
$\bar{n}_e$	1.4×10^{20} m^{-3}
$T_e(0)$	5 keV
$T_i(0)$	17 keV
W	3.6 MJ
τ_E ($P_{HEAT} = 2.8$ MW)	0.34 s
$n_e \tau_E$	0.39×10^{20} m^{-3} keV s
$n_e T_i \tau_E$	2×10^{20} m^{-3} keV s
H-mode duration	10.3 s

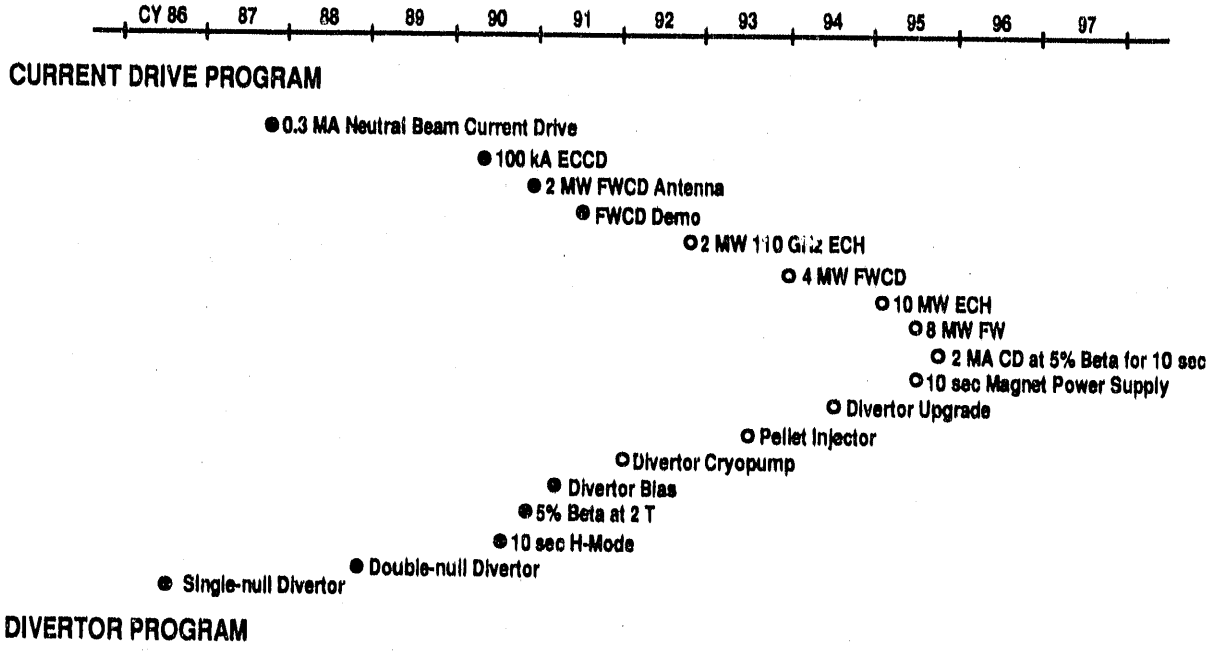

Fig. 1.1-5. DIII–D intermediate term integrated program plan.

TABLE 1.2-1
OVERVIEW OF FY91 RESEARCH RESULTS

- Tokamak Operations
  - — First machine boronization in May 1991.
  - — Increased neutrabl beam energy capabilities from 80 to 93 keV.
  - — First demonstration of digital plasma control system.
  - — Development of a disruption control/avoidance program activity.
  - — Started new disruption database and modeling activities.
  - — Installed new diagnostics.
  - — Improved the advanced divertor electrical insulation and cooling.
  - — Installed the third and fourth 110 GHz ECH antennas.
  - — Improved the fast wave antenna.
  - — Implemented an equipment preventive maintenance system.

- Divertor and Boundary Physics
  - — Gaseous divertor demonstrated without affecting confinement.
  - — Biased divertor ring used to control plasma collisionality.
  - — Divertor heat loading characterized at reactor relevant power.
  - — First edge plasma profiles with fast scanning Langmuir probe.
  - — Demonstrated neutral particle flux control with biased divertor ring.
  - — Reduced impurity concentrations with boronized walls.
  - — Identified fluctuation time scales after L–H transition.
  - — Developed modeling codes supporting biased advanced divertor experiments.
  - — Implemented an edge/divertor database protocol.

- Core Physics
  - — Achieved central beta of 44% in controlled manner.
  - — Discovered very high confinement VH–mode with confinement 3.6 × L–mode.
  - — Produced high inductance H–modes with improved confinement.

TABLE 1.2-1 (Continued)

- Core Physics (Continued)
  - — Operated with core plasma in second stable region.
  - — Demonstrated DIII–D TAE relevant operational regime.
  - — Operated with highly peaked current profiles.
  - — Established machine size scaling for H–mode operations.
  - — Increased fusion triple product to 2×10^{20} m^{-3} s keV.
  - — Evaluated the effects of plasma rotation on locked modes.

- Radio Frequency Heating and Current Drive
  - — Demonstrated strong fast wave electron heating at 32 MHz.
  - — First fast wave current drive experiments with 140 kA of noninductive current.
  - — Produced high confinement H–mode using only fast wave heating.
  - — Observation of nondiffusive transport in ECH heat pulse studies.
  - — First 110 GHz ECH gyrotron was installed and operation initiated.

- National and International Collaborations
  - — LLNL staff contributed to DIII–D divertor and transport physics.
  - — LLNL operated Motional Stark Effect diagnostic.
  - — LLNL installed an electron cyclotron emission diagnostic.
  - — ORNL staff assignments at DIII–D were increased.
  - — ORNL used codes to predict advanced divertor pressures.
  - — Installed ORNL capacitance manometer under divertor ring.
  - — ORNL initiated pellet injector collaboration.
  - — Sandia operated fast scanning Langmuir probe with UCLA.
  - — UCLA reflectometer and laser diagnostics supported L–H studies.
  - — JET neutral beam and cryopump information used for DIII–D.
  - — Textor boronization techniques applied to DIII–D.
  - — Tore Supra expanded DIII–D boundary layer collaboration.
  - — First ergodically diverted LHCD results from Tore Supra.
  - — JFT-2M ergodic limiter H–mode studies of interest for DIII–D.

SECTION 2

BOUNDARY PLASMA RESEARCH PROGRAM/SCIENTIFIC PROGRESS

2. BOUNDARY PLASMA RESEARCH PROGRAM/ SCIENTIFIC PROGRESS

2.1. BOUNDARY RESEARCH PROGRAM OVERVIEW

The DIII–D divertors along with a relatively thin boundary region just inside the magnetic separatrix and the so-called scrapeoff layer (SOL) just outside the magnetic separatrix play a key role in establishing the overall performance capabilities of the tokamak. Plasma properties found in these regions can be extremely demanding when operating near conditions required for the highest levels of machine performance. It is, therefore, understood that significant progress in enhancing the performance and efficiency of the tokamak's operation must involve a better understanding of boundary layer physics processes and requires the development of advanced boundary layer control technologies.

The DIII–D experimental boundary layer research program is organized into three key areas of activity. Each of these activities is complemented by strong support from theory and modeling groups both within the DIII–D organization and outside it. The key research areas cover: (1) basic divertor and edge physics activities including heat flux characterizations near reactor relevant power levels, studies of edge plasma/neutral particle transport and control, development of radiative divertor concepts for power control, and biased divertor experiments designed to explore control techniques utilizing edge electric potential modifications; (2) high confinement H–mode physics activities which are designed to determine the connecting between edge plasma parameter profile (such as the radial component of the electric field, the plasma rotation, and the electron temperature), and reductions in edge electron density fluctuation level observed at the onset of the H–mode phase; and (3) impurity production, transport, and control physics. A summary of significant findings and advancements made in each of these areas, as well as an overview of the theory and modeling work supporting these activities, is given in this section.

Some of the key results in the boundary plasma research program are:

- The characterization of high heat flux divertor and SOL parameters at reactor relevant power levels of 5 MW/m^2.

- Demonstrated that the radiative divertor concept significantly reduces the thermal load on the target plates with little or no reduction in the energy confinement time.
- The first measurements of SOL density and temperature profiles and fluctuations in the vicinity of the separatrix with the fast scanning Langmuir probe.
- The first Advanced Divertor Project (ADP) biased divertor experiments which demonstrated that cold electrode operation is practical and introduces no deleterious effects.
- The initial development of an edge database for modeling future reactor divertor designs.
- Demonstrated controlled collisionallity reductions with the new ADP ring during biasing experiments.
- Demonstrated that divertor biasing can be used to control neutral fluxes and pressures under the ADP baffle ring.
- Observations of two turbulence suppression time scales in two different regions of the plasma at the transition between low confinement L–mode and high confinement H–mode suggesting that improved H–mode interior confinement results from changes in the boundary after the initial L–H transition.
- The first boronization, which was remarkably successful, resulting in a reduction of the plasma impurity content and made a significant impact on the routine operation of DIII–D.
- Observation of a very high confinement VH–mode with 1.8 times H–mode energy confinement time after boronization.

2.2. DIVERTOR PHYSICS OVERVIEW AND SUMMARY

The DIII–D divertor physics group is actively pursuing a broad based program aimed at understanding basic physical processes which affect the performance limits of poloidally diverted tokamaks. The group's activities are designed to provide timely input for critical International Thermonuclear Experimental Reactor (ITER) design issues while allowing opportunities to explore options which appear to be attractive for increasing the capabilities of diverted tokamaks. Substantial 1991 program progress was made in: characterizing high heat flux divertor performances and SOL parameters, developing radiative boundary techniques which may provide greater control over ELMing high confinement H–mode

discharges, with edge localized modes (ELM), performing comprehensive measurements of plasma properties such as density and potential fluctuations and profiles in the SOL for a variety of discharge conditions, performing experiments and modeling with the newly installed DIII–D Advanced Divertor, developing edge specific diagnostic systems such as those shown in Fig. 2.2-1 to support expanded experimental efforts over the next few years, and compiling a database for edge modeling and comparative studies. The DIII–D divertor program is expanding to meet the needs of the ITER Design Activity while continuing to make substantial progress in acquiring a fundamental understanding of key physics issues which will be needed to enhance the performance capabilities of tokamaks reactors in the future.

2.2.1. HEAT FLUX CHARACTERIZATIONS

Heat flux scaling studies at peak power levels of $\approx$5 MW/m^2 on the divertor targets were carried out in order to characterize the divertor and SOL properties relevant to the parameters being anticipated for ITER [1]. Heat flux variations with changes in the plasma current I_p, toroidal magnetic field B_T, and edge safety factor q_{95} were less significant than effects due to locked modes on the $q = 2$ surface. These locked modes cause a broadening of the SOL profiles which lowers the peak heat flux at the target plate. When locked modes are not present the peak divertor heat flux $Q_{div,peak} \propto I_p$.

2.2.2. HEAT REDUCTION AND RADIATIVE EFFECTS DURING DEUTERIUM D_2 INJECTION IN H-MODES WITH EDGE LOCALIZED MODES (ELMs)

The introduction of large D_2 neutral gas fluxes, via an externally controlled valve, provided an effective method of reducing the target plate heat flux on the divertor floor [2]. The peak heat flux could typically be reduced by a factor of four or more with little, if any, reduction in the plasma energy confinement. A representative example of the single-null divertor configuration for the range in parameters investigated: I_p = 1.0-2.0 MA, B_T = 1.4-2.1 Tesla, injection power P_{inj} = 5-15 MW is shown in Fig. 2.2-2.

The SOL and divertor region are modeled with an impurity transport code recently developed at Sandia called NEWT1-D. Preliminary results indicate that 80-90% of the radiated power in the SOL and divertor is due to deuterium line radiation, assuming carbon to be the dominant impurity species. This suggests that an intrinsic (or injected) impurity specie may not be necessary to reduce heat flux at the divertor target. Low measured values of electron temperature T_e (5 eV) and high neutral gas pressures (>50 mTorr) near the divertor targets indicate that processes other than line radiation are also significant.

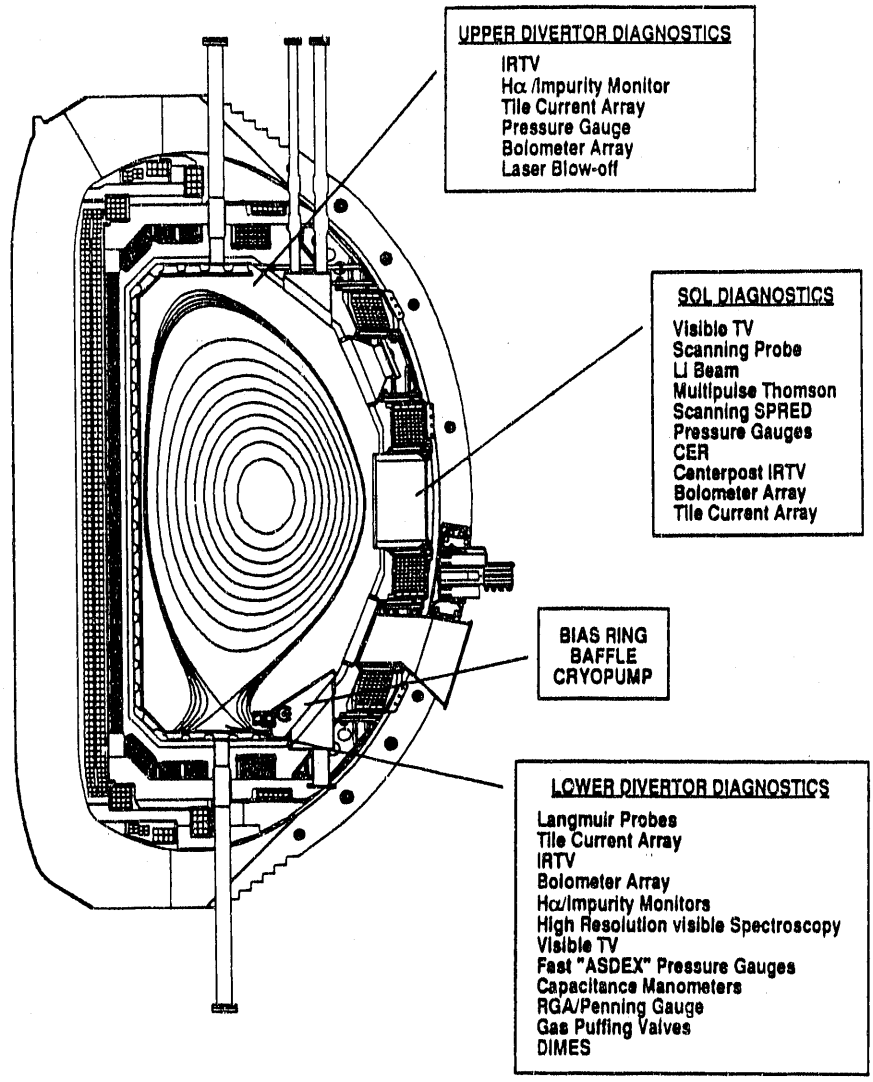

Fig. 2.2-1. An extensive array of edge diagnostics are currently available on DIII–D. With the addition of new diagnostic systems proposed for installation during the next several years, DIII–D will be capable of addressing most of the important issues needed for improved divertor performance.

Under these conditions, charge-exchange and ion-neutral elastic collisions can be expected to play important roles in peak heat flux reduction and momentum loss along field lines in the divertor.

2.2.3. NEUTRAL PRESSURE MEASUREMENTS AND MODELING

The newly installed Advanced Divertor baffle forms a partially closed divertor. The baffle develops neutral gas pressures in excess of 10 mTorr during ELMing H–modes [3],

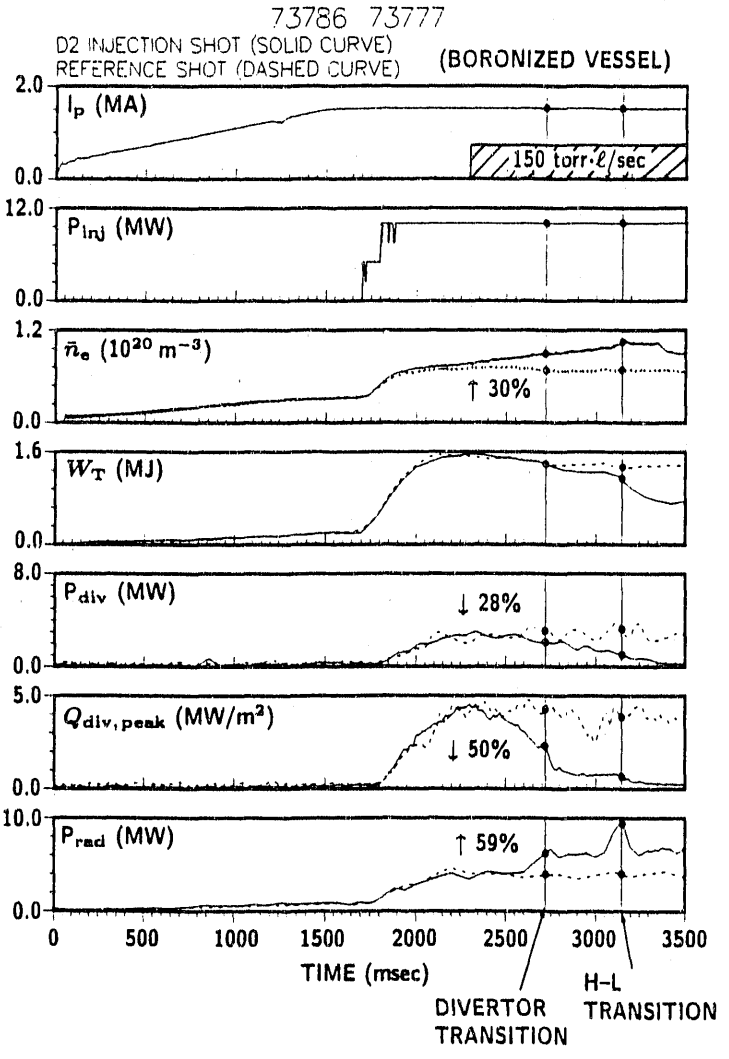

Fig. 2.2-2. D_2 injection was effective in reducing both peak heat flux ($Q_{div,peak}$) and total integrated particle heat flux across the divertor (P_{div}) with only modest degradation in the plasma stored energy (W_t), prior to the H → L mode transition. The solid line is the D_2 injection shot, while the dashed line is the reference shot. Most of the total radiated power (P_{rad}) is coming from the X–point and divertor region, not the plasma core [2].

and such high pressures bode very well for particle removal by the cryopump to be installed under the baffle in FY92 and in future experiments. The pressure increases with both neutral beam heating power and plasma current. The pressure is a rather sensitive function of the distance between the divertor magnetic separatrix and the edge of the baffle, with a full width at half maximum (FWHM) $\approx$ 3 cm [4].

The measured pressures are an order of magnitude greater than predicted by simple simulations. However, recent self-consistent simulations (using measured SOL plasma parameters and divertor heat flux as inputs to the B2 edge plasma simulation code for modeling the SOL plasma temperaure T_e and density n_e, and iterating to convergence with the DEGAS neutral particle transport code) correctly predict the measured pressure. It is found that the baffle raises the divertor recycling to the extent that the divertor electron temperature is lowered to $\approx$2 eV, which lets more neutrals escape from the plasma and contribute to pressure under the baffle than would otherwise be possible. The experimental absence of carbon CII radiation at the divertor plate supports the low simulation T_e. Additional calculations are in progress to estimate the attainable particle removal by pumping when self-consistent plasma effects are included [5].

2.2.4. EDGE AND SCRAPEOFF LAYER (SOL) MEASUREMENTS

Edge plasma properties play an important role in determining the dominant physics of the divertor and in establishing the overall performance capabilities of the divertor. Concentrated efforts are presently underway to measure edge n_e and T_e profiles during varied operational conditions for comparisons with the divertor data and to determine edge plasma parameter scalings [6]. Fluctuation measurements and calculation of the $\vec{E} \times \vec{B}$ particle fluxes are also made in order to help quantify transport mechanisms in the plasma boundary [7]. These measurements utilize the SNL/UCLA fast scanning Langmuir probe array, installed on DIII–D in December 1990, and now fully operational. The probe consists of a pneumatically driven, 3 m/s drive tube equipped with five graphite tips. These tips are used to simultaneously measure the plasma profiles (n_e, T_e, floating potential ϕ), and the fluctuating quantities $\tilde{n}_e(k,\omega)$ and $\tilde{\phi}(k,\omega)$. The associated $\vec{E} \times \vec{B}$ particle transport is calculated using both time domain and spectral analysis techniques. The probe is capable of measuring these parameters up to 2 cm inside the separatrix in low power ($\leq$5 MW) discharges.

Initial profile measurements indicate that Ohmic and low confinement L–mode discharges exhibit similar density (exponential) and temperature (bi-exponential) decay in the SOL. High confinement H–mode discharges, however, display a faster spatial decay reflecting at least a factor of 2 decrease in the perpendicular diffusion coefficient. Equilibrium floating potential profiles exhibit a sharp negative dip near the separatrix during H–mode, and a slower transition to negative values in L–mode discharges. These floating potential profiles also display quasi-stationary ($t \leq 200$ ms) structures in the SOL in all confinement regimes.

Studies of the electrostatic fluctuations in the SOL indicate that the characteristics of the turbulence are similar in Ohmic, L, and H confinement regimes. Wave numbers are typically 1 $cm^{-1} \leq k_\theta \leq 2$ cm^{-1}, and fluctuation levels are $\tilde{n}/ < n > \approx$ 30%-40% and $\tilde{\phi}/ < \phi > \approx$ 25%-40% across the SOL. The associated fluctuation-driven particle transport is also nearly independent of confinement regime in the SOL. This is in contrast to the observed shortening of the SOL widths from L– to H–mode, indicating that the relative importance of fluctuation-driven transport in the SOL may change from L– to H–mode. Initial measurements inside the separatrix indicate that the density fluctuation levels are reduced, consistent with reflectometry measurements, while potential fluctuation levels remain unchanged. The associated fluctuation-driven transport inside the separatrix is also reduced.

2.2.5. BIASED DIVERTOR EXPERIMENTS

The biased divertor on DIII–D affords a unique approach to control and improve tokamak performance [8]. It is intended to supply a means of density control in H–mode plasmas, to produce low collisionality plasmas for current drive experiments and to break the present linkage between n_e and I_p for transport studies. It is also intended as a method to modify influential boundary processes, such as electric potential profiles, which are instrumental in determining the edge plasma rotation profiles, and edge current density distributions, which influence the stability of edge modes.

The first year of operation has demonstrated that cold electrode operation is practical, within the limits of divertor ion saturation current, and introduces no deleterious effects. The divertor electrode has operated at up to 550 V and 12 kA to date. Core plasma impurity content and energy confinement are unaffected by electrode operation. Divertor bias changes the core plasma density. Density decreases were accompanied by corresponding temperature increases, thereby demonstrating a controlled reduction of collisionality.

Divertor bias has marked effects on baffle chamber gas pressure, see Figs. 2.2-3(a) and 2.2-3(b), and divertor recycling. These effects are attributed to $\vec{E} \times \vec{B}_{Tor}$ driven flows on the order of 1000 m^3/s. Both radial and poloidal flows are important. Baffle chamber pressure rises substantially for $\vec{E} \times \vec{B}_{Tor}$ toward the baffle entrance for all operating modes tested: Ohmic, L–mode and ELMing H–mode. Furthermore, the pressure is much less sensitive to separatrix location than in the absence of bias. This feature could be extremely useful to sustain divertor exhaust while the separatrix position is continuously varied or swept

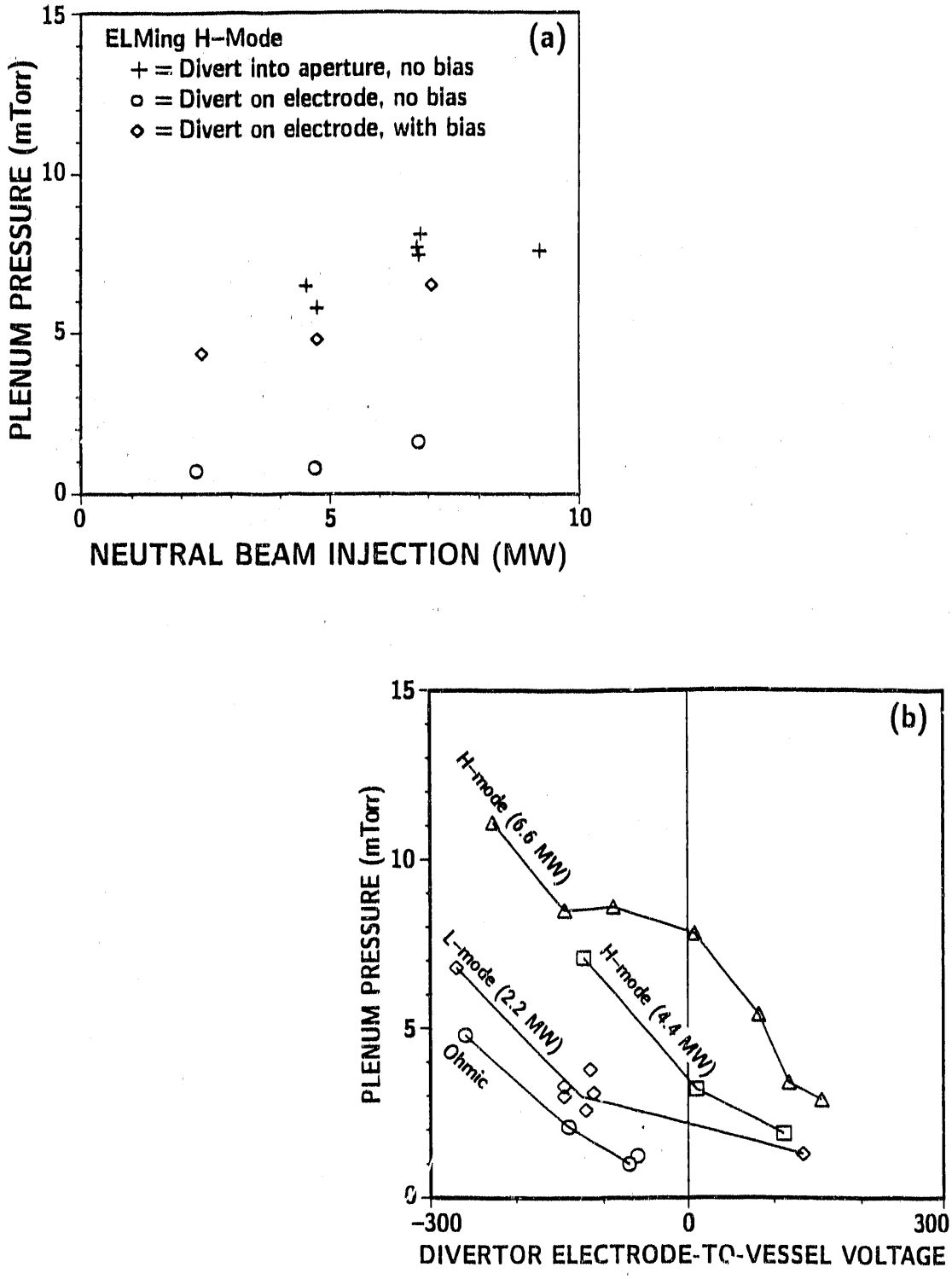

Fig. 2.2-3. (a) The divertor bias overcomes sensitivity of pressure to separatrix position [10]. (b) Plenum gas pressure at optimum position versus bias for four plasma conditions. Ohmic and L–mode chord average electron densities are 2.3 $\sim$ 2.5 $\times$ 10^{19} m^{-3}. All points are for 1 MA and 2.1 T.

in order to distribute the exhaust power over a wide surface. The $\vec{E} \times \vec{B}_{Tor}$ flow might also combine favorably to stem backflow of plasma from a radiative divertor.

Divertor bias alters the power threshold of the L $\rightarrow$ H–mode transition. Large bias of either sign raises the L $\rightarrow$ H threshold power, $P_{L\rightarrow H}$, by as much as a factor of 4 with a –400 V bias. Minimum $P_{L\rightarrow H}$ (of $\approx$1.2 MW as opposed to $\approx$2.1 MW with no bias) is at a bias of +75 to +100 V. Because the bias for minimum $P_{L\rightarrow H}$ is independent of the sign of $\vec{B}_{Tor}$ the $\vec{E} \times \vec{B}_{Tor}$ drift is ruled out as an explanation. Radial profiles of the toroidal and poloidal rotation speeds are different for positive and negative biasing, but the interpretation is inconclusive due to uncertainty of the exact location of the magnetic separatrix. Identification of the cause of the effect of divertor bias on the L $\rightarrow$ H transition might help to understand the nature of the H–mode.

In anticipation of the biased divertor experiments a quasi-2D transport code was developed [9] for comparison with experimental data. The code includes classical parallel transport relations, as well as current and thermoelectric terms usually absent from SOL models, but essential for biasing simulations. The model equations also include the $\vec{E} \times \vec{B}$ particle drifts which are shown to be responsible for the observed heat flux asymmetries at the target plates of DIII–D. A simple diffusive model of turbulent radial transport of heat and particles is also included. Recently, the neutral ionization model has been improved and a simple radiation model has been added for the recycling zones near the target plates. As more complete experimental data sets become available, detailed comparisons will be made to test the validity of the model equations.

2.2.6. MODELING AND DATABASE

Modeling codes provide an important perspective for planning, interpreting, and comparing divertor and boundary physics experiments [11,12]. Combinations of the B2 edge plasma modeling and DEGAS neutral transport codes are used to analyze divertor pressure data in DIII–D while a one dimensional impurity code, called NEWT1-D, is applied to the radiative divertor experiments. In addition, an implicit B2 code, called IMPB2, has been developed for divertor modeling studies. Results from IMPB2 emphasize the importance of accurate neutral models when simulating divertor physics. These modeling codes can best be validated by comparisons with experimental data from DIII–D. A DIII–D edge physics database [13] has been established for validating the codes and for making comparisons with data from other divertor experiments such as JET.

2.2.7. EDGE DIAGNOSTICS

A number of new edge, SOL, and divertor specific diagnostics have come into operation during FY91. An array of 28 tile current monitors was instrumental in tracing the flow of injected current from the bias electrode [14]. The monitors detected unusually large natural SOL current during VH–mode, but the origin of this effect is not yet identified. The array also measured large plasma "halo" currents during disruptions. Most of the monitors were eventually damaged by disruptions, and they are presently being ruggedized. A fast scanning Langmuir probe array at the equatorial plane (see Section 2.2.4) and a divertor target plate Langmuir probe array were used to help characterize the edge and SOL parameters under different operating conditions. A capacitance manometer was installed to make direct pressure measurements. The manometer measurement is independent of the gas species, as opposed to an ionization gauge which is sensitive to the mass and ionization potential of each species [15]. A divertor spectrometer, equipped with both a broad bandwidth (150Å) OMA and a fast multichord OMA was also brought into operation during FY91.

Edge diagnostic systems which are soon to be commissioned include a new bolometer diagnostic which will consist of two arrays viewing from different poloidal angles and a Lithium Beam Diagnostic System. The new bolometer allows localized measurements of plasma radiated power which is a particularly important measurement for the radiative divertor experiments. The object of the Lithium Beam Diagnostic System is to examine the density profile and investigate associated fluctuations in the DIII–D boundary layer. An intense, low energy (E $\approx$ 5-30 keV) neutral lithium beam is injected into the edge region and collisionally induced line fluorescence (at λ = 6708Å) is observed with the system's viewing optics. Because of the favorable atomic properties of lithium (*i.e.*, high excitation rate, low beam temperature, and a resonant wavelength which is well separated from H_α line emissions) the fluorescence should provide detailed information about the plasma density several centimeters inside the separatrix with good spatial (<1 cm) and temporal (<10 ms) resolution. Initial data is expected during the spring of 1992 [16].

References for Section 2.2.

[1] Hill, D.N., *et al.*, "Divertor-Plasma Characterization in DIII–D Plasmas," *Bull. Amer. Phys. Soc.* **36** (1991) 2325.

[2] Petrie, T.W., *et al.*, "Radiative Experiments in ELMing H–mode Plasmas in DIII–D," *Bull. Amer. Phys. Soc.* **36** (1991) 2471.

[3] Klepper, C.C., *et al.*, "Divertor Neutral Pressure Enhancement with a Baffle in DIII–D," to be submitted to *Nuclear Fusion.*

[4] Schaffer, M.J., *et al.*, "Effect of Divertor Bias on Particle and Power Flows in the Tokamak Divertor Scrapeoff Layer," General Atomics Report GA-A20474, submitted to *Nuclear Fusion.*

[5] Hogan, J., *et al.*, "Plasma Modeling of Baffle Pressure Scaling Studies in the DIII–D Advanced Divertor Experiment," *Bull. Amer. Phys. Soc.* **36** (1991) 2503.

[6] Watkins, J.G., *et al.*, "DIII–D Edge Profile Characterization With the SNL/UCLA Fast Scanning Langmuir Probe," *Bull. Amer. Phys. Soc.* **36** (1991) 2472.

[7] Moyer, R.A., *et al.*, "Initial Characterization of Fluctuations in the Edge Plasma With the SNL/UCLA Fast Reciprocating Langmuir Probe," *Bull. Amer. Phys. Soc.* **36** (1991) 2472.

[8] Schaffer, M.J., *et al.*, "Particle Control in the DIII–D Advanced Divertor," General Atomics Report GA-A20631, to be published in Proc. 14th IEEE Symp. on Fusion Engineering, San Diego, 1991.

[9] Staebler, G., *et al.*, "Transport Modeling of Divertor Bias Experiments," *Nucl. Fusion* **31** (1991) 729.

[10] Schaffer, M.J., *et al.*, "Biased Divertor Experiments on DIII–D," *Bull. Amer. Phys. Soc.* **36** (1991) 2325.

[11] Campbell, R.B., *et al.*, "A Calculation of Impurity Transport in the DIII–D Scrape-off Layer," *Bull. Amer. Phys. Soc.* **36** (1991) 2471.

[12] Rensink, M.E., *et al.*, "Modeling of DIII–D Divertor Plasmas at ITER-Like Power Levels," *Bull. Amer. Phys. Soc.* **36** (1991) 2472.

[13] Jong, R.A., *et al.*, "Edge Physics Database for DIII–D," *Bull. Amer. Phys. Soc.* **36** (1991) 2472.

[14] Schaffer, M.J., and B.J. Leikind, "Observation of Electric Currents in Diverted Tokamak Scrape-off Layers," *Nucl. Fusion* **31** (1991) 1750.

[15] Klepper, C.C., *et al.*, "Divertor Neutral Pressure Enhancement With a Baffle in DIII–D," *Bull. Amer. Phys. Soc.* **36** (1991) 2325.

[16] Thomas, D.M., *et al.*, "The DIII–D Lithium Beam Edge Diagnostic," *Bull. Amer. Phys. Soc.* **36** (1991) 2473.

2.3. HIGH CONFINEMENT H-MODE PHYSICS

An active and diverse experimental program has led to a deeper understanding of the physics of the H-mode in DIII-D. These studies were aided by several diagnostic improvements, including the increased spatial resolution of the edge charge exchange recombination (CER) system, the implementation of a carcinotron source for FIR scattering, the advent of the multipulse Thomson scattering system and increased spatial resolution of the edge Thomson points. These studies featured a strong collaboration between the GA physics' team and researchers from UCLA, UCSD, and UC Berkeley.

After several experimental scans, the theoretical idea [1,2] that a transition into the H-mode is triggered by a reduction in edge turbulence due to an increase in the radial electric field E_r shear remains an attractive paradigm for designing and analyzing experiments. These scans included variations of the toroidal field, target density, plasma current, and heating power. In addition, data were taken with plasma current ramps and in ohmic H-modes. The picture supported by all of these scans is that at the low to high L-H confinement transition, E_r in a thin layer just inside the separatrix rapidly becomes more negative forming a "well" like structure in which density fluctuations are reduced. Furthermore, the well region is the location in which the transport barrier is formed, as is demonstrated by the development of large gradients of the ion temperature T_i, electron temperature T_e, electron density n_e and carbon density (Fig. 2.3-1). Impressive values of T_i at the plasma edge are routinely observed. Ion temperature gradient ∇T_i values of 1.2 keV/cm and values of T_i of 2-3 keV within 1-4 cm of the separatrix have been readily obtained. For many cases, the edge values of T_i are much larger than the values of T_e.

The reduction of density fluctuations is inferred from the reflectometer signals which show marked reductions in the shear layer within 100 μs of the drop in the deuterium D_α recycling signal. This conclusion has been greatly strengthened with measurements from the far infrared (FIR) system which also show that the electron density fluctuation level $\tilde{n}$ drops in the shear layer within 100 μs of the transition. This conclusion is made possible by the fact that the negative E_r in the shear layer causes a frequency shift of the FIR scattered spectra which is opposite in direction to the shift produced by the positive E_r further into the plasma core.

The radial electric fields as measured by the CER system show no precursors within the error bars prior to the transition. However, large changes are observed in E_r within 1 ms of the drop in the D_α signal. Thus, the idea that changes in E_r cause the reduction

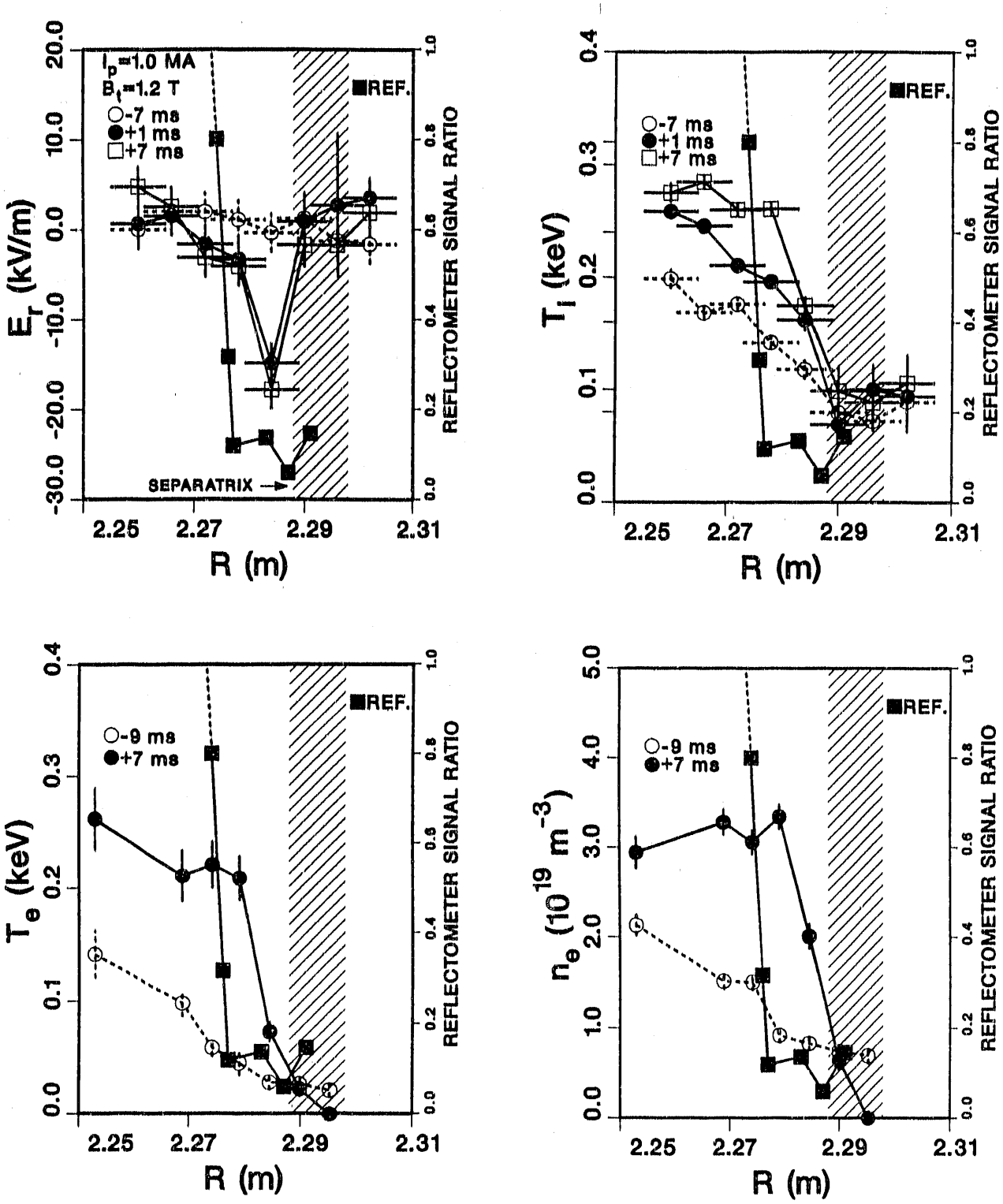

Fig. 2.3-1. Reflectometer data (indicated by solid black squares) overlaid on profiles of E_r, T_i, T_e and n_e. Each reflectometer point is ratio of total detected fluctuation power after the transition to power before the transition. Times shown are relative to L–H transition. Region of well structure in E_r coincides with region in which reflectometer signals drop in H–mode. Gradients of T_i, T_e, and n_e all increase in this region after the transition.

in microturbulence can neither be proven nor disproven. In fact, recent theoretical ideas which treat E_r and the plasma transport self-consistently suggest that E_r and the fluctuation levels may evolve simultaneously [3,4]. Thus, there may be no clear precursor.

The widths of the E_r well and of the region in which the reflectometer signals are suppressed are observed to be in the range 1-3 cm and the depth of the E_r well is in the range of 20-40 kV/m for the wide variations in plasma conditions which have been studied. Some variation in the width and depth have been observed, but the controlling parameter for the edge E_r is not yet understood.

In addition to the initial rapid suppression of fluctuations observed at the edge of the plasma in the H–mode phase, the FIR scattering data clearly show that suppression of fluctuations also occurs on a slower timescale in the interior of the plasma after the H–mode is established [5]. (Spatial resolution with the FIR system is achieved by studying parts of the scattered spectrum with different Doppler shifts due to $\vec{E}\times\vec{B}$ rotation as has been discussed above.) For the second phase of suppression, $\tilde{n}/n_e$ is observed to drop over a period of tens of milliseconds by a factor of roughly two. Transport analysis has also shown that there is a reduction of transport coefficients in this same interior region by about a factor of two and that the reduction also occurs over a period of tens of milliseconds [6]. Thus, there is circumstantial evidence for a link between turbulence and transport but this cannot be concluded firmly at this time. The observation of two timescales and two spatial regions for changes in confinement and turbulence in the H–mode suggest that the improved interior confinement of the H–mode is made possible by changes in the boundary conditions of the plasma after the initial L–H transition.

The Thomson scattering data show that the electron pressure gradient at the very edge of the plasma quickly reaches the ideal ballooning limit after the L–H transition. The gradient then grows into the plasma for some time until an ELM is triggered. (Three types of ELMs have been identified. The discussion here is restricted to Type I or "Giant" ELMs.) The T_i gradient also exhibits similar behavior. Thus, although ballooning modes may limit the edge pressure gradient, it is not at all clear that the ELM is due to a ballooning mode. The reflectometer system shows that a Type I ELM has a precursor which is a general rise in broadband turbulence levels which grow for many milliseconds prior to the ELM and culminates in the ELM itself. The precursors are localized to the vicinity of the "knee" in the n_e gradient; the knee corresponds to the inner edge of the transport barrier. Precursors have not been observed with other quantities such as T_e, T_i, n_e, or E_r.

References for Section 2.3.

[1] Biglari, H., P.H. Diamond and P.W. Terry, *Physics of Fluids B* **2** (1990) 1.

[2] Shaing, K.C., E.C. Crume, Jr., *Phys. Rev. Lett.* **63** (1989) 2369.

[3] Hinton, F.L., *Phys. Fluids B* **3** (1991) 696.

[4] Diamond, P.H., *Bull. Am. Phys. Soc.* **36** (1991) 2454.

[5] Phillipona, R., R.J. Groebner, K.H. Burrell, E.J. Doyle, P. Gohil, N.C. Luhmann, Jr., H. Matsumoto, W.A. Peebles, C.L. Rettig and R.D. Stambaugh, "Two-Stage Turbulence Suppression and $E \times B$ Plasma Flow Measured at the L–H Transition," General Atomics Report GA-A20516, submitted to *Phys. Rev. Lett.*

[6] Kurki-Suonio, T.K., R.J. Groebner, K.H. Burrell, "Changes in Local Confinement After an L–H Transition in DIII–D," General Atomics Report GA-A20450, submitted to *Nucl. Fusion.*

2.4. IMPURITY CONTROL ON DIII–D

2.4.1. THE EFFECT OF BORONIZATION ON IMPURITIES

During FY91 DIII–D, following the lead of TEXTOR, implemented boronization. Boronization, similar to carbonization previously employed on DIII–D, is the process of depositing a thin, hard boron film on the internal vacuum components. This thin film provides a low Z, low sputter rate first wall and has been shown to significantly reduce impurities and recycling. Boronization has been demonstrated to be superior to carbonization, primarily due to the passivation of oxygen by boron. This process has proven so successful on DIII–D that it has made a significant impact on the routine operation of the machine. In this section we will discuss the observed reduction of impurity content of the plasma following the first boronization, the effects on impurities during the course of five months of operation during which several boronization procedures were carried out, and briefly touch on impurity behavior during VH–mode operation.

The first boronization on DIII–D was completed on Saturday, May 18. The gas mixture used on this date was 90% helium (He) and 10% deuterated diborane B_2D_6, producing a 100 nm film consisting mostly of boron. The effect on intrinsic impurities during operation was dramatic. Shown in Fig. 2.4-1 are impurity line traces as measured by the survey, poor resolution, extended domain (SPRED) spectrometer and other relevant data for two similar discharges, No. 72130 taken before boronization and No. 72190 taken

on May 20. The nickel (Ni) lines are down by an order of magnitude, the oxygen OVIII line is down by more than a factor of five, and the carbon line is also significantly reduced. There is also a significant reduction in the radiated power. These two shots are typical of standard ELMing H–mode discharges taken prior and post boronization and demonstrate the remarkable success of this process.

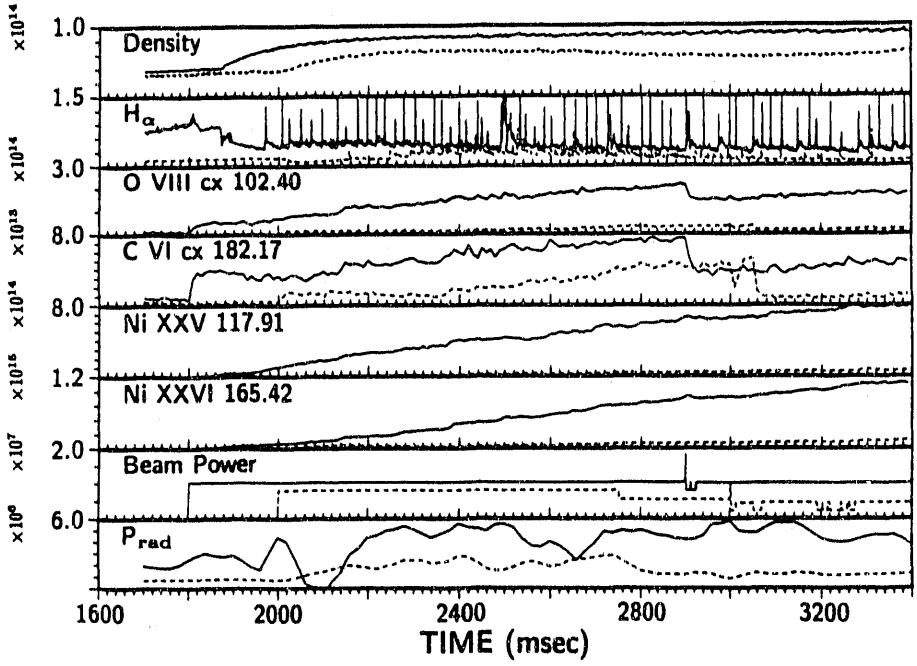

Fig. 2.4-1. A comparison of discharge properties before, Shot 72130 (solid lines), and after, Shot 72190 (dashed line) boronization. Both discharges are lower single null and enter an ELMing H–mode phase soon after the application of neutral beam heating. Impurity line intensities and radiated power are significantly reduced following boronization.

During the course of the summer of 1991, five separate boronization coatings were completed, spaced approximately one month apart. Since DIII–D is routinely run on a two-week-on/two-week-off schedule, this represents a boronization for every two-week run period. The history of an oxygen line intensity as measured by SPRED during the ohmic phase of discharges with plasma current between 0.9 and 1.5 MA is shown for many discharges over the summer in Fig. 2.4-2 (nickel and carbon line intensities are similar). In all cases, the levels remain low compared to the pre-boronization levels. The data show that the impurity levels are remaining constant during the run period, indicating the effect

of the film has not degraded during the two weeks of run time. Because of the fairly high frequency of recoating the vessel, data on the longevity of a single coating is not presently available.

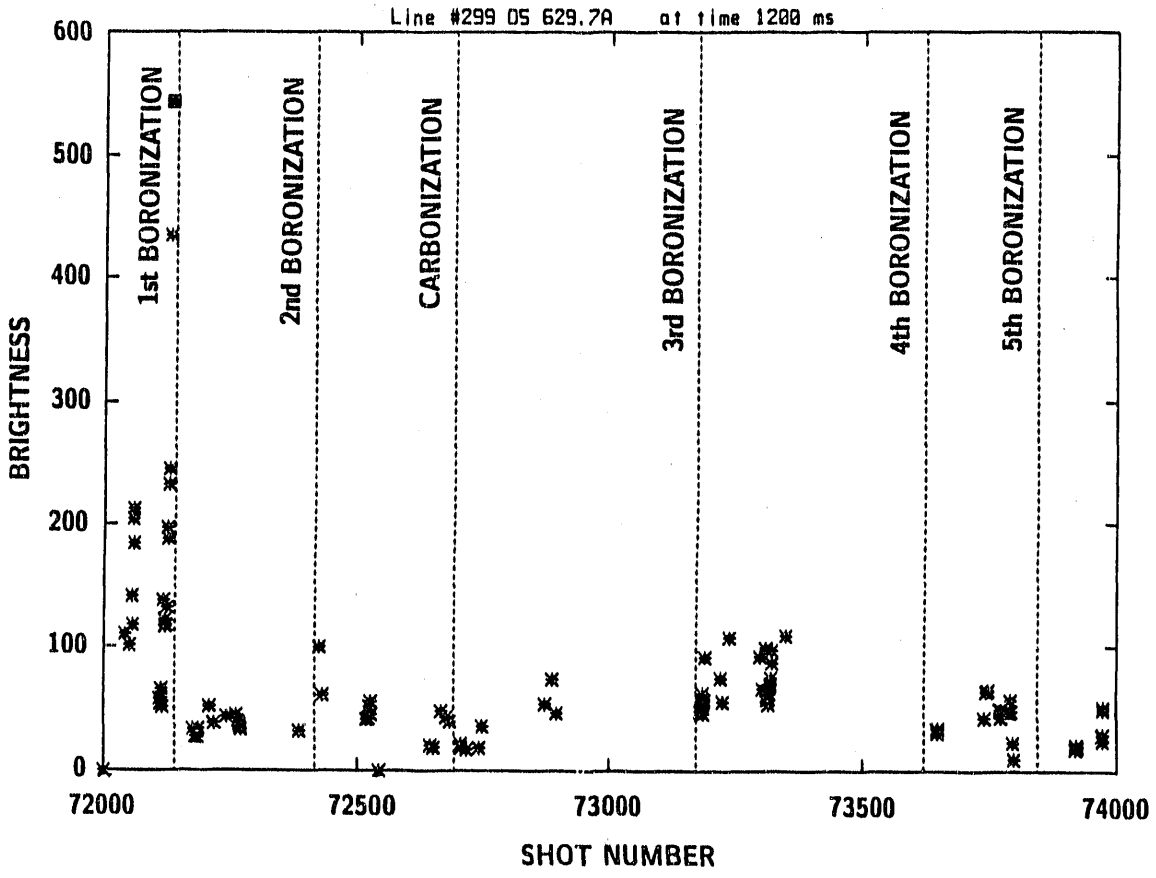

Fig. 2.4-2. The history of the OV line at 629.7Å, measured by SPRED, during the ohmic phase of the plasma over the course of the summer 1991 campaign. Data shown is for discharges with plasma current between 0.9 and 1.5 MA, typically 1200 ms after discharge initiation. Typically, there is a one month lapse between boronizations, including two weeks of discharge operation and two weeks of maintenance.

Boronization does not completely solve the impurity problem on DIII–D. Shown in Fig. 2.4-3 is the time history of discharge No. 73313, taken after the third boronization. This discharge enters a quiescent H–mode about 500 ms after the application of beam heating. During the quiescent H–mode, impurity line intensities are seen to grow dramatically, and the radiated power is observed to increase until it equals the beam power. At this point, the plasma returns to an L–mode condition. This behavior is consistent for

standard quiescent H–mode plasmas throughout the summer, and is taken as evidence that the coating is not uniformly protecting the plasma facing surfaces. Because of this observation, the coating process was altered during the course of the summer. As can be seen from Fig. 2.4-2, the impurity levels during the ohmic phase were somewhat higher after this coating.

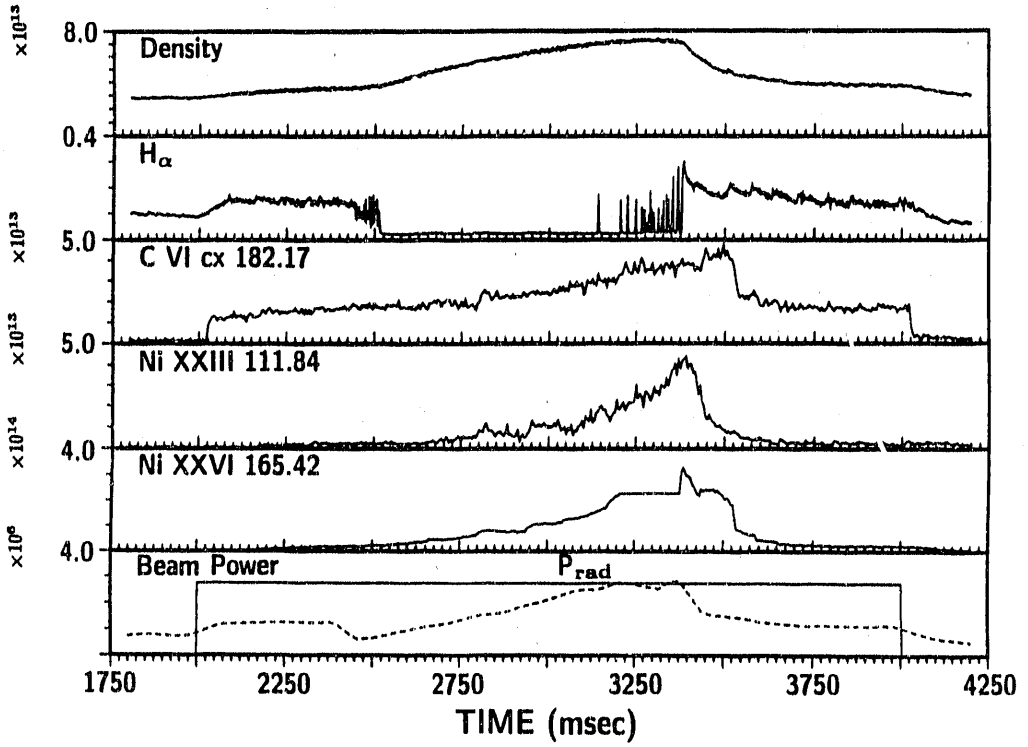

Fig. 2.4-3. Discharge No. 73313 exhibits impurity accumulation and high radiated power during a standard quiescent H–mode even after boronization.

Beginning with the second boronization, a second B_2D_6 gas injector was added to the vessel, approximately 180° from the first. For the third, a pulsed glow technique was implemented. Because laboratory experiments at KFA Jülich have indicated that the glow discharge breaks up the B_2D_6 into extremely reactive radicals that strongly adhere to the wall on the first collision, it was felt that uniformity might be improved if the glow were turned off for a sufficient time to allow the B_2D_6 to fill the volume of the vessel, then the glow would be turned on for a sufficient time to deposit that B_2D_6. Based on calculations, a 33% duty cycle with a 3 s period was implemented. At the present time, the only indicator of deposition uniformity is the plasma behavior, which is usually complicated to interpret.

However, the general feeling is that the performance after the last two boronizations was somewhat superior to the previous coatings.

Bromine (Br) was introduced accidentally into the vessel during 1990 and has resisted clean-up efforts. It is normally apparent only for a few run days after a high temperature bakeout. However, after the third boronization, the Br levels were quite high. In order to reduce the Bromine content, the post-boronization high temperature bake of the vessel was eliminated after subsequent boronizations (Nos. 4 and 5). The result was as anticipated; Br lines were quite low. The original intent of the bakeout was to reduce recycling from deuterium left in the film from the deposition process. However, recycling was observed to be low even without the bake, indicating the efficacy of pure He glow in removing the deuterium from the outer layers of the film.

The behavior of impurities during the quiescent VH–mode is observed to be very different from that observed during standard quiescent H–mode. Shown in Fig. 2.4-4 is discharge 73182, which exhibits a VH–mode phase between 2050 and 2700 ms and a quiescent H–mode between 3150 and about 3600 ms. During the VH–mode phase, the impurity line intensity is low and does not increase throughout the 650 ms duration. However, during the H–mode, the line intensities are observed to increase dramatically, ultimately saturating the Ni signal. The plasma then reverts to a low confinement L–mode. The behavior of impurities during VH–mode will be the subject of experimental work during FY92 operations.

2.4.2. RADIATIVE DIVERTOR

Experiments to reduce the heat load to the divertor by creating a high density, radiating divertor plasma were carried out during FY91. As expected, the experiments also had a significant effect on the impurity content of the plasma. The injection of neutral deuterium D_2 gas into ELMing H–mode plasmas has reduced both nickel and low-Z impurities in the core plasma. Figure 2.4-5 demonstrates such reductions by comparing a D_2 injection case (solid) with a noninjection reference case (dashed). The roughly 30% decrease in the effective charge of the plasma Z_{eff} during D_2 injection is not merely due to dilution. The Ni influx into the core plasma and the concentrations of oxygen and carbon are significantly lower in the injection case. As typical of ELMing H–mode, the increase in the radiated power is mainly in the divertor region; increased radiation in the core occurs only after reversion to L–mode at 3100 ms.

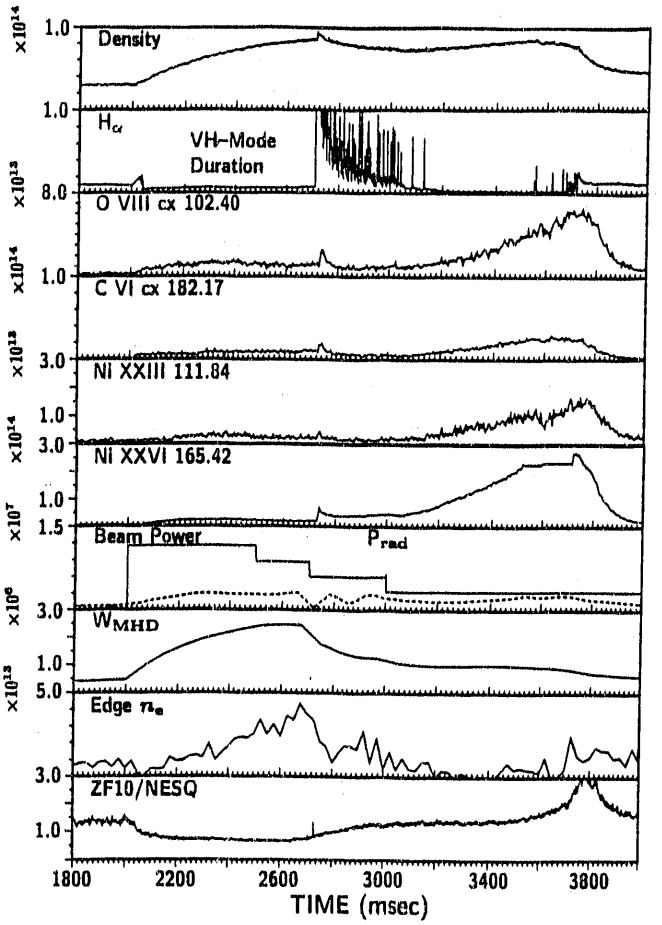

Fig. 2.4-4. Shot No. 73182 exhibits a VH-mode period between 2050 and 2700 ms and a standard quiescent H-mode between 3130 and about 3600 ms. During the VH period, impurity line radiation and radiated power do not increase.

Reduction in impurities in the core plasma during D_2 injection were especially pronounced prior to the first boronization. After boronization, the reduction of impurities was considerably less striking, since impurities were already very low.

2.4.3. SURVEY, POOR RESOLUTION, EXTENDED DOMAIN (SPRED) SPECTROMETER SYSTEM IMPROVEMENTS

SPRED Edge Scanner: A device which allows the SPRED to obtain spatially resolved views across the DIII-D midplane was built, installed, and employed during operations. The system has a potential uninverted spatial resolution of 1 cm at the point of tangency in the plasma, and a sweep rate of up to 10 Hz, covering the inner and outer thirds of the plasma. These capabilities will allow a much improved determination of

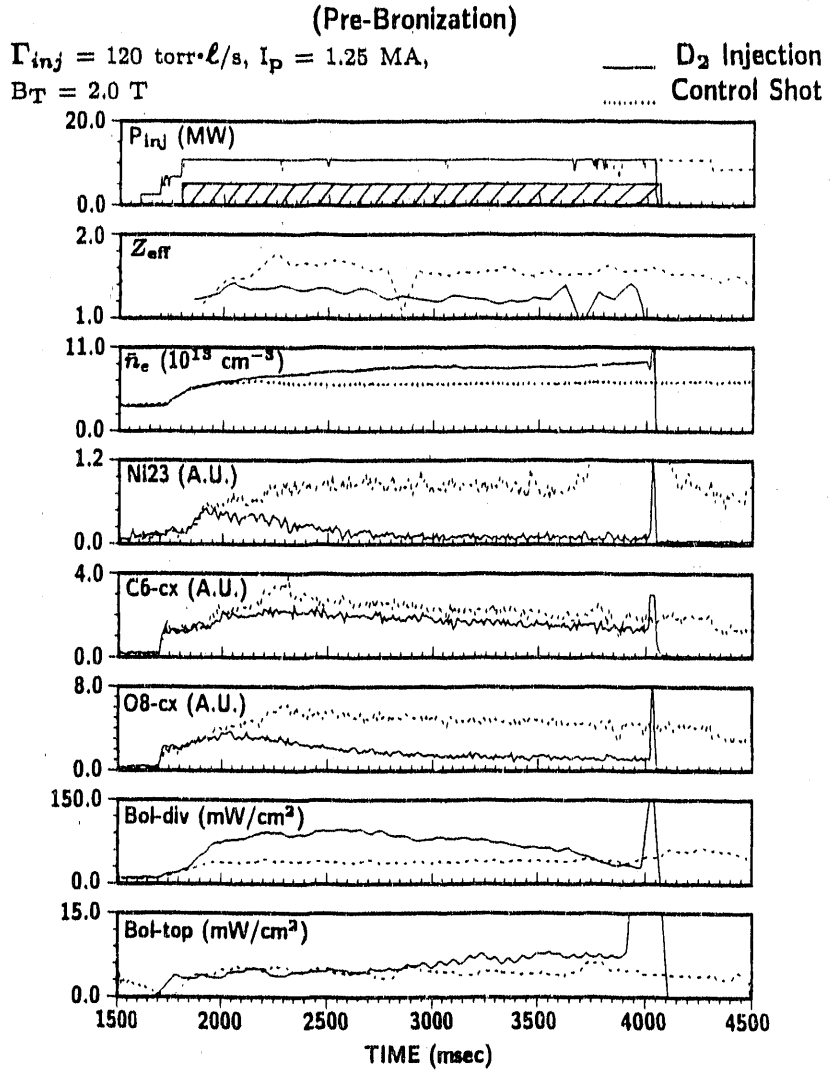

Fig. 2.4-5. Comparison of discharges with (solid line) and without (dashed line) high D_2 gas injection. Both discharges are lower single-null diverted prior to boronization.

impurity transport, and using line brightness ratio techniques, will allow a comparison of electron density and temperature at the inner and outer midplane edge plasma.

Initial results were encouraging in both the transport and plasma diagnostic respects. Figures 2.4-6(a) and 2.4-6(b) show the measured and modeled time histories of selected argon (Ar) lines during a discharge in which argon was injected and the SPRED view was swept at 2 Hz. The adjacent argon ArVII and ArVIII states, which are only 19 eV apart in ionization energy, have different spatial signatures, indicating the potential for detailed impurity transport modeling. Already, significant differences with the multiple impurity

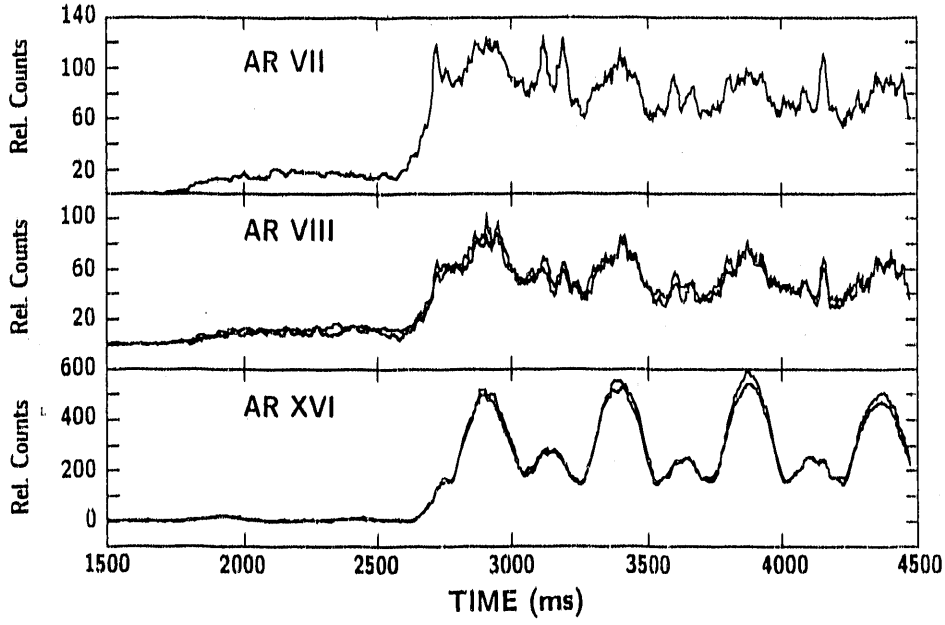

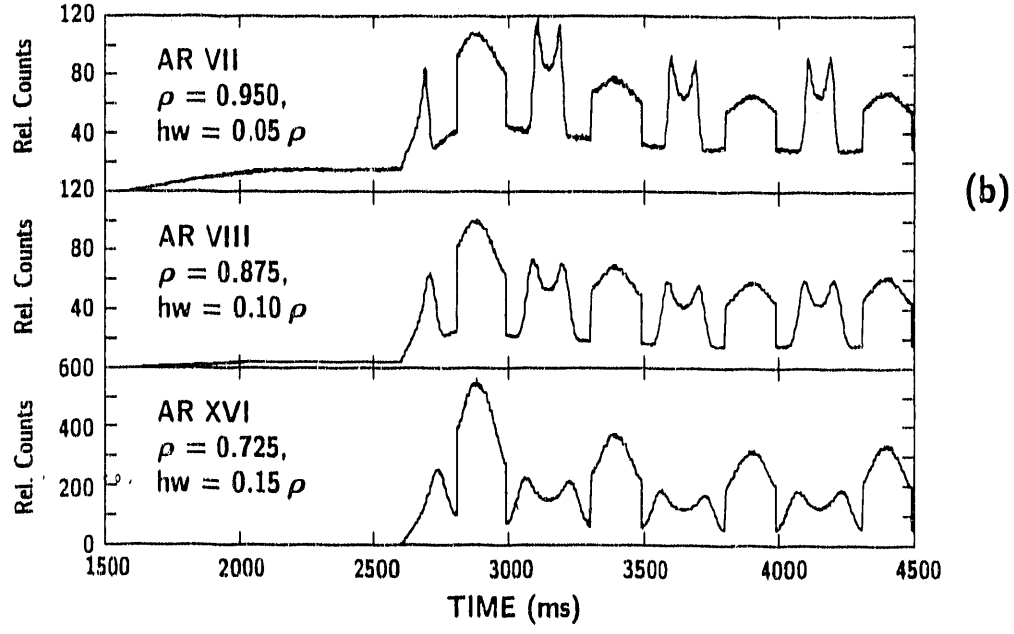

Fig. 2.4-6. Intensities of selected Argon impurity lines from DIII–D (a) observed with the SPRED Edge Scanning System, and (b) modeled using the MIST code. A scan frequency of 2 Hz was used. Sharp peaks are seen as the scan passes through the narrow radiation shell near the centerpost for the low charge states. The model used measured n_e and T_e profiles obtained from Thomson scattering.

species transport (MIST) code predictions have been observed and will be investigated further.

2.4.4. MULTILAYER MIRROR SPECTROMETER DEVELOPMENT

As part of a new collaboration between General Atomics and Johns Hopkins University, a prototype soft X–ray scanning monochromator was mounted on DIII–D from May-Sept. This high throughput spectroscopic diagnostic uses a variety of flat multilayer mirrors (MLMs) in a near normal configuration to cover the region from 10-170Å with a resolution 0.25-10.8Å, depending upon the particular MLM. Below 50Å, where the monochromator is photometrically calibrated, the spectrum is dominated by hydrogen HI-like and helium HeI-like carbon and boron. Below 120Å, the resolution of the MLM blends the L–shell emission from bromine and nickel. However, current analysis at Hopkins will show that with the appropriate software (developed at General Atomics and modified at Hopkins), it is possible to deconvolute this type of MLM-based spectrum into a resolved spectrum.

During a series of radio frequency (rf) experiments, the ratio of Lyman-α/Balmer-α [33.7Å/182Å (measured by SPRED)] in HI-like carbon was monitored. This ratio is currently being modeled with the MIST impurity transport code in an attempt to determine the effects of the rf pulse on the transport of carbon. This is directly related to the next phase of the collaboration, scheduled to begin next year, of mounting a soft X–ray MLM-based diagnostic capable of performing a multichordal measurement of HI-like carbon or boron across the lower divertor floor.

2.5. THEORY AND MODELING WORK

2.5.1. TWO-DIMENSIONAL DIVERTOR TRANSPORT CODE

Work began on the development a two-dimensional divertor transport code. This involves solving a general nonlinear elliptic partial differential equation in two dimensions using a finite element multigrid method. In order to simplify the problem, the ion heat equation was considered initially by itself. The solution domain is defined by flux surfaces just inside and just outside the separatrix. For simplicity, the magnetic field is calculated from seven discrete current loops. The results of the calculation show that the constant temperature contours closely follow the flux surfaces except near the X–point, where they depart significantly from them. With the ion grad-B drift toward the X–point, in a single-null configuration, the peak in the heat flux to the divertor plate shifts strongly to the

inboard side, while with the opposite direction of the toroidal magnetic field, it shifts strongly to the outboard side. The poloidal variation of temperature on the inner boundary was found to be significant, casting doubt on the use of a constant-temperature boundary condition.

2.5.2. ONE-DIMENSIONAL SCRAPEOFF LAYER TRANSPORT MODEL

A one-dimensional computer model of the transport in the SOL of a diverted tokamak was developed, and used to simulate the application of a bias voltage to one of the neutralizer plates intercepting the separatrix. When the divertor plates are grounded, an asymmetry of the temperature, energy flux and ion flux at the target plates is produced by the $\vec{E} \times \vec{B}$ drift. Application of a bias to one target plate can substantially change these asymmetries, as well as the ion impact energy, the current and the total ion flux to the divertors. The scaling of SOL parameters and divertor heat flux with toroidal field and input power was studied using this computer model. A weaker dependence of the divertor heat flux on the scrape-off power was found than previously expected.

SECTION 3

RADIO FREQUENCY HEATING AND CURRENT DRIVE

3. RADIO FREQUENCY HEATING AND CURRENT DRIVE

3.1. RADIO FREQUENCY PROGRAM OVERVIEW

Radio frequency (rf) waves and high frequency microwaves are expected to provide efficient methods of heating the plasma, driving large toroidal currents needed to confine and stabilize the discharge, and controlling the radial current profile which may result in improved plasma performance. The rf heating and current drive program on DIII–D calls for the aggressive development of advanced rf systems suitable for assessing the complex technical standards which will be encountered during high power, long pulse (quasi-steady state) fusion reactor operations. These systems, when fully integrated into the DIII–D experiment, will be used to demonstrate the feasibility of maintaining noninductively driven currents of up to 2 MA for periods of order 10 seconds in discharges with 5% beta (the ratio of the plasma pressure to the magnetic pressure). Interim rf program activities will also support a number of basic physics studies designed to better understand the influence of the current density profile on: improving the energy confinement, increasing the beta limit, transient effects associated with high frequency magnetohydrodynamic (MHD) mode activity, so-called second stability operations, and very high confinement VH–mode discharges.

RF heating and current drive in the 30–60 MHz frequency range, using the fast (magnetosonic) wave (FW), was a key component of the FY91 rf experimental activity on DIII-D. Fast wave current drive (FWCD) is of particular importance because FWs have good penetration to the plasma core at the plasma densities required in fusion reactors (as opposed to lower hybrid waves) with good current drive efficiency. Since the FW is poorly absorbed by the electrons unless their temperature is high, the development of advanced electron cyclotron heating (ECH) methods at 60 GHz and 110 GHz is viewed as an essential part of the FWCD program. ECH has also been used to study the transport properties in DIII–D. The results from experiments using off-axis ECH have revealed the presence of an inward heat flow; this result presents a serious challenge to the usual models of transport in tokamaks.

The principal rf program results obtained in FY91 included:

- The demonstration of strong heating during 32 MHz hydrogen minority heating in deuterium majority plasmas and verification of good launching efficiencies for FWs.
- The development of engineering techniques required for efficiently phasing the rf antennas to carry out high power FWCD experiments.
- Production for the first time anywhere of a high confinement H-mode using FWs in the electron heating mode.
- The first experiments on FWCD with up to 140 kA of noninductive current in a 400 kA discharge.
- The observation of non-diffusive heat transport effects in off-axis ECH experiments and identification of a inward "heat pinch."

3.2. ELECTRON CYCLOTRON HEATING

The DIII-D 60 GHz ECH system continued to be a key tool in performing critical experiments required for understanding and advancing the tokamak concept of magnetic confinement. ECH is a unique heating technology in that the energy is coupled to the electrons in a localized spatial region of the plasma. The location is controlled by adjusting the toroidal magnetic field thereby moving the resonance to the desired location. A series of well planned experiments utilizing this capability revealed clearly an anomalous inward flow of the added electron thermal energy, in contrast to the predictions of standard techniques used to model energy transport in the tokamak. Identification of this "heat pinch" has already stimulated new theoretical activity in the community and resulted in a General Atomics paper which was accepted for publication in the *Physical Review Letters*. An understanding of this unexpected effect will hopefully be the key to unlock the overall puzzle of electron thermal transport, which still remains unexplained.

The versatile ECH system has also been used as an enabling technology for FWCD experiment on DIII-D. ECH is used to heat the electrons to temperatures of or greater than 2 keV in order to provide the necessary coupling to the 60 MHz fast magnetosonic wave launched with the DIII-D Ion Cyclotron Range of Frequency (ICRF) system. The FWCD experiments were successful in generating up to 140 kA of noninductive current.

Extended ECH capability will become available with the completion of the 110 GHz system development presently underway. Progress on this system is described in Section 6.3.

3.2.1. HEAT PINCH

Transport of energy and particles across magnetic flux surfaces in tokamaks has been known for many years to be anomalously large when compared with theoretical predictions based upon particle collisions. Models attempting to explain this transport normally assume that the time evolution of the temperature, T, of each species in the presence of some form of turbulence is still governed by a fluid-like equation of the form:

$$\frac{3}{2}\frac{\delta n \mathrm{T}}{\delta t} + \nabla \cdot \vec{q} = Q \quad ,$$

where $\vec{q}$ is the heat flux. The heat sources and sinks are combined into Q. In the diffusive model, the heat flux $\vec{q}$ is assumed to be proportional to the gradient in T (∇ T) and the proportionality constant is the thermal conductivity (κ). The thermal diffusivity (χ) is related to κ by $\kappa = n\chi$ where n is the species density. The diffusivity could be a function of T and ∇ T, which makes the equation nonlinear, and it could also be a function of n and the gradient in n (∇n), which couples the density and temperature evolution.

Experiments utilizing localized heat deposition with ECH have shown that this equation coupled with any of the above diffusion models cannot explain the observations. A term must be added which causes an inward energy transport for the electrons, up the density gradient. In these studies, the DIII–D ECH system was configured to launch microwaves from the high magnetic field side of the plasma at 60 GHz. The total ECH power launched was $\leq$1.25 MW, far in excess of the total ohmic heating power in these discharges. Experimental electron temperature profile shown in Fig. 3.2-1 provides immediate evidence of transport not in accord with purely diffusive models. The temperature profile should be flat inside of the heating location (Q_{ECH}) if the off-axis heating is the only power input. In this case, calculations indicate that more than 80% of the input power is deposited outside of $\rho = 0.5$ (ρ is the radial magnetic coordinate), yet the electron temperature profile remains peaked. Measurements of the soft X–ray emission at various ρ confirm the power is deposited locally, as shown, in agreement with the absorption pattern calculated by the TORAY ray tracing code.

A power balance analysis is performed with the ONETWO tokamak transport code, using measured plasma density and temperature profiles, and the experimental magnetic surface topology. This analysis shows that in order to maintain the measured electron temperature profile shown in Fig. 3.2-1, heat must be transported inward as shown by the negative electron heat flux (q_e), in Fig. 3.2-2. A dramatic reversal of the electron

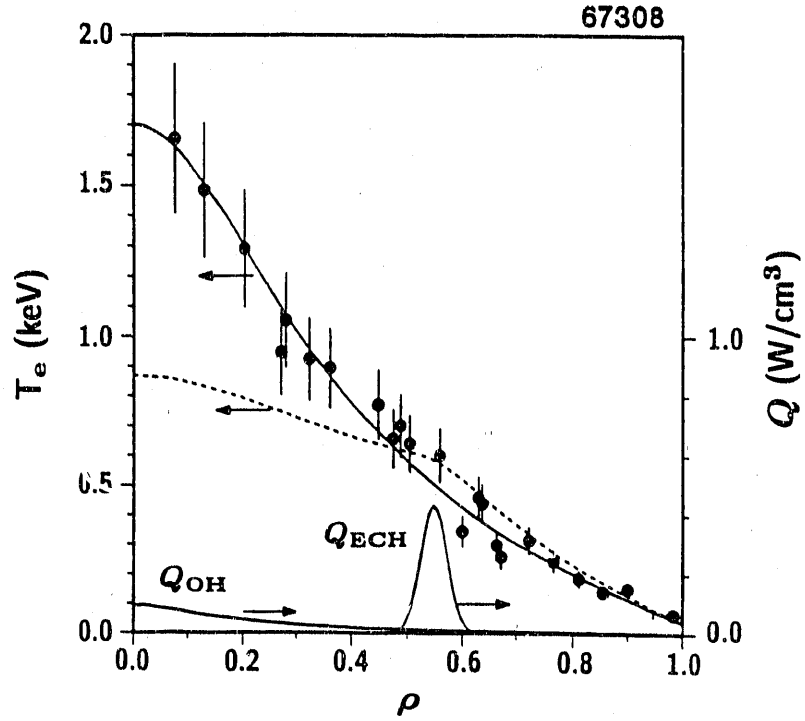

Fig. 3.2-1. Experimental electron temperature profile as a function of the radial magnetic coordinate ρ measured by electron cyclotron emission and Thomson scattering. The plasma parameters are $\bar{n} = 2.2 \times 10^{19}$ m^{-3}, $B_T = 1.7$ T, plasma current I = 600 kA, and $P_{ECH} = 1.25$ MW. The calculated power deposition profile for the ECH is also shown. The dashed curve is a simulation based upon a diffusive model utilizing measured diffusion coefficients from perturbation experiments.

heat flux occurs at the ECH resonance location (ρ_{res}) as indicated on the figure. (This location moves as the location of heat deposition is moved.) No corresponding change in the ion heat flux is seen. To our knowledge, this is the first measurement of radial heat flux reversal in a tokamak plasma. Thus, there must be a transport mechanism which is effective at transporting energy to regions of higher temperatures. This mechanism is clearly not diffusive, since diffusion would act to equilibrate the temperature everywhere.

Another way to display the heat pinch effect is to solve the standard transport equations given the ECH and ohmic heating power deposition profiles as source terms. This results in the dotted electron temperature curve shown in Fig. 3.2-1, clearly unable to explain the measured central temperature. For this calculation, a measured diffusive thermal transport coefficient was used. (This measurement was from another experiment

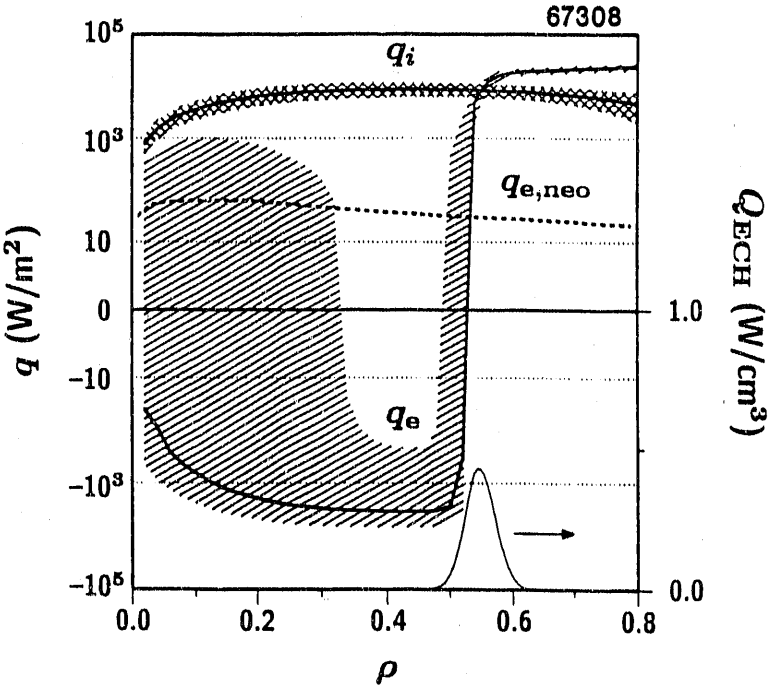

Fig. 3.2-2. Power balance calculations of the electron and ion heat flux and the neoclassical electron heat flux as a function of ρ for the same discharge as in Fig. 3.2-1. The ECH deposition profile is shown again for reference.

in which ECH pulses were modulated temporally, and the local diffusion of the heat away from the deposition point was measured.)

At present, there is no theoretical explanation of this heat pinch. The data obtained during these experiments place severe constraints on possible theoretical explanations. Net inward transport of energy cannot be explained by purely diffusive models even with χ as a function of T_e or ∇T_e. Models with critical temperature gradients are also excluded because these models still have neoclassical conduction as a minimum outward transport. Calculations of drift-wave transport including density gradient driven heat flux can give net inward flow of the electron energy, but a theory of this type which depends only on local variables cannot explain the sensitivity of the flux reversal to the heating location rather than the local fluid variables. Either there is a nonlocal transport mechanism at work in these plasmas or the appropriate local variables have yet to be identified.

3.2.2. ELECTRON CYCLOTRON HEATING FOR FAST WAVE CURRENT DRIVE

The 60 GHz ECH system was used in the FWCD experiments (Section 3.3) to raise the electron temperature to provide the necessary target conditions for the FW. ECH again was launched from the inside of the torus in the X–mode of polarization. Power levels in the range of 0.6 to 1 MW were incident on the plasma. Results from these experiments are described in the next section.

3.3. FAST WAVE HEATING AND CURRENT DRIVE

FWCD has been selected as a backup technique for driving current noninductively near the center of the plasma of the International Thermonuclear Experimental Reactor (ITER) tokamak [1]. FWs have the advantages of good penetration to the plasma core and high efficiency of current drive. However, FWCD has not yet been verified, and this is one objective of the present DIII–D experiments.

FWs may be damped directly by the electrons through the processes of electron Landau damping and transit-time magnetic pumping (TTMP). These damping processes are rather weak, but they increase strongly as the electron temperature is raised. This allows the waves to penetrate to and be absorbed near the center, even in a reactor-like plasma of very high electron temperature (unlike the much more strongly damped lower hybrid wave, which is absorbed near the edge under reactor-like conditions). This behavior makes FWs highly suitable for reactor applications, but it makes studies of FW absorption difficult in plasmas with low electron temperature. We take advantage of the ECH system of DIII–D to raise the electron temperature (T_e) and increase the damping strength.

A long-range goal of the DIII–D program is the improvement of the tokamak concept. One possible way to improve the confinement of energy or the beta limit is to optimize the current density profile. Peaking of the current density profile $j(r)$ (as measured by increasing internal inductance ℓ_i) has been shown to accomplish both of the above objectives in near-circular DIII–D discharges, where the increase in ℓ_i is accomplished transiently by ramping the plasma current [2]. This may also be accomplished in steady-state through noninductive current drive techniques like FWCD. Therefore, in order to carry out its long-term mission an intermediate objective for the DIII–D program is a demonstration of full noninductive current drive with good confinement in a high beta divertor plasma.

Modeling of the DIII–D plasma using the ONETWO transport code shows that full noninductive current drive may be obtained under a variety of conditions using a

combination of FWCD, electron cyclotron current drive (ECCD), and a bootstrap current [3]. Here, the ECH plays a dual role of raising T_e so that absorption of the FW improves as well as contributing to the noninductive current drive and to the plasma pressure which drives the bootstrap current.

The FY91 experiments represent the first steps of the FWCD program. The experiments are meant to demonstrate the basic physics of the FW interaction with electrons and to advance the numerical models for FW heating and current drive by providing a body of experimental data for comparison. At the low rf powers involved at this stage of the program, large noninductive currents are not expected.

The DIII–D tokamak is well suited to a study of FWCD. The FW antenna occupies a pair of midplane ports on the outer wall of the vacuum vessel, while the ECH antennas are located on the inboard wall 13 cm above the midplane of the vessel. The FW antenna shown in Fig. 3.3-1 has four independently phased current carrying straps spaced 22 cm between centers. The straps are 11 cm wide and 45 cm high. The antenna was made at Oak Ridge National Laboratory (ORNL). The transmission line, tuning, and phasing scheme is described in Ref. [4]. The antenna is driven by a rf source with power up to 2 MW and frequency of 30 to 60 MHz. (This is the same rf source and transmission system used in the FY90 ion Bernstein wave heating experiments on DIII–D which had a different ORNL antenna.) A key to the technical success of these experiments has been the General Atomics engineering development of the tuning and phasing scheme coupled with the hardware support by ORNL.

Experiments on minority heating were performed at 32 MHz, and all FWCD experiments used 60 MHz. At 60 MHz and with the phasing between straps set to 180° ("π-phasing") the power spectrum is symmetric (equal powers are launched in both toroidal directions), and the major peaks are at $n_{||} = \pm 11$. ($n_{||}$ is the ratio of the speed of light to the phase velocity of the wave in the toroidal direction, so that smaller $n_{||}$ the faster the wave.) With $n_{||} \simeq 11$ the wave is resonant with electrons of about 2 keV of energy. For FWCD, the phasing between straps is set to 90° ("$\pi/2$ phasing") to generate a toroidally asymmetric spectrum to preferentially drive current in one direction. The forward spectrum peaks at $n_{||} \simeq 5.5$ which is resonant with $\simeq$8 keV electrons. Accurate numerical models are being developed to understand how the antenna spectrum is transformed into the wave spectrum launched in the plasma.

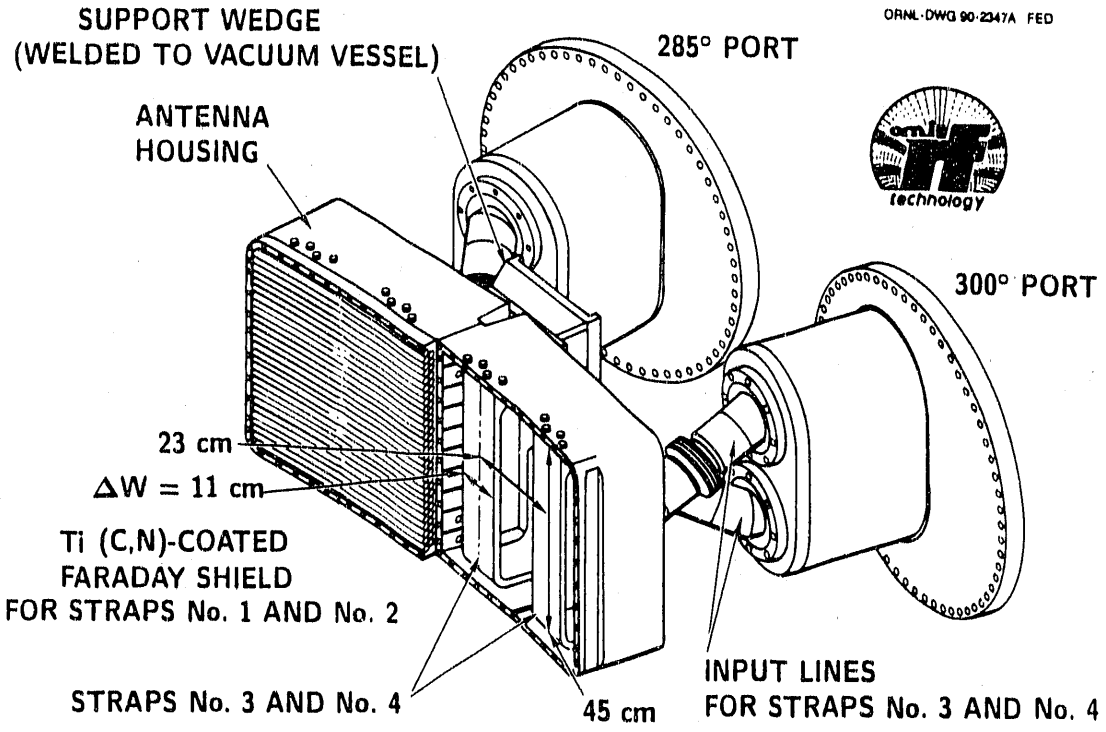

Fig. 3.3-1. Fast wave current drive antenna for DIII-D (30-60 MHz, 2 MW, 2 s, four straps with arbitrary phasing).

3.3.1. FUNDAMENTAL MINORITY ION HEATING

The first experiments done using the FWCD antenna were aimed at testing the effectiveness of the antenna at launching the FW [5]. One way to do that is to try heating a hydrogen minority in a deuterium majority plasma, thereby making contact with a very large body of experimental heating results from other tokamaks. The effectiveness of the antenna can be estimated from the experimental heating efficiency. The experiments were done at a frequency of 32 MHz, which places the fundamental cyclotron frequency of hydrogen at the center of the plasma for a toroidal field of 2.1 tesla.

Under these conditions, strong plasma heating was found, as shown in Fig. 3.3-2. In this figure, hydrogen minority heating in a deuterium plasma is compared with neutral beam injection heating at the same 1 MW power level. Figure 3.3-2 shows that the increase in stored energy determined from MHD analysis is very nearly the same for the two heating methods. When the energy confinement time with FW minority using heating π-phasing is compared to that expected from the ITER low confinement L-mode scaling law, good agreement is found, indicating that the antenna is in fact launching the FW

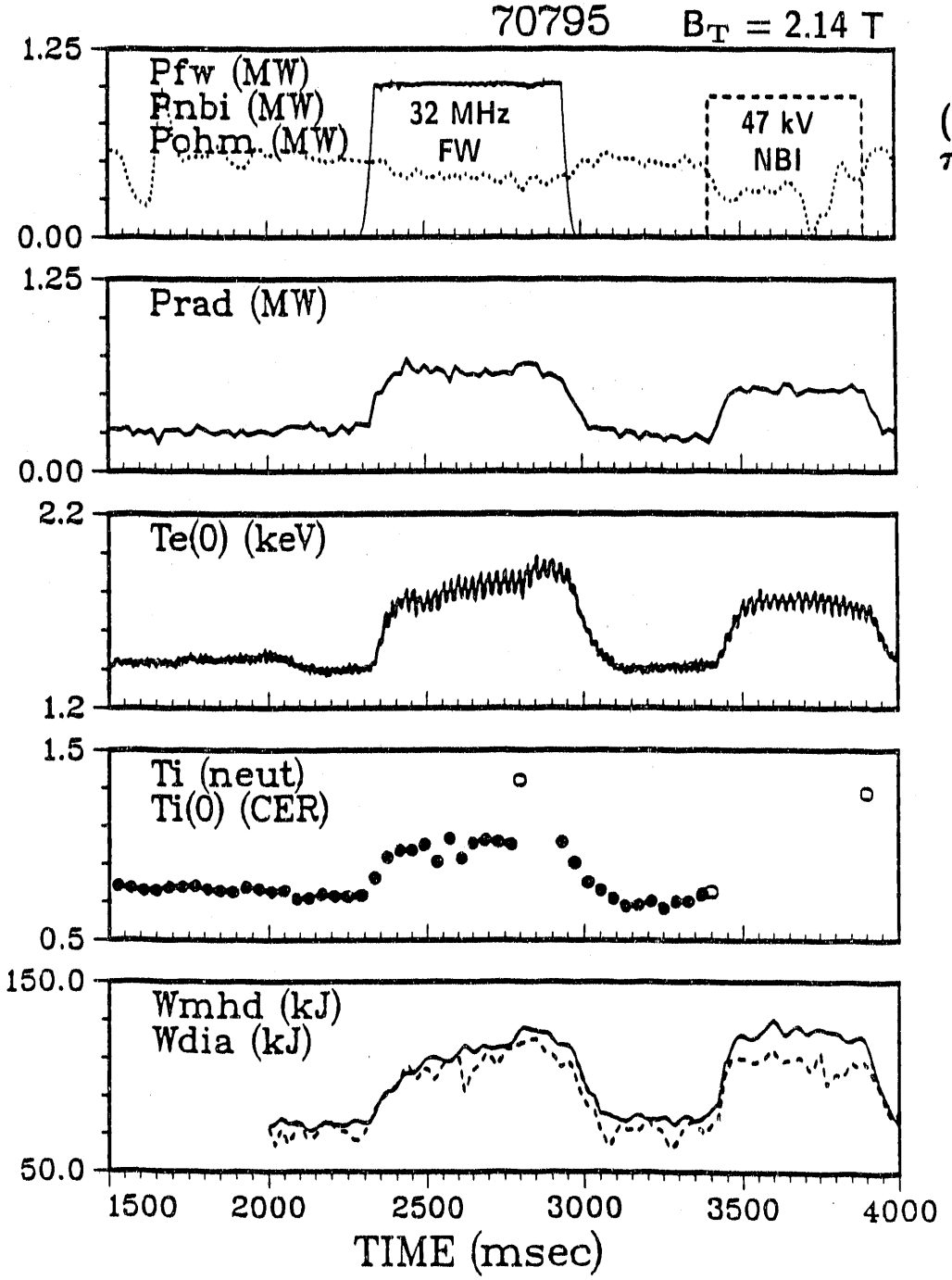

Fig. 3.3-2. Example of minority plasma heating for a deuterium plasma with a 2% hydrogen minority. The magnetic field is 2.14 T, which places the fundamental cyclotron frequency for hydrogen near the magnetic axis, for the applied frequency of 32 MHz. The plasma density is 2.0×10^{19} m^{-3}, and the plasma current is 0.7 MA. The antenna is phased (0, π, 0, π).

with high efficiency, and that most of the FW power is propagating into the plasma and being absorbed.

3.3.2. INTERACTION OF FAST WAVES WITH ELECTRONS

In order to drive current efficiently with the FW, the wave must interact with electrons much more strongly than with any other sink, such as ions or the plasma boundary. The first tests of electron damping were done using symmetric π-phasing of the antenna straps to test the theory of single pass damping [6]. Two of the key theoretical parameters determining the strength of this damping are the ratio of the wave parallel phase velocity to the electron thermal velocity, and the strength of the equilibrium magnetic field. Both of these parameters can be controlled experimentally.

Strong FW absorption as evidenced by plasma heating was found during application of symmetrically launched FWs. Figure 3.3-3 shows the increase in electron temperature, ion temperature, and plasma stored energy for two pulses of FW heating. The stored energy increases to 200 kJ with application of 1.05 MW, for a gross energy confinement time of 0.13 s. The fractional radiated power is about 0.4 for both the ohmic and the FW phases of the discharge. The electron heating tends to be peaked near the plasma center.

Analysis of the discharges with modulated FW power for determination of the heating profile shows that the profile is strongly peaked near the center of the plasma, in agreement with results from a full wave code.

As a final test of FW electron heating, the high confinement H–mode was obtained with FW electron heating alone. Figure 3.3-4 shows a case with the toroidal magnetic field $B_T = 1$ tesla with about 0.75 MW of FW power. At 2850 msec, the plasma goes into H–mode, as signaled by the drop in the deuterium D_α recycling emission and the rise in density and stored plasma energy. The H–mode has a relatively high amount of edge localized mode (ELM) activity. The transition power is somewhat below the observed scaling for threshold power for neutral injection or ECH, and after the transition the FW power drops further due to the change in the density profile near the edge which reduces the coupling. Because of the ELMs and the proximity of the heating power to the threshold power, the increase in energy confinement time compared to the low confinement L–mode is only 60%. Attainment of the H–mode is often viewed as a stringent test of a heating technique since even a small introduction of impurities is usually enough to suppress the H–mode. Boronization of the DIII–D vacuum vessel helps greatly in suppressing the introduction of impurities, especially high-Z metallic impurities.

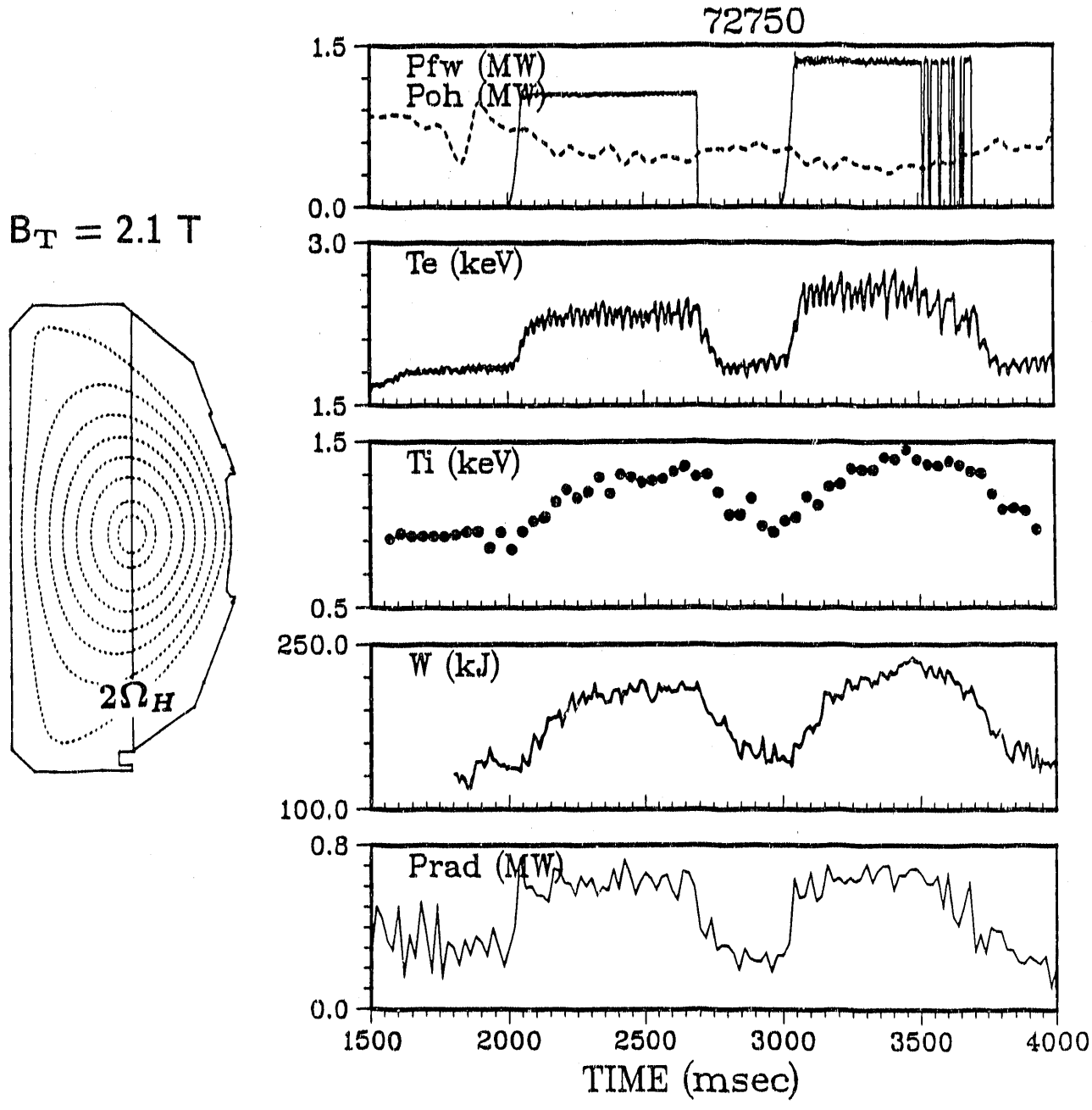

Fig. 3.3-3. Example of electron heating for a deuterium plasma. The toroidal field is 2.0 T and the density is 2×10^{19} m^{-3}. The hydrogen minority fraction is less than 3%. The antenna phasing is (0, π, 0, π) and the frequency is 60 MHz.

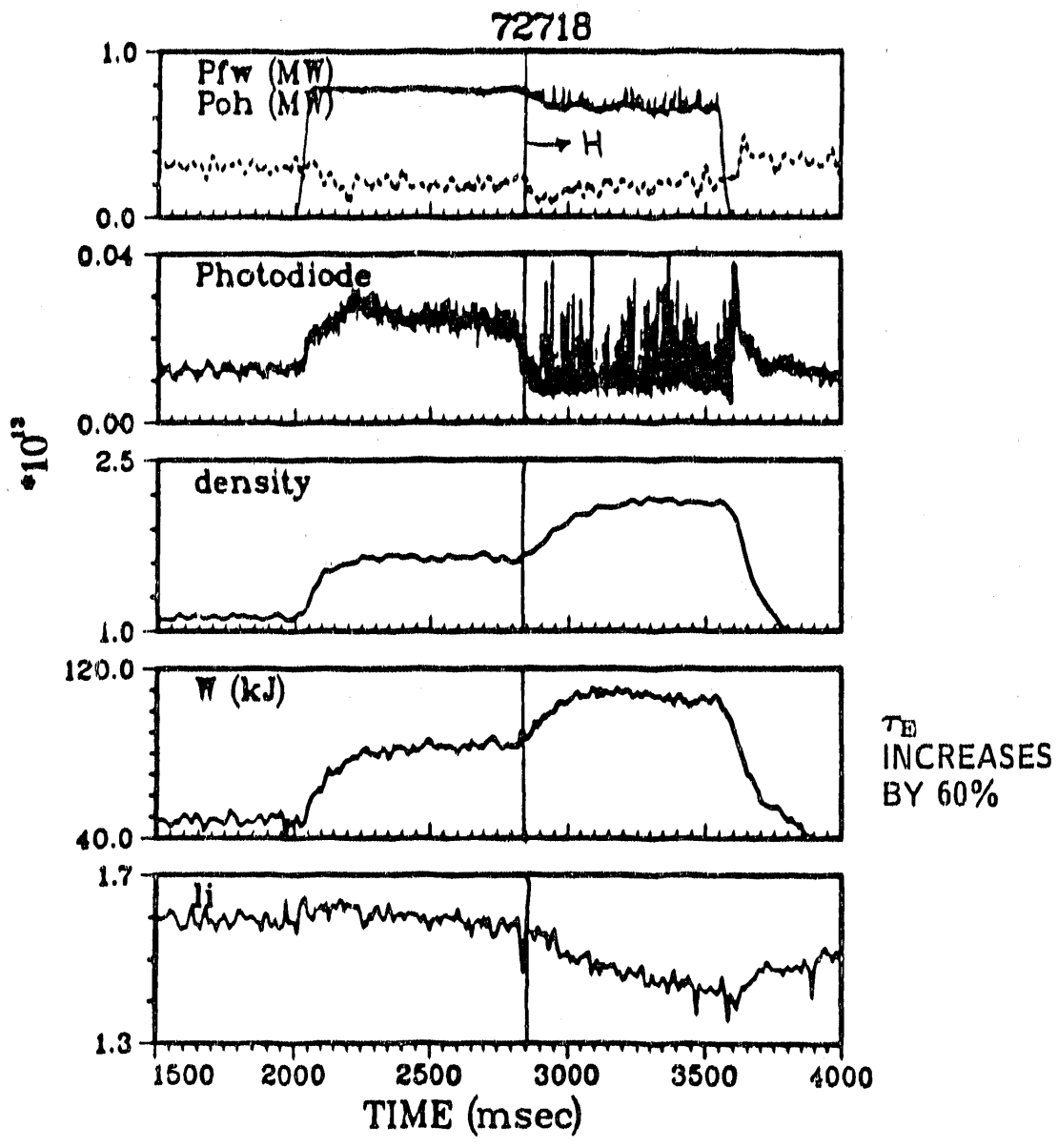

Fig. 3.3-4. Data from a discharge which enters the H–mode at 2860 msec. The toroidal field is 1 T and the plasma current is 0.5 MA.

3.3.3. FAST WAVE CURRENT DRIVE

A series of FW experiments with $\pi/2$ antenna phasing used for producing a strongly directional wave spectrum demonstrated for the first time that noninductive FWCD could be attained with a properly phased antenna module. FWCD was inferred from a comparison of the observed plasma resistance (V/I_p) with that calculated from the profiles of electron temperature and the effective charge (Z_{eff}), assuming neoclassical resistivity.

When FW power is applied, electron heating and a loop voltage drop is observed. This is the same technique used for ECCD experiments on DIII–D [7]. Analyses performed in this manner find driven currents of up to 140 kA, out of 400 kA. However, reversal of the direction of the launched wave from the co-current direction to the counter-current direction has little effect on the driven current determined in this manner.

Figure 3.3-5 shows a discharge with FWs applied with co-current drive at a power level of 1.2 MW. The toroidal magnetic field is 1 tesla and the plasma current is 0.4 MA. A preheating pulse of ECH at 0.6 MW overlaps the beginning of the FW pulse. The voltage at the surface of the plasma, Fig. 3.3-5(b), is determined using the equilibrium fitting code EFIT code to subtract the effects of changing major radius and changing internal inductance. The central electron temperature is found from electron cyclotron emission, Fig. 3.3-5(c). It rises to about 2 keV prior to the FW, then 3 keV during the FW heating. The density, Fig. 3.3-5(d), also rise during the FW heating, which moderates the increase in electron temperature.

Analysis of the loop voltage predicted by neoclassical resistivity during the ohmic phase at 2100 msec [dashed line in Fig. 3.3-5(b)] shows excellent agreement with the observed loop voltage. Similar analysis during ECH + FWCD at 2450 msec [dotted line in Fig. 3.3-5(b)] and during FWCD alone at 2900 msec [solid line in Fig. 3.3-5(b)] shows significant discrepancies between the predicted and the observed loop voltages. These discrepancies can be interpreted as current drive, about 140 kA out of a total current of 400 kA. There is an additional current calculated to be 20 kA due to the neoclassical bootstrap current. Analysis of these discharges is continuing, but it appears that the discrepancy between the measured and the calculated loop voltages is well outside the error in the measurements.

The direction of the wave spectrum may be changed by changing the phasing of the antenna straps in order to drive counter-current. When this is done and the experiment illustrated in Fig. 3.3-5 is repeated, the result is the same: the measured loop voltage is less than the calculated loop voltage by about the same amount. Further analysis, including modeling with a Fokker-Planck code, will be done to understand these results.

References for Section 3.3.

[1] "ITER Conceptual Design Report," ITER Documentation Series No. 18 (IAEA, Vienna, 1991).

[2] Ferron, J.R., *et al.*, *Bull. Amer. Phys. Soc.* **36** (1991) 2324.

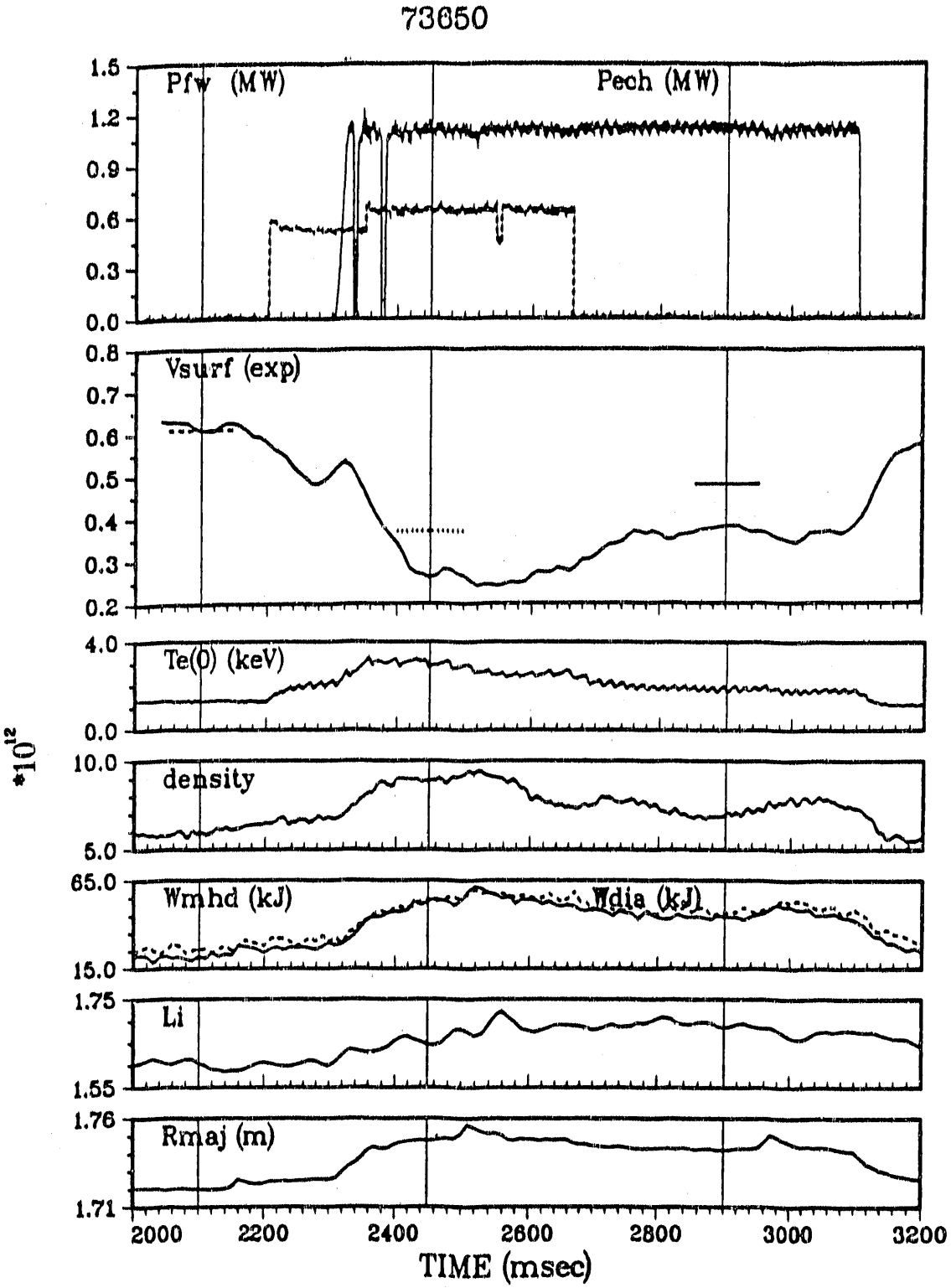

Fig. 3.3-5. Data from a discharge with (0, $\pi/2$, π, $3\pi/2$) phasing of the FW antenna. The toroidal field is 1 T, the plasma current is 0.4 MA, the configuration is full-sized divertor.

[3] Luce, T.C., *et al.*, "Modeling of Fast Wave Current Drive Experiments on DIII–D," General Atomic Report GA-A20691 (1991); to be published in Proc. 9th Topical Conf. on Applications of Radio-Frequency Power to Tokamaks, Charleston, 1991.

[4] Mayberry, M., *et al.*, "Fast Wave Current Drive Antenna Performance on DIII–D," General Atomics Report GA-A20694 (1991); to be published in Proc. 9th Topical Conf. on Applications of Radio-Frequency Power to Tokamaks, Charleston, 1991; Pinsker, R.I., *et al.*, "30-60 MHz FWCD System on DIII–D: Power Division, Phase Control and Tuning for a Four Element Antenna Array," to be published in Proc. 14th IEEE Symp. on Fusion Engineering, San Diego, 1991.

[5] Petty, C., "Fundamental and Second Harmonic Hydrogen Fast-Wave Heating on DIII–D," General Atomics Report GA-A20693 (1991); to be published in Proc. 9th Topical Conf. on Applications of Radio-Frequency Power to Tokamaks, Charleston, 1991.

[6] Porkolab, M., to be published in Proc. 9th Topical Conf. on Applications of Radio-Frequency Power to Tokamaks, Charleston, 1991.

[7] James, R., *et al.*, Proc. 17th EPS Conf. on Controlled Fusion and Plasma Heating, Amsterdam, 1990.

SECTION 4

CORE PHYSICS

4. CORE PHYSICS

4.1. CORE PHYSICS PROGRAM OVERVIEW

The core physics research program includes activities related to high beta (the ratio of plasma pressure to magnetic pressure) stability and confinement, to producing scaling information for future machine designs, and to providing a basic understanding in several areas of plasma transport research. High confinement H–mode studies continued to contribute to the International Thermonuclear Experimental Reactor (ITER) H–mode database, and a joint effort with the JET team in England has resulted in definitive transport scaling conclusions. Based on direct comparisons of corresponding discharges in DIII–D and JET new results were derived for machine size scaling effects on H–mode confinement properties. Basic studies utilizing the multipulse Thomson laser system and perturbative transport techniques have provided a greater depth of understanding of interior transport processes.

An important new DIII–D experimental result is the identification of Toroidal Alfvén Eigenmodes (TAE) modes destabilized by fast neutral beam ions. This demonstrates that DIII–D is capable of detailed TAE mode studies and because of its ability to operate at high densities with low magnetic fields is particularly well suited to achieve high betas needed for producing energetic super Alfvénic ions with the 20 MW DIII–D neutral beam systems.

State-of-the-art DIII–D plasma control capabilities were utilized to dynamically control the current profile (current ramp) and plasma shape (elongation ramp) in order to study the effect of magnetic shear on beta limits and plasma confinement. These experiments demonstrated the importance of profile control for enhanced confinement and high normalized beta operations envisioned in high performance tokamaks.

The synergysm between wall conditioning and confinement was demonstrated by boronization of the vacuum vessel. In addition to effectively reducing the radiative loss, as predicted, we achieved the very high confinement VH–mode (over H–mode) regime with energy confinement times approaching a factor of 1.8 those found in H–mode. Access to a

second stable edge and an increase of the transport barrier due to enhanced electric field shear are possible candidates responsible for the VH–mode.

Highlights in the Core Physics research area in FY91 include:

- Simultaneously attainment of enhanced plasma confinement and high normalized beta using current profile and plasma shape control.
- The discovery of very high confinement VH–mode after boronization with enhancements of up to 1.8 times JET/DIII–D H–mode scaling and a fusion triple product of 2×10^{20} m^{-3} s keV.
- The identification of high frequency magnetohydrodynamic (MHD) activities on DIII–D as TAE modes driven by super Alfvénic energetic ions. Significant loss of fast particles was observed.
- Very high beta, peaked pressure profile discharges with plasma core in the second stable regime were reproduced with dynamic profile control.
- Dramatic reduction of effective diffusivity and/or the possible existence of a heat pinch have been observed with off-axis ECH and corroborated by off-axis NBI.
- Analysis, with the inclusion of ASDEX data in the JET/DIII–D database, confirmed the strong major radius scaling in H–mode confinement scaling.

These and other significant progress will be discussed this section.

4.2. STABILITY PHYSICS

4.2.1. TOROIDAL ALFVÉN EIGENMODES

Finite toroidicity can substantially modify the continuous Alfvén spectrum, breaking it up by inducing finite gaps with isolated toroidicity-induced Alfvén eigenmodes (TAE) appearing inside the gap. These TAE modes are global in nature and can be destabilized by resonances with energetic particles, alpha particles in a burning plasma or fast beam particles in a beam heated plasma. This instability can result in large radial transport and direct loss of the alpha particles or fast beam particles, giving a much reduce heating efficiency and perhaps a greatly reduced NBI current drive efficiency.

The TAE mode is evaluated experimentally in DIII–D by using fast beam particles to drive the mode unstable. The beam particles simulate alpha particles in a burning plasma. Simple theory requires a particle velocity parallel to the magnetic field ($v_{||}$) to

be approximately equal to the Alfvén wave velocity $v_{\text{Alfvén}}$ for instability. In the DIII–D experiments, comparison of near tangential vs more perpendicular neutral beam injection (NBI) is used to vary $v_{\|}$, and the toroidal field and density are changed to vary $v_{\text{Alfvén}}$. Experimentally, the mode was more easily destabilized by injection of the left neutral beam sources than by the right sources at the same power. This is consistent with identifying the instability as an Alfvén mode, since the left sources create ions with a larger parallel velocity, closer to the Alfvén speed. The mode was also more easily destabilized as $v_{\|}/v_{\text{Alfvén}}$ was increased in a toroidal field scan.

The frequency of the TAE mode in DIII–D is found to vary linearly with toroidal field, as expected from simple theory [1]. More detailed analysis with the GATO stability code shows a good quantitative agreement between the predicted and observed frequencies [2,3]. In addition, the calculated frequency of fast particle destabilized ballooning modes does not agree with the observed frequency of the mode, giving further evidence that the observed modes are TAE modes. The frequency dependence of the mode is shown in Fig. 4.2-1.

The importance of this instability is shown by its strong effect on fast ion confinement. Analysis of the 2.5 MeV neutron emission indicates that as much as 50% of the injected beam power is lost during intense TAE activity. Damage to material surfaces on the outer wall has been correlated with these large fast ion losses. Copper foil activation and silicon diode measurements indicate that confinement of fusion products (1.01 MeV tritons and 0.83 MeV He^3 ions) also deteriorates in the presence of the TAE modes [4]. The loss of the the fast ions by TAE modes is shown in Fig. 4.2-2, where the fast ion beta is shown to saturate with a decrease in the toroidal field and an increase in the TAE mode amplitude.

In order for a global TAE mode to be unstable and cause serious loss of fast particles, a gap in the shear Alfvén continuum must exist over most of the plasma cross section. The location and structure of the gap has been evaluated using two numerical tools: the CONT code and GATO. The CONT code computes the frequencies at which irregular continuum modes exist by solving the corresponding dispersion relation. The CONT code has been modified to evaluate DIII–D equilibria [5]. GATO has been modified to search for the location of the gaps and is used to evaluate the structure of the continuum modes and the TAE modes [6]. We have found several important features of the gap structure. We have found a second order gap from the toroidal coupling of poloidal mode numbers m and $m+2$: the "more usual" TAE mode is from the toroidal coupling of m and $m+1$. Noncircularity introduces additional gaps in the continuum: elongation greatly enlarges

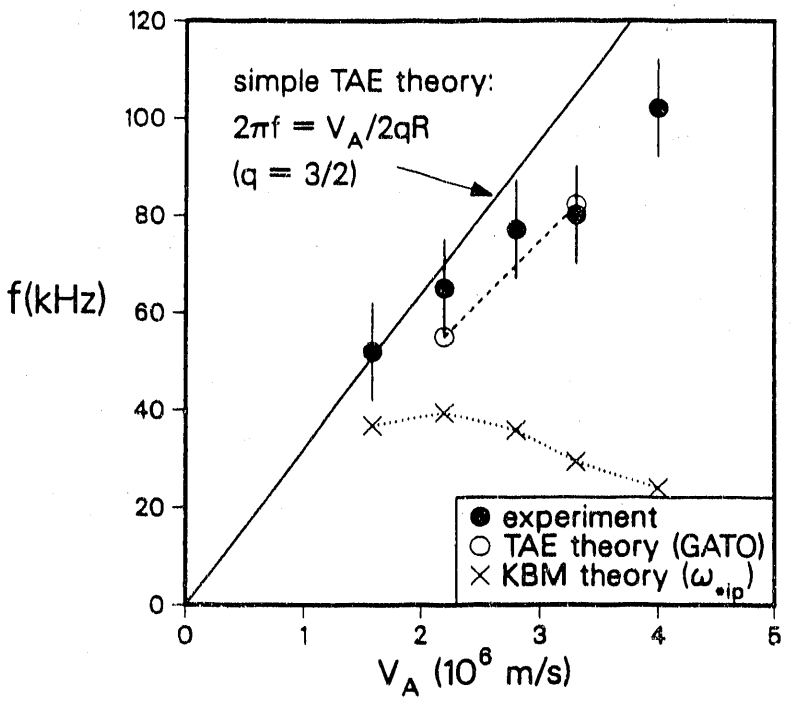

Fig. 4.2-1. Observed frequency is consistent with TAE modes. Observed frequency agrees well with GATO prediction and simple TAE mode theory. Frequency is not consistent with kinetic ballooning modes at $\omega_{*ip} = k_\theta \rho_i v_{ti} d(\ell_n p_i)/dr$. Toroidal field scan at constant I_p = 0.6 MA, $n_e = 3 \times 10^{19}$ m^{-3}, P_{NB} = 5 MW, L-mode.

the gap from coupling of m and $m+2$, and triangularity introduces a gap from the coupling for m and $m+3$. A counterpart to the TAE mode exists in the gap produced by the elongation and is called the ellipticity-induced Alfvén Eigenmode, or EAE mode [7]. Finite β also changes the gap structure. Increasing beta increases the width (in frequency) of the primary gap. Also the frequency of the gap is increased slightly. Coupling of the acoustic and shear Alfvén waves at finite beta introduces a zero order gap with a width in frequency of order $w^2/w_A^2 \approx \beta$.

Detailed calculations of the gap structure and the structure of the TAE modes have been evaluated with CONT and GATO, using the experimentally determined equilibria including the measured density profiles, and including the effects of the DIII–D wall. The calculations show the existence of the TAE mode for $n = 3$, one of the mode number observed in the experiment. The basic $m = 3$, $m = 4$ TAE component lies near the bottom of the associated gap and is coupled to several other m, $m+1$, TAE components as well as the $m = 3$ continuum Alfvén mode. This coupling splits the TAE into several

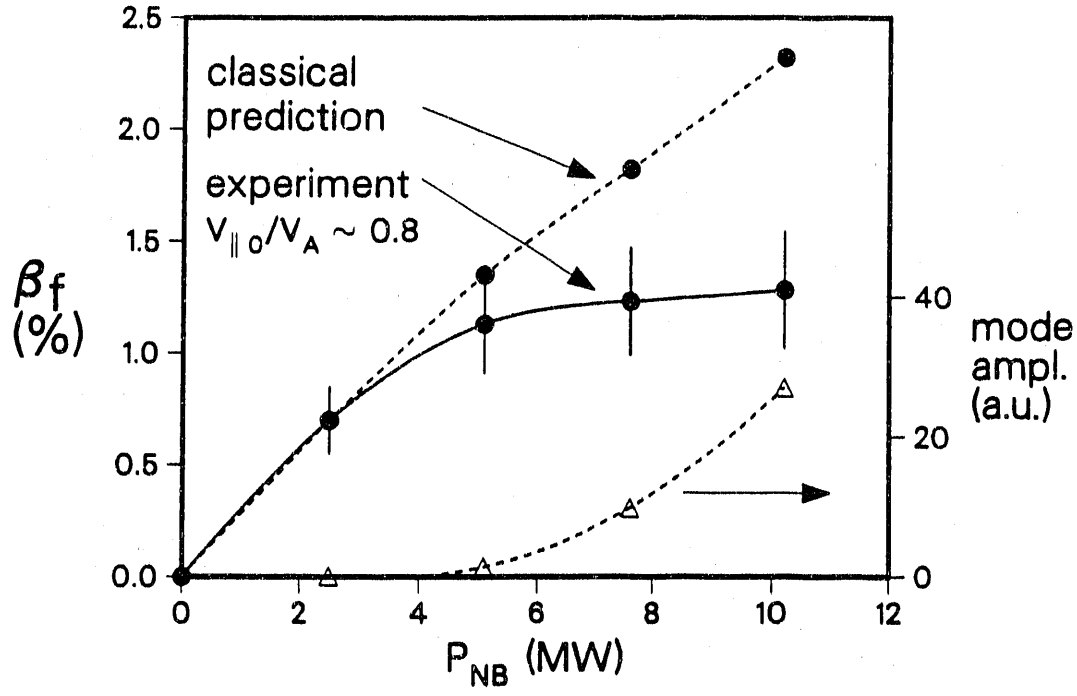

Fig. 4.2-2. TAE mode causes strong saturation of fast ion beta. TAE mode amplitude increases rapidly as β_f exceeds 1%. Fast ion beta saturates at $\beta_f \sim 1.3\%$. Classical slowing-down prediction from the ONETWO transport cod.e Fast ion loss estimated from neuron emission. B_T = 0.8 T, I_p = 0.6 MA, n_e = 3-4 × 10^{19} m^{-3}, L–mode.

modes analogous to the splitting of degenerate energy states in quantum mechanics by small perturbations. The EAE mode (also split several times by coupling to other modes) has also been confirmed in GATO calculations for two experimental discharges. The gap structure and the structure of the mode for one DIII–D experimental equilibrium is shown in Fig. 4.2-3.

The coupling of the TAE mode to the continuum is expected to provide a significant damping of the mode and thus destabilization would require a larger population of fast particles than in the absence of the continuum damping. It is found that for most experimental equilibria, at a given frequency, the gap in the shear Alfvén continuum extends only over a part of the discharge. Detailed structure of the modes evaluated with GATO show that the TAE mode found in the gap is in most cases strongly coupled to the continuum. Collaborations with theorists from the University of Texas have been developed in an effort to quantitatively evaluate the continuum damping of the mode.

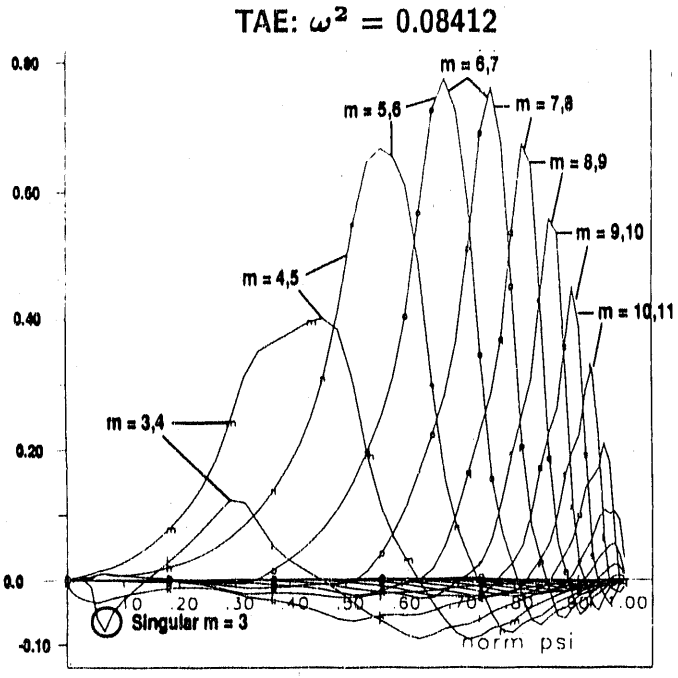

(a)

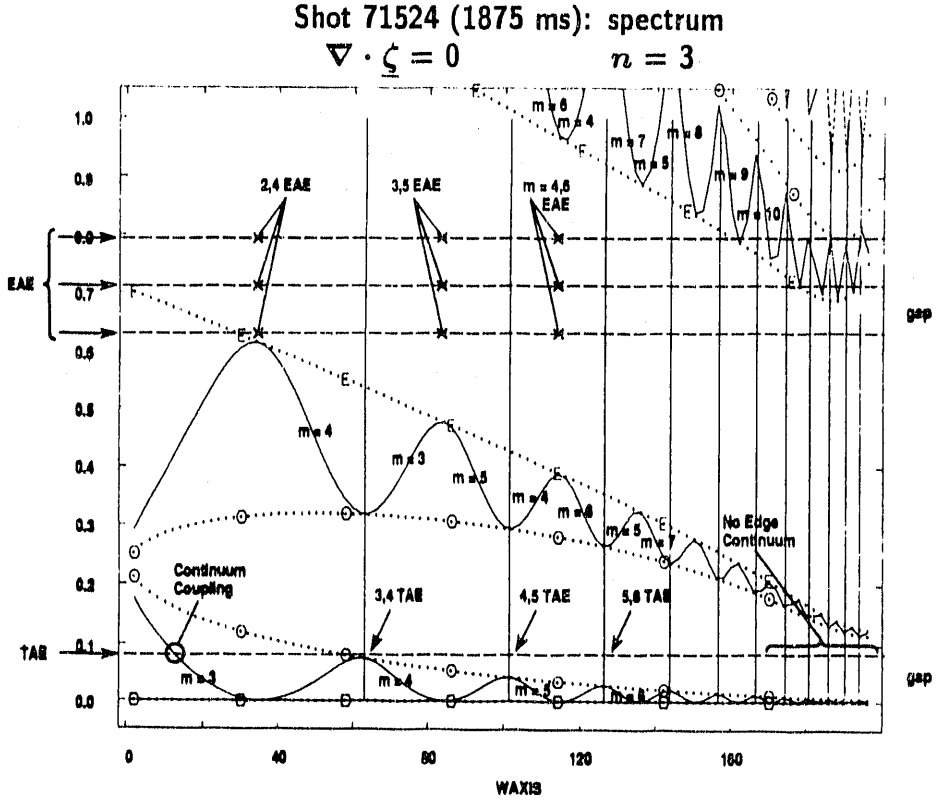

(b)

Fig. 4.2-3. (a) A TAE mode which "threads the gap" (no continuum coupling except internal $m = 3$) was found at $\omega^2 = 0.08412$. (b) Three split EAE modes were found. One appears to have split into the lower global gap, eliminating all continuum coupling.

We are also attempting to evaluate the effect of continuum damping on the stability of the mode experimentally. Changing the shape, the current profile, and the density profile of the discharge is calculated to change the structure of the gap and the continuum damping. Elongating the plasma at constant q had a stabilizing effect as expected. The mode was stabilized by increasing the internal inductance with a plasma current rampdown, as expected, because of the higher shear in the outer part of the plasma.

4.2.2. DEPENDENCE OF STABILITY AND CONFINEMENT ON THE CURRENT PROFILE

Experimentally, we have found that both the maximum achievable beta and the energy confinement time increase with a peaking of the current density profile, or increasing internal inductance, ℓ_i. This observation suggests that the confinement degradation in heated discharges is related to the beta limit and leads us to consider more seriously pressure gradient driven turbulence transport models. Establishing a firm connection between increased beta limits and improved confinement would allow us to use a well understood and thoroughly tested ideal MHD theory as a tool to identify operational regimes of improved plasma performance. The dependence of the beta limit on the internal inductance against ideal ballooning modes has been derived analytically for large aspect ratio circular geometry [8].

The effect of the current profile on the $n = 1$ kink stability also has been evaluated, including both zero and finite edge current density [9,10]. For both zero and finite edge current density, the maximum normalized beta $\beta_N = \beta/(\mathrm{I}/aB)$ stable to $n = 1$ kinks, $\beta_{\mathrm{NO}}^{n=1}$ increases almost linearly with internal inductance, ℓ_i, over the range of $0.7 < \ell_i < 1.2$. The effect of the inclusion of edge current on the $n = 1$ kink stability is similar for both circular and divertor equilibria. As the edge current increases, the central as well as the edge shear becomes weakened, which makes these equilibria unstable to the kink mode.

To confirm the scaling of beta with internal inductance, current ramp experiments were performed in lower field (1.4 tesla), near circular discharges (*i.e.*, with an elongation parameter $\kappa = 1.2$). With negative current ramps, values of ℓ_i greater than 2 were obtained. The maximum operational normalized beta achieved for these circular discharges increases with increasing internal inductance, $\beta_N \propto li$; and a normalized beta of $\beta_N > 6.0$ was achieved at $\ell_i = 2$. The experimental high β_N values along with the numerically calculated ballooning limits are shown in Fig. 4.2-4. In constant current discharges, which remained at the lower value of internal inductance, the highest normalized beta was 3.5.

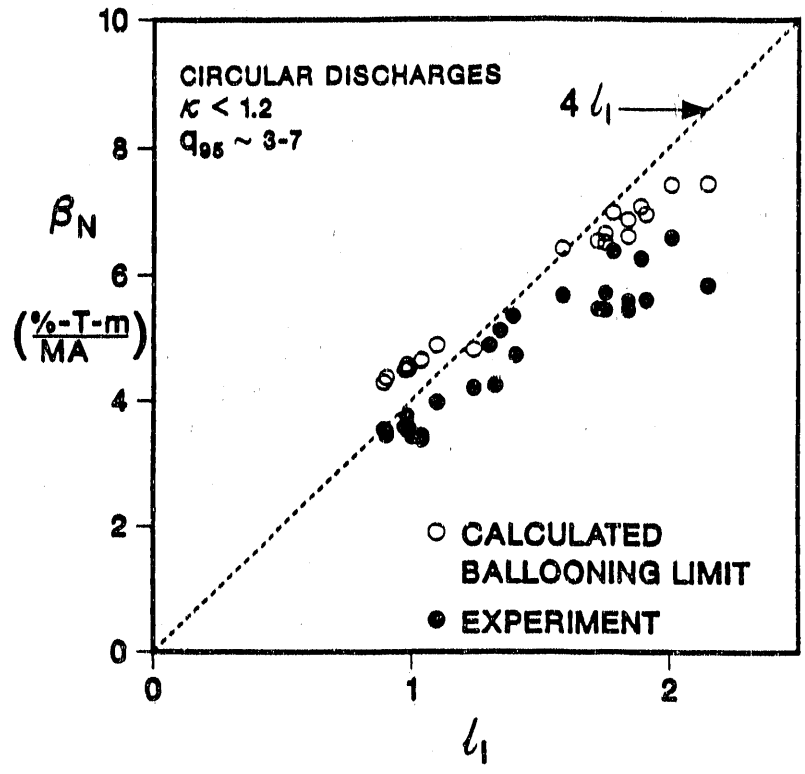

Fig. 4.2-4. Maximum normalized beta increases with ℓ_i. Discharges with high β_N are near the calculated ballooning mode limit. Operational beta limit is consistent with $\beta_n = 4\,\ell_i$

The previous highest value of β_N obtained in DIII–D is 5, and for comparison, the predicted Troyon limit is 2.8.

A rapid decrease in the plasma current has been used in DIII–D to induce transient changes in the current density profile in order to study the effect on confinement. With a decrease in the current by a factor of 2 and a current ramp rate of $dI/dt \approx -4$ MA/s, the internal inductance (ℓ_i) increased from 1 to as high as 2.75. In near circular $\kappa = 1.2$, inside wall limiter, low confinement L–mode discharges with constant auxiliary heating power the stored energy drops by less than 10% during the current ramp with no measurable change in the density or temperature profiles. After the current ramp, on a time scale of approximately 0.5 s (>10 energy confinement times $-\tau_E-$), ℓ_i decreases to the preramp value and the thermal energy content drops by a factor of 2 to the value predicted by L–mode confinement scaling. Over several discharges, there is an approximately linear scaling of τ_E/I_p with ℓ_i [11]. In contrast, double-null high confinement H–mode, ELMing

discharges have stored energy decreases of 35% on the time scale of the ramp even though there is an accompanying large increase in ℓ_i. There is a drop in electron density of as much as 60%, primarily in the outer half of the discharge, and a 30% drop in the electron temperature.

A rapid increase in the discharge elongation (κ) has also been used to make the current profile more peaked. Changing κ from 1.2 to 1.8 in 200 ms with constant beam power injection resulted in an increase in ℓ_i from 1.1 to 1.7. With κ below 1.8, the discharge remained in L–mode and the energy confinement time (τ_E) was observed to depend only weakly on ℓ_i, which is qualitatively consistent with the current ramp experiments. However, when the maximum value of κ exceeded 1.8, H–mode was obtained. In H–mode discharges obtained with an elongation ramp τ_E varied almost linearly with ℓ_i and the thermal energy confinement time as great as 1.8 times the value predicted by H–mode confinement scalings was obtained [12]. The ratio of the experimentally obtained thermal energy confinement time to the JET-DIII–D ELM-free confinement scaling is shown to increase linearly with ℓ_i in Fig. 4.2-5 for the H–mode elongation ramp data and the current ramp L–mode data. If the peaked current density profile can be maintained in H–mode discharges, there is promise in obtaining a regime of high energy confinement (3 to 4 times L–mode scaling) in discharges that have a high beta limit $\beta_{CRIT} > 4\,I/aB$.

4.2.3. SECOND STABLE CORE PLASMAS

Accurate equilibrium reconstruction and detailed stability analysis of a strongly shaped, double-null, high average beta ($\beta = 11\%$) discharge [13] shows that the plasma core is in the second stable regime. The equilibrium reconstruction using all the available data (coil currents, poloidal magnetic loops, motional Stark effect data, the kinetic pressure profile, the magnetic axis location, and the location of the two $q = 1$ surfaces) shows an inner negative shear region, an outer positive shear region, and a low shear region connecting the two. The inner negative shear region allows a large positive shear region near the boundary, even at low q ($q_{95} = 2.6$) permitting a large outer region pressure gradient to be first regime stable. The inner region is in the second stable regime, consistent with the observed axial beta [$\beta(0) = 44\%$]. The low shear region remains stable since pressure gradients vanish. A summary of the high n stability analysis is shown in Fig. 4.2-6. An $n = 1$ kink mode stability analysis shows the plasma is unstable to an internal mode which is consistent with the experimental observations of a saturated internal $m/n = 1/1$ mode. The core plasma pressure, not being limited by ballooning stability, appears to reach a local isodynamical equilibrium limit at the magnetic axis.

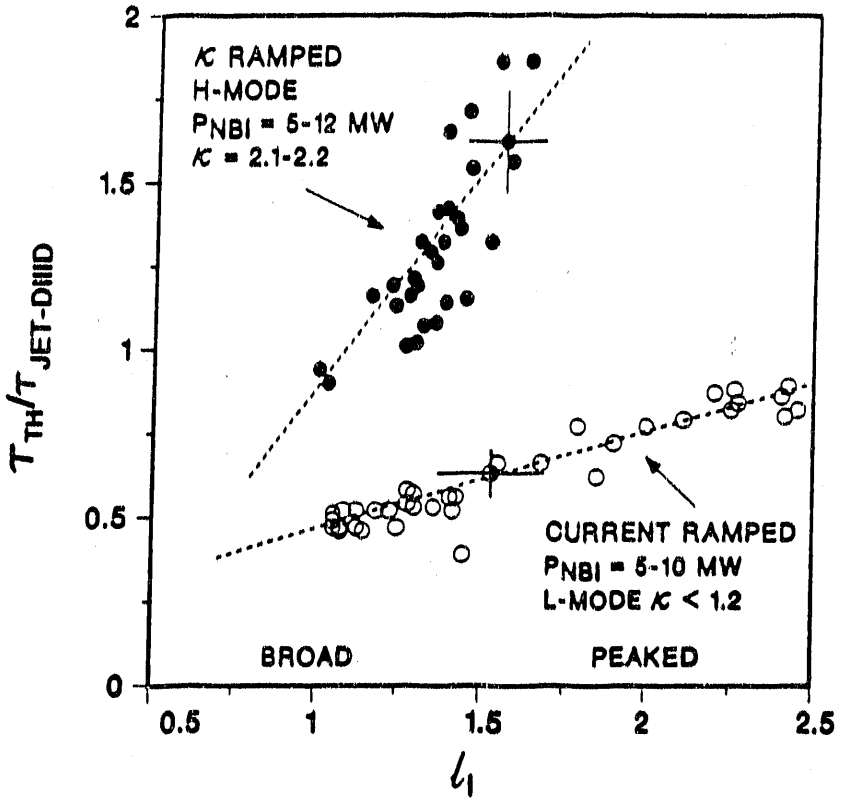

Fig. 4.2-5. Energy confinement increased with ℓ_i and strong shaping. $\tau_{JET/DIII-D} = 0.11\ P_L^{-0.46}\ I_P^{1.03}\ R^{1.48}$, H-mode scaling.

Two days of experiment were devoted to further evaluating discharges with high central beta; second stable core plasmas. We were successful in obtaining five discharges with $\beta \approx 11\%$ and with discharge behavior very similar to the previous $\beta = 11\%$, $\beta(0) = 44\%$ discharge. We believe that complete analysis of these discharges will again show a second stable core plasma. Many discharges were operated within a few percent of the ideal $n = 0$ stability limit with an elongation parameter $\kappa \approx 2.5$. Most disruptions were beta limited and not axisymmetric instability.

4.2.4. LOCKED MODES AND NONAXISYMMETRIC MAGNETIC ERROR FIELDS

Tokamak discharges generally disrupt following mode locking; which places limits on the operation space. Understanding locked modes may lead to expansion of operation space, particularly to lower density target plasmas, crucial for very high confinement VH–mode discharges and rf current drive discharges.

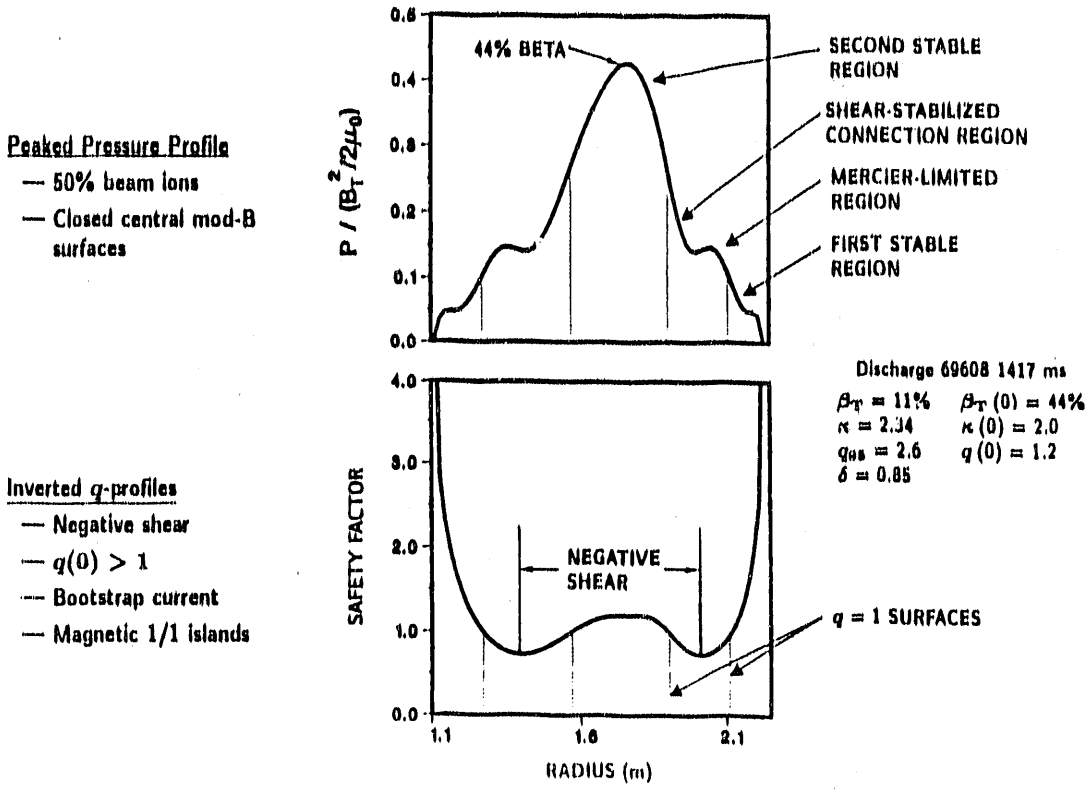

Fig. 4.2-6. Second stability DIII–D core with 44% beta.

An experiment to evaluate the dependence of the locked mode stability on the magnitude of the external magnetic error field was carried out in collaboration with Culham Lab in England. Results from the COMPASS-C tokamak and the DIII–D tokamak were compared and give a much better understanding of locked modes. These locked mode experiments were carried out in both DIII–D and COMPASS in ohmic deuterium discharges at an edge safety factor, $q = 3.5$. In both devices, a low density locked mode is observed: for a fixed value of the external error field, as the density is lowered below a certain value, a nonrotating locked mode becomes unstable; or for a fixed electron density, as the external error field is increased, the locked mode becomes unstable. The behavior of COMPASS discharges to error fields producing disruptive locked modes is similar to DIII–D except that COMPASS is much more robust, *i.e.*, it takes about an order of magnitude higher relative $m = 2, n = 1$ error field to trigger a locked mode [14]. The explanation is in agreement with a theory that fast rotating small tokamaks shield out the error field requiring a higher critical error field to penetrate and induce a locked mode. Comparing the measurements and theory predictions from COMPASS to DIII–D to BPX to ITER, the ratio of the critical error field for instability to the toroidal magnetic field

is 1×10^{-3} for COMPASS, 1×10^{-4} for DIII-D, $2 - 5 \times 10^{-5}$ for BPX, and 1×10^{-5} for ITER. The dependence of the critical density on the magnitude of the error field is shown for DIII-D and COMPASS-C in Fig. 4.2-7.

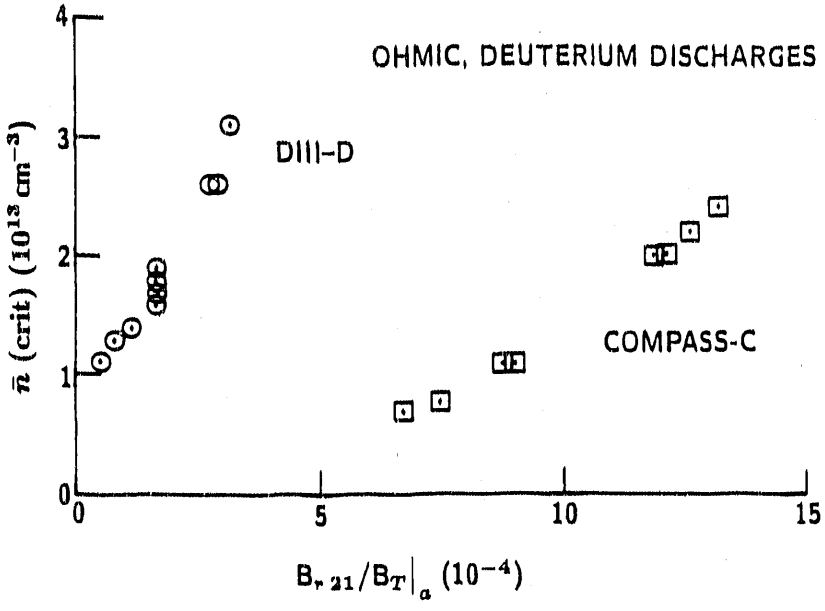

	COMPASS-C	DIII-D
R_0 (m)	0.56	1.67
B_T (T)	1.2	1.3
f_{Mirnov} (kHz)	13	1.6
Configuration	Limited, circular with $q_L = 3.5$	Single-null divertor with $q_{95} = 3.6$

Fig. 4.2-7. Smaller, faster rotating COMPASS-C plasma is less sensitive than DIII-D to error fields inducing a locked mode.

A means to make the discharge rotate faster toroidally such as neutral beams, biased plates, or ac helical fields should make a discharge less sensitive to error fields. A recent experiment has been carried out on DIII-D to evaluate the dependence of the locked mode threshold on the rotation: neutral beams were used to vary the toroidal rotation speed. In each discharge, an $n = 1$ perturbation coil current was slowly increased to add to the intrinsic DIII-D F-coil error field and the critical magnetic error field for locked mode onset was determined as a function of plasma rotation. The effect of rotation speed on the locked mode threshold is compared in discharges with similar stored energy by

comparing discharges with near tangential and perpendicular injection: DIII–D plasmas rotate faster when driven by nearly tangential injection, but the achieved β depends only on the absolute power and not angle of injection. It is found that in otherwise similar discharges, a larger magnetic error field is required to destabilize the locked mode as the toroidal rotation is increased [14]. However, as the discharge approaches the beta limit at higher beam powers, less and less error field induces a locked mode.

4.2.5. HIGH BETA WORKSHOP

A workshop on high beta research in tokamaks was held at General Atomics July 15-17. There were approximately 40 active participants from GA, PPPL, MIT, Columbia, JET, JAERI, ORNL, Grumman, DOE, LLNL, Los Alamos, and UCLA. 33 talks were presented covering experimental and analysis work on DIII-D, TFTR, JET, JT-60 and PBX-M. There was active discussion on a wide range of topics and the general response seemed to be that it was a very productive workshop.

Talks at the workshop demonstrated that progress in the area of high beta tokamak physics has been substantial, including the achievement of significantly increased plasma parameters and the advancement of analysis techniques for both experimental equilibria and stability. The workshop produced a compilation of the similarities and differences between high beta discharges and analysis of DIII-D, JET, JT-60, PBX-M and TFTR which will be issued as a summary of the workshop.

References for Section 4.2.

[1] Heidbrink, W.W., *et al.*, "An Investigation of Beam Driven Alfvén Instabilities in the DIII–D Tokamak," *Nuclear Fusion* **31** (1991) 1635.

[2] Heidbrink, W.W., "TAE Modes in DIII–D," Invited presentation, *Bull. Amer. Phys. Soc.* **36** (1991) 2402.

[3] Strait, E.J., *et al.*, "Stability of TAE Modes in DIII–D," *Bull. Amer. Phys. Soc.* **36** (1991) 2324.

[4] Duong, H.H., *et al.*, "Confinement of Fast Ions During TAE Instabilities," *Bull. Amer. Phys. Soc.* **36** (1991) 2477.

[5] Chu, M.S., *et al.*, "Alfvén Continuum Gap and the High n Gap Mode in a Noncircular Tokamak," 1991 Int. Sherwood Fusion Conf., April 22-24, 1991, Seattle, Washington, paper 1C26.

[6] Turnbull, A.D., *et al.*, "The Structure of Ideal MHD Alfvén Modes," presented at the 1991 Int. Sherwood Fusion Conf., April 22-24, 1991, Seattle, Washington, paper 1D4.

[7] Turnbull, A.D., *et al.*, "Toroidicity Induced Alfvén Eigenmodes," to be submitted to *Phys. Fluids B.*

[8] Lao, L.L., *et al.*, "Effects of Current Profile on the Ideal Ballooning Mode," General Atomics Report GA-A20593, submitted to *Physics of Fluids B.*

[9] Lao, L.L., *et al.*, "Effects of Current Profile on MHD Stability," in *Controlled Fusion and Plasma Physics* (Proc. 18th European Conf. Berlin, 1990) Vol. 15C, Pt. IV, EPS, Petit-Lancy (1991) 73.

[10] Taylor, T.S., *et al.*, "Profile Optimization and High Beta Discharges and Stability of High Elongation Plasmas in the DIII–D Tokamak," in *Plasma Physics and Controlled Nuclear Fusion Research* (Proc. 13th Int. Conf. Washington, D.C., 1990) Vol. 1, IAEA, Vienna (1991) 177.

[11] Ferron, J.R., *et al.*, "The Effect of Current Profile Changes on Confinement in the DIII–D Tokamak," *Bull. Amer. Phys. Soc.* **36** (1991) 2324.

[12] Lao, L.L., *et al.*, "Dependence of Plasma Stability and Confinement on the Current Density Profile," *Bull. of Amer. Phys. Soc.* **36** (1991) 2477.

[13] Lazarus, E.A., *et al.*, "An Optimization of Beta in the DIII–D Tokamak," General Atomics Report GA-A20571, submitted to *Nuclear Fusion.*

[14] La Haye, *et al.*, "Plasma Rotation, Error Fields, and Mode-Locking in DIII–D," presented at the IEA Workshop on MHD Effects on Transport, Princeton, New Jersey, November 11-12, 1991.

4.3. CONFINEMENT

4.3.1. TRANSPORT STUDIES

Transport studies are important for predicting the performance characteristics of reactor grade tokamak designs such as ITER. Since the energy confinement time (τ_E) is a key fusion ignition parameter, it is essential to ascertain if a particular reactor design is capable of achieving high confinement H–mode operations or better. If the design is over conservative, excessive construction and operational expenditures will result. On the other

hand, if a better understanding of transport physics is obtained, a significant reduction in the cost of the reactor will be realized. Considerable resources within the DIII–D core physics program are focussed on important aspects of tokamak confinement and transport studies.

Several transport experiments this past year were focused on studying local plasma transport properties as a function of the heating profile. Motivated by results from previous off-axis electron cyclotron heating ECH heating experiments in low confinement L–mode discharges [1], energy transport was investigated in two identical high confinement H–mode target discharges with different neutral beam deposition profiles. These off axis heating experiments [2] were conducted using 75 keV NBI as the auxiliary power source. The H–mode experiments were conducted in a diverted deuterium plasma with values of plasma current $I_p = 0.65$ MA, toroidal magnetic field $B_T = 2$ T, electron density $\langle n_e \rangle = 4.5 \times 10^{19}$ m^{-3}, aspect ratio $R/a = 1.83/0.48 = 3.8$, and elongation $\kappa = 1.5$. Off axis heating was accomplished by vertically displacing the plasma 0.30 m; 85% of the auxiliary heat was deposited outside the normalized minor radius of $\rho = 0.4$. The application of 7.5 MW of deuterium neutral beam power resulted in the plasma transitioning into the high density H–mode confinement regime with equal electron and ion temperatures. The two discharges had similar density, temperature, and impurity profiles even though in one case the heating was peaked at the center and in the other case it was off-center (see Fig. 4.3-1). The global thermal energy confinement was not affected by changing the heating location. Three interpretations of the data are possible. The results of a one-fluid power balance analysis employing the $1\frac{1}{2}$ dimension ONETWO transport code and assuming purely diffusive heat transport found that the effective diffusivity changes with the changing heating profile. Specifically, Fig. 4.3-2 shows that the thermal diffusivity χ is reduced by up to a factor of 10 inside the peak heating location. This surprising result is similar to previous L–mode results on DIII–D with both ECH [1] and neutral beam heating [3]. An alternate interpretation of the data is to allow for an inward heat flow to exist during off-axis heating thereby allowing χ to remain unchanged. The maximum power flow is obtained at the peak of the auxiliary heating deposition which is similar to what was observed during the ECH discharges. Finally, it is also possible that the appropriate local variables that describe local transport have not been identified or that local transport is not completely determined by local variables.

Results from DIII–D now demonstrate that the power balance diffusivity changes with the heating location for each of the two different heating schemes; ECH and NBI. Therefore, we are left to conclude that this plasma transport behavior is a general result

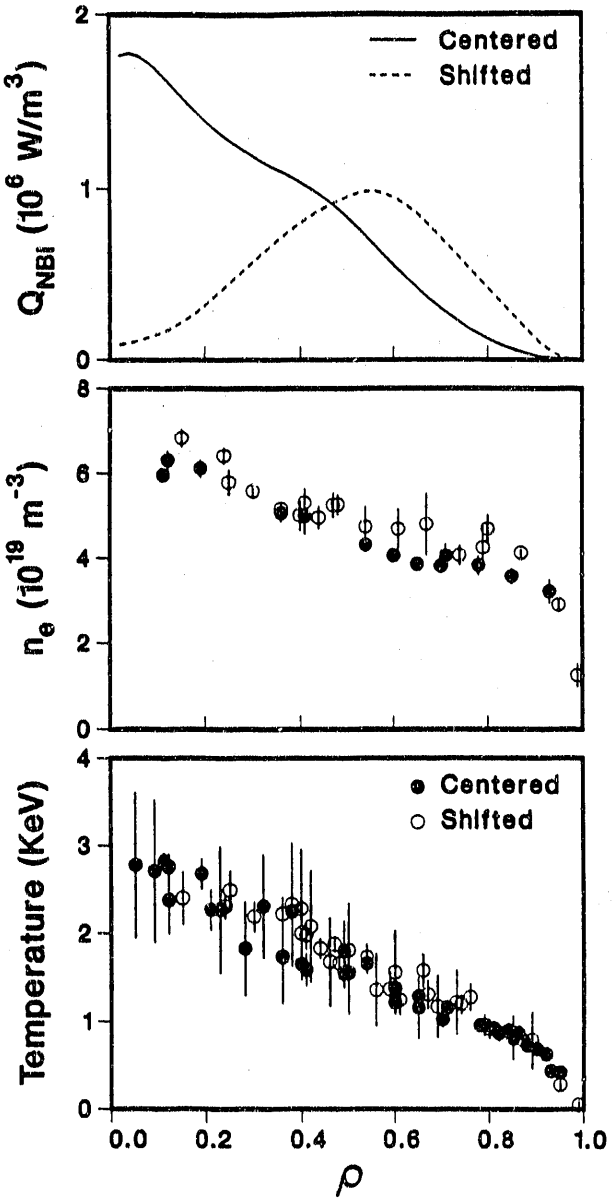

Fig. 4.3-1. NBI heating, electron density, and temperature profiles showing no change in n_e or T profiles for two very different heating profiles.

and not specific to just one type of heating scenario. In the future, we propose to operate discharges with a locally negative radial heat flux by heating further off axis with the neutral beam systems and/or by enhancing the core plasma radiation thereby conclusively addressing the inward heat flow issue. Furthermore, by running discharges in which the electron and ion transport can be separately determined will allow a direct comparison to

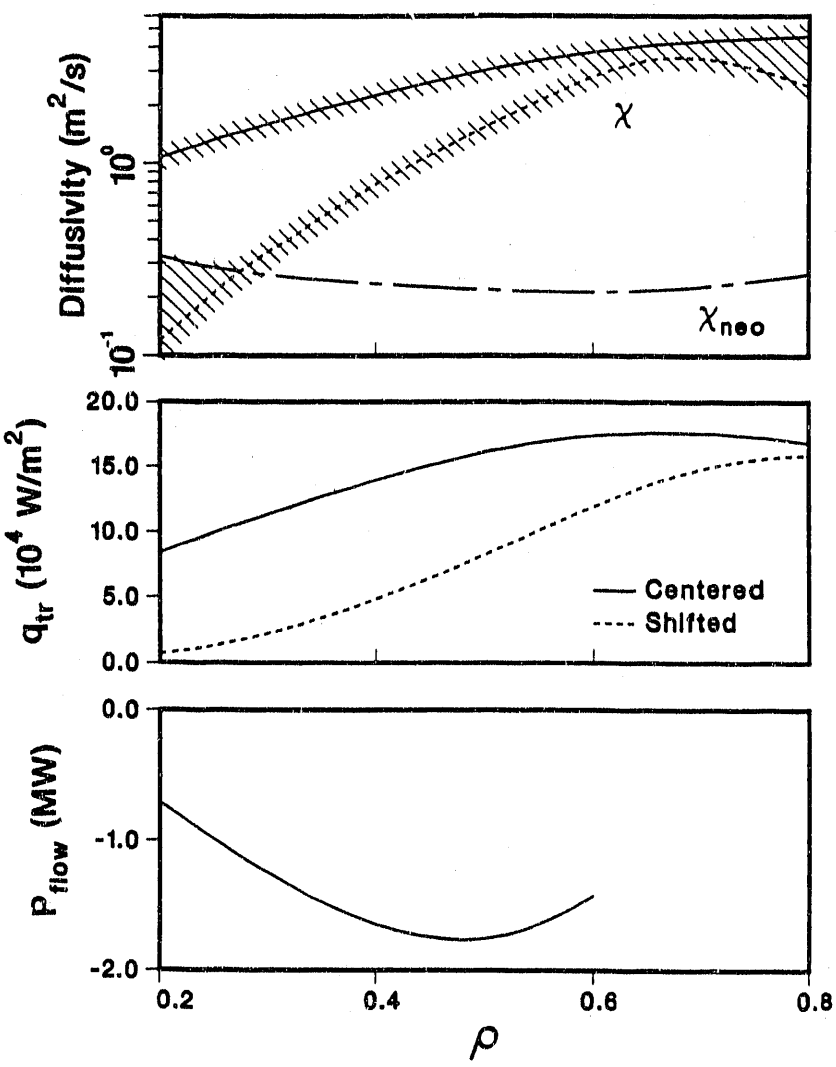

Fig. 4.3-2. Profiles of power balance diffusivity χ, radial heat flux q_{tr}, and inward power flow P_{flow} required to have χ remain unchanged for centered and off-axis heating cases.

the changing electron behavior in the ECH case. Understanding whether just the electron transport responds to the input heat or if the ions behave similarly should help reduce the number of possible theoretical descriptions of plasma transport.

Following boronization, double-null divertor discharges with thermal confinement time values of 1.8 times greater than the DIII-D/JET H-mode scaling relation were observed [4]. In this very high confinement time phase (VH-mode), no edge localized modes ELM or significant sawtooth activity is observed and the plasma energy increases with time until an event, usually correlated with an increase in magnetohydrodynamic MHD

activity, causes the discharge to begin ELMing and revert back to H–mode confinement values. Detailed time dependent transport analysis of a typical discharge indicates that the improved confinement in VH–mode as compared to H–mode corresponds to a reduction in the single-fluid diffusivity, χ_{eff}, by a factor of 2-3 in the outer half of the plasma. This improvement is evident from increases in both the ion and electron temperature gradients, while the change of the density profile is minimal. Also, there is a broadening of the region where significant bootstrap current flows near the edge. This is thought to be related to the entrance of a large portion of the plasma volume to second stability based on ideal stability calculations using the MBC and CAMINO numerical codes. Figure 4.3-3 shows the increase in the thermal confinement, the calculated bootstrap current, and the fraction of the discharge in the second stable regime. A cause and effect relationship of transport improvements and second stability has not been established, but there does appear to be a correlation.

4.3.2. GLOBAL CONFINEMENT SCALING

The knowledge of how the H–mode energy confinement τ_E depends on different parameters is of crucial importance to the performance predictions for next generation devices. Historically, these designs have made the unsatisfactory assumption that H–mode τ_E will scale as L–mode τ_E with an H–mode enhancement factor of order two. In an effort to reduce the uncertainty in the predicted H–mode τ_E, two different studies were undertaken: an investigation of the scaling of edge localized mode ELM-free thermal H–mode confinement (τ_{th}) and a more broad based study involving participation in the ITER H–mode database activity.

The τ_{th} scaling study was a joint effort between the JET and DIII–D research teams [5] and found the relationship $\tau_{th} \propto I_p^{1.0} P_L^{-0.5} L^{1.5}$ where I_p is the plasma current, P_L is the loss power, and L is a plasma linear dimension. This year, the JET/DIII–D thermal database has been expanded by adding 53 discharges from ASDEX and 9 discharges from PBX-M. The preliminary regression analysis gives an expression which also has a relatively weak dependance on the minor radius (a); the discharge elongation (κ), and the magnetic field.

The ITER H–mode database activity continued this past year with detailed analysis of the database which resulted in the publication of a large ITER report documenting the database and discussing data selection and main features, the condition of various datasets from a statistical point of view, and several scaling expressions [6]. The power law expression arrived at for ELM-free discharges (see Fig. 4.3-4) gives a confinement time

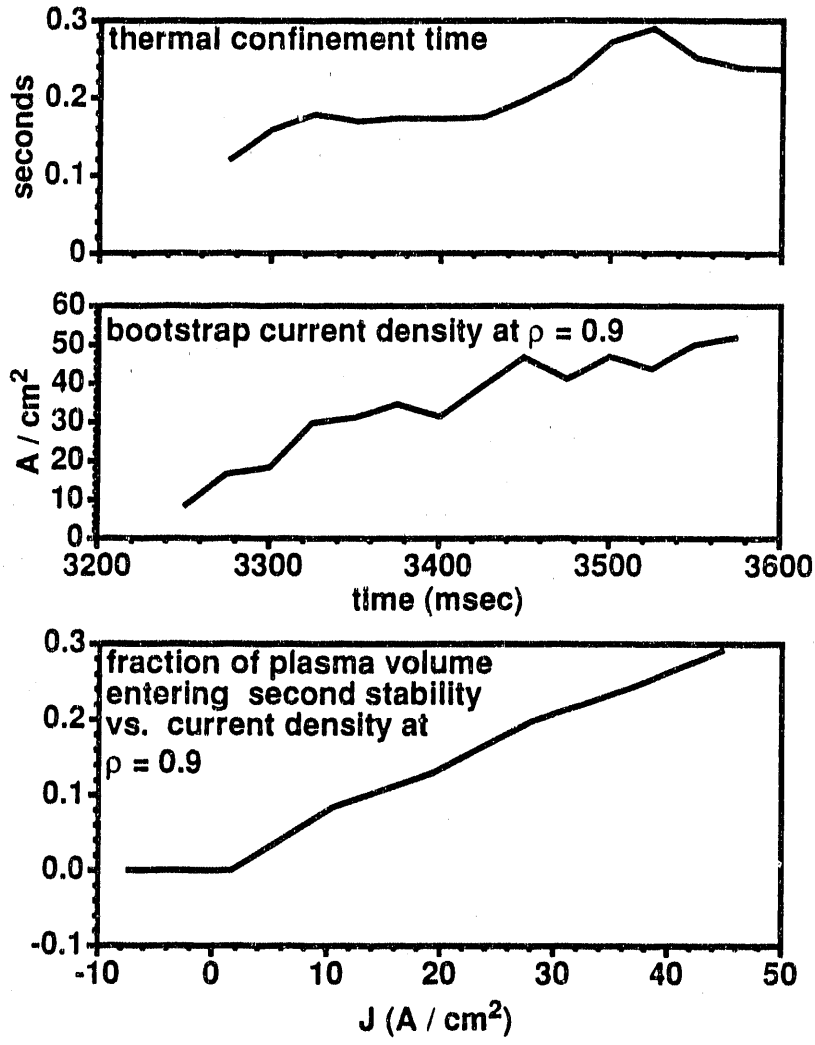

Fig. 4.3-3. Increasing thermal confinement time is correlated with an increasing edge current density and an increasing fraction of the plasma volume entering second stability.

for ITER of 5.4 s assuming the ITER design values of 22 MA, 4.85 T, 160 MW, effective mass of 2.5, major radius of 6 m, and elongation of 2.2. The ITER report was edited and submitted to *Nuclear Fusion*. Midway through the year, additional H–mode data was added to the database from ASDEX, DIII–D, JET, and JFT-2M with the intent of preparing a short description of the new data and a brief summary of any impact the new data may have on the scaling expressions once the new database was put together. It was also decided that the group should create a threshold database for H–mode discharges

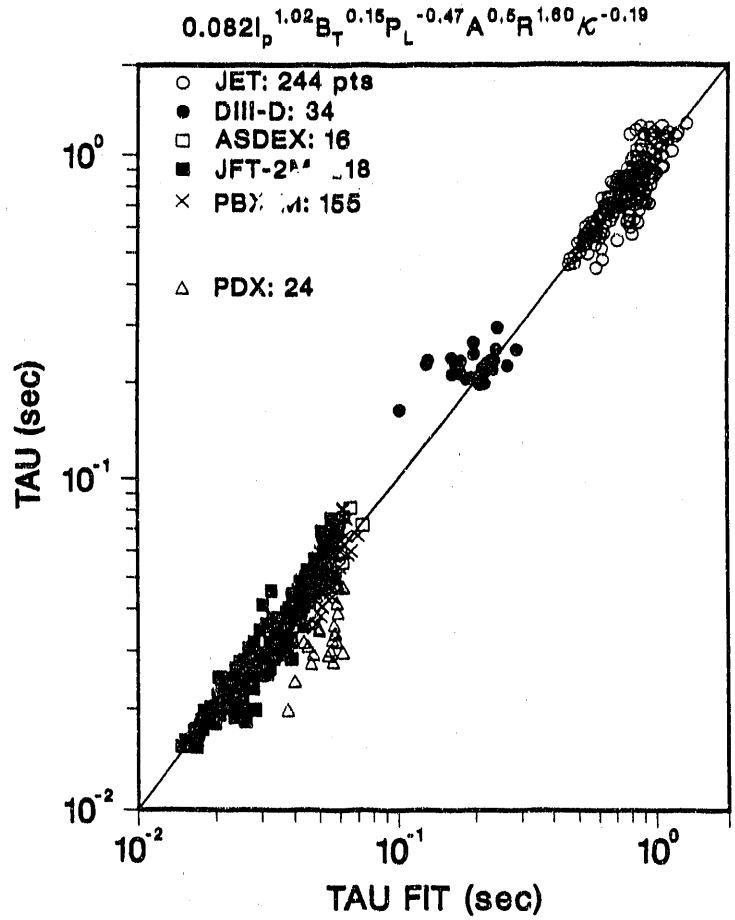

Fig. 4.3-4. Comparison of measured with fit valves of confinement time from the ITER H–mode database. PDX data is compared with the fit but was not used in determining the fit.

with the first task being a definition of what parameters should be included. This task is still in progress.

The effect on H–mode energy confinement of operating at low values of the plasma safety factor q was previously investigated experimentally on the DIII–D tokamak. This past year, detailed analysis and comparison with a model was performed accepted for publication in *Nuclear Fusion* [7]. Operationally, the linear increase of H–mode energy confinement with plasma current ceases for I_p/B_T larger than $\approx$1 MA/tesla. I_p/B_T, instead of q, was found to be the correct parameter to describe the boundary of current scaling in DIII–D. Experimentally, it has been determined that this saturation of confinement is not the result of a ceiling imposed by saturated Ohmic confinement, by the plasma reaching a β limit, by enhanced plasma radiation, or by ELMs. The observed

confinement saturation is found to be quantitatively consistent with a model of global energy confinement degradation resulting primarily from the macroscopic phenomena of sawteeth. Future work in this area includes focusing on a universal way to describe the confinement degradation boundary. The ratio of I_p/B_T was a good indicator for DIII–D but is clearly not universal since a different size device like JET observes degradation at a different value of I_p/B_T.

4.3.3. THOMSON SCATTERING SYSTEM

The multipulse Thomson scattering diagnostic began operation during the fall of 1990, with two lasers and 28 spatial channels. During 1991, operation of the system became routine with availability approaching 100% for at least one laser, producing high-quality data in support of virtually all experiments on DIII–D. To date, we have measured a wide range of plasma parameters: $5\ \text{eV} \leq T_e \leq 6\ \text{keV}$ and $2 \times 10^{18}\ \text{m}^{-3} \leq n_e \leq 2 \times 10^{20}\ \text{m}^{-3}$. Several improvements were made to enhance the capabilities of the system and improve reliability [8]. An example of the new systems capabilities are shown in Fig. 4.3-5.

Early in the year, the system was upgraded from the original 28 spatial channels to 40 channels. The old channels were rearranged in order to give improved coverage of the plasma edge, with the new ones filling in several gaps nearer the center of the plasma. The ten new channels use five filter polychromators, with the two removed filters being at spectral locations only needed for relatively cold plasmas. This new spatial arrangement allowed profile measurements with high spatial resolution, 1.5 cm at the edge, for a wide variety of plasma shapes.

A method was developed to use the Rayleigh scattering data to measure the response of each spatial channel at the laser wavelength much more accurately than was previously done. With this method, we were able to correct systematic errors that occurred in the density measurement. In the future, we will improve this procedure further, in order to reduce the error bars on our density profiles.

Late in the year, we began installation of six new YAG lasers. At the completion of this upgrade, we will have a total of eight lasers capable of profile measurements at a combined 160 Hz rate. We will also be able to perform synchronous (for 2 msec every 50 msec) and asynchronous (event-triggered single-shot) burst modes at rates of at least 4 kHz. The new lasers require a great deal of new hardware, including a redesign of the entire beamline. This upgraded system is expected to be operational early next year.

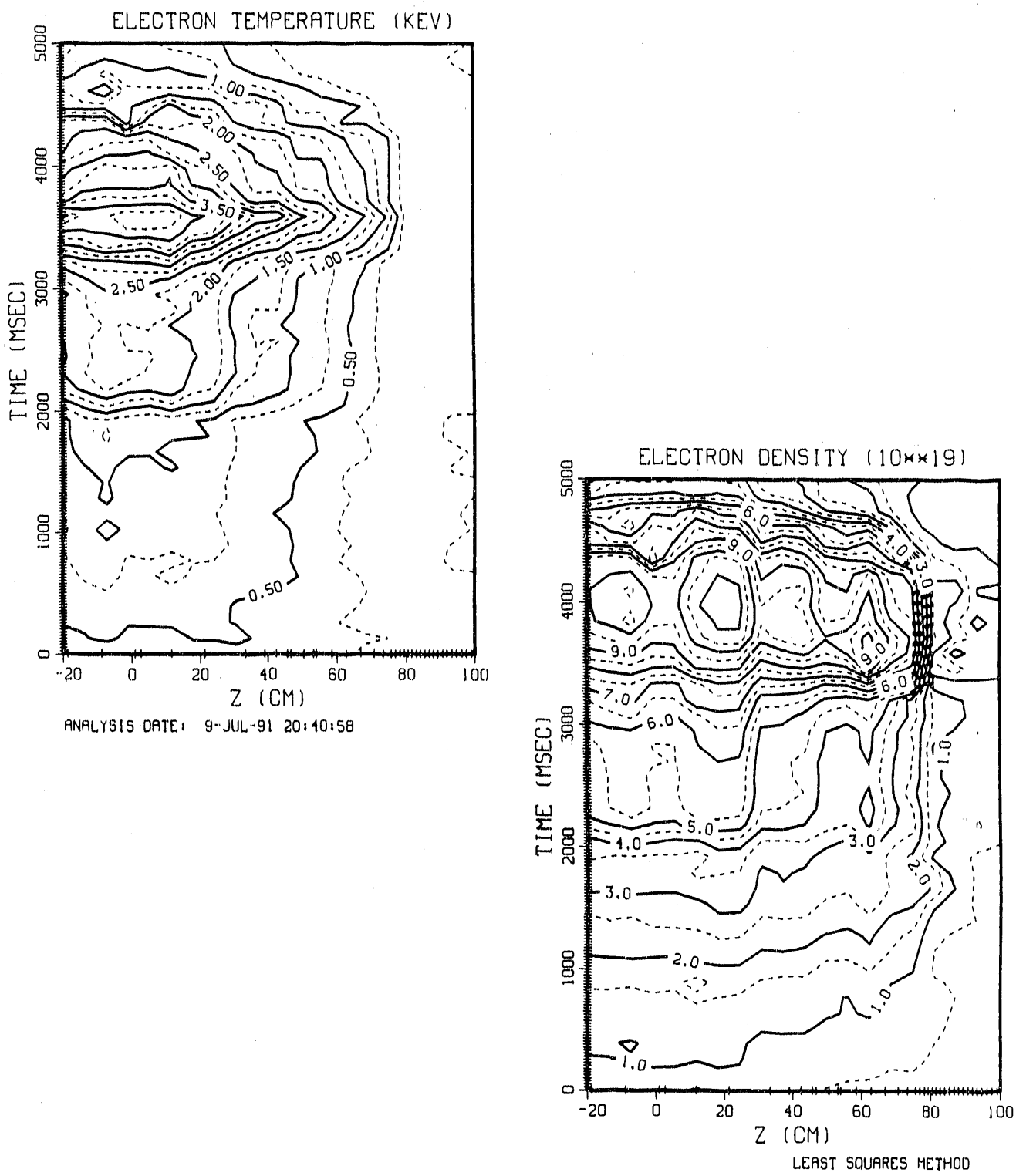

Fig. 4.3-5. Contour plot of T_e and n_e as a function of time and space for an entire plasma discharge measured by the multipulse Thomson scattering diagnostic. The H-mode period from 3300 ms to 4500 ms can be identified by the steep edge density gradient. The tick marks along the axes indicated actual times and locations where the measurement was made.

References for Section 4.3.

[1] Petty, C.C., *et al.*, in *Controlled Fusion and Plasma Physics* (Proc. 18th European Conf. Berlin, 1990) Vol. 15C, Pt. I, EPS, Petit-Lancy (1991) 241; see also T.C. Luce, *et al.*, General Atomics Report GA-A20541 (1991), submitted to *Phys. Rev. Lett.*

[2] Schissel, D.P., *et al.*, "An Examination of Heat Transport During Off Axis Neutral Beam Injection in DIII–D," General Atomics Report GA-A20696 (1991), submitted to *Nucl. Fusion Lett.*

[3] DeBoo, J.C., R.E. Waltz, T. Osborne, in *Controlled Fusion and Plasma Physics* (Proc. 18th European Conf. Berlin, 1990) Vol. 15C, Pt. I, EPS, Petit-Lancy (1991) 173.

[4] Jackson, G.L., *et al.*, *Phys. Rev. Lett.* **67** (1991) 3098.

[5] Schissel, D.P., *et al.*, *Nucl. Fusion* **31** (1991) 73.

[6] Christiansen, J.P., *et al.*, "A Global Energy Confinement H–mode Database for ITER," JET's ITER Project Report ITER-IL-PH-4-1-1 (1991).

[7] Schissel, D.P., *et al.*, "An Examination of DIII–D Energy Confinement at Small Values of the Plasma Safety Factor," General Atomics Report GA-A20438 (1991), submitted to *Nucl. Fusion.*

[8] Carlstrom, T.N., "The Multipulse Thomson Scattering Diagnostic on the DIII–D Tokamak," General Atomics Report GA-A20614 (1991); to be published in Proc. 14th IEEE Symp. on Fusion Engineering, San Diego, 1991.

SECTION 5

DIII-D OPERATIONS

5. DIII-D OPERATIONS

DIII-D Operations comprises all of the operating activities of the DIII-D program. The past year has been extremely productive. First results were obtained with the fast wave current drive system and the first 110 GHz gyrotron was installed. The installation of the advanced divertor ring and baffle has led us into a new era of divertor control and exciting results. The new boronization capability provided reduced impurity levels key to the fast wave program and also led to the discovery of enhanced plasma energy confinement in the VH-mode. Attention to understanding the latent capabilities of the neutral beam system resulted in the ability to increase the beam energy from 50 keV to 93 keV and the power output from 2.8 MW to 3.8 MW per source. This provides the opportunity to raise the total system output to 30 MW at nominal cost.

During the year, substantial new effort was initiated in the Plasma Control System and related Disruption Avoidance/Control areas. A new plasma control system is being developed for DIII-D based on a digital processor. This system will substantially enhance the capability and flexibility of DIII-D plasma control. It will provide the capability of precise long-pulse control of the plasma needed for the current drive and divertor programs. This system will also provide the basis for a more comprehensive plasma control system including disruption avoidance and control.

A renewed effort on disruption issues has focussed in the operations group. An aggressive program of modeling and analysis has begun.

A special effort is being made to identify those areas where modernizing existing hardware, some of which dates back to the 1970s, would benefit the program. In addition a review process to examine those events and mistakes that significantly detract from the efficiency of DIII-D operations has been initiated. Safe operation of the facility continued to be an important priority. Particular attention was paid to the safe implementation of new tasks, review of the existing procedures for hazardous work, and the training of personnel. Boronization, a process that uses a toxic and pyrophoric gas, was designed and implemented with careful attention to details that would lead to safe operation and thorough review through our Hazardous Work Authorization procedures. Experts from

both the company and other laboratories were involved. Continued emphasis on reliable and efficient operation should help enhance safety.

Continuing attention was also paid to radiation safety. Radiation levels at the site boundary were 5.5 mrem. The DOE guideline is 20 mrem and background in San Diego is about 100 mrem. Particular attention was paid to maintaining the integrity of the neutron shield. Radiation training of the staff was carried out.

5.1. TOKAMAK OPERATIONS

5.1.1. INTRODUCTION

Boronization and the experimental results that followed provided the highlight of the FY91 tokamak operations year. This new vacuum vessel conditioning method paved the road for the discovery of an exciting new very high confinement VH–mode which is described in the preceding physics sections. The Advanced Divertor Project (ADP) ring, which was installed in the DIII–D vessel at the end of FY90 and was used for experiments in FY91, also produced promising results, but its electrical insulation proved to be problematic.

The boronization and the ADP technical work will be described below together with other items that affected the tokamak operation. A statistical review of the operation year will be given and finally some of the plans for new installations will be mentioned.

5.1.2. BORONIZATION

Boronization is a process by which a vacuum vessel is coated by a layer of boron, using a glow discharge in a gas mixture of 90% helium and 10% diborane. Diborane is a very toxic and explosive gas, therefore considerable effort was spent in designing the boronization system, writing and reviewing the Hazardous Work Authorization (HWA). The task engineer visited ASDEX and Textor in Europe and TFTR at Princeton to see their boronization and safety systems. A scientist, who had done the first boronization in Textor, was involved in the design of the DIII–D system and writing the HWA. Several safety meetings were held to explain the process, the hazards, and how they were going to be handled to all the personnel on site.

The reduction in both metal and low Z impurities was significant after the first boronization and the new higher confinement mode, VH-mode, was discovered. There were, however, several indications that the boron layer was not deposited uniformly around

the torus. A second gas inlet port about 180° from the first one was installed to correct this problem. The port chosen was the Ion Cyclotron Heating (ICH) antenna port, which gave the additional benefit, that a heavier layer of boron would be deposited on the antenna and, therefore, cut down the impurities released from the antenna. We found, that carbonization was superior in terms of reducing ICH antenna impurities. Methane gas was, therefore, added to the helium/diborane mixture in the following boronizations and the glow was pulsed to improve the toroidal uniformity of the boron layer.

An added benefit from boronization is fast recovery after vents of the vessel to air since boron reacts very readily with both oxygen and nitrogen. This was demonstrated several times during the year.

5.1.3. ADVANCED DIVERTOR PROJECT RING

The purpose of the advanced divertor ring and its associated baffle plates is to control the edge density of a diverted plasma. Plasma particles moving along the outboard field lines outside the separatrix, strike the floor near the ring, bounce under it, and get trapped. Measurements of the density in the plasma and the pressure under the baffle plates confirm that an adequate pressure buildup occurs to allow meaningful pumping. This pressure can be increased by biasing the ring with respect to the vessel.

Several other benefits arise from the possibility of biasing the ring: (1) sweeping the divertor strike point by sweeping the voltage on the ring and thereby minimizing the local heat deposition, and (2) injecting helicity into the plasma and thereby driving plasma current. These potential benefits are the reason for assuming the arduous engineering task of submerging a biased ring, that has to be electrically isolated from the vessel, into an environment with a varying magnetic field, plasma, and low neutral pressure. To avoid breakdown between the ring and the vessel, any path along the magnetic field lines is blocked by an insulator. To protect the insulating material on the feed lines, which cross the toroidal field, from any potential plasma in the baffled area, ground shields are installed over it. The insulation is further complicated since the materials have to be vacuum compatible and can only be tested during plasma shots. To illustrate the problems an account of the last year's experience with the ring is given below.

Soon after the ring was installed in FY90, leaks developed from the water cooling channels into the primary vacuum. These were found to be due to faulty weld processes. They were repaired, and after two operating periods the leak problems have not reappeared. Failures in the electrical insulation have not been so easy to address. After

a short period of plasma operation, where encouraging physics results were obtained, a severe breakdown occurred between the shield and one of the water feed lines, which punctured. Some water leaked into the vessel and it was subsequently pumped out. The water, which contained small amounts of tritium, was separated from the pump oil and had to be treated as radioactive waste.

The insulation between the water lines and their shield was then increased during a month long vent, and the system was high potted to 3 kV in air as it was reassembled. Instrumentation monitoring the voltage on the ring was improved to allow fast spikes to be detected, and the bias power supply shut off. The voltage protection varistors were also moved as close to the ring as possible.

A series of exciting experiments with the ring were then performed. Eventually, the ring standoff voltage had dropped to a level below that considered safe for operating with the ring in the bias mode. Operation with the plasma resting on the ring continued without biasing until a second water leak occurred. The vessel was vented again, the ring inspected, and the leak fixed. The decreasing stand-off voltage was found to be due to coating of the boron nitride tiles used as insulators on the ing and the floor, and the leak was caused by breakdown arcs generated by plasma induced voltages on the floating ring, eroding the water line. A redesign of the ring was at this time in full progress, thus it was decided to ground the ring and operate without water cooling. This limited the parameter space within which operation could be done. By installing a gaseous nitrogen cooling system the operating space was increased somewhat. At the beginning of FY92, the vessel was vented and the ring supports, feed lines, and insulation was redesigned. The test voltage has been increased to 5 kV.

5.1.4. OTHER OPERATION ISSUES

It has been noticed over the last few years that a few events, are collectively responsible for a large amount of the accumulated tokamak downtime. Five such events in FY91 were responsible for 41% of the downtime. Two water leaks from the ADP ring accounted for about half of this time. Toroidal power supply failures occurred which were caused by master gate drive boards having components that rattle loose during shots. The master gate driver boards are scheduled to be replaced during FY92. The fourth problem occurred in the neutral beamlines (NB), where the incorrect gas was fed to several ion sources and damaged them. This event was reviewed and new procedures were established to avoid a repetition. The fifth event was a ground fault on the toroidal field coil. This fault only occurred during full field shots, when both the toroidal and the ohmic heating

coils were energized. It took several days to develop the technique to measure and find the 5 to 20 A ground fault current in the background of the normal 120,000 A in the coil. The fault path was found to be a bolt on an F–coil case bracket, which during a shot touched the nearby B-coil and eventually rubbed through the insulation, thus grounding the coil. The machine was inspected and no other similar situation was found.

5.1.5. TOKAMAK OPERATIONS DATA

During FY91, the DIII–D facility was operated for 22 weeks. This was more weeks than originally planned because more funding became available and a planned vent was delayed from the end of FY91 to the beginning of FY92 in order to pursue key technical results following boronization.

The DIII–D operation schedule is shown in Fig. 5.1-1. The typical operating cycle was five days per week, 8 h per day, operating two weeks in a row separated by two weeks of maintenance. Six vents were needed during the year to inspect and repair the ADP insulation and fix vacuum leaks. Only one of these was planned. The recovery from these vents was significantly faster than in the past due to the boronization. Machine availability (Fig. 5.1-2) averaged 71.5% for FY91.

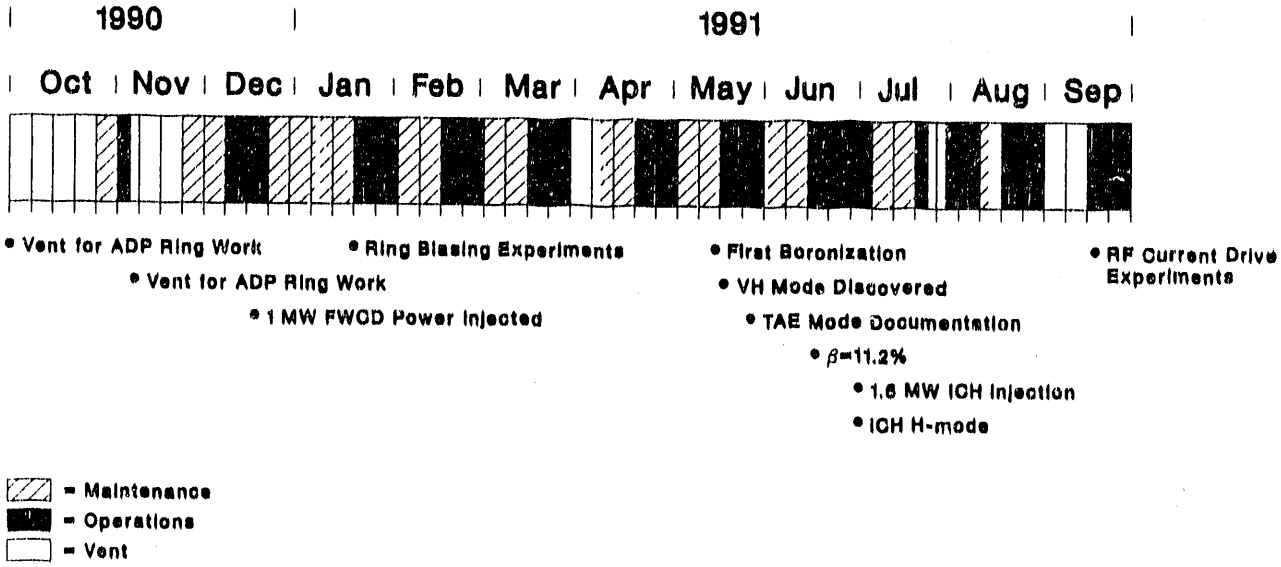

Fig. 5.1-1. DIII–D FY91 weekly operations schedule.

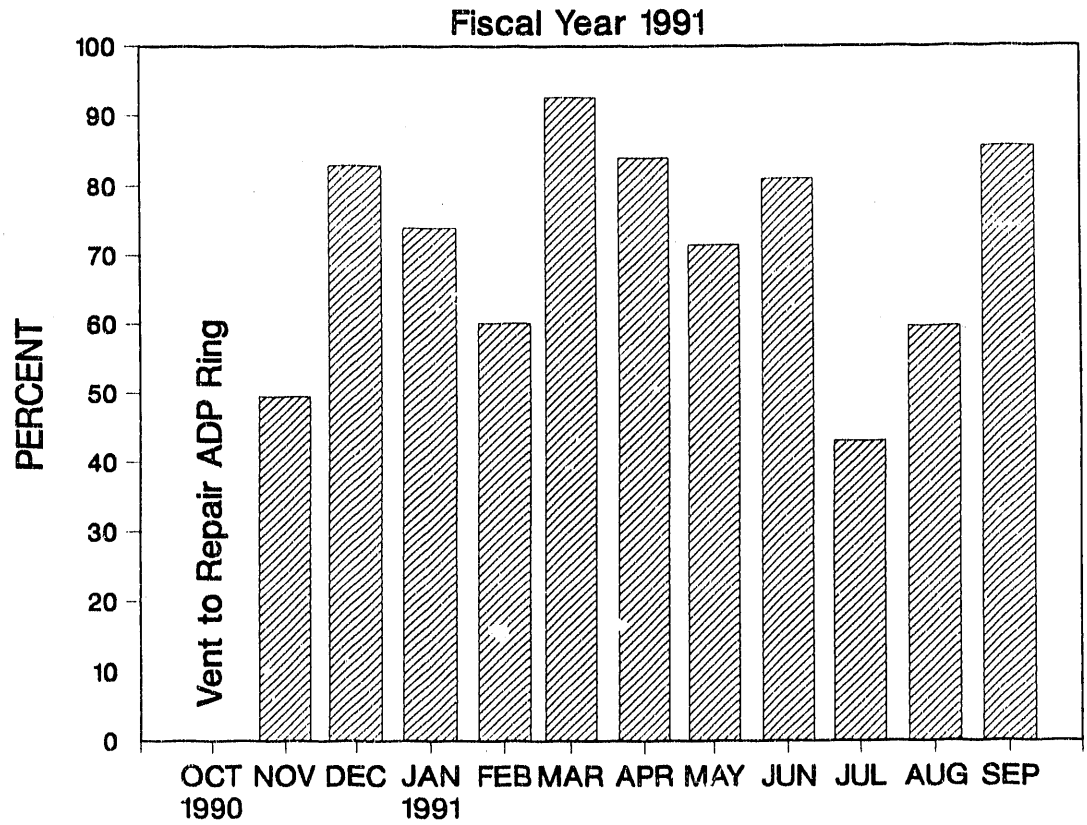

Fig. 5.1-2. DIII–D machine availability.

5.1.6 PLANNED NEW INSTALLATIONS

As the machine is operated more routinely at higher currents and higher power input, more damage to the vessel wall tiles is expected to occur and a complete coverage of the outer Inconel wall with protective tiles will be needed. During the spring vent, melting on the edges of the upper Inconel tiles was noticed. This occurred due to bombardment by energetic plasma particles. As a first step, a toroidal graphite band two tiles wide will be installed on the upper outer wall during the first quarter of FY92. Design of the remaining armor to cover the whole outer wall is in progress and is expected to be installed during a vent in the beginning of FY93.

Control of locked modes is essential for operation at lowest density, and low density operation is needed for rf current drive experiments. Previous experiments with a crude coil have demonstrated the effectiveness of an error compensation system.

A new correction coil, C–coil, is being designed. The new coil will consist of several square segments, which are wrapped around the machine at the midplane. The current in the different sections can, through a patch panel, be adjusted to unequal levels.

5.2. NEUTRAL BEAM OPERATIONS

5.2.1. OPERATIONS SUMMARY

Twenty-two weeks of plasma heating experiments were supported by NB in 1991. For the first half of the year, eight ion sources were available. In July, one of the NB transformers was removed from neutral beam use and temporarily converted for 60 GHz Electron Cyclotron Heating (ECH) operation leaving seven ion sources available. 20 MW of NB power has been routinely injected in support of the DIII–D physics program.

The group has adapted in response to specific requirements of the ECH and Ion Cyclotron Resonant Heating (ICRH) physics program, developing the capability of modulating NB pulses, and with a view to providing reduced power levels more comparable to the power levels of the present rf systems, routinely operating at voltages as low as 40 kV.

The NB group has achieved remarkable results in providing available power levels far greater than the NB systems' original design criteria. The source operating voltage was increased to 93 kV from the the design value of 80 kV; this allowed the output power to be increased to 3.8 MW from 2.8 MW. All told, this system is now capable of producing nearly twice the power per source in deuterium as the original design value for hydrogen operation. Modest changes in the support hardware remain to be carried out in order to achieve this level of operation with all eight sources. Improvements have also been made in the efficiency and measurement of injected power.

5.2.2. SYSTEMS IMPROVEMENTS AND MAINTENANCE

During the second quarter of 1991, a study was done to assess the feasibility of operating the Common Long Pulse Ion Source at voltages higher than the nominal 80 kV rating. Based on the accelerator grid geometry of the ion source, it was determined that 93 kV would be a reasonable operating limit. The 30° left ion source was chosen for actual testing because the high voltage transformer used in this system had been recently rewound with the capability of providing 130 kV, open circuit. During the third quarter of 1991, this source was successfully conditioned up to 93 kV over the course of three days.

The power yield from this 93 kV operation was 3.8 MW, as compared to 2.8 at 80 kV, a 35% increase!

To date, three ion sources have been operated at 93 kV. Two Transrex systems have been individually conditioned to 93 kV; however, operation at these levels with the present transformers is marginal. A second UVC Transformer was removed from service to be rewound and will be installed during January 1992. If the remaining six transformers were upgraded, the DIII–D NB would be capable of injecting almost 30 MW, twice the original nominal specifications in hydrogen.

Improvements have been obtained in two other important areas, one being the neutralization efficiency of the beam systems which directly affects the injected beam power, the other being the accuracy with which this quantity is measured. Injected power has been increased by assuring an adequate density of gas in the neutralizer throughout the shot. This has been accomplished by installing new gas puffing hardware and control room monitoring diagnostics. The measurement accuracy of injected power as measured by waterflow calorimetry has been improved by means of regular calibration under the DIII–D Preventive Maintenance Program, and by real time readings of calorimeter water flows in the control room. Reionization losses, previously subject to a wide range of estimates, have been measured and are under 5%. In the future, attention will be turned to improved calculation of shine-through losses (the amount of NB energy that does not heat the plasma, but rather is deposited on the far walls of the tokamak).

There was an increase in the amount of ion source maintenance encountered in 1991. A water fitting failed, external to the 150° left ion source, spraying several hundred gallons of water over the enclosure and source. The cause was traced to a compression type fitting that was never properly swaged at the factory. It proved impossible to dry the ion source *in situ* to the degree necessary to stand off the high voltages involved, and the source was removed to the source lab for servicing.

In the course of preparing to provide ion source operation in helium, several sources were accidentally operated in argon with helium operating parameters. This caused breakdowns on several insulating gaskets requiring their replacement. In all, four sources were affected. The experience has resulted in refinement of the ion source preventative maintenance program and spares inventory. In addition, procedures have been instituted to prevent the recurrence of this type of accident. Gas types are checked after every bottle change by two individuals, and residual gas analysis RGA scans are run to verify the gas type.

Most ion source problems experienced during the year have involved the failure of insulating gaskets between copper plates in the arc chamber assembly. Other problems have involved defects in the original machining of two such plates. Adherence to the DIII-D preventative maintenance program has often revealed impending failures before an actual breakdown, allowing for orderly repairs. A program has been undertaken to insure that we have a good inventory of spare parts for our Common Long Pulse Ion Sources (CLPS).

5.2.3. SYSTEMS AVAILABILITY

Overall average availability for the year is excellent at 91.1%, which compares favorably to FY90. Availability of the NB systems by month is shown in Fig. 5.2-1. Since the emphasis this year has been on physics experiments utilizing ICRH and ECH, there are times when only a small fraction of the available beam power is being used. This explains the difference between the "Available" and "Injecting" categories.

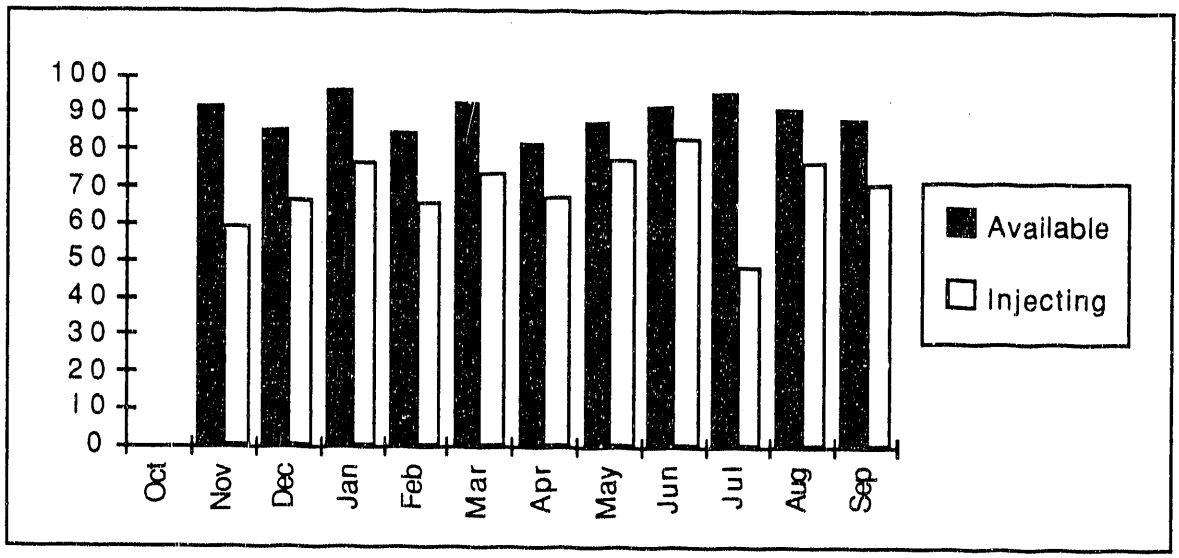

Fig. 5.2-1. Neutral beam availability by month.

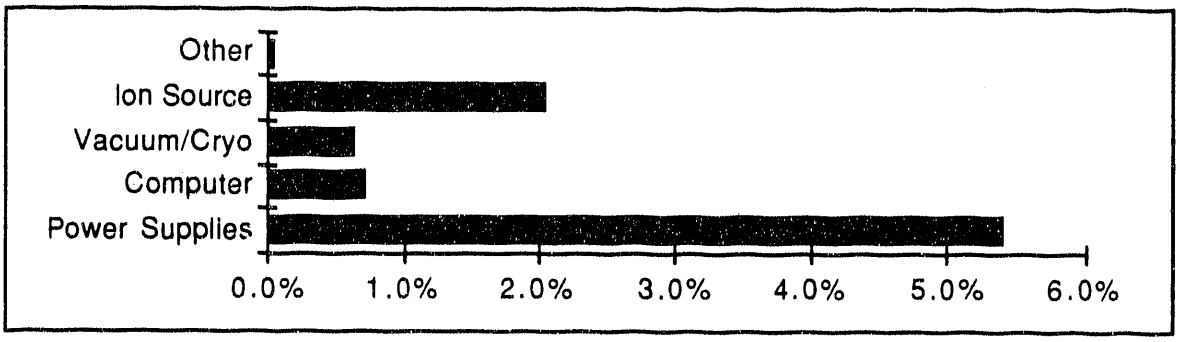

Fig. 5.2-2. Neutral beam system unavailability by cause.

The various causes for downtime are shown in Fig. 5.2-2. Vacuum, cryogenic, and computer problems each account for less than 1% of the total, ion source problems approximately 2%, while power supply problems account for almost 5.5%.

While overall availability was excellent, the group is always striving to improve performance. A power supply reliability task force has been established to identify subsystem upgrades and improvements which will decrease downtime due to NB power supply problems.

5.3. ELECTRON CYCLOTRON AND ION CYCLOTRON HEATING OPERATIONS

5.3.1. ELECTRON CYCLOTRON HEATING OPERATIONS

During FY91 the ECH system was used for a total of ten days to conduct plasma experiments. For the first three quarters, the vault area underwent major modifications for the future installation of the 110 GHz systems. The system was used for standalone experiments and in conjunction with the 60 MHz system for radio frequency current drive experiments. Due to the 110 GHz system space requirements, two 60 GHz tanks had to be removed from the area which left only eight operational gyrotron systems. Due to a waveguide launcher bias problem and a failed gyrotron output window, there were only six gyrotrons available for most of the reporting period. The cause for the window failure is not known at this time but it is felt that fatigue, possible water absorption, and slightly higher operating pressure of the system may have all contributed. The gyrotron window was replaced and the tube is now operational but the bias problem will have to wait until the machine vent in early FY92. All operations were conducted using the inside launch

as described in last years report and Fig. 5.3-1. Due to the high priority of the 110 GHz gyrotron testing, the 60 GHz system had to borrow the use of a NB power supply for operations.

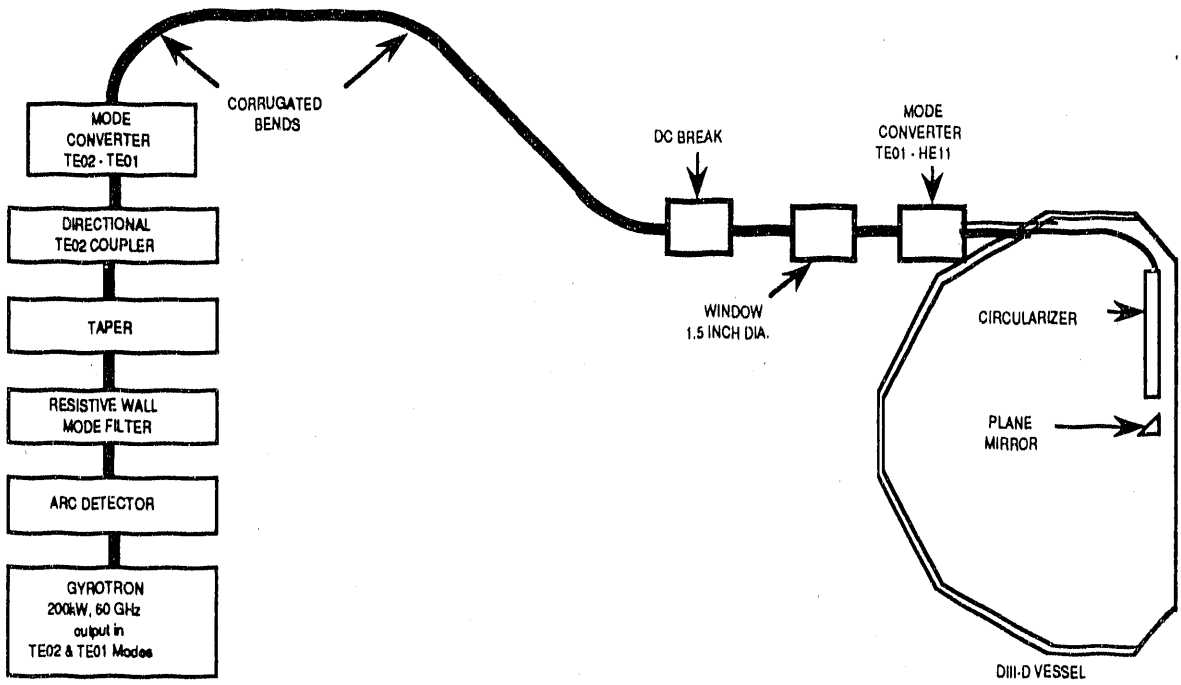

Fig. 5.3-1. ECH inside launch schematic.

5.3.2. ION CYCLOTRON HEATING AND FAST WAVE CURRENT DRIVE OPERATIONS

There were ten days of Fast Wave Current Drive (FWCD) experiments this year with injected power levels of greater than 1.7 MW. Early in the year, vacuum leaks developed in the antenna vacuum feedthrough. These leaks were corrected by Oak Ridge National Laboratory (ORNL) personnel who replaced the ceramic feedthroughs.

In the second quarter, the Final Power Amplifier (FPA) was disassembled for the upgrade of a tetrode which had been in operation since original installation of the system at General Atomics. The new tetrode has a higher plate dissipation which should allow for higher output power. After preliminary low power testing, an attempt at higher power operation was made. The tube failed to hold off the required 25 kV, and a spare tetrode similar to the original was installed. The amplifier was reassembled and tuned for operation at 54 MHz where vacuum conditioning of the antenna was done. At some point during

this conditioning, the dc break in line "A" failed. The break was subsequently repaired with some modifications being made to increase its voltage hold-off capability. While repairs of the break were under way, high power dummy load testing of the amplifier was started. Due to, as yet, unknown causes, an FPA cavity arc developed in the region of the tube ceramic-to-anode transition. This arc went unnoticed until a vacuum leak in the tube envelope developed. Upon further investigation and correspondence with the tube manufacturer, it was discovered that a tube loss of this nature had been encountered by the equipment manufacturer (Varian-Eimac) during system development. The manufacturer has expressed concern over the situation and has suggested possible corrective measures to be taken. New protection sensors have been added to detect this arcing. At present, it looks like the limiting factor in injected power is the transmission line voltage holdoff and FPA output power. The transmission lines are currently being pressurized with CO_2 but plans are under way to use Freon 116 which should enable the holdoff voltage to be doubled. The FPA is also scheduled to receive several modifications which should allow for operation at higher power levels without over stressing the screen grid (this has been the limiting factor to present). Both of the above modifications will be completed early in FY92.

5.4. DISRUPTIONS/PLASMA CONTROL

5.4.1. DISRUPTION STUDIES

During the past year, the disruption studies program at General Atomics has expanded its scope in order to better address the various disruption design issues of fusion devices and to lay the ground work for a program of disruption control. The topics presently under investigation include behavior of the plasma current during disruptions, development of a disruption and operations database, computer simulation of disruptions, measurement of electron temperature and density profiles during disruptions, toroidal symmetry of poloidal disruption currents, and runaway electron generation during disruptions.

Disruptions often result in large forces on the vacuum vessel and in-vessel components, and the magnitude of these forces is much larger if the disruption is accompanied by a vertical instability of the plasma column. Previous research on DIII–D [1-4] has explained the origin of these forces and direct measurements have confirmed the existence of the poloidal currents predicted to be responsible for much of the force. This disruption data is now being used to benchmark plasma simulation codes available within the fusion community. Two such efforts that have begun this year involve the TSC code in

collaboration with Oak Ridge, and Princeton and the DINA code in collaboration with the Khurchatov Institute in the Soviet Union. Preliminary simulations have been performed utilizing the DIII–D geometry, magnetic data, current measurements, and the actual feedback algorithms for plasma shape, position, and current control.

Critical information needed for the proper simulation of these discharges is the electron temperature in the plasma scrapeoff layer, or halo region, surrounding the last closed flux surface. This temperature strongly affects the current flowing in this region, the drift speed of the plasma, and thus the forces that result from the disruption. This data has now been obtained for the first time using the multipulse Thomson scattering system. During the drifting phase of the vertical displacement event (VDE) the temperature in the halo region ranges from 25 to 30 eV at the plasma edge to 10 eV near the edge of the halo region. The density increases sharply from below 1×10^{13} cm^{-3} before the motion begins to values up to 1×10^{14} cm^{-3} when the plasma is 40 cm off axis. Additional measurements with the improved Thomson scattering system this coming year should greatly increase the database for disruption simulations.

Another major factor in determining the vessel forces is the time behavior of the plasma current during the disruption. Measurement of the current has been improved by construction of new circuitry to evaluate Ampere's law inside the vacuum vessel using internal magnetic probes. This eliminates the effect of the large vessel currents during disruptions and permits measurements of changes in the plasma current on time scales shorter than the vessel time constant. These studies have indicated that the average current decay rate during disruptions increases linearly with the value of the predisruption plasma current. Further examination revealed that the decay rate for discharges in which a vertical instability precedes the disruptions is as much as 50% larger than for discharges that disrupt with the plasma vertically centered. Despite a significant reduction in the influx of oxygen and metallic impurities after boronization of the vessel, the current decay rate during disruptions was unchanged. The dependence of the current decay rate on impurity content, plasma density, and other plasma parameters will be investigated in the coming year.

Development of a disruption and operations database of discharges has also begun this year. This database will permit analysis of the statistical frequency of disruptions in different operating regimes, the identification of the dominant causes of disruptions, as well as many other issues relevant to plasma disruptions and operation.

In contrast to other high current tokamaks, disruptions in DIII–D do not generate a persistent high current, high energy runaway electron tail. To investigate this anomaly, we are installing an array of high speed hard X–ray detectors around the vessel to look for the characteristic X–rays that are generated when the runaway electrons strike the vessel surface. A particle trajectory code was written to identify the likely areas of interaction of the electrons and the vessel surface for the different magnetic configurations in DIII–D. In collaboration with Sandia National Laboratory (SNL), Albuquerque, two of our disruptions have been modeled using a simplified circuit model of the plasma, vessel, coils, and runaways electrons. Results of the model confirm that the high density observed on many DIII–D disruptions significantly reduces the runaway generation rate. In addition, the inward plasma motion after the thermal quench may account for a rapid loss of runaways electrons on the inside wall before they have been accelerated to very high energies. In the coming year, we will try to test these hypotheses experimentally using the improved diagnostic capability. The measurements of the electron temperature and density during the disruptions should permit much more accurate modeling of the runaway generation.

5.4.2. PLASMA CONTROL

An advanced plasma control system is being implemented for the DIII–D tokamak utilizing digital technology. This system will regulate the position and shape of tokamak discharges that range from elongated limiter to single-null divertor and double-null divertor with elongation as high as 2.6. It will also be used for research on real time optimization of discharge performance for disruption avoidance, current and pressure profile control, optimization of radio frequency antenna loading, or feedback on heat deposition patterns through divertor strike point position control. Development of this system is expected to lead to control system technology appropriate for use on future tokamaks. This digital system is unique in that it is designed to have the speed necessary to control the unstable vertical motion of highly elongated tokamak discharges such as those produced in DIII–D and planned for the International Thermonuclear Experimental Reactor (ITER). A 40 MHz Intel i860 processor is interfaced to 112 channels of analog input signals. The commands to the poloidal field coils can be updated at 80 μs intervals for the control of vertical position with less than 80 μs delay between sampling of the analog signal and update of the command. The shape control algorithm is based on linearization near a target shape of the controlled parameters as a function of the magnetic diagnostic signals. The digital system will allow for increased precision in shape control through real time adjustment of the control algorithm to changes in the shape and discharge parameters.

References for Section 5.4.

[1] Jensen, T.H., and D.G. Skinner, *Phys. Fluids B* **2** (10) (1990) 2358.

[2] Strait, E.J., L.L. Lao, J.L. Luxon, E.E. Reis, *Nucl. Fusion* **31** (1991) 527.

[3] Kellman, A.G., *et al.*, *Fusion Technology* **2** (1990) 1045.

[4] Lao, L.L., and T.H. Jensen, *Nucl. Fusion* **31** (1991) 1909.

5.5. DIAGNOSTICS

5.5.1. OVERVIEW

The DIII–D diagnostic effort in FY91 concentrated on improving and expanding the ADP diagnostics. Improvements to the kinetic profile diagnostics were also made, including increasing the number of spatial points and the spatial resolution of the multi-pulse Thomson scattering system. There are 35 major diagnostic systems operating on a routine basis on DIII–D with an additional seven diagnostic systems under development. Table 5.5-1 lists the major diagnostic systems along with the quantities measured. As can be seen from the table, many of the diagnostic systems involve national or international collaborative efforts. These efforts have been beneficial to both the DIII–D program and to the collaborators and we expect this trend to continue.

5.5.2. NEW OR UPGRADED OPERATIONAL DIAGNOSTICS

In FY91, relatively few new diagnostic systems were added to DIII–D; however, a number of improvements and upgrades to existing systems were completed. Most of the improvements and additions to the DIII–D diagnostic set were made to diagnostics dedicated to measuring edge or divertor parameters. In a collaborative effort with SNL, a fast stroke Langmuir probe was installed that measured the edge $n_e(r)$ and $T_e(r)$ profiles. This new Langmuir probe can make measurements deeper into the plasma than the probe assembly that it replaced since the probe can be inserted into the plasma for short time (50 ms) during a plasma discharge. A divertor visible spectrometer was made operational. This spectrometer is designed to study impurity behavior inside the advanced divertor ring region and was installed in a collaborative effort with ORNL. A modification to the survey, poor resolution, extended domain (SPRED) spectrometer diagnostic completed in FY91 allows measurements of edge impurity profiles. Upgrades of the data acquisition systems for the infrared (IR) divertor TV and the divertor Langmuir probes have substantially improved the quality of the data from those systems.

TABLE 5.5-1
PLASMA DIAGNOSTICS

Diagnostic	Quantity Measured	Comments
Operations-Related Diagnostics		
Magnetics	$\dot{B}$, Magnetic	2 poloidal (58), 1 toroidal (8) mag. probe arrays with 50 kHz response; 41 flux loops, 9 diamagnetic loops, 30 saddle loops, 3 I_p Rogowskis
Hard X–rays		2 toroidal locations, 4 detectors, 1 kHz response
Plasma TV	Visible TV	Radial view, 180° limiter, divertor
IR cameras	Heat load to armored surfaces	180° limiter, upper divertor; inside wall lower divertor (LLNL)
Photodiodes	H_α radiation, recycling	H_α filtered, 16 locations, 10 kHz response
Neutron detectors	Fusion and photo-neutrons	3 toroidal locations, 200 Hz response
Soft X–ray arrays	Internal fluctuations	1 vertical, 1 horizontal, 32 ch. ea. >250 kHz response, ~4 cm resolution, 4 toroidal locations, 12 ch. ea. 100 kHz
Electron Profiles		
ECE grating radiometer	$T_e(r,t)$	Radial profile, 10 ch., 0.1 msec
Multipulse Thomson profile	$T_e(r,t)$, $n_e(r)$	Multiple lasers, 20 ms (upgrade to 6 ms), vertical profile, 40 pts., <1 cm in edge resolution, 20 keV > T_e > 10 eV
CO_2 interferometers	$\bar{n}_e$	Vertical, 3 chords; radial, 1 chord
ECE Michelson	$T_e(r,t)$	Radial profile, each 25 msec

TABLE 5.5-1 (Continued)

Diagnostic	Quantity Measured	Comments
Fluctuations		
Microwave reflectometer	$n_e(r,t)$, $\tilde{n}_e(r,t)$	UCLA collaboration – broadband; system gives profile in 5 ms, narrowband system, 400 kHz bandwidth
Correlation reflectometer	Radial correlation lengths in $\tilde{n}$	UCLA
FIR scattering	$\tilde{n}_e(r,t)$	UCLA collaboration – 4 MHz bandwidth
CO_2 scattering	$\tilde{n}_e(r)$	MIT collaboration – phase contrast 1kHz, 100 MHz bandwidth
Ion Temperature and Rotation		
Charge exchange recombination	$T_i(r,t)$, $v_\phi(r,t)$, $v_\theta(r,t)$	16 channels bulk plasma; 16 channels edge plasma; 3 mm T_i edge resolution; 6 mm v_ϕ, v_θ, edge resolution
Impurities and Boundary Parameters		
Visible bremsstrahlung	$Z_{eff}(r,t)$	Radial profile, 16 chords, 1 kHz
Bolometer array	Radiated power	Radial profile, 21 ch., 1 kHz
SPRED (dual range)	Impurity concentrations	280-1200Å; 100-290Å, spectrum every 1 msec; edge profiles with scanning capability
H_α TV	Divertor H_α	LLNL
Divertor IR camera	Heat load to divertors	LLNL, GA, 125 msec for a profile
Langmuir probes	Edge $T_e(t)$, $n_e(t)$	On divertor tiles
Laser blowoff system	Impurity injection	Impurity transport
Fast stroke langmuir probe	Edge $T_e(t)$, $n_e(t)$	SNL

TABLE 5.5-1 (Continued)

Diagnostic	Quantity Measured	Comments
Impurities and Boundary Parameters (Cont.)		
Fast pressure gauges	Neutral pressure	Near divertor region (ASDEX, LLNL), 2-3 msec response
Tile current monitors	Poloidal tile currents	Includes tile currents in the ADP
Divertor visible spectrometer	Divertor impurity concentrations	ORNL
Divertor Baratron gauge	Neutral pressure	ORNL – verified ASDEX gauge measurements
Fast Ion Diagnostics		
Scintillator	Neutron fluctuations	50 kHz response time
E||B charge exchange	Beam-ion density profile	Conventional charge exchange analyzer coupled with H_α detectors used to measure beam neutral density profile, scannable, spectrum in 1 ms
Fusion products	Fast neutrons tritons He^3, other fast ions	UCI collaboration; movable probe assembly
Current Drive Diagnostics		
Motional stark effect (MSE)	$B_p(r)$	Scannable single channel upgraded to 6 radial channels; 2 cm resolution, 5 msec response
ECE Michelson	Microwave emission	Detects tail population in the electron distribution function, profile in 25 msec (LLNL and Maryland)
SXR pulse height	High energy X–ray spectrum	Soviet collaboration; detects tail population in electron distribution; spectrum every 100 ms

TABLE 5.5-1 (Continued)

Diagnostic	Quantity Measured	Comments
In Development		
Multipulse Thomson	$n_e(r,t)$, $T_e(r,t)$	Upgrade to eight 50 Hz lasers
Bolometer upgrade	Radiated power	2 arrays – 20 ch. ea., 1 kHz
DIMES	Surface erosion	DIvertor Material Exposure System
ADP RGA	Neutral gas mass spectrometer	ADP physics RGA
Second lower divertor IR TV	Heat load to divertor	Designed to measure toroidal asymmetries
Li beam	Edge $\tilde{n}(r,t)$	Turbalance measurement near the edge
Fast magnetic probe array	$\tilde{B}_\theta$	Frequency response >500 kHz

The phase contrast interferometer, a collaborative effort with MIT and designed to measure density fluctuations, became operational in FY91. The radial viewing carbon dioxide (CO_2) interferometer channel was modified to better handle the carbon coating of the inside wall mirror. A 3.3 micron HeNe laser was incorporated to compensate for vibrations of the mirrors. This new configuration closely matches a proposed ITER interferometer design.

5.5.3. DIAGNOSTICS UNDER DEVELOPMENT

Our FY92 diagnostic plans emphasize strengthening of the radio frequency (rf) relevant diagnostic set and improvements in our fluctuations measurement capabilities.

In the rf area, a reflectometer incorporated into the ICH antenna is planned in collaboration with ORNL and UCLA. This new reflectometer will be used to study the local density profile in front of the antenna. In collaboration with LLNL, the Motional Stark Effect (MSE) diagnostic that measures the poloidal magnetic field B_p, will be upgraded to six spatial channels in late FY91. This will provide single-shot plasma current profiles, useful for current drive studies, and greatly improve the quality of our magnetic equilibrium calculations. A second rf magnetic probe will be installed to measure toroidal asymmetries produced by the ICH current drive.

Fluctuation measurements will be enhanced by a new lithium beam diagnostic and a new magnetic probe array. The lithium beam was developed at General Atomics and will be used to measure density fluctuations at the edge. The lithium beam and associated detection hardware will be installed in the first part of calendar year 1992. A high speed magnetic probe array has been built and will be installed in early FY92. The magnetic probe array, which has better high frequency response and spatial resolution then probes previously installed on DIII–D, will primarily be used to study TAE modes.

The very successful multipulse Thomson scattering system is being upgraded to include eight lasers each operating at 50 Hz. This will provide a complete 40 point temperature and density profile every 6.25 ms during the entire plasma pulse. A second divertor IR TV camera (LLNL) will be installed in order to study possible toroidal asymmetries in the heat load to the divertor tiles. A more complete list of diagnostics that are under development can be found in Table 5.5-1.

5.6. RELIABILITY AND AVAILABILITY

5.6.1. INTEGRATED PREVENTIVE MAINTENANCE PROGRAM

The DIII–D Project has implemented an Integrated Preventive Maintenance Program (IPMP) which places all of the preventive maintenance tasks into a common computerized database. The IPMP utilizes a database program named Maintstar. Previously, each of the various technical groups which support the DIII–D Project were responsible for their own preventive maintenance (PM) program. This created a large array of widely differing PM programs. Currently, the following group's equipment is in the IPMP;

1. Vacuum Systems
2. Water Cooling Systems
3. Air Systems
4. Cryogenic Systems
5. Prime Power/Motor Generator (MG)
6. B, E, and F–Coils Power Systems
7. Neutral Beamlines Power Systems
8. Neutral Beamlines Mechanical
9. Diagnostics
10. Electron Cyclotron Heating Systems
11. Ion Cyclotron Heating Systems
12. Mechanical Systems
13. Electronic Systems
14. Operations
15. Facilities

Equipment PM data was taken from manufacture's manuals whenever possible, or past maintenance practices, or engineering estimates were made. PM work orders are issued twice monthly to the lead technicians. The lead technicians are responsible for ensuring that the PM task gets completed in a timely manner. Additionally, they verify

the accuracy of the completed PM work order sheet. Besides labor hours and parts and material costs, all pertinent information and observations about the equipment are noted on the PM work order sheet. The information about the completed PM tasks is then fed back to the IPMP via the work order. Any maintenance changes to the equipment are noted in the IPMP and is followed up at the next maintenance period or as needed. The PM task is then closed out. Corrected Maintenance (CM) or nonscheduled tasks are handled in a similar manner. Thus, a complete maintenance history (both PM and CM) is being developed for each piece of equipment within the IPMP. Eventually, each of the groups shown above were brought into the IPMP on a group-by-group basis. At the end of this reporting period, there were 861 pieces of equipment in the IPMP.

5.6.2. SIGNIFICANT EVENT REVIEW

In March of this year, DIII–D Management initiated a Significant Event Review (SER) procedure. The purpose behind these reviews is to learn from past events what causes the problem and thus permanently eliminating the reoccurrence of events which result in unanticipated costs or expended effort. The philosophy is to avoid problems with better design, procedures, *etc.* The SER brings together key personnel involved in the event with key people from related parts of the organization to discuss the event and propose courses of action. The SER is followed up with a Significant Event Report.

There have been three SERs held during this reporting period. The SERs were held regarding: (1) damage to three NB arc chambers; (2) design, installation, operation, and scheduling problems for the Edge SPRED Diagnostic; and (3) the rupture of a plastic line that carried city water for fire protection and equipment relying on tower cooling for operations. The course of action followed for these SERs resulted in changes to documentation such as procedures, drawings, *etc.*

5.7. RADIATION MANAGEMENT

The total neutron radiation dose at the site boundary for FY91 was 3.8 mrem, the total gamma radiation was 1.7 mrem, giving a total site dose for the year of 5.5 mrem. (This is below the SAN DOE annual guideline limit of 20 mrem and the California annual limit of 500 mrem.)

The total exposure dose personnel received (which also includes the dose from being on-site during operations) was kept below the DIII–D procedural limits of 25 mrem per day, 100 mrem per week and 300 mrem per quarter. The highest dose accumulated by an

individual from pit runs and vessel entries for FY91 was 75 mrem; 88 people had doses less than 25 mrem; 6 people had doses between 26 and 50 mrem, and 3 people had doses between 50 and 100 mrem. All doses were logged in the database of personnel radiation doses.

Radiation safety training was provided for new personnel. The DIII–D work authorization was reviewed with the "DIII–D Radiation Procedures" and the "DIII–D Access Control Procedures" revised. The updated procedures were approved by the General Atomics Health Physics Department.

A portable weatherproof monitoring station to house a neutron and a gamma detector was built for use in performing site boundary surveys and the periodic (every 2 years) survey of the site boundary radiation began. Data for all the site positions along the public boundary have been collected and the permanent site monitoring station continues to be the highest radiation point as in the past.

A radiological safety inspection of the DIII–D facility was conducted by the General Atomics Health Physics organization; five findings were identified and all required actions were completed in a timely manner. The facility and its radiation producing devices were also inspected by a county inspector.

Plans for penetrating the shield wall for the ADP cryoline were discussed and calculations were made of the increase in site radiation. Calculations give an increase in site radiation of 1% for the 4-in. hole required for the line and an increase in radiation 15 ft from the wall of 13% for the 4-in. hole if no additional shielding is provided. The radiation outside the pit run door was remeasured to provide a basis for comparison after the hole is made.

Gaps in the pit shield wall were discovered and filled with shielding material and penetrations were made for installation of ECH waveguide.

A large number of items removed from the machine pit have been checked for activation and those with radiation levels above background are in storage.

5.8. ELECTRICAL ENGINEERING

The electrical engineering activities centered on upgrades to the existing electrical power capabilities, system improvements, and preventative maintenance. Several tasks were completed; regulation accuracy of the 80 kV Modulator/Regulator power supply used for ECH operation was improved, and improvements were made to the crowbar systems in

the NB power supplies resulting in more reliable beam operation. One new power regulator (chopper) for use in the field shaping coil system was constructed. A study was conducted on possible increased current operation of the toroidal field power supplies. The toroidal field power supplies have been routinely operated at 126 kA near the design maximum value. The thyristor phase control rectifier ratings limit the toroidal power supply system to approximately 0.75 s maximum pulse length at an increased toroidal coil current of 146 kA.

Several new diagnostic, vacuum, and cryogenic system related tasks were completed by the instrumentation and control system group; Thomson Multipulse alignment system upgrades were completed and checked out. ADP ring cryopumping hardware and software was installed for vacuum/cryocontrol. Vacuum vessel conditioning boronization interlocks and control system were completed. An upgrade of the prestress monitor system was completed. Installation of remote signal interfaces from the ECH control room were completed. A heater blanket control rack was assembled and installed for the 110 GHz system.

The following new tasks are in progress: implementation of an Advanced Plasma Control System for DIII–D is continuing, studies are under way to define needed upgrades to the DIII–D electrical systems in support of long pulse experiments. A new control system and control panel for the D1 power supply has been constructed and is currently being installed. The DIII–D facility electrical panel documentation is being reviewed and updated.

A systematic review of recurring problems has been initiated with aim to improve the overall reliability and availability of the power systems. This process has already identified areas of needed improvements. Design improvements are currently being made to the master gate drive circuits for the toroidal and poloidal power supplies. Uninterruptible power supplies which have been in use since the start of the Doublet III program are now in the process of being replaced. All DIII–D electrical systems have now been integrated into the new preventative maintenance program.

Major preventative maintenance was performed on two high voltage transformer-rectifier (HVTR) sets. This involved untanking and reshimming of coils. One additional HVTR is currently being upgraded with new coils for higher voltage operation at a transformer manufacturers facility. Higher voltage (90 kV) beam operation was tested successfully with one upgraded HVTR, and then four additional NB systems were upgraded and

operated at the 90 kV voltage level. The latter four HVTRs were of a design permitting higher voltage operation without rewinding of the secondary coils.

5.9. MECHANICAL ENGINEERING

5.9.1. TOKAMAK SYSTEMS

5.9.1.1. Divertor Material Exposure System (DIMES). This system provides a means to insert material samples into the machine without the need for venting the vessel. This is done by remotely operating a vertical ram mechanism upward through an isolation valve into a bottom vessel port. The samples are made, initially from graphite, although other materials may be selected for future studies.

The mechanism originally selected was an acme threaded screw system driven by an electric gear motor through a gear train. Although the basic system was simple, an unacceptable amount of internal friction developed during the test phase. Additional design studies have since been made to develop a device which does not require sliding surface friction. The current design uses a telescoping hydraulic cylinder arrangement coupled with a bellows to provide the primary vacuum seal.

The vacuum and control system designs for the overall diagnostic have been completed and are ready for final installation.

5.9.1.2. Outer Wall Tile Upgrade. A series of graphite tile arrays has been designed for installation on the outer wall inside the vacuum vessel. One tile array consisting of two horizontal courses surrounds the outer wall just below the existing ceiling tiles. Three additional arrays, oriented poloidally, are spaced at approximately uniform intervals around the vessel at 55°, 190°, and 305°. These poloidal arrays are one tile wide and extend vertically from the $R-1$ area to the $R+2$ area. In addition, a group of 14 Inconel tiles is being fabricated for installation around the 255° $R+1$ port to protect the 110 GHz ECH launcher assemblies.

The 260 new graphite tiles provide additional coverage equal to about 10% of the outer wall surface exposed to the plasma. The tiles are not intended to function as a primary limiter, but rather to provide protection for the vessel and to minimize plasma contact with high-Z atomic mass materials. Installation of the new tiles is expected to occur during the first quarter of FY92.

5.9.1.3. Replacement of the Faraday Shield on the Fast Wave Current Drive (FWCD) Antenna. Work is in progress at ORNL to design and fabricate a replacement Faraday

shield for the FWCD antenna. The new shield is designed to install directly onto the existing antenna housing. The replacement shield consists of a single layer of Inconel rods oriented at a 15° angle with the horizontal to more closely match the field lines. Some minor modifications are required on the antenna housings to accommodate the thermal and mechanical stresses which develop with the slanted rod arrangement.

In addition, a series of four reflectometer horns is also being designed by ORNL to install in the narrow space immediately adjacent to the FWCD antenna in the 285°-300° port area of the vessel. The waveguides for these rf horns will exit the vessel through small instrumentation ports installed in the 300° port cover for that purpose.

5.9.1.4. Belt Bus Joint Monitoring and Replacement. DIII–D contains a total of 96 belt bus flexible joints in the toroidal field system. A small number of these joints have either shown or developed high resistance over the past few years based on routine monitoring. As a result of this program, two of these joints were replaced during the last fiscal year, while an additional five joints were either tightened in place, or else removed, reworked, and reinstalled. In each case except one, the resistance of these joints returned to normal and has remained satisfactory since being serviced. One joint continues to show signs of increasing resistance over the long term. A replacement is planned for next fiscal year.

A belt bus redesign effort has been undertaken to develop a more robust and reliable joint. The Italian firm of Istituto Gas Ionizzati, Padova, Italy, has already developed and tested a similar joint for use on the RFX toroidal field coils using an electron beam welding procedure. Samples of these joints have been inspected and preparations are in progress at DIII–D to develop a replacement joint based on this design.

5.9.1.5. Diagnostic Support Activities. Mechanical Engineering has provided design and analytical support for a number of diagnostics during FY91. Some of these activities involve extensive projects while others are simple modifications designed to improve existing equipment.

1. New Bolometer Array. Two arrays of 48 sensors each are being designed for installation in two vacuum vessel ports: 195° $R-1$, and 210° $R+2$. Engineering work involving electromagnetic shielding, electronics, and vacuum compatibility has been addressed through the end of FY91. The sensors selected have also been analyzed for temperature stability and level of outgassing.

2. Lithium Beam Diagnostic. The Lithium beam diagnostic is planned for installation in the R+1 port at 75° on the vacuum vessel. The diagnostic instrument is being developed by the physics division, with the actual supports and installation being

designed and fabricated by mechanical engineering. A magnetic shield box required for this diagnostic is being fabricated from a special 4750 nickel-iron alloy. Availability of this material was difficult, but sufficient lead time for delivery was provided in the program to avoid scheduling problems.

Modifications have been made to the local platform area to provide the necessary access for the diagnostic and its supports. The vessel interface valves and fittings are scheduled for installation during the first quarter, FY92, with the actual diagnostic installation to follow in the second quarter.

3. High Frequency Magnetic Probe Diagnostic. This diagnostic incorporates a group of five magnetic pickup coils mounted on a small stainless steel structure suspended from a port flange. The coils are wound on machinable macor ceramic, with the leads carefully threaded through alumina insulators to a ceramic feedthrough on the port flange. This equipment was designed by the physics division, and engineered, fabricated, and assembled by mechanical engineering. Installation is scheduled for the first quarter FY92.

4. Edge SPRED Diagnostic. This is a very lightweight mechanical structure which supports and positions two gold plated mirrors designed to reflect extreme ultraviolet light at a very low angle of grazing incidence with the mirror surface. The mirror structure is supported on a long arm which is driven in a sinusoidal manner by a stepping motor.

   This equipment is installed at 330°, $R - 0$, adjacent to one of the NBs. A special double bellows design has been incorporated to allow input of the sinusoidal motion through the vessel vacuum boundary. Installation of this diagnostic occurred in April 1991.

5.9.2. FLUID SYSTEMS

5.9.2.1. New Helium Liquefier System. Based on planned future increases in capacity requirements, procurement activities were initiated for a new helium compressor and liquefier. Steady state liquid helium usage was projected for the next two years. The projections include usage by: NBs, the ADP cryopump, ECH magnets, and a pellet injector. The steady state usage is estimated to be 120 ℓ/h. Our present liquefier has a capacity of 80 ℓ/h.

5.9.2.2. Advance Divertor Prototype Demonstration. In support of the ADP, a prototypic cryopump was built and tested to assure that the pump will perform in a stable manner

at the higher than expected pressures being observed under the divertor baffle. Testing was also performed to determine the critical heat flux of the cryopump. All tests were satisfactorily completed and confirmed the design basis.

Design of the cryosystem, external to the vessel, that will supply liquid helium and liquid nitrogen for in-vessel cryopumping was completed. The 30 meter cryo-transferline purchased from Kabelmetal Company, Germany was received. Fabrication of other major system components: the cryostat and the cryogenic distribution is nearing completion.

5.9.2.3. New Water Cooling System. The fabrication and erection task for the high capacity, low pressure, deionized water cooling system for vessel auxiliary heating components was recommenced. This task was stopped in 1989 in order to redirect available funds and be consistent with the need date of the extended 2 MW, ECH program schedule. The design was reviewed for current validity and procurement activities initiated.

5.9.2.4. Boronization Program. In support of the decision to do vessel boronization at DIII-D, two facilities, TEXTOR and ASDEX in Germany were visited to learn about their systems to boronize tokamaks. A system design for DIII-D was prepared, reviewed, and approved. The boronization system including the transmission line was fabricated, assembled, and installed. The entire system was checked out using helium gas. The boronization Hazardous Work Request (HWA) was prepared by engineering, reviewed, and approved by the Fusion Safety Committee and the system placed in operation. The vessel's first boronization was satisfactorily performed on May 18, 1991. Subsequent boronizations have been successfully performed.

SECTION 6

PROGRAM DEVELOPMENT

6. PROGRAM DEVELOPMENT

6.1. PROGRAM DEVELOPMENT OVERVIEW

There were two main DIII–D program development activities in FY91. These were the Advanced Divertor Project (ADP) and the 110 GHz Electron Cyclotron Heating (ECH) and Current Drive (ECCD) program. These programs are targeted at providing new capabilities which will facilitate DIII–D experimental programs oriented toward the development of steady state current drive and boundary layer control technologies. Since these areas are recognized as critical points in the development of fusion reactor designs, we expect that results from these DIII–D activities will be of particular importance during the next few years.

6.2. ADVANCED DIVERTOR PROJECT

6.2.1. INTRODUCTION

The implementation of hardware supporting the ADP provides a unique opportunity to carry out DIII–D experiments aimed at developing new boundary layer control techniques. Results from these experiments are expected to open up improved performance parameter regimes and lead to an overall reduction in critical component failure risks. The principal experimental attributes associated with the ADP are: (1) provide density control during the high confinement H–mode phase of the discharge for transport and current drive studies, (2) produce low collisionality plasmas for current drive experiments, (3) break the linkage which is typically found to exist between the plasma current and the electron density, (4) provide a means of injecting helicity into the discharge for steady state current drive, (5) to control and minimize energy deposition profiles on the divertor target plates by sweeping the bias ring voltage, and (6) study the effects of edge currents on the plasma stability.

6.2.2. ADVANCED DIVERTOR STUDIES

Results obtained during the ADP experiments in FY91 were very positive. These have been reviewed earlier in Sections 2.2.3 and 2.2.5 of this report. Results which are

of particular significance for the future development of the program include those related to pressure buildup under the divertor ring and implications coming out of the biasing experiments. For example, in the area of helium ash removal, a critical issue for ITER and other future long pulse ignition devices, our observations indicate that helium accumulations can be prevented with a moderate pumping speed. In addition, biasing affects heat and particle flow to the divertor as well as the power required to achieve high confinement H–mode. Further, while biasing does not seem to affect edge localized mode (ELM) stability, it can alter the time duration of an ELM, and affects edge magnetic fluctuations in rapidly ELMing plasmas.

In addition to our experimental ADP programs, numerical modeling has been instrumental in gaining a quantitative understanding of the ADP pressure scaling results. A version of the plasma transport B2 code was applied to the analysis of the scaling experiments, in concert with neutral partical transport simulations obtained from the DEGAS code. While estimates made during the conceptual design phase indicated pressures of approximately 1 mTorr (without pumping), these estimates were made before including B2 modeling effects on the divertor pressure. The modified DEGAS results, using the B2 fluxes, indicate a pressure of roughly 5 mTorr for a neutral beam power $P_{NB} = 7$ MW (experimentally pressures of 7.5 mTorr were measured) and pressures in the 8–14 mTorr range for $P_{NB} = 14$ MW (experimental values of 12 mTorr). The remaining discrepancy is very sensitive to details of the electron density and electron temperature distributions in the wings of the scrapeoff layer. Efforts to obtain information about these profiles will be undertaken in FY92.

6.2.3. HARDWARE DEVELOPMENT

6.2.3.1. Divertor Ring and Baffle. The first phase of the Advanced Divertor was completed in the summer of 1990. When two new major components were installed in the tokamak. The first is an electrically isolated toroidally continuous ring electrode in the outer lower divertor region that is biased with a 1 kV–20 kA power supply. The second major addition is a toroidally continuous gas baffle between the outer wall and the biased ring. The volume created behind the toroidal baffle is equipped with neutral gas pressure gauges and will be equipped with a cryogenic pump in 1992. Either divertor bias or divertor baffle modes can be run by adjusting the position of the outer divertor strike point using the field shaping coils. In the bias mode, an external power supply drives scrapeoff layer currents in experiments to study particle transport modification, second stability limits, and helicity injection current drive. The baffle mode tests density control, particle

exhaust and tokamak operation with net particle throughput. Finally, by moving the lower divertor strike point further inward, the plasma can be removed from interaction with the Advanced Divertor which was designed for minimal intrusion on the plasma volume and minimal limitations on normal plasma operation.

The toroidally continuous ring electrode is made of Inconel 625 for its strength, relatively high electrical resistivity, and high temperature capability. The ring has two parallel coolant channels machined and welded into it. This coolant channel is connected to the same air/water system used for the walls and ports of the DIII–D vessel. During bakeout, hot air flows through the channels while water flows during operation. The ring electrode is armored with graphite tiles made of the same basic design and material as the vessel armor tiles. The ring is supported off the vessel floor by 24 local Inconel 625 brackets. The supports are sufficiently flexible in the radial direction to accommodate modest differential thermal growth.

Experience with the biased ring in FY91 has revealed several weak points in the original insulation design. An arc to a water lead during the first quarter of FY91 caused an in-vessel water leak. The arc damage was quickly repaired and a campaign to upgrade the ADP electrode insulation system to withstand ± 3 kV in air and vacuum was completed. In addition, a peak voltage detector and a wide band voltage divider to detect and characterize possible fast voltage spikes on the electrode was installed. During subsequent operations, the 3 kV standoff capability slowly degraded to 2 kV, and ring biasing operations were suspended. The ring was grounded at the power supply. The peak voltage detector has recorded very fast disruption driven voltage spikes in excess of 5 kV in this configuration. These spikes are possible in this grounded configuration due to the inductance of the system. A subsequent in-vessel water leak due to arc damage occurred while the ring was grounded.

Post-operations visual inspections have revealed some common sites for arcing. Moderate to severe arc damage has been seen at the ring-support interface, most notably at the lower outer corner of the support bracket; at the insulating bolt joint between ring and support; and at the water leads near the ring. Evidence of arcing along insulator surfaces which have been partially coated by metal and carbon vapor during extended operations has also been seen on the the underside and top of the ring.

A redesign of the insulation in all of these areas has been accomplished. See Fig. 6.2-1 for a comparison of existing with redesigned insulation. The support bracket outer lower corner has been redesigned to accommodate a ceramic corner between the ring and the

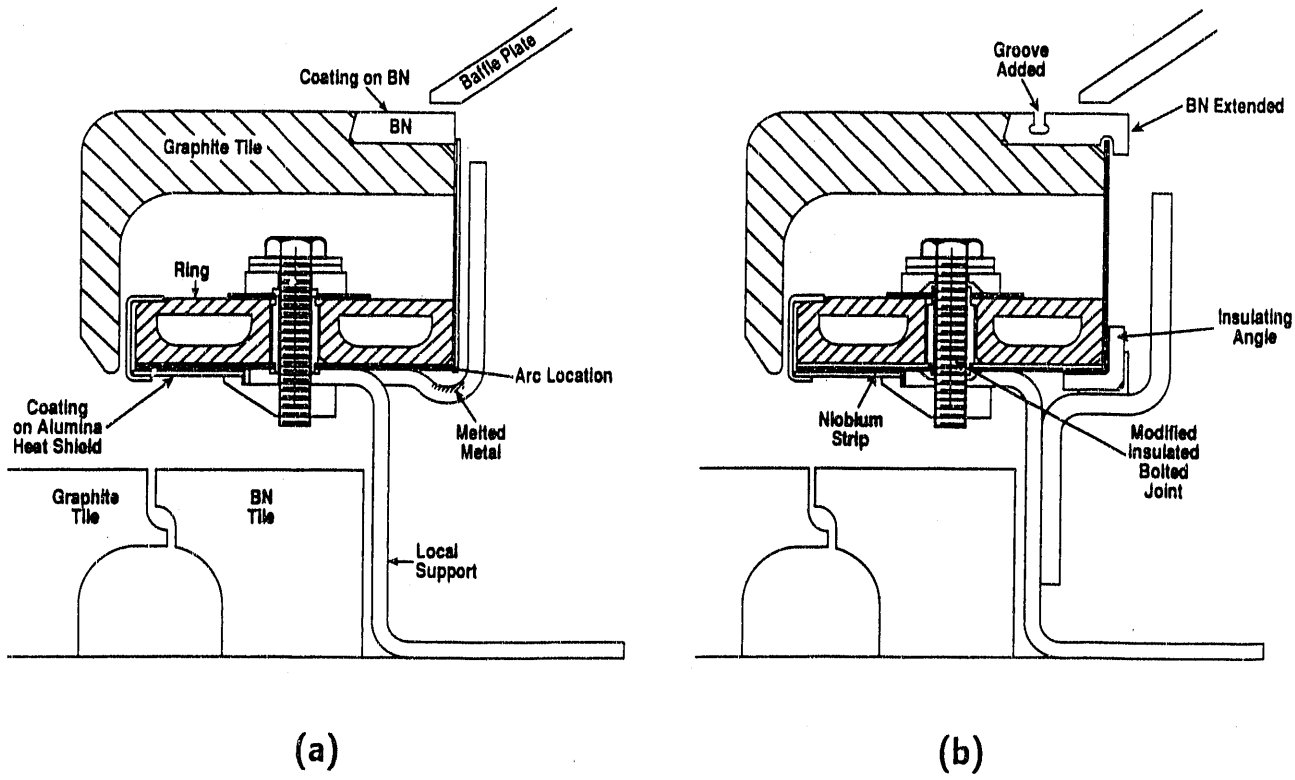

Fig. 6.2-1. Original (a) and redesigned (b) ring cross sections: (a) indicates some of the common arc areas discovered during FY91 operations, and (b) indicates redesigns of these areas.

support. This ceramic corner now captures a Mica Mat sheet insulating the outer face of the ring, replacing a butt joint that had several arc failures. In addition, a policy of radiusing all corners in critical areas has been adopted. This includes the outer lower corner of the ring, and all relevant corners in the insulating ring support bolt joint. The boron nitride insulation located at the ring top outer corner now has deep path-lengthening shadowing grooves cut toroidally to inhibit the formation of a continuous metal vapor coated surface extending from the graphite ring tile to the baffle plate.

The water and current feeds and feedthroughs have been completely redesigned. Water leads have been reduced to two from four, and run colinearly with the electrical feeds. The electrical feeds are now very rigid and straight, with all motion due to thermal growth and magnetic forces accommodated by an internal pivot and an insulated bellows port. The combination electrical/water feeds are now insulated with removable machined ceramic dam shells from the bellows region up to the ring. Grounded metal shield cans

surround the insulation to prevent surface charge driver arcs. These shield cans will have current monitors to detect arcing between the cans and the water leads within.

The installation of the redesigned ring insulation and feeds will take place during the long vent in the first quarter of FY92. Biased ring operations will begin early in the second quarter of FY92.

6.2.3.2. Diagnostics and Analysis Tools. We have added or upgraded a number of edge plasma diagnostics and analysis codes to help interpret the experimental results. The central diagnostic task for divertor biasing will be to determine the path of current flow in the scrapeoff layer plasma and to document how it affects transport. For the pumping and baffling experiments, we must determine the particle throughput to the pumps, as well as the distribution of gas in the plasma boundary. A summary of the ADP diagnostics which are currently in use is given in Table 6.2-1.

TABLE 6.2-1
SUMMARY OF CURRENT ADVANCED DIVERTOR PROJECT DIAGNOSTICS

Diagnostic	Measurements	Collaborator
Tile Current Arrays (Poloidal and Toroidal)	Poloidal current flow into the divertor and inner wall armor	GA
Baffle Plate Current Monitors	Poloidal current flow into the baffle plate	GA
Fast Insertion Langmuir Probe	Edge plasma n_e, $\tilde{n}_e$, T_e, ϕ, $\tilde{\phi}$	UCLA/SNLA
Divertor Langmuir Probe Array	n_e, T_e at divertor target plates	SNLL/GA/LLNL
Divertor Visible Spectroscopy	Divertor and impurity line profiles	ORNL
Fast Neutral Pressure Gauges	Neutral gas pressure under the baffle and divertor target vicinity	ORNL/GA
Divertor H_α TV	Divertor image from a tangential view	LLNL
Divertor IRTV	Power flux to divertor floor	LLNL/GA
Bias Ring Instrumentation	Ring voltage, current, and temperature	GA
Ring Feed Shield Monitors	Ground shield current and voltage	GA

The tile current monitors are used to obtain a detailed picture of the poloidal current flow patterns. Some of the individual tile current monitors were damaged during FY91 operations. These will be repaired during the first quarter FY92 vent. In addition, two baffle plates separated roughly 90° toroidally will have current monitors added. These monitors are similar in design and capability to the tile current monitors, and will complement tile current data.

In order to more closely monitor arcing to the water leads, each of the grounded feed shield cans will have current monitors to detect arcs which terminate on the shields.

The fast insertion Langmuir Probe is now fully operational and will be available to ascertain the scrapeoff layer radial potential profile with a biased ring. This data can be extended in past the separatrix for Ohmic and low power neutral beam heated plasmas. This new data will both complement and extend the data measured by the existing divertor floor Langmuir Probe Array.

The effects of biasing and cryopumping on divertor particle flux will be monitored with the existing divertor spectroscopy systems and neutral gas pressure gauges. A capacitance nanometer was installed in the fourth quarter of FY91 to measure neutral gas pressure in the private flux region. This gauge complements the existing fast ASDEX type neutral pressure gauges located in the baffle and private flux regions. Power flux to the divertor floor region is monitored by an existing infrared camera. The data from these measurements can be interpreted by DEGAS and B2 computer codes to give divertor recycling and power flux in the divertor channels.

Ring voltage, current and temperature monitors are now in place. In addition to monitoring the current driven into the he plasma, the current and voltage monitors provide some information about arcs from ring to vessel. This information was inadequate to locate arcs in critical areas. In order to more closely monitor arcing to the water leads, each of the current/water feed shield cans will be grounded through a low impedance current shunt monitor. This will allow detection of arcs which terminate on the shield cans.

6.2.3.3. Advanced Divertor Cryopump. The choice of a cryopump located in the baffle region over other pumping schemes was made in FY90. A practical conceptual design was completed and favorably reviewed by the JET team working on a similar cryopumped divertor. A detailed design was completed in the first quarter of FY91. In this detailed design, pumping of the divertor region is achieved by cryocondensation on a surface cooled to 4.3°K by liquid helium. The pumping surface is a tubular configuration and is protected from energetic particles and thermal radiation by two concentric shields. The innermost

shell is liquid nitrogen cooled and the outer shield "floats" between liquid nitrogen temperature and ambient temperature. The whole assembly has been designed to withstand the extreme temperature excursions due to baking (700°K). The use of a single feed point for all cryogenics has reduced the high mechanical loads due to induced eddy currents and allows the use of low heat leak supports to reduce the cryogen consumption. The total steady state heat load to the helium is less than 10 W. Analysis shows that a liquid helium flow rate of 5 gm/s is required to ensure flow stability in the liquid helium cooled tube. A particle removal rate of approximately 20 torr-ℓ/s has been predicted using numerical modeling codes.

Biased ring experiments have measured baffle pressures of order 10 mtorr. This raised the question of ability of the cryopump design to handle the higher heat load from the elevated pressures. A heat loading experiment was performed on a prototype section of cryopump. The experiment showed that the higher heat loads to the cryopump would not significantly affect pump stability for deuterium operation but would be marginal for long (20 s) pulse hydrogen operation.

The question of a possible arcing fault of the cryopump due to disruption voltage transients and the resultant consequences were studied intensively. It was determined that electrical insulation against arcing could not be guaranteed and the resulting high arc currents would result in forces that would fail the cryopump mechanically. Therefore, it was decided to postpone the installation of the cryopump until Spring 1992 to allow time for the additional analysis and design work. Following this decision, we initiated conceptual design studies for a pump that would survive high current disruptions. Three concepts were investigated:

- A ruggedized pump which is toroidally continuous, both electrically and mechanically.
- A ruggedized pump which is only electrically toroidally continuous.
- A toroidally segmented pump which is exposed to disruption voltages too low to cause arcing.

The first concept was considered to be the most reliable, however, it was rejected since a design concept which could satisfy conflicting thermal and mechanical constraints was not found. The other two concepts were shown to be feasible and are presently subjects of intensive thermal and mechanical design studies.

An experiment was designed to test plasma sprayed ceramic insulation techniques in a hydrogen glow plasma environment similar to the ADP baffle environment. Tests revealed that relatively thick plasma sprayed coatings can routinely hold off kilovolt potentials. However, the ability of vendors to cover large irregular areas without fault is still an issue, as is the coatings' reliability over repeated thermal cycles.

Design of the out-of-vessel cryosupport system was completed in FY91, subject to possible rerouting of the feed lines as required by the final cryopump design chosen. Design of the cryostat and radiation shield was completed and the cryostat is about 70% assembled. All major components have been received. The distribution box is designed, and one liquid helium and liquid nitrogen transfer line was specified and received from Kabelmetal GmbH. One of the cryopump options now being considered would require a redesign of the transfer system at a significant cost increase.

6.3. 110 GHz ECH SYSTEM

6.3.1. INTRODUCTION

The DIII–D radio frequency (rf) heating program targeted to address specific needs not being considered on other devices and fosters DIII–D programatic goals in the areas of confinement improvement, high beta operation, and long pulse operation. A unique application of the DIII–D ECH system is to raise the temperature and beta of the electron component so that the damping of the traveling fast wave is strengthened. It is expected that 10 MW of ECH 110 GHz with 8 MW of fast wave current drive at 120 MHz 2 MA of noninductive current at 5% volume-averaged beta in DIII–D. The first phase of this program is to develop and operate a system with 2 MW at 110 GHz for up to 10 seconds.

The basic arrangement of the 110 GHz ECH system is shown in Fig. 6.3-1. Besides the rf unit, which efficiently produces and transmits the high power microwave energy to the DIII–D tokamak, several other pieces of equipment are needed to support the rf unit. It is important for overall system reliability that each subsystem operate at rated performance with high efficiency.

The ECH system consists of four 500 kW gyrotrons to generate 110 GHz microwave power with pulse widths up to 10 seconds. Low loss transmission systems transmit this power to the DIII–D tokamak. The overall specifications are given in Table 6.3-1.

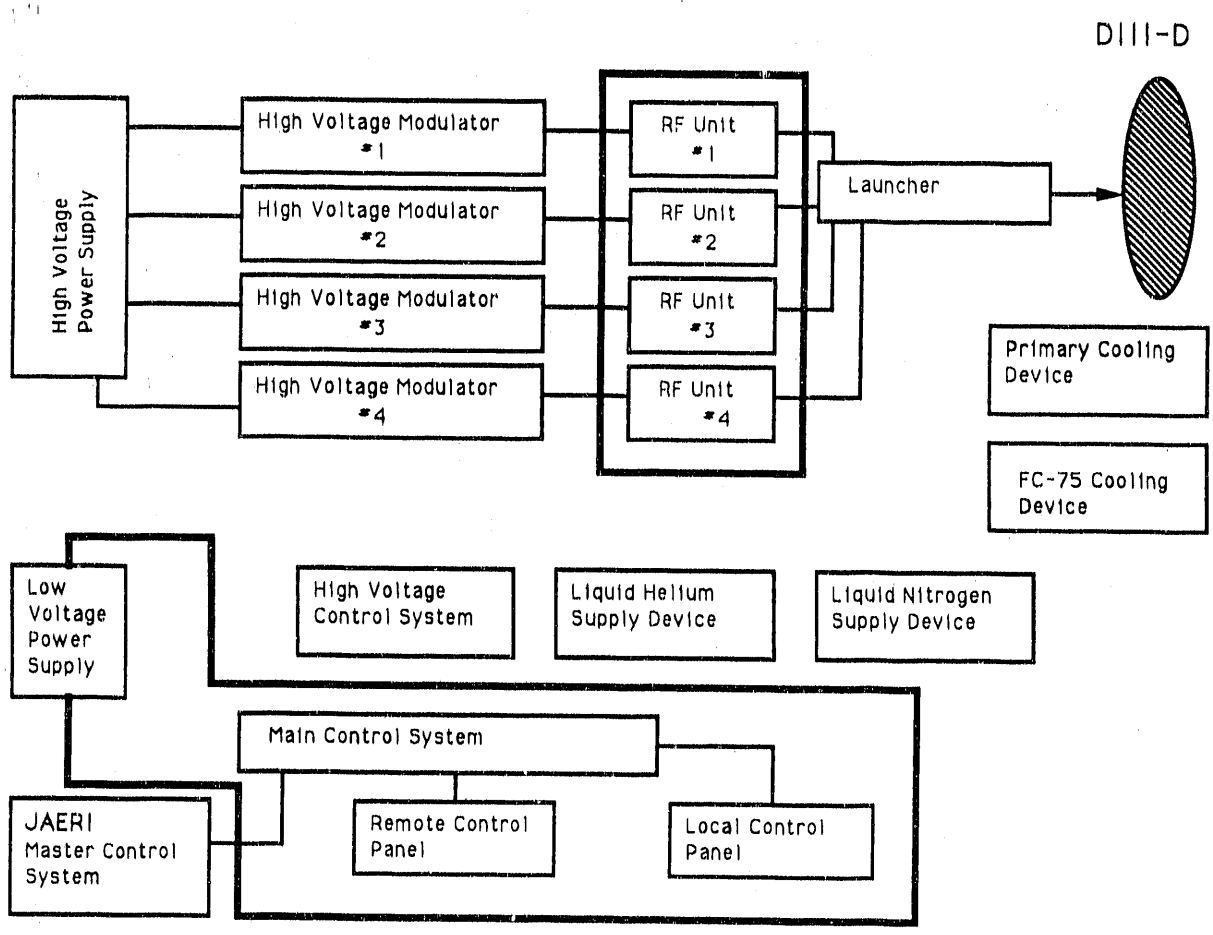

Fig. 6.3-1. Basic arrangement of the 110 GHz ECH system.

6.3.2. GYROTRON

The gyrotron tube is the device that can most reliably generate high frequency (>100 GHz), high power microwave with pulse lengths approaching continuous operation. The gyrotrons currently being developed by Varian Assoc., Palo Alto California are specified to operate for 10 seconds with a power of 500 kW at a frequency of 110 GHz. Three gyrotrons have been fabricated with two of them being tested. One of the gyrotrons has been pulsed at 500 kW for 1 s and 300 kW for 2 s, the other gyrotron has been pulsed at 540 kW for 100 msec and has reached 700 kW for 1 msec. Parts for two more gyrotrons have been fabricated and are awaiting assembly. Difficulties in extending the pulse length capabilities of these gyrotrons are associated with an inability to dissipate the energy generated in the tube's cavity during the rf production process.

The first gyrotron has been delivered and is being used to pulse test the transmission line components, a picture of its installation is shown in Fig. 6.3-2.

TABLE 6.3-1
RF UNIT SPECIFICATIONS

Power level	500 kW
Frequency	110 GHz
Pulse length	10 s
Duty cycle	1%
Transmission system	Evacuated corrugated waveguide
Overall transmission efficiency	75%

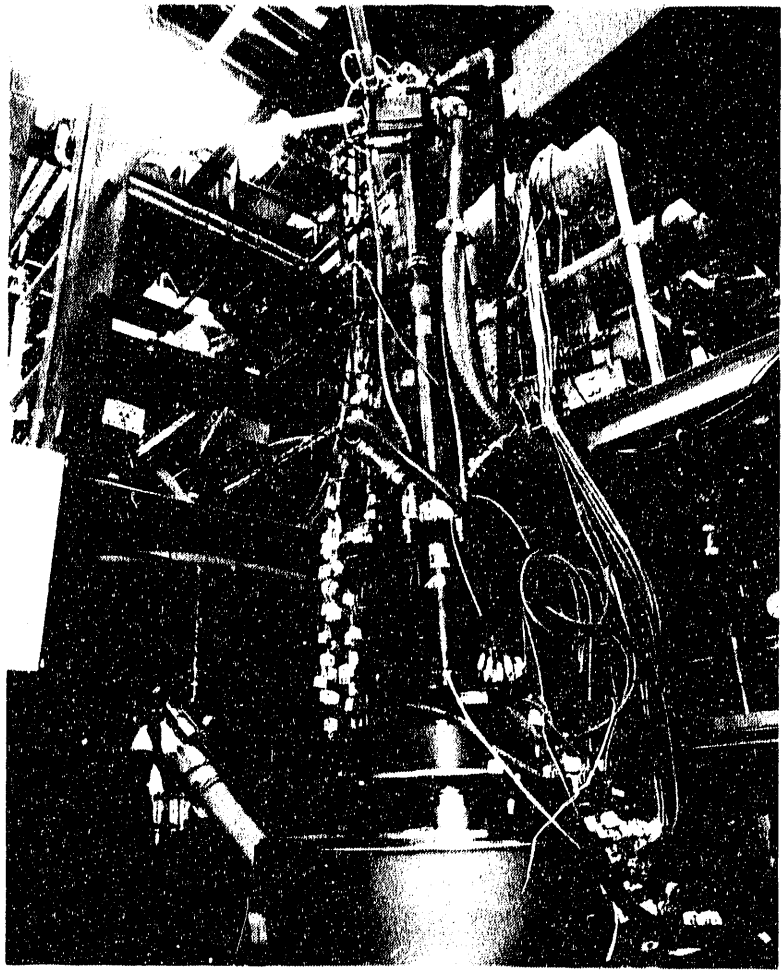

Fig. 6.3-2. Prototype gyrotron installation.

6.3.3. GYROTRON MAGNET

The gyrotron magnet is a superconducting magnet system that is designed and built to Varian Specification 255001 and is designated as the VYW-8011 Magnet System by Varian. As shown in Fig. 6.3-3, the magnet system consists of a set of four coaxial superconducting solenoids and four pairs of transverse trim coils. The superconducting magnets are maintained in a helium environment by use of a vacuum dewar with liquid nitrogen shield. All coils are powered by independent power supplies. All of the magnets have been built. Two were built by General Atomics and two by Oxford Instruments.

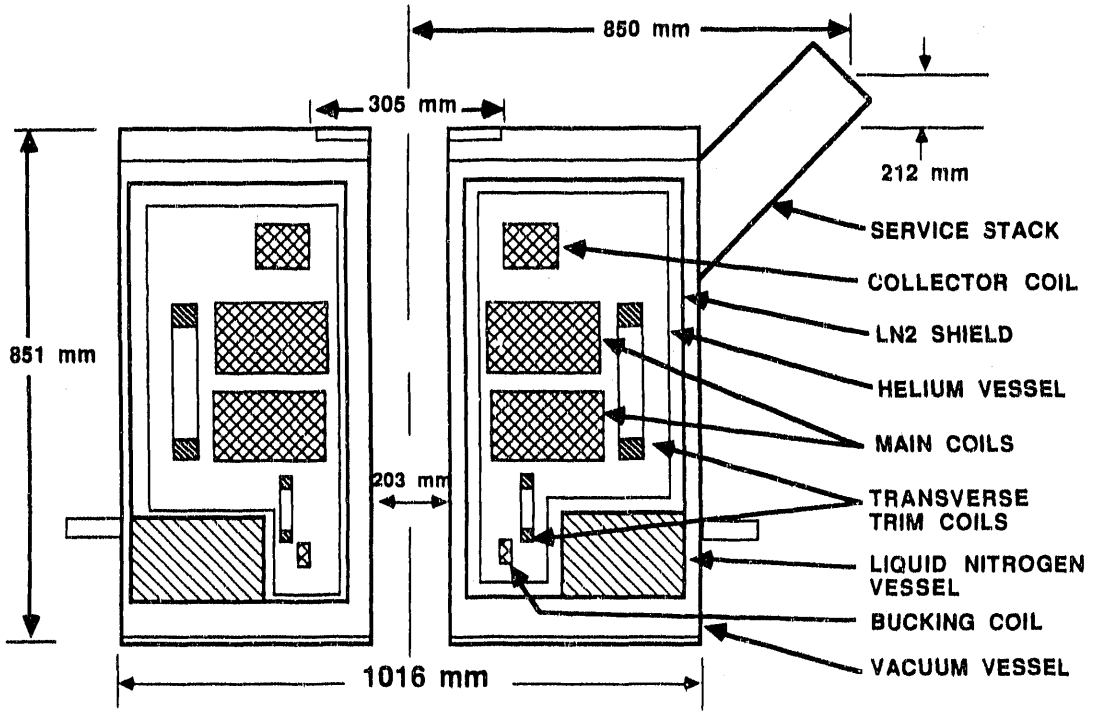

Fig. 6.3-3. Magnet cryostat cross section.

6.3.4. GYROTRON TANK

The gyrotron tank supports the gyrotron tube and the gyrotron magnet, and it supplies power for the cathode heater and gun anode. It also supplies instrumentation and control functions for all electrical connections to the gyrotron. The electrical interfaces of the gyrotron tank to the primary power system, to the high voltage power system, and to the control system are shown in Fig. 6.3-4. The tank is made of aluminum plate, coated with epoxy paint, and it is filled with transformer oil to reduce the chance of electrical breakdown. One tank has been installed for gyrotron testing and the other three tanks are in fabrication with installation expected to occur during the spring of 1992.

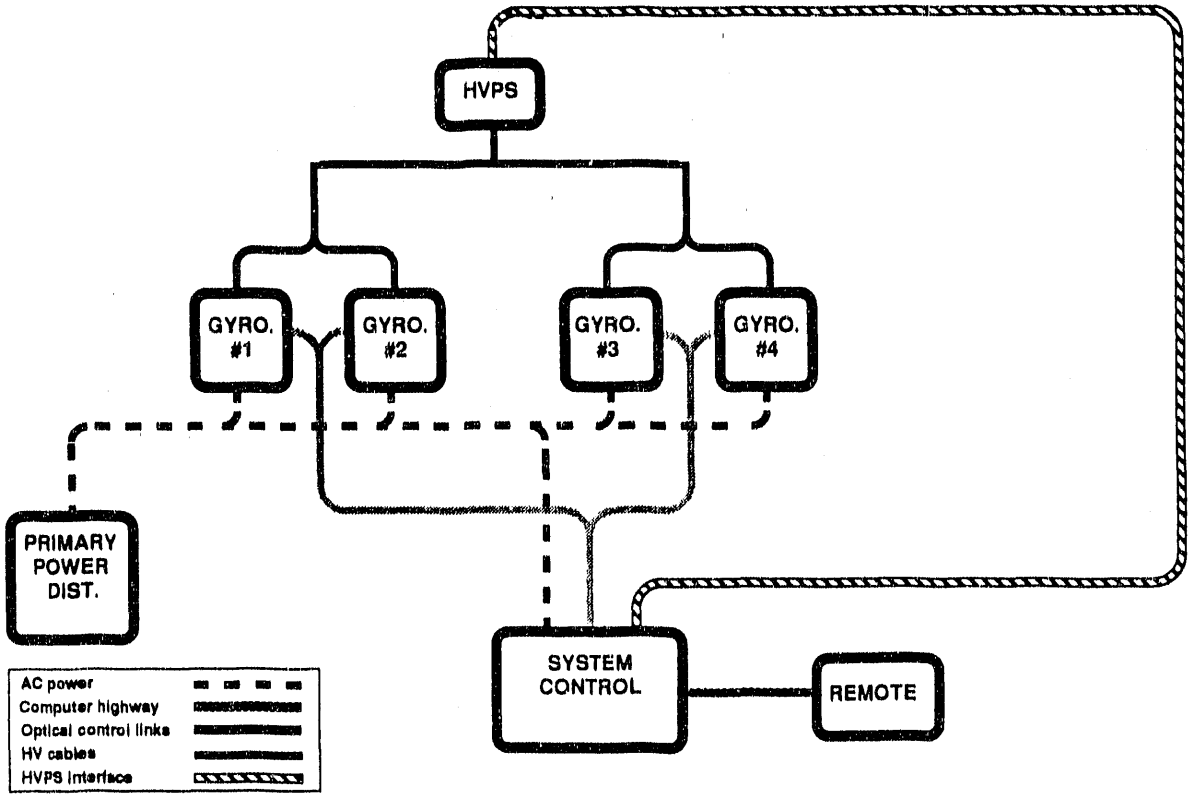

Fig. 6.3-4. Control system block diagram.

6.3.5. RADIO FREQUENCY TRANSMISSION SYSTEM

The waveguide system is designed to balance the conflicting goals of low ohmic loss, low mode conversion, high power handling capability, and insensitivity to the mechanical misalignments. Additional considerations are introduced by particular components, such as the mode converter, which transforms the gyrotron output mode into one which is more suitable for transmission.

A Gaussian HE_{11} waveguide mode will be used in the transmission line. This facilitates a "strongly guided" waveguide approach in which the corrugated waveguide diameter is small enough that extreme sensitivity to mechanical misalignment (especially small changes in direction) is avoided. The diameter chosen is 31.8 mm, for which unintended mode conversion can be controlled and the ohmic losses are tolerable (0.05%/m). The average power density in this waveguide is 63 kW/cm^2 for 500 kW input. In order to propagate this high average power without breakdown, the waveguide must be evacuated to pressures below 10^{-3} torr.

The waveguide system is shown in Fig. 6.3-5, and the status of the components is given in Table 6.3-2, photographs of some of the key components are shown in Figs. 6.3-6 and 6.3-7. The overall transmission efficiency of this system is expected to be above 75%. Most of the system is low enough in dissipation that convection cooling of components will be sufficient. A few components require cooling, even at 1% duty cycle, including the mode converter and the mirrors of the mitre bends.

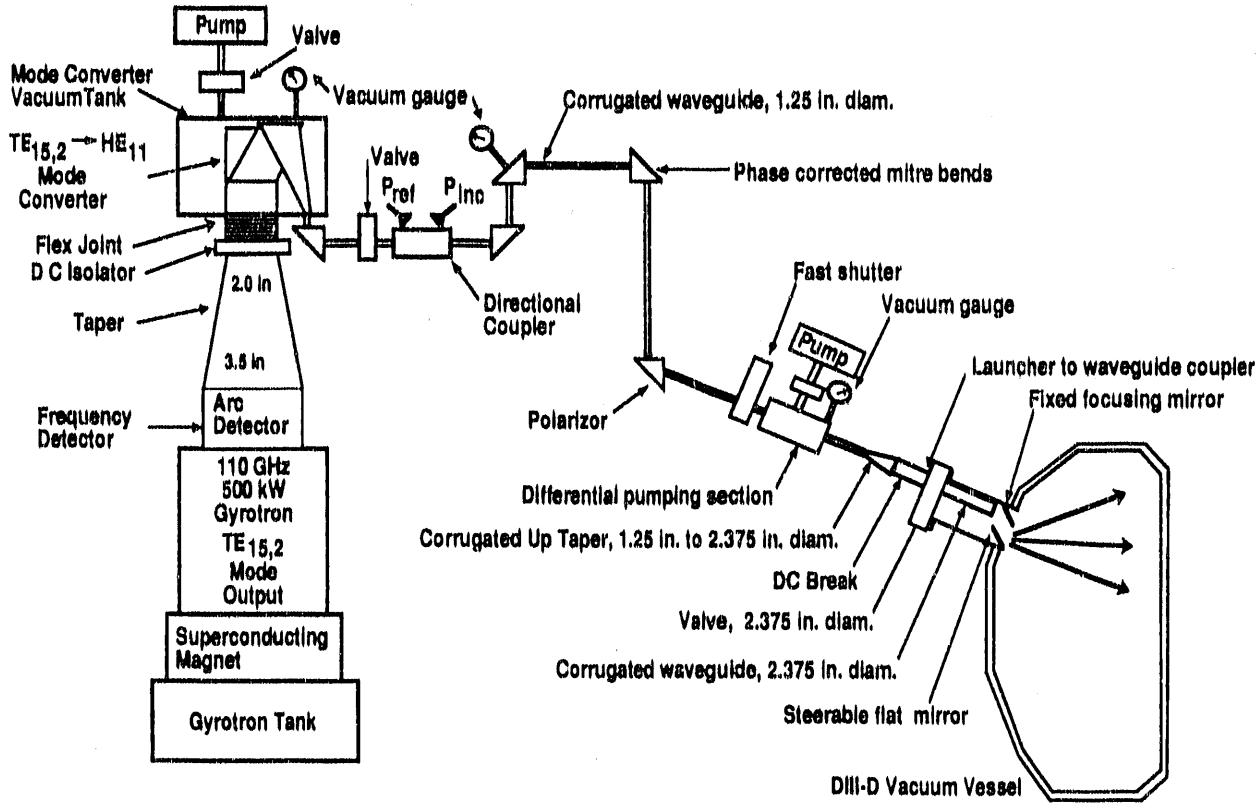

Fig. 6.3-5. Waveguide system.

TABLE 6.3-2
110 GHz TRANSMISSION LINE COMPONENTS

Item No.	No. Required	Element	Status					
			Not Started	In Design	In Fab	Parts In-House	Complete	Installed
1	4	Arc detector					3	1
2	4	Down taper				2	1	1
3	4	Electrical isolator					3	1
4	4	Flex section		4				Prototype
5	4	Mode convention, TE15,2 > HE1,1		4	4			Prototype
6	4	Vacuum tank and supports					1	1
7	2	Pump station				1		1
8	4	waveguide valve			3			1
9	4	Directional coupler				4		Prototype
10	100	Corrugated waveguide				60	10	30
11	100	Corrugated waveguide couplers					70	30
12	100	Corrugated waveguide hanger					75	25
13	100	Corrugated waveguide seal					70	30
14	20	90° miter bend					13	7
15	8	Polarizer		6			2	
16	4	Pumped section					3	1
17	4	UP taper 3.18 > 6.03				2	1	1
18	2	Joint to launcher				1		1
19	4	Corrugated waveguide heaters					3	1
20	4	Heater insulation					3	1
21	4	Electrical break				3		1
22	4	Second vacuum station				2	1	1
23	4	Fast shutter and controls				2	1	1
24	4	waveguide valve					2	2
25	4	Launcher						4
26	1	Dummy load						1

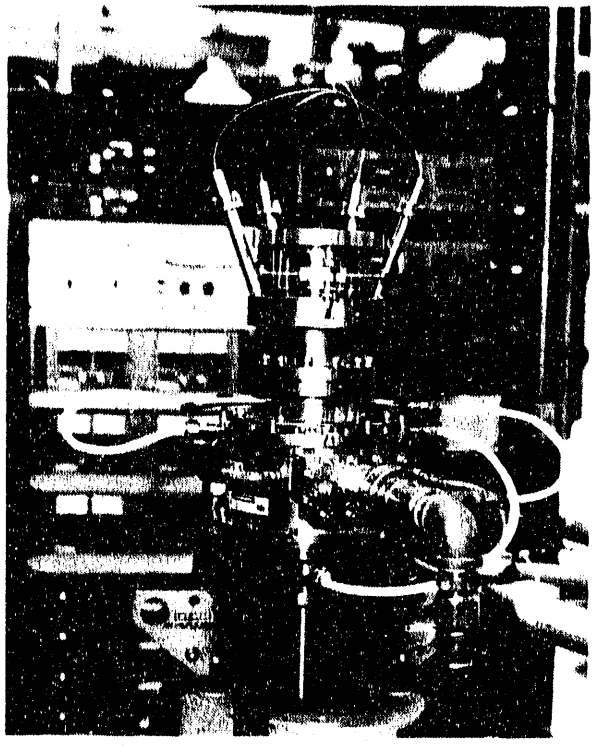

(a)

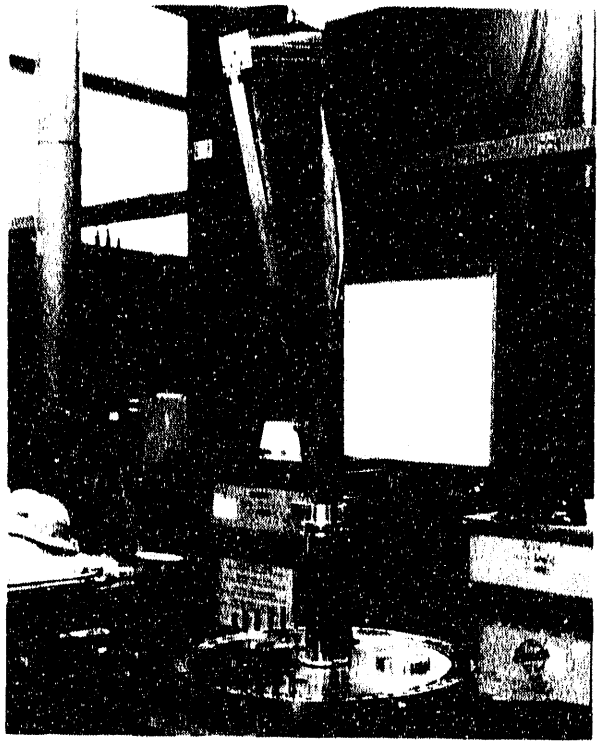

(b)

(c)

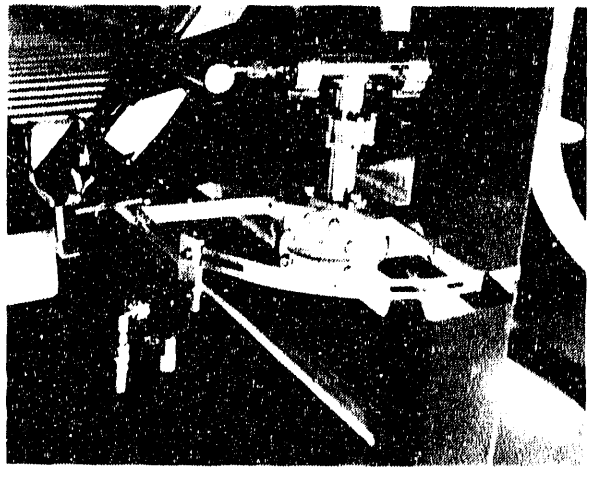

(d)

Fig. 6.3-6. Transmission line components (a) arc detector, (b) mode converter, (c) mitre bend, and (d) directional coupler.

(b)
(a)

SECTION 7

SUPPORT SERVICES

7. SUPPORT SERVICES

7.1. QUALITY ASSURANCE

Fusion Quality Assurance (QA) engineers, inspectors, and support personnel maintained a high level of activity during 1991. Significant projects were the 110 GHz Electron Cyclotron Heating (ECH) System, ECH Gyrotron Superconducting Magnets, Advanced Divertor Project (ADP), and the DIvertor Material Exposure Systems (DIMES).

7.1.1. DESIGN SUPPORT

1. Reverse-engineered a quick shut-off valve utilizing the Coordinate Measuring Machine (CMM) for the ECH Design Group.
2. Assisted Fusion Engineering in the development of a technique to measure a relatively inaccessible 45 degree angled seat on the DIMES experiment.
3. Developed tooling and a technique to measure the ECH gyrotron-to-cryostat concentricity accurately. The tooling was also used to adjust the gyrotron accurately within the cryostat bore.
4. Fabricated tooling to measure curvature change of Advanced Divertor prototypes during welding.
5. Performed load versus deflection evaluations on Advanced Divertor leaf spring samples.
6. Reverse-engineered a 35 mm high speed turbopump ball bearing assembly for the DIII–D Vacuum Systems Design Group.
7. Performed bore straightness evaluations on 7 ft waveguides and mode converters to evaluate design and production parameters.
8. Reviewed and approved all DIII–D design drawings, specifications, procedures, and purchase requests. Participated in design reviews, and chaired the Material Review Board (MRB).

7.1.2. INSPECTION SUPPORT

1. The majority of Quality Control (QC) activities during the year involved receiving and source inspections of purchased and fabricated parts, subassemblies, and assemblies. Inspection activity was particularly heavy for the 110 GHz ECH system and the ADP.

2. QA also witnessed several hydrotests of ASME Code vessels and final acceptance tests of gyrotron magnets for the 110 GHz ECH system. QA also conducted in-process inspections of 110 GHz ECH gyrotron tank circuit boards and assemblies, and receiving inspections and tests of purchased cryogenic units for the ADP project.

3. Since the majority of Fusion manufactured components are produced locally by a limited number of smaller machine shops, Fusion QA has adopted a policy of conducting periodic in-process inspections during fabrication. This practice has resulted in discovering machine setup problems, design drawing misinterpretations, machine programming errors, and machinist errors in sufficient time to prevent scrapping the part. Prevention of errors and the commensurate schedule preservation more than compensated for the additional labor required.

7.1.3. AS-BUILT MEASUREMENT SUPPORT

1. Provided as-built measurements on several DIII–D ports and port flanges for Fusion design engineers.

2. Performed a series of in-process measurements to determine the degree of weld distortion on experimental Advanced Divertor split tube weldments.

3. Recorded as-built dimensions on selected 110 GHz ECH subassemblies. This data was used during system assembly to reduce tolerance accumulation.

7.1.4. OPTICAL TOOLING/LAYOUT/ALIGNMENT SUPPORT

1. Performed mechanical layouts for the 110 GHz gyrotron magnets.

2. Performed semi-annual subsidence measurements of the Building 34 neutron shielding wall columns and footings. No unexpected settling has been noted.

3. Conducted numerous calibrations of the 110 GHz Superconducting Magnet warm bore axis measurement tool.

4. Completed a layout of the 110 GHz waveguide run from the DIII–D machine port to the ECH vault. An optical tooling transit, a precision sight level, a and a water level were utilized to transfer the elevation across an intervening wall. A second layout was completed utilizing a first-surface stellite mirror and a helium-neon laser.

5. Optically aligned ECH pumpout tees utilizing an optical tooling transit with autocolimator.

6. Provided optical alignment of the lithium beam accelerator internal components for the DIII–D Physics Department.

7.1.5. QA SYSTEM IMPROVEMENTS

1. Initiated and performed a Total Quality Management (TQM) Feasibility Study in conjunction with Fusion Management. The purpose is to determine the potential of TQM implementation for the Fusion Group.

2. Participated in a Fusion Group effort to revise and improve Engineering Procedures. This effort is continuing.

3. Fusion QA has developed a new form, the Quality Assurance Action Request, which is designed to expedite required changes to design documents, and to track the required changes to a successful closeout. This form augments, but does not replace, the existing design document approval and release system.

   A second new form, the Rework/Discrepancy Report, has been designed to document nonconformances which may be reworked to satisfy design requirements. A copy of the report is left with the supplier in order to assure complete communications relative to the required action to be taken. Nonconformances which require a use-as-is or repair disposition are documented on a Nonconformance Report as usual.

4. Fusion QA initiated trend reports on supplier performance in an effort to increase awareness of poor performance. The first trend report resulted in a Corrective Action Request being submitted to one supplier.

7.1.6. OTHER SUPPORT

1. Conducted the quarterly visual inspections of all DIII–D hoisting and rigging equipment.

2. Witnessed a large number of High Consequence Lifts of DIII–D equipment in accordance with DOE and GA Hoisting and Rigging Manuals.

3. Assisted DIII–D Engineers in developing production travelers for 110 GHz ECH waveguide production.

4. Performed dye penetrant evaluations on tube-to-helium vessel welds on the #3 gyrotron superconducting magnet.

7.2. PLANNING AND CONTROL

The Planning and Control Group supported operation and maintenance of the DIII–D facility. Planning and control provided long-term program planning, as well as day-to-day scheduling (cost control, preparation of Field Task Proposals and Cost and Fee Proposals), processing of purchase requests, expediting and reporting of status. These support activities are essential to the performance of the program within prescribed budgets and schedules. These planning activities (budget, schedule, resource) enabled us to maximize the utilization of available resources for accomplishment of program goals.

Major planning activities during FY91 included 2 MW 10 GHz System, Advanced Divertor Project, and Machine Operations, Maintenance and Vents.

7.3. COMPUTER OPERATIONS

During FY91, data was taken for 3389 tokamak or test shots. The largest single shot was 56.3 Mbytes of data. Over 109 Gbytes of data was collected during the year.

The data acquisition system for the DIII–D signals and results was modified so that it can handle 64-bit timing information. This was a major project which was started in FY90. Almost all programs and databases were changed as part of this work, and the new results are available to the physics user on request, which means that application programs did not need to be changed.

The rewrite of the neutral beam routines to be compatible with existing MODCOMP operating system levels was completed. This project has been under way for over a year and the major objectives were completed. All codes are now more flexible, have a better user interface, can be more easily modified and use the InterTask Communications features of the standard MODCOMP operating system. This has allowed all systems to be brought up to the current operating system levels, and current levels of other software. Additionally, new hardware and hardware features are now available because of the operating system

level. A standard database product has been used and will also be available for other improvements on the systems.

Software changes were made so that data acquired during glow discharge cleaning between shots is available in the next shot. Changes were made in timing of the thermocouple data collection so that it does not conflict with lockout times. This was all in support of the advanced divertor experiments.

Many changes were made to the VAX systems. In order to keep up with the increasing number of diagnostics run on separate diagnostic systems, a central console unit was installed. There are now 18 VAXes in the cluster; these can all be monitored and controlled from the central console. The VAX 6310 was upgraded to a 6410. This has helped to keep the compression of shot data from long lags behind the actual data collection and also helps to get the large uncompressed shot files moved off to tape quickly, thus keeping more total shots on disk. The 6410 has also been used extensively at night for shot analysis. A dedicated VAXstation 3100-38 was added for performing equilibrium fitting EFIT analyses between shots.

An additional 8 mm 2.3 Gbyte tape drive was installed and procedures were setup to do full system backups to the two units. This has saved several hours of operator time each week. New 5 Gbyte 8 mm tape units have been purchased for trial and, at the end of the year, were undergoing testing for suitability in our environment.

The Building 34 site and Building 13 were wired for AppleTalk in all offices. All MAC users can reach the central server and share files. Applications have been set up on the server which allow for specific numbers of concurrent users, and this has greatly aided the management of licensing and software, and has made more software available to every user. These tools have greatly added to productivity. The Energy Sciences Network (ESnet) became fully functional. It was installed in October at which time the old MFEnet was disabled. The MFE satellite ground station, including the related computer equipment, was deinstalled and removed. All hardware pertaining to the MFEnet was returned to NERSC. The ESnet has performed exceptionally well, with noticeable improvements in throughput over the MFEnet.

The Multiflow computer was not highly utilized. Although some physics calculations were done, most users shied away from the UNIX operating system. The D version of the DIII–D equilibrium fitting (EFITD) code and associated data translation programs were converted. A problem with the DISSPLA software from Computer Associates (CA) which made the software unusable was never fully resolved by CA. Without DISSPLA,

the output from EFTID could not be interpreted. Due to lack of user interest and poor vendor support, the decision was made to decommission the Multiflow. The Multiflow minisupercomputer was deinstalled and returned to GE Capital in September after an early buy out of the lease was arranged.

The User Service Center (USC) developed an upgrade plan to increase the VAX computer power after extended measurements showed the VAXes were very loaded during prime time causing poor response. The upgrade plan was presented to management, the user community, and sent out to other Fusion labs for peer review. The accepted plan replaced two obsolete VAXes with two VAX 4000-300s, moved one 8650 to DIII–D, and added a VAX workstation and terminal servers. There was a total increase in VAX MIPS at the USC of 16 and 4.5 at DIII–D. The equipment was installed in August. The VAX 4000-300s are general purpose computers, accessible to all Fusion users, while the VAXstation is dedicated to EFITD calculations during run periods. Before these VAXes could be joined to the existing USC cluster, all systems were upgraded to VMS 5.4-2. Access by terminal to these VAXes also required the upgrading of the Xyplex communication equipment to the LAT protocol. A second S1032 database license was purchased for one of the VAX 4000-300s. Installtion of new Micro Technologies communication boards made the VAX 4000-300s full cluster members rather than satellite nodes, dramatically improving in system performance.

The Computer Security Plan for sensitive visitors was modified to expand the access on the USC VAXes for the visitors from sensitive countries, and thereby improved the computational collaboration with other DIII–D participants. This modified plan was approved by the DOE-SAN. The USC Statement of Strategy was also updated and submitted to DOE-SAN. It, too, was subsequently approved. Login banners on all Fusion computers were modified to reflect the DOE directives. The purpose of the banner is to notify everyone who accesses the computer that only authorized users are permitted on the system. The USC participated in a CIAC security workshop held at LBL.

The pending switch at NERSC from the CTSS operating system to UNICOS has created a great deal of work. Many of the production physics codes being run on the Crays were written using the CIVIC fortran compiler. These need to be converted to CFT77 fortran and compiled under UNICOS.

The NCAR graphics package was purchased. This software runs on all platforms and is cost effective. It is compatible with the NERSC UNICOS Crays. It is a possible replacement for DISSPLA.

Optimization of EFIT has been undertaken by the USC. The first step involved two major modifications to the IMSL bicubic spline routines in an effort to improve performance. To date, about a 15% overall reduction in CPU time has been realized.

7.4. ENVIRONMENT SAFETY AND HEALTH

7.4.1. OVERVIEW

The DIII–D safety program is established to provide safe operation of the DIII–D facility and to provide a safe working environment for its employees and visitors. The areas that are stressed include high voltage and current, vacuum, ionizing radiation, microwave radiation, cryogenics, and industrial safety. Therefore, a special two-volume Safety Manual set exists entitled, "DIII-D Safety Procedures for Facility and Equipment Operation." Volume 1 contains policies and Volume 2 contains procedures. These two manuals point out the specific safety rules and operating procedures to be adhered to while at the DIII–D site. Both manuals refer to the company manual for general safety rules and regulations. The DIII–D safety program is supported by the General Atomics safety program which provides expertise in areas such as health physics, industrial hygiene, and industrial safety.

DIII–D has a Safety Committee that is made up of representatives from all facets of DIII–D, from top management to the hands-on technician. Its chairman is the DIII–D program director and the Fusion Safety Officer acts as the assistant chairman and full-time secretary. The Safety Committee can also solicit specialized help from any one of the three Safety Subcommittees when additional help is required in the areas of lasers, electrical, or vacuum. The Safety Committee met twice a month to discuss safety activities and concerns such as: new hazardous work requests, radiation work authorizations, accident reports or near misses, equipment malfunctions with potential safety hazards, accident avoidance through personnel training and supervisor involvement, access control in hazardous areas and the potential hazards in high voltage areas. Minutes of each meeting are published by the Fusion Safety Officer and become the basis for discussion at the next meeting.

When new employees arrive on site to work, they go through a thorough and comprehensive safety indoctrination by the Fusion Safety Officer and Pit Coordinator. At that time, they were made aware of the specific potential hazards that are present and the safety precautions and rules that apply. Subcontractors also went through a similar indoctrination.

The DIII–D Emergency Response Team consists of individuals from various areas involved directly with maintenance and operation of the DIII–D equipment. They were all trained in CPR, first aid, SCBA and fire extinguisher usage, evacuation and crowd control, and facility familiarization. The team can respond within seconds to provide immediate first aid assistance while the company EMTs are enroute.

The neutron and gamma radiation produced at DIII–D is constantly monitored during operations at the site boundary with the level kept below 20 mR per year. Personnel dosimeters are worn by all individuals while on the DIII–D site and if entrance into the machine pit is required between shots, and alarming dosimeter is worn in addition to the TLD badge. Prior to unrestricted machine pit access, the pit is surveyed and the necessary areas are cordoned off until a safe reading is achieved.

A series of Safety Inspections occur throughout the year in keeping with our active Hazard Prevention Program. The inspections are conducted by both DIII–D and General Atomics personnel and by outside consultants with a report provided to the Fusion Safety Committee for action. The inspection topics are: monthly site inspection, yearly electrical inspection, voluntary OSHA consultant inspection, insurance carrier inspection and the General Atomics Safety Committee Hazards Survey site inspection. The Fusion Safety Officer is responsible for tracking the progress and ensuring compliance.

Training is all-important to the safety of both personnel and equipment. Due to the complexity of the DIII–D site and its operation, numerous safety training classes were offered throughout the year or whenever necessary. These classes include but are not limited to: confined space entry, back injury prevention, radiological safety, laser safety, hazard communication, cryogenic safety, crane and forklift operation, lockout/tagout, the national electrical code, shop tool usage, and basic industrial safety.

7.4.2. FY91 SAFETY

A final copy of the DOE Multi-Disciplinary Review was received at the beginning of FY91. Copies were distributed to appropriate individuals for correction and 51% were completed immediately. A follow up audit was conducted by the DOE/SAN office During the second quarter, and they were pleased with the response to the action items noted. The last inspection discrepancy noted by this audit was corrected July 7, 1991.

Also during their visit, a previously scheduled Multi-Response Emergency Drill was conducted. The visitors were given observers badges and were asked to participate in the critique of the drill. The drill included Emergency Response Team members, the

General Atomics Emergency Services Department, General Atomics Security, Hartson Ambulance Service, Scripps Memorial Hospital, and a representative from the San Diego office of Emergency Preparedness. The scenario was based on the occurrence of a large earthquake and the release of a poisonous gas. There were many scheduled as well as surprise casualties, which provided the opportunity for many lessons to be learned.

A Boronization Team was implemented into the DIII-D program this year. This was necessary because of the new designs and safety reviews of the proposed Boronization system. PPPL, Hughes, and the General Atomics materials laboratory were visited to gain first-hand information on sites that are currently utilizing Diborane. All team members are now trained in First Aid, CPR, and the use of self-contained breathing apparatus (SCBA). At the close of FY91, five boronization processes have occurred.

The Fusion Safety Officer was given the opportunity to visit Tiger Teams at various DOE facilities. These visits included the opening and closing Tiger Team sessions at PPPL and closing Tiger Team session at LBL. Information was gathered regarding the purpose, scope, objective, and methodology of a Tiger Team. He also visited ORNL and conducted research on their machine guarding program for which they received a noteworthy practice on from their last Tiger Team audit.

The Fusion Safety Officer also attended a Tiger Team training session presented by the DOE for prospective Tiger Team members and interested contractors. The information gained in this comprehensive week of training will prove to be invaluable in fine-tuning the fusion safety program.

A fire and emergency evacuation drill was conducted by General Atomics Emergency Services Department which exercised the DIII-D Emergency Response Team as well as the emergency preparedness of all DIII-D personnel.

The DIII-D Safety Manual continued to be updated with seven procedures having been totally rewritten and reviewed.

The DIII-D Safety Committee Membership was reviewed, brought up to date, and temporary rotating members were replaced by new members. This committee met a total of 26 times to accomplish the following tasks.

1. Reviewed and approved 32 Hazardous Work Authorizations after appropriate recommendations and changes by the committee and select subcommittees.
2. Approved the implementation of a new incident/near miss report to be used in cases where no injury or property damage occurred. This form will help the

committee to investigate and correct potential problems before they become more serious.

3. Reviewed three incidents which involved no lost time or property damage, and six accidents all of which were minor first aid cases with the exception of one lost time.

4. A new DIII-D safety check in form was developed and implemented for the use of the DIII-D Safety Officer to ensure that each new employee, job shopper, or visitor receives a proper and complete safety indoctrination.

5. Implemented a policy that each person involved with a HWA be required to sign a verification sheet indicating that they have read the HWA they are working on. This sign-off sheet would be the responsibility of the requestor to circulate around to each person listed on the "personnel involved" section and, upon completion, to ensure that it is included in the original copy in the reception area. The sign-off sheet will be spot checked by the Fusion Safety Officer and will be reviewed for compliance at each yearly review cycle.

A number of inspections were made of the DIII-D site. These include a request from the Fusion Safety Officer for the CAL/OSHA Industrial Hygiene consultation services, an Electrical Consultant Inspection, a General Atomics Hazard Survey Inspection, monthly Fusion Safety Committee inspections, daily walk around inspections, and follow up visits from the San Diego Fire Marshal's Hazardous Materials Inspection Team and the DOE Multi-Disciplinary review committee. In all, a total of 231 safety discrepancies were noted, and at the close of FY91, 203 of these discrepancies have been corrected. Of the remaining 28, 25 were noted during an electrical inspection in which the safety department requested the services of a private consultant. The magnitude of these electrical discrepancies will require the services of our on-site electrical contractor, and the repair work is estimated to cost about $9,200.00.

An extensive Emergency Response Team Training schedule has been drawn up and is scheduled to be executed the first quarter of FY92. This will include training in SCBA, CPR, First Aid, Crowd Control, Fire Extinguisher Usage, Hydrant Hookup, Facility Familiarization, and a Confined Space Evacuation Drill.

A chemical inventory was conducted of the entire DIII-D facility, cataloging all hazardous substances. Manufacturers and distributors of these chemicals were notified for request of Material Safety Data Sheets and have now been cataloged for employee access

in the Safety Library and the Fusion Safety Office. These data sheets have also been cataloged in the computer database system for easy reference and back up.

During FY91, 53 new employees and visitors received a safety indoctrination from the Fusion Safety Officer

An individual was added to the Fusion Safety Staff, and brings with him three years of safety experience. This has allowed us to tackle a backlog of unresolved inspection findings and other important safety related issues.

7.5. VISITOR AND PUBLIC INFORMATION PROGRAM

Tours of the DIII–D facilities are open to organizations and institutions interested in fusion development (colleges, schools, government agencies, manufacturers, and miscellaneous organizations). These tours are conducted on a noninterference basis and are arranged through the DIII–D tour coordinator whose responsibilities include security, arranging tour guides, and scheduling tours as required. During the year, 1,618 people toured DIII–D to give a total of 2,836 during the last seven years.

Special tours during the year included:

- UCSD Physics Club
- San Diego City College Environmental Biology
- ITER Business Sponsors
- La Jolla Day School 7th Grade Class
- IEEE Fusion Engineering Conference
- Cub Scout Group
- Salk Institute
- University of Washington Group
- Gulftronics
- EDUCOM Convention
- Packaging and Handling Engineering Convention
- IEEE Power Engineering Conference
- Numerous Congressman and Staff

- San Diego City Console
- ITER Joint Central Team Members
- Rancho Bernardo Philosophy Club
- Society of Women Engineers
- American Society of Mechanical Engineers
- Lutheran High School Chemistry Class
- UCLA Physics Students
- North American Electrical Reliability Console
- UCSD ASME Club
- Heart Elementry School 6th Grade Science Class
- SDSU Physics Club
- Helix High School Physics Class
- UCSD Nuclear Energy Physics Class
- Rancho Bernardo Masonic Lodge
- Torrey Pines High School Physics Class
- Naval Civil Engineers
- Explorer Scout Group

SECTION 8

ITER CONTRIBUTIONS

8. ITER CONTRIBUTIONS

The DIII–D program has made substantial contributions to the Physics R&D Program over the last several years. The ITER Short-Term Physics R&D Program was carried out during the ITER conceptual design phase and was completed at the beginning of the fiscal year. A summary of the rather extensive final report is shown in Table 8-1. Following this, a plan was developed to address the ITER Physics R&D Needs for 1991, 1992 and beyond, as described in an ITER document by the same name. This plan addresses almost all of the areas of research proposed by ITER. The plan is summarized in Table 8-2.

Research to fulfill this obligation began in FY91. The report of this work is summarized in Table 8-3. In addition, DIII–D staff members participated in the Home Team Physics activities including leadership in the Disruptions and Operations and Physics R&D areas and active participation in the additional areas of Diagnostics, Divertor Physics, and rf heating. In addition, there was active participation by many staff members in ITER workshops and planning sessions.

The ITER Long Term Physics R&D Needs is a comprehensive program to identify the physics needs for ITER. Fifty-one topics are collected into five major categories. The DIII–D program will contribute to 43 of these topics. Major contributions are anticipated in the areas of Power and Particle Exhaust Physics and Enhanced Confinement where our program is expected to provide key physics input. The rf program is anticipated to provide electron cyclotron and fast wave current drive results. The DIII–D disruption program has been strengthened in response to ITER needs and this effort is expected to provide responses on a wide range of disruption issues. In the area of Physics of Burning Plasmas, the DIII–D program expects to make substantial contributions to the Physics of Burning Plasmas through studies of alpha particle losses.

TABLE 8-1
SUMMARY OF DIII–D SEPTEMBER 1990 ITER R&D RESPONSES

Topic	Ongoing DIII–D Contribution	Investigator	Collaborators
Design Related			
1. Power and helium exhaust	√	Hill	LLNL, SNL
2. Helium radial distribution	√		
3. Radiative edge	√	Mahdavi	LLNL
4. Divertor sweeping	√	Hill	LLNL
5. Low-Z PFC materials	√	Hill	LLNL, SNL
6. High-Z PFC materials			
7. Characterization of disruptions	√	Kellman	PPPL
8. Disruption control	√	Kellman	
9. RF plasma formation and preheating	√	Prater	Culham
10. RF current initiation			
11. Inductive volt-second consumption	√	Hogan/Taylor	ORNL
12. Alpha-particle ripple losses			
13. Plasma diagnostics	√	Snider	
Performance Related			
14. Steady-state enhanced confinement	√	Gohil	ASDEX
15. Tests of theoretical transport models	√	Burrell	JET, JAERI
16. Control of MHD activity	√	Strait	
17. Density limit	√	Petrie	
18. Plasma performance at high kappa	√	Lazarus	ORNL, Lusanne
19. Alpha particle simulations	√	Heidbrink	U.C. Irvine
20. Electron cyclotron current drive	√	Politzer	LLNL
21. Ion cyclotron current drive	√	Politzer	ORNL
22. Alfvén wave instability	√	Heidbrink	U.C. Irvine
23. Advanced fueling techniques			

TABLE 8-2
PLANNED DIII-D CONTRIBUTIONS
TO ITER LONG-TERM PHYSICS R&D

	DIII-D
1. Power and Particle Exhaust Physics	
1.1. SOL and Divertor Physics	√
a. Divertor Conditions	√
b. Geometry Variations	√
c. Hot Spots	√
d. CD Divertor Conditions	√
e. Impact of Fueling	√
f. ELMs	√
1.2. Impurity Radiation and Transport	√
a. Radiating Plasma Edge	√
1.3. He and H Exhaust	
1.4. Divertor Control	√
1.5. Plasma-Facing Materials	√
a. Conditioning Methods	√
b. Conditioning Between Shots	√
1.6. Alternative Divertors	
2. Disruption Control and Operational Limits	
2.1. Disruptions Characterization	√
a. Runaway Electrons	√
b. Soft Current Quench	√
2.2. VDEs	√
2.3. Disruption Avoidance and Control	√
a. Disruption Pre-Cursors	?
2.4. Beta Limits	√
a. Profile Effects	√
b. Equilibrium Inductive Operation	√
c. Sawteeth Effects	√
d. Fast Ion Effects	√
2.5. Density Limit	√

TABLE 8-2 (Continued)

	DIII–D
3. Enhanced Confinement	
3.1. Steady-State Operation	√
a. Energy Confinement Scaling	√
b. Plasma Particle Transport	√
c. Momentum Transport	√
3.2. Control of MHD Activity	√
3.3. Transport Mechanisms	√
a. Plasma Turbulence	√
4. Optimization of Operation Scenario and Long-Pulse Operations	
4.1. Long-Pulse Operation	√
a. Bootstrap Current	√
b. Lower Hybrid Physics	√
c. FWCD	√
d. ECCD	√
e. NBCD	√
f. Advanced CD	√
4.2. Optimization of Startup	
a. LHCD Ramp-up	
4.3. Plasma Shutdown	√
4.4. ICRH	?
4.5. Pellet Ablation Models	
a. Compact Toroids	√
5. Physics of a Burning Plasma	
5.1. Single Particle Effects	√
a. Ripple Fast Ion Losses	
5.2. Collective Effects	√
5.3. DT and Alpha Particle Physics	

TABLE 8-3
SYNOPSIS OF DIII–D CONTRIBUTIONS TO ITER LONG-TERM PHYSICS R&D NEEDS

NOVEMBER, 1991 REPORT

(COLLABORATORS ARE NOTED IN PARENTHESES)

1. Power and Particle Exhaust Physics

PH 1.1a Divertor Power Load Profiles. Peak divertor heat fluxes increase linearly with plasma current and reached values of up to 5.3 MW m^{-2} for ELMing H–mode plasmas at 1.5 MA plasma current and 15 MW beam power. In double-null ELMing H–mode plasmas, the divertor heat flux could be shifted between the divertors continuously by altering the magnetic configuration and deuterium gas injection reduced the peak divertor heat flux at both upper and lower strike points. (LLNL, ORNL, SNLL, SNLA, UCLA)

PH 1.1b Impact of Divertor Geometry Variation. The addition of divertor baffling has led to very high pressures of 10–20 mtorr under the baffle plate when the divertor plasma is positioned at the baffle entrance with no bias and with up to 15 MW of beam power. The pressure increases nearly linearly with the applied neutral beam injection power. (LLNL, ORNL, SNLA)

PH 1.1c Hot Spots on Plasma Facing Components. Measurements of the divertor heat flux show that the heat flux varies linearly as the cosine of the angle between the field lines and the normal to the tile. Carbon blooms are not observed even for total input energy levels of 40–50 MJ into the plasma. (LLNL, Culham)

PH 1.1e Impact of Fueling. Model calculations using the DEGAS code indicate that the density rise during the H–mode results from both an improved particle confinement in the plasma core and a reduction in neutral shielding by the SOL plasma. Experimental results indicate that fueling from either the midplane or from the region between the strike points produces the same fueling efficiency (less than 10%) for ELMing H–mode plasmas. (LLNL, ORNL, SNLA)

PH 1.1f ELMs and Other Edge Transients. ELMs regulate the time-averaged plasma parameters such as the particle flux, electron density and temperature, and the neutral gas pressure. ELMs are important for maintaining a quasi-stationary H–mode discharge. Three types of ELMs have as yet been identified in DIII–D. (LLNL, ORNL, SNLA, UCLA)

PH 1.2 Impurity Radiation and Transport in the Bulk, Scrape-Off Layer and Divertor Plasmas. (a) Experimental comparisons before and after boronization at DIII–D show that without boronization deuterium puffing produces substantial reductions in impurity levels, whereas with boronization no further reduction from the initial low levels is observed. (b) Improved impurity screening observed in VH–mode when T_e is high at the separatrix is under further investigation. (LLNL, ORNL)

PH 1.2a Powerfully Radiating Plasma Edge. For a wide range of plasma parameters, injecting deuterium gas into the edge of ELMing H–mode plasmas reduces the divertor heat flux by a factor of four or greater, with only a modest degradation in plasma energy confinement. (LLNL, ORNL, SNLA)

PH 1.3 Exhaust of Helium and Hydrogen. This study will be delayed to 1992 and is through a collaboration with GA and Oak Ridge National Laboratory. The main objectives will be to measure time dependent helium density profiles after helium gas injection into a steady-state plasma, and to model this profile evolution to determine diffusive and convective transport coefficients. (ORNL)

PH 1.4 Active Control and Optimization of Divertor. Experimental studies with the new divertor bias ring and divertor baffle provided important results on neutral pumping requirements and power threshold for H–mode plasmas. (a) High neutral gas pressures (>10 mtorr) were obtained under the baffle with optimized localization of the separatrix with respect to the baffle entrance. (b) A minimum of the power threshold for the L–H transition was obtained for a positive bias between +75 to +100 volts, with the threshold increasing by a factor of four with a negative bias of –400 volts. (LLNL, ORNL, SNLA)

PH 1.5 Wall Conditioning Methods. Surveys of erosion of the divertor tiles are being performed with the most significant utilizing the DIMES sample changer assembly. (SNLL)

2. Disruption Control and Operational Limits

PH 2.1 Characterization of Disruptions. The upper limit to the average current decay rate of DIII–D disruptions is linearly proportional to the pre-disruption plasma current. The maximum instantaneous current decay rate also increases with the pre-disruption current and is about 1.5 to 2 times the average value.

PH 2.1a Disruption-Produced Runaways. The absence of high current runaway electrons after disruption in DIII–D may be attributed to the behavior of the plasma motion following the disruptions. Specifically, the rapid inward motion can lead to the early loss of runaway electrons before the energy or runaway content can become large. (SNLA)

PH 2.2 Plasma Motion During Disruptions. Simulation codes are being utilized in an effort to reproduce DIII–D disruptive discharges. The codes incorporate the magnetic data together with models for the shape and position contral feedback system and the actual power supply configurations used on the discharges. (ORNL, Kurchatov Ins.)

PH 2.4a Profile Effects on the Beta Limit. Theoretical and computational studies are described which indicate that the current density and pressure profiles can strongly influence the beta limits determined by ideal kink and ballooning modes. Experimental values of β_N as high as six were achieved by increasing ℓ_i to approximately 2 using a rapid negative current ramp. (ORNL)

PH 2.4b Steady-State Pressure and Current in Inductive Operation Profiles. The highest experimental value of normalized beta obtained varies from 3.5 at $q_{95} < 3$ to 6 at higher values of q. For low q values, the discharges are terminated by disruptions caused by external and global kink modes whereas at higher q, the disruptions are less frequent and are limited by slowly growing resistive modes, fishbones and possibly by ballooning modes. (ORNL)

PH 2.4c MHD Impact on High Beta Operations. Investigation of the sawtooth crash and determination of the inversion radius have been performed for high beta discharges. The sawtooth period is well described for ohmic, L–mode, and H–mode discharges.

PH 2.5 Density Limit. The density limit for ELMing H–mode discharges is observed to increase linearly with the plasma current while appearing to be independent of the toroidal field. Degradation of the energy confinement by 20% to 30% is observed on approaching the density limit. (LLNL, ORNL)

3. Enhanced Confinement

PH 3.1 Steady-State Operation with Enhanced Confinement. This field includes (a) detailed investigations of the L–H transition and the influence of the edge radial electric field and the suppression of microturbulence at the plasma edge, (b) increased input to the H–mode databases for ITER and ASDEX, (c) studies of H–mode confinement with high aspect ratios, and; (d) the discovery of a new very high confinement regime (VH–mode). (UCLA, Jülich GmBH)

PH 3.2 Control of MHD Activity. MHD activity and its influence on the sawteeth behavior have been studied with the result that the sawtooth inversion radius scales as $1/q_{95}$ and the mixing radius scales as $1/q_{95} + 0.3$. Investigations of locked mode instabilities indicate that the instability threshold is dependent on the interactions of resonant magnetic perturbations with rotating plasmas.

PH 3.3 Transport Mechanisms. Studies of plasma transport have involved off-axis heating experiments utilizing both electron cyclotron heating and neutral beam injection. Localized electron cyclotron heating of the electrons results in an inward electron heat flux inside the heated region with no change in the ion heat flux. This behavior would tend to rule out nonlinear diffusion and critical gradient models for transport processes. (LLNL, ORNL)

4. Optimization of Operation Scenarios and Long-Pulse Operation

PH 4.1 Long Pulse Operation. The major effort in this field has been focused on preparing for fast wave current drive in DIII–D. Efficient direct electron absorption of fast waves was achieved and an H–mode plasma was obtained using only fast wave heating of electrons at 60 MHz. (ORNL)

PH 4.4 Control of Hot Ions With IC Waves. Fast waves were successfully launched from the fast wave current drive antenna and efficient heating of a hydrogen minority in a deuterium plasma was demonstrated. Experiments also showed that there is a strong dependence of impurity generation on the phasing of the four antenna straps.

5. Physics of a Burning Plasma

PH 5.1 Fast Ion Single-Particle Physics. Time resolved measurements of 14 MeV neutron emission and 15 MeV proton emission demonstrated that, the temporal behavior and magnitude of the signals arising from the burnup of 1.0 MeV tritons and 0.8 MeV ^{3}He ions agree with classical predictions. (UC Irvine)

PH 5.2 Fast Ion Collective Effects. Unstable TAE modes are being studied at DIII–D. The instability can cause up to 50% of beam power being lost from the plasma. The largest losses are accompanied by low frequency MHD bursts with the losses scaling linearly with the magnitude of the TAE activity. (UC Irvine)

SECTION 9

BURNING PLASMA EXPERIMENT CONTRIBUTIONS

9. BURNING PLASMA EXPERIMENT (BPX) CONTRIBUTIONS

General Atomics scientists supported BPX as part of the nationally distributed Physics Team. Dr. Ronald Stambaugh continued to serve as Deputy Head of Physics. His principal activity was to complete the Physics R&D Plan for BPX. This plan was distributed in February 1991. Subsequently, the Office of Fusion Energy desired to establish level one milestones for the Alcator C–mod, DIII–D, and TFTR programs for research tasks of primary importance to BPX. Dr. Stambaugh coordinated the negotiation and creation of those milestones. Dr. Stambaugh presented the Physics R&D Plan at the BPX Conceptual Design Review and at the Field Task Proposal Presentations. Dr. Stambaugh also coordinated the interaction of DIII–D research input with BPX and served on advisory panels on the relation of other devices research programs to BPX. With Lang Lao, he completed and submitted for publication, "A Study of the Dependence of the Maximum Stable Plasma Elongation on Aspect Ratio."

Dr. Ronald Waltz served as Confinement Physics Task Leader. He led dimensionally similar discharge transport experiments on DIII–D aimed at distinguishing between Bohm and gyro-Bohm scaling. Discharges with various vertical shifts were employed in order to vary the neutral beam heating profile. Transport analysis was performed on these discharges. The basic result was that the transport process can not simply be described by an effective diffusivity. The overall confinement time and the temperature profiles were insensitive to the heat deposition location. These results were similar to the heat pinch results previously obtained with electron cyclotron heating (ECH). They make it impossible to sensibly discuss the transport in terms of Bohm or gyro-Bohm scaling until the role of the heat pinch or whatever produces "profile resiliency" is clarified. Dr. Waltz also participated in analyzing the TFTR dimensional similarity experiments. He presented a summary of national confinement research in support of BPX at the BPX Conceptual Design Review.

Some work on disruptions was done in support of BPX. Efforts were made to calibrate the TSC code to DIII–D data. Dr. Royce Sayer of Oak Ridge National Laboratory (ORNL) came to General Atomics and worked with Dr. Arnold Kellman for this purpose. DIII–D magnetics data and halo current measurements were given to Sayer.

Dr. Ronald Prater supported BPX with some conceptual work on ECH launching schemes. He presented this work at the Physics Design Review Meeting at ORNL.

Dr. Robert La Haye provided extensive support to BPX in the area of field errors and construction tolerances on the coils. He performed locked mode studies on DIII-D and COMPASS tokamak at Culham and reported the results in many forums, including an invited paper at the American Physical Society meeting. These results were made available to BPX. He performed calculations of error fields in BPX that would result from deformations of each individual poloidal coil. He assessed the size of magnetic islands that the resulting field errors would form and also assessed the effect of the error fields on the heat flux patterns on the divertor plates. He proposed a set of additional field error correction windings be implemented on BPX.

SECTION 10

COLLABORATIVE EFFORTS

10. COLLABORATIVE EFFORTS

10.1. DIII–D COLLABORATION PROGRAMS OVERVIEW

Fusion collaboration programs at General Atomics encompass a broad spectrum of activities ranging from those which result directly in work on the DIII–D tokamak to those in which DIII–D staff member travel to other fusion facilities in order to acquire new technical information or carry out specialized experiments required for the development of advanced concepts. These collaboration activities are not only economically effective but provide a tremendous degree of technical support for the development and execution of DIII–D programs while encouraging exchanges which are needed stimulate new ideas necessary for solving difficult technical problems. It is implicitly clear from the discussions of new DIII–D results given in preceding sections of this report that collaborations with other fusion research laboratories, both in the United States and in foreign countries, have played a key role in the internationally acknowledged success of the DIII–D program.

This section of the report explicitly highlights the benefits resulting from interactions with scientists and engineers from: the Japanese Atomic Energy Research Institute (JAERI); the Lawrence Livermore National Laboratory (LLNL); the Oak Ridge National Laboratory (ORNL); Sandia National Laboratories in Albuquerque, New Mexico (SNLA), and Livermore, California (SNLL); Princeton Plasma Physics Laboratory (PPPL); and university programs located at: the University of California at Los Angeles (UCLA), at Berkeley (UCB), at Irvine (UCI), and at San Diego (UCSD); as well as: the University of Maryland, the Massachusetts Institute of Technology (MIT), the University of Washington, the University of Wisconsin, and Johns Hopkins University. The largest FY92 collaborations were with LLNL and ORNL while the JAERI collaboration continues to be the longest ongoing activity.

10.1.1. JAPANESE ATOMIC ENERGY RESEARCH INSTITUTE (JAERI)

Two JAERI scientists participated in the DIII–D program. H. Matsumoto was here on a long term assignment. He worked on low to high confinement transition physics studies reported in Refs. [1-3] and the particle transport studies [4]. H. Kawashima participated

in the electron cyclotron heating (ECH) program and he ran the soft X–ray pulse height analyzer diagnostic for the radio frequency (rf) current drive studies [5].

References for Section 10.1.1.

[1] Matsumoto, H., *et al.*, "Suppression of the Edge Turbulence at the L to H Transition in DIII–D," submitted to *Plasma Physics and Controlled Fusion.*

[2] Doyle, E.J., *et al.*, "Modifications in Turbulence and Edge Electric Fields at the L–H Transition in the DIII–D Tokamak," *Phys. Fluids B* **3(8)** (1991) 2300.

[3] Philipona, R., *et al.*, "Two-Stage Turbulence Suppression and E × B Plasma Flow Measured at the L–H Transition," submitted to *Phys. Rev. Letter.*

[4] Matsumoto, H., *et al.*, "Perturbative Particle Transport Study of DIII–D H–mode Plasma," *Bull. Amer. Phys. Soc.* 8T16, **36** (1991) 2476.

[5] Prater, R., F.W. Baity, S.C. Chiu, H. Kawashima, *et al.*, "Initial Fast Wave Current Drive Experiments on DIII–D," *Bull. Amer. Phys. Soc.* 3E9 **36** (1991) 2324.

10.1.2. NATIONAL LABORATORIES

10.1.2.1. Lawrence Livermore National Laboratory. Livermore personnel participated in several areas of the DIII–D research program in FY91, continuing to contribute to divertor physics studies, the development of a current profile diagnostic, and transport physics.

In the divertor physics area, a database of plasma parameters relevant to studies of the boundary plasma was developed. This database employs the same techniques as those implemented in the confinement database. Using the same basic parameters as the confinement database, we also incorporate the value of the plasma density and temperature at the separatrix, parameters which define the magnetic geometry outside the last closed flux surface, and parameters at the divertor floor, including the power, density, and temperature. Most of the analysis procedures required to extract this data have been automated, and about 100 time slices currently reside in the database.

In addition to the database work, experiments required to explore BPX-relevant questions such as the ability to control divertor heat depositions by varying the geometry between lower single null, double null, and upper single null were carried out. The results indicate that it is possible to sweep the heat load from the lower to upper divertor tiles by controlling the separatrix position to within about 1 cm. Divertor characterization experiments were also completed to simulate heat loads which are expected during the

operation of the International Thermonuclear Experimental Reactor (ITER). Heat loads as high as 5 MW/m^2 at the divertor target plates were achieved and data on heat load distribution as a function of plasma current and toroidal field were obtained.

Progress continued in the development of edge modeling codes. An automated grid generation procedure, which starts with an equidisk produced by the EFIT equilibrium code, was developed for the B2 and DEGAS code. This procedure implemented a smooth grid which covers both the core plasma and the scrapeoff layer while minimizing the required user input. In addition, a fully implicit version of the B2 code was developed and coupled to the DEGAS code. This new code uses a diffusion model to simulate the neutral transport and has alerted us to the sensitivity of the results to the neutral model. Preliminary results indicate higher densities and lower temperatures near the divertor plates than obtained using only the B2 code.

The divertor Langmuir probe data was examined for information on the so-called sheath transmission factor (γ). Experimental values of γ lie in the range 2-8 rather than the theoretically expected value of 8. This suggests that less power is carried out per electron than expected, and may mean the ion energy is lower than expected. This result is consistent with a simple theory which includes the effect of ion-neutral collision in the sheath. Conclusions based on this work will have significant impact on the design of the ITER divertor as they imply a lower ion energy at the divertor floor and, hence, lower sputtering rates.

The successful operation of a prototype single-channel Motional Stark Effect diagnostic was followed by the installtion of a six-channel instrument during the fall vent with initial operation scheduled for early 1992. This diagnostic measures the magnetic field pitch angle, which can be used to calculate the current profile, at positions well inside the core plasma.

In the area of transport physics, work has continued on the development of X–ray tomographic analysis. We have examined the behavior of the "X–ray hole" which is frequently seen in hot ion mode operation. The feature is initiated by the development of a region of high emission on the outside of the plasma, near the midplane where the value of the safety factor q is rational. This localized region remains stationary for a time on the order of 100 ms, then begins to slowly rotate over the top of the machine and to the inside. The emission drops dramatically on the outside, producing the feature called a hole. The emission gradients are very steep after the development of the hole, and it is not clear our detector spacing is sufficient to resolve the profile.

We have installed additional electron cycltron emission (ECE) diagnostics to permit better determination of the central electron temperature. The HECE is an interferometer which is used to determine the emission at the third harmonic during 2 tesla operations. This diagnostic provides measurements of the central temperature during fast wave current drive (FWCD) experiments.

10.1.2.2. Oak Ridge National Laboratory (ORNL). During FY91, ORNL has increased the number of on-site staff working on DIII–D. D. Hillis and M. Wade have begun one-year assignments in August/September 1991, adding to the existing assignments of E. Lazarus, C. Klepper, and M. Menon. Shorter visits by other ORNL staff also increased. Contributions to the DIII–D program were made in the following areas: FWCD, high-beta tokamak operation, experimental scaling studies on divertor baffle pressure, load testing on a divertor cryopump prototype, B2 and DEGAS modeling and interpretation of the divertor plasma and neutral pressure, initiation of an experimental program on helium transport and exhaust, and assistance in tokamak operations and disruption studies. Planning for a future pellet program was begun.

Advanced Divertor Program. Progress was made in the understanding of the Advanced Divertor Project (ADP) pressure scaling experiments. The scaling experiments showed that baffle pressures in excess of 10 mTorr could be maintained under stationary conditions. In addition, neutral beam power scaling and some current scaling data were obtained. A version of the B2 plasma edge code was applied to the analysis of the scaling experiments, in concert with DEGAS calculations. Details of this work are given in Section 2.2.3 and 6.2.1 of this report.

The DEGAS code, which is used to make predictions of particle exhaust with the ADP cryopump, indicates that approximately 50% of the neutrals entering the baffle are pumped. The neutral flux itself, however, depends sensitively on the divertor plasma response to active pumping. The effects of baffle pumping on the divertor plasma are being investigated with the B2 code and with an internal recycling model on the DEGAS code. Once these effects are known or predicted, better estimates of the particle throughput can be made with self-consistent plasma/neutral transport calculations.

Diagnostic capabilities in the divertor area have been improved by installing a capacitance manometer to measure absolute pressures under the baffle as well as in the private flux region. It has provided independent pressure measurements and increased

the confidence in the earlier measurements from the ASDEX-type gauges. The capacitance manometer was also used during gaseous divertor experiments to confirm the very high pressures in the private flux region, indicated by the saturation of the ASDEX-type gauges. A combination of the ORNL divertor spectrometer with the fast optical multichannel analyzer (FOMA) provided by General Atomics was successfully used to monitor carbon impurities (CIII) in the X–point region.

The high pressures in the divertor baffle region, while beneficial for particle exhaust, raised concern with respect to the thermal loads on the divertor cryopump. An experiment was conducted in which the maximum heat load anticipated from the pressure buildup was simulated by pulsed resistive heating of a cryogenic loop, dimensionally similar to the cryopump. The experiment revealed that the pump will be stable for 20-s pulses at high heat loads with deuterium, but will be marginal with hydrogen.

With General Atomics staff, studies were initiated on the effects of disruptions and vertical displacement events. For this purpose, an analysis of the relationship between tile currents and vessel motion was begun.

The studies on helium transport and exhaust were initiated in August. These studies focus on the transport of helium in diverted H–mode plasmas to compare with ORNL's earlier L–mode transport studies in the TEXTOR/ALT-II program and with related work at TFTR. The ultimate goal is to understand transport and exhaust of helium ash in a burning device like ITER. Initial experiments were conducted by puffing helium into the plasma (~20 ms) during the last 1 to 2 s of the discharge, resulting in a helium concentration of 5% to 8%. The time dependence of the He^{++} ion density profiles in the plasma core is measured by charge-exchange recombination (CER) spectroscopy at 16 radial locations with 10 ms time resolution. It was typically observed that the helium puffed in at the divertor floor tile, arrived in the center of the discharge after ~80 ms. Modeling of the helium transport and exhaust experiments is being performed with the PPPL Multiple Impurity Species Transport (MIST) code and the Oak Ridge ORTC code. The results of the helium studies will be compared with those obtained on TEXTOR, TFTR, Joint European Torus (JET), and JT-60.

Fast Wave Current Drive Program. Successful antenna operations with $\pm\pi/2$ phasing was obtained. To accomplish this, the power splitter feeding the two transmission lines into the DIII–D enclosure was replaced by a simple tee, allowing unbalanced power to be fed to the two lines. A new tuning algorithm was developed to calculate, on a shot-to-shot basis, the tuning element settings that would produce $\pm\pi/2$ phasing between neighboring

straps, equal currents and voltage amplitudes on all four lines, and an impedance match at the transmitter. It also was possible to switch from $+\pi/2$ phasing to $-\pi/2$ phasing in a single shot, using measurements made during the former shot to predict the tuner settings for the latter.

Experiments have been performed in both a "low absorption" regime and a "high absorption" regime. In the latter case, power levels above 1.3 MW were achieved for both $+\pi/2$ phasing and $-\pi/2$ phasing. Most of the data in both cases was obtained with a gap between the plasma separatrix and the front surface of the antenna Faraday shield of 3 cm. In this case, values for the tuning element settings converged after two or three shots. Operation also has been attempted with a 5 cm gap, in order to increase the directivity of $k_{||}$ spectrum at the plasma surface. In this case, the tuning algorithm did not converge to a satisfactory solution within a small number of shots. It is not clear whether the algorithm was converging at all within the four shots allotted to the tuning sequence. Work is under way to develop an improved algorithm to alleviate this problem. It does not appear that there are other limitations, such as power handling considerations, which would prevent operation with the larger gap.

A replacement Faraday shield is planned that should improve antenna performance substantially. The new shield has only a single tier of rods for increased plasma loading and hence higher power handling capability. The new shield will have a plasma-sprayed coating of boron carbide to reduce impurities. (Titanium from the titanium carbo-nitride coating on the present shield is one of the tell-tale signs of impurity influx during radio frequency operation.) In addition, a microwave reflectometer will be incorporated into the new shield design (in collaboration with UCLA) to provide edge density profiles in front of the antenna. This profile information is needed to establish the directivity of the launched wave spectrum in the plasma.

Pellet Injector. The JET pellet injector will be made available for use on DIII–D. It was agreed that injector operations would be concluded on JET early in CY92 and that the injector would be available for shipment to ORNL around February 1992. A decision was made to use the injector on JET after the limited tritium operation scheduled for November. This decision was based on an assessment of the likely levels of tritium exposure to the injector and the consequences relating to future use of the injector at ORNL and DIII–D. According to present DOE guidelines, it is possible that the injector will be considered tritium contaminated in the event of a worst-case accident scenario, but the level of contamination is not expected to be serious enough to preclude use of the equipment.

A preliminary schedule has been prepared for installation of the injector on DIII–D and tentative agreement has been reached between ORNL and General Atomics on the scope and division of responsibility of work associated with the pellet injector system modification and installation subtasks.

At present, it is estimated that the level of effort required at ORNL will dictate a project duration of about 1-1/2 years with operations on DIII–D expected to start in the fourth quarter of FY93.

10.1.2.3. Sandia National Laboratories. Sandia Albuquerque (with UCLA) operated the fast stroke probe carriage on DIII–D. J. Watkins used it to measure plasma profiles in the scrapeoff layer of DIII–D. Sandia Livermore continued to support divertor tile erosion and Langmuir probe measurements on DIII–D with electronics, probe tips, and analysis. John Cuthbertson took up full-time residence at DIII–D to support Langmuir probe analysis.

10.1.2.4. Princeton Plasma Physics Laboratory (PPPL). R. Waltz worked with PPPL staff on dimensional similarity experiments. We continued to interact with M. Zarnstorff on confinement improvement experiments via fast ion orbit loss.

10.1.3. UNIVERSITY PROGRAMS

UCLA projects on DIII–D include reflectometer and far infrared (FIR) scattering systems (supported by General Atomics and DOE-APP) and the fast stroke probe (with Sandia). The reflectometer and FIR systems continued to support low to high confinement (L–H) transition physics studies. Important advances were made in spatially localizing the turbulence detected by the FIR system by making use of the spatially varying Doppler shift from $\vec{E} \times \vec{B}$ rotation of the plasma. Ed Doyle presented an invited paper on L–H transition physics at the 1990 American Physics Society (APS) meeting. The turbulence data played an important role in the physics of the very high confinement VH–mode as presented at the 1991 APS meeting. The fast stroke probe was brought into operation in 1991. The probe was plunged into the separatrix and first data on profiles and turbulence in the SOL were obtained.

The University of Maryland continued to support the vertical and horizontal ECE systems. Scott Janz completed his Ph.D. work at DIII–D.

From MIT, Mikos Porkolab continued to participate in the ECH and FWCD programs on DIII–D. A Ph.D. student, Stefano Coda, continued to work on the Phase Contrast Imaging System.

Professor Fowler's group at UC-Berkeley continued to support a variety of transport investigations on DIII–D. T. Kurki-Suonio completed transient transport analyses showing the temporal and spatial evolution of the transport reduction in high confinement H–mode. Q. Nguyen completed a drift orbit code. D. Finkenthal took up residence at General Atomics to work on his Ph.D. in helium transport.

The plasma theory group at UCSD (M. Rosenbluth, P. Diamond, Y.B. Kim) supported DIII–D in the areas of H–mode physics, plasma rotation effects, and the rotation driver.

W. Heidbrink of UC-Irvine presented an invited paper on toroidal Alfvén eigenmodes at the 1991 APS meeting. A thesis student, H. Duong, studied triton burnup in DIII–D and maintained the Charge Exchange Analyzer.

The low safety factor confinement paper written jointly with J. Callen and Z. Chang of the University of Wisconsin was sent to *Physics of Fluids*. R. Fonck advised us on a possible Beam Emission Spectroscopy system on DIII–D.

D. Orvis of the University of Washington spent the summer at General Atomics analyzing DIII–D divertor bias data.

Johns Hopkins University scientists field tested a developmental multilayer mirror spectrometer on DIII–D.

10.2. INTERNATIONAL COOPERATION

General Atomics currently carries out active international collaboration programs: in England on JET, in France on the Tore Supra tokamak, in Germany on the ASDEX tokamak, and in Japan on the JFT-2M tokamak.

10.2.1. JET COLLABORATION

DIII–D continued to maintain one full-time staff member at JET. Dr. Robin Snider completed a seven-month assignment at JET, working on X–ray tomography, and was succeeded by Dr. Chandrakant Baxi. Dr. Baxi spent four months at JET working on the following issues: neutral beams (the effect of nitrogen and helium spillage); cryopump (quench of the helium panel, cooldown of the nitrogen panel by liquid nitrogen, and analysis of the argon spray system); and the JET Advanced Divertor (performance of the hypervapotron). Dr. Baxi was succeeded by Mr. Thomas Hodapp, who will work on the

JET Advanced Divertor System. Dr. Thomas Carlstrom of General Atomics was sent to JET to observe the historic tritium experiment.

10.2.2. TORE SUPRA COLLABORATION

U.S.-France collaboration activities in 1991 have continued to support investigations of ergodic divertor physics in Tore Supra. In addition, new activities centered around experiments in divertor and boundary layer physics were initiated in 1991 as part of a comparative program on power and particle control processes in the DIII–D poloidal divertor and in the Tore Supra ergodic divertor. Dr. Todd Evans ended a 39-month long assignment at Tore Supra on July 23, 1991 during which time he served as an experimental program leader in the area of ergodic divertor physics. A workshop on boundary layer physics issues in DIII–D and Tore Supra was held in Cadarache from May 27-31, 1991 to discuss the status of the two experiments and exchange ideas for collaboration activities.

The 1991 Tore Supra ergodic divertor program was divided between experiments with high power lower hybrid current drive (LHCD) or ion cyclotron heated (ICH) plasmas and impurity screening studies in ohmic plasmas with either gas or pellet fueling. Results from these experiments were presented at a series of International Conferences, Meetings, and Workshops including: the Washington International Atomic Energy Agency (IAEA) Conference; the 32nd and 33rd Annual American Physical Society Meetings; the 9th European Tokamak Program Workshop in Arles, France; the 18th European Physical Society Conference; the 9th Topical Conference on Radio Frequency Heating in plasmas; and in a paper published in *Nuclear Fusion*.

Within the Tore Supra ergodic divertor program, General Atomics' activities have continued to emphasize goals which provide a better understanding of physical mechanisms responsible for magnetically induced particle and energy confinement time improvements in ohmic and additionally heated discharges [1-3]. Optimized conditions were found in which ohmic plasma confinement times could be improved by as much as 60% above the standard linear confinement regime [1] and a series of 2.0 MW ICH experiments with perturbed magnetic boundaries were completed in deuterium plasmas. The ICH experiments demonstrated that magnetically perturbed boundaries reduce the radio frequency power coupled to the core plasma by approximately 40%. This reduction can, in principle, be corrected in real time by actively tuning the ICH antenna during the magnetic perturbation phase. Once the coupling problem is overcome, we intend to test basic physical models describing heat and particle transport across the ergodic layer and power scaling implications connected with the control of recycling, radiation, and impurity screening

processes. Based on theoretical arguments, it is expected that impurity screening efficiencies in addition to the overall effectiveness of the ergodic layer for controlling heat and particle transport will improve with increasing power flow into the boundary due to high power additional heating. A sharp transition, similar to the low to high confinement L–H transition in poloidally diverted tokamaks, is expected to occur at ICH power levels in the 10-12 MW range for a limiter plasma with a circular cross section, such as Tore Supra, when an ergodic layer is located near the plasma boundary. No evidence of such a transition was observed during our initial low power ICH experiments in Tore Supra but we have observed boundary layer effects which indicate that the power scaling argument is valid in this range.

Another confinement control approach being explored exclusively by General Atomics is to position small, time independent, magnetic islands near the plasma boundary while pushing the plasma against the high-field side axisymmetric limiter [1,2]. High power LHCD pulses combined with small amplitude magnetic perturbation pulses have resulted in large particle confinement transition [2] in deuterium plasmas with this configuration. These results are similar to earlier observations in helium fueled ohmic plasma [1] but with much larger particle confinement time increases. An example of this type of magnetically induced transition event, with 2.0 MW of LHCD input power, is shown in Fig. 10.2-1. The helical coil current I_H used during this shot is a factor of two below the computed threshold for producing an ergodic layer. We see an initial increase in the volume averaged density during the unperturbed LHCD phase followed by a larger increase in the density during the magnetically perturbed LHCD phase. No external gas fueling was introduced after the initial plasma current ramp up portion of the discharge and the hydrogen neutral flux from the inner wall decreased by $\approx$25% throughout the LHCD pulse. The energy stored in the plasma goes up when the LHCD pulse is introduced and again when the magnetic perturbation pulse starts. At the same time, the carbon concentration in the core plasma goes down by more than a factor of two [1,2] and the central electron and ion temperatures increase [2].

In addition to our confinement control studies with the Tore Supra ergodic divertor coils, we have completed several impurity injection and high flux gas puffing experiments. Neutral penetration probabilities are strongly reduced by the ergodic layer. In some cases, it is no longer possible to use gas fueling to control the core plasma density. It was shown that deuterium pellets can be used to compensate for the reduction in gas fueling efficiency in these cases. Theoretical work on the effects of error fields in tokamaks was strongly coupled to the experimental work on Tore Supra. As a result of this, we were able to

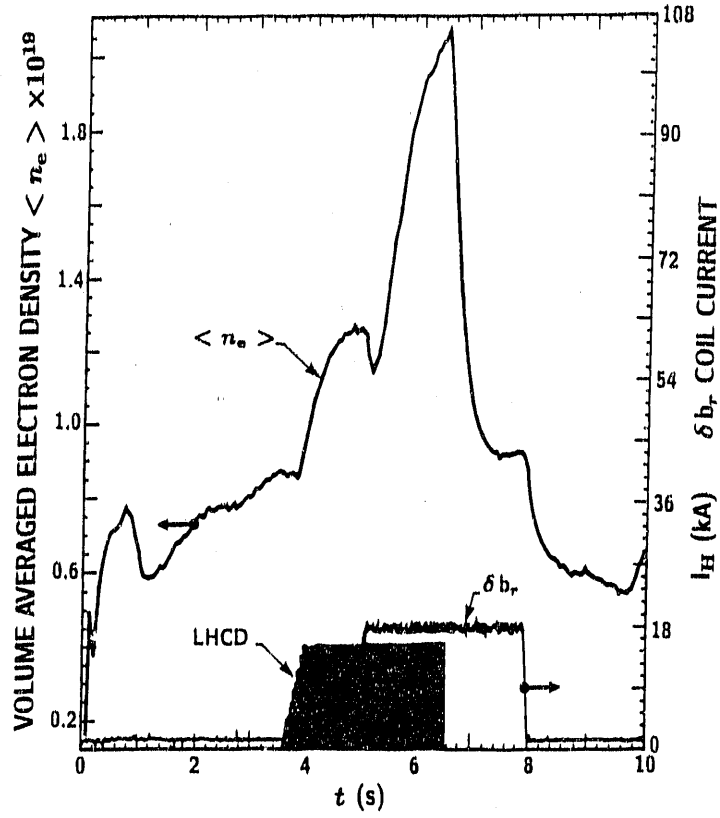

Fig. 10.2-1. Volume averaged electron density $< n_e >$ increases with LHCD and with LHCD + I_H [2].

formulate a number of predictions concerning the size and locations of intrinsic magnetic islands in Tore Supra as well as in TFTR. Some evidence supporting these predictions has begun to emerge from the two machines. In general, a greater appreciation of the importance of resonant magnetic perturbation effects on the overall performance capabilities of given tokamak has resulted from the Tore Supra experiments and the theoretical work which was developed to support these experiments.

References for Section 10.2.2.

[1] Evans, T.E., *et al.*, "Plasma Performance Control During Ergodic Divertor Experiments in Tore Supra," in *Bull. Amer. Phys. Soc.* **35** (1990) 1998.

[2] Evans, T.E., *et al.*, "First Results from Combined Ergodic Boundary Layer and LHCD Experiments in Tore Supra," in *Bull. Amer. Phys. Soc.* **36** (1991) 2367.

[3] Evans, T.E., *et al.*, "Plasma Performance Control During Ergodic Divertor Experiments in Tore Supra," CEA Euratom DRFC/CAD Report EUR-CEA-FC-1419 (March 1991)

10.2.3. ASDEX COLLABORATION

G. Jackson and T. Hodapp visited ASDEX to gain knowledge of the ASDEX boronization system that was very useful in implementing boronization on DIII–D. Their principle contact was H. Poschenreider. R. Harvey represented General Atomics at the ASDEX/U.S. Executive Committee Meeting held in Frascati. He also was attending the Lower Hybrid Workshop at that time. Dr. Harvey made major contributions to the review of the ASDEX L–H program given by Soldner at the IAEA meeting. F. Ryter worked with J. DeBoo and D. Schissel at General Atomics to add ASDEX data to the JET/DIII–D H–mode confinement database. This work has resulted in the publications:

- Schissel, D.P., *et al.*, "H–mode Energy Confinement Scaling from the ASDEX, DIII–D, and JET Tokamaks," in Plasma Physics and Controlled Nuclear Fusion Research (Proc. 18th European Conf. Berlin, 1991); General Atomics Report GA-A20548 (1991).
- Ryter, F., *et al.*, "Expression for the Thermal H–mode Energy Confinement Time under ELM Free Conditions," General Atomics Report GA-A20707, submitted to *Nucl. Fusion.*

Dr. P. Parks went to ASDEX and worked with Drs. Lengyel and Lackner of the Max-Planck Institute to produce an improved model of pellet ablation. The work resulted in the report "An Ablation Model for Time-Dependent Pellet Ablation Studies at Max-Planck Institute," IPP 5/40 (June 1991). Dr. T. Evans worked with ASDEX staff on the effect nonaxisymmetric error fields on mode locking and confinement. The work was included in, "Statistical Properties of Intrinsic Topological Noise in Tokamaks," in *Plasma Physics and Controlled Nuclear Fusion Research* (Proc. 18th European Conf. Berlin, 1991) and in Max-Planck Institute report, "Measurements of Poloidal and Toroidal Energy Deposition Asymmetries in the ASDEX Divertors," IPP III/154 (March 1991). Dr. K. McCormick consulted with Dr. D. Thomas at General Atomics on lithium beam diagnostic systems and analysis codes. Dr. U. Schneider of ASDEX worked on analysis of very high confinement VH–mode discharges in DIII–D and fostered the start of some comparison of these discharges to unusually high confinement discharges in ASDEX during a visit

at General Atomics. Dr. H. Zohm has recently arrived to work on ELMs and locked modes in DIII–D.

10.2.4. JFT-2M COLLABORATION

Drs. Anthony Leonard and Torkil Jensen of General Atomics completed visits of seven weeks and two weeks respectively at JFT-2M as part of a continuing collaboration on edge plasma modification experiments. While there, they participated in experiments involving the new internal coils that have been recently installed on JFT-2M. One set of coils is designed to be an Ergodic Magnetic Limiter (EML) and decrease the sharp edge gradients in H–mode by applying magnetic perturbations to the plasma edge. The new EML coil set was found to have less of an effect than the old coil set which is external to the vacuum vessel. A careful computer analysis of the magnetic structure produced by the new EML coil set revealed a smaller magnetic diffusion than for the old EML coil set. A greater current capacity in the new EML coil set will be needed in order to meet or exceed the performance of the old EML coil and properly test the EML concept applied diverted H-mode plasmas.

A second set of recently installed internal coils are designed to interact with the magnetic structure of the interior plasma. These coils provide a $m/n = 2/1$ perturbation and create magnetic islands on the $q = 2$ surface. Collaborative experiments using these coils attempted to modify the plasma rotation profile in a test of a recent model by T.H. Jensen and A.W. Leonard concerning the interaction of plasma rotation and magnetic islands. However, the coil set was unable to slow the toroidal rotation induced by neutral beam injection, while the old EML coil set was effective in slowing rotation. A more complete model must be made in order to understand the experimental results. The experimental data is also useful for understanding plasma rotation and locked mode experiments on DIII–D.

SECTION 11

FY91 PUBLICATIONS

11. FY91 PUBLICATIONS

Allen, J.C., R.W. Callis, W.P. Cary, T.E. Harris, and A. Nerem, "Eight Channel–16 Bit, Bidirectional Analog to Digital Monitoring and Control System," in Proc. 14th Symp. on Fusion Engineering, IEEE, San Diego, California, September 30–October 3, 1991; General Atomics Report GA-A20604 (1991).

Baxi, C.B., "Thermal Analysis of JET Cryopump Nitrogen Shield," General Atomics Report GA-A20371 (1991).

Baxi, C.B., P. Anderson, A. Langhorn, M. Menon, K. Schaubel, and J. Smith, "Thermal Design, Analysis, and Experimental Verification for a DIII–D Cryogenic Pump," in Proc. 2nd Int. Symp. on Fusion Nuclear Technology ISFNT-2, June 2-7, 1991, Karlsruhe, FRG; General Atomics Report GA-A20464 (1991).

Baxi, C.B., A. Langhorn, K. Schaubel, J. Smith, "Thermal Analysis of a Coaxial Helium Panel of a Cryogenic Vacuum Pump for Advanced Divertor of DIII–D Tokamak," in Proc. 1991 Cryogenic Engineering Conf., June 11-14, 1991, Huntsville, Alabama; General Atomics Report GA-A20589 (1991).

Baxi, C.B., G.J. Laughon, A.R. Langhorn, K.M. Schaubel, J.P. Smith, A.M. Gootgeld, G.L. Campbell, M.M. Menon, "Verification Test for Helium Panel of Cryopump for DIII–D Advanced Divertor," in Proc. 14th Symp. on Fusion Engineering, IEEE, San Diego, California, September 30–October 3, 1991; General Atomics Report GA-A20589 (1991).

Baxi, C.B., W. Obert, "Optimization of Thermal Design for Nitrogen Shield of JET Cryopump," in Proc. 14th Symp. on Fusion Engineering, IEEE, San Diego, California, September 30–October 3, 1991; General Atomics Report GA-A20587 (1991).

Bramson, G., "Timing System for Neutral Beam Injection on the DIII–D Tokamak," in Proc. 14th Symp. on Fusion Engineering, IEEE, San Diego, California, September 30–October 3, 1991; General Atomics Report GA-A20640 (1991).

Burrell, K.H., and the L to H Transition Physics Task Group, "Comparison of Theories of the L to H Transition with DIII–D Results," in Bull. 33rd Annual American Physical Society Meeting, November 4-8, 1991, Tampa, Florida (Abstract), **36** (1991) 2474.

Callis, R., W. Cary, C. Moeller, R. Freeman, R. Prater, D. Remsen, L. Sevier, "110 GHz ECH Heating System for DIII–D," in Proc. 9th Topical Conf. on Radio Frequency, August 19-21, 1991, Charleston, South Carolina; General Atomics Report GA-A20627 (1991).

Carlstrom, T.N., K.H. Burrell, J.C. DeBoo, G.L. Jackson, P. Gohil, R.J. Groebner, M.A. Mahdavi, T. Osborne, R. Philipona, "Scaling of H–mode Threshold Conditions in DIII–D," in Bull. 33rd Annual American Physical Society Meeting, November 4-8, 1991, Tampa, Florida (Abstract), **36** (1991) 2476.

Carlstrom, T.N., G.L. Campbell, J.C. DeBoo, R.G. Evanko, J. Evans, C.M. Greenfield, J.S. Haskovec, C.L. Hsieh, E.L. McKee, R.T. Snider, R.E. Stockdale, M.P. Thomas, P.K. Trost, "The Multipulse Thomson Scattering Diagnostic on the DIII–D Tokamak," in Proc. 14th Symp. on Fusion Engineering, IEEE, San Diego, California, September 30–October 3, 1991; General Atomics Report GA-A20614 (1991).

Cary, W.P., J.C. Allen, R.W. Callis, J.L. Doane, T.E. Harris, C.P. Moeller, A. Nerem, R. Prater, D. Remsen, "110 GHz ECH on DIII–D: System Overview and Initial Operation," in Proc. 14th Symp. on Fusion Engineering, IEEE, San Diego, California, September 30–October 3, 1991; General Atomics Report GA-A20632 (1991).

Chiu, S.C., M.J. Mayberry, R. Pinsker, C.C. Petty, M. Porkolab, "Theory of Ion Bernstein Wave Coupling at Low Edge Densities," in Proc. 9th Topical Conf. on Radio Frequency, August 19-21, 1991, Charleston, South Carolina; General Atomics Report GA-A20608 (1991).

Clow, D.D., D.H. Kellman, "Computer Control of the High Voltage Power Supply for the DIII–D Electron Cyclotron Heating System," in Proc. 14th Symp. on Fusion Engineering, IEEE, San Diego, California, September 30–October 3, 1991; General Atomics Report GA-A20606 (1991).

Coda, S., M. Porkolab, T.N. Carlstrom, M.J. Mayberry, C.C. Petty, R.I. Pinsker, "Phase Contrast Interferometry on DIII-D," in Bull. 33rd Annual American Physical Society Meeting, November 4-8, 1991, Tampa, Florida (Abstract), **36** (1991) 2473.

Colleraine, A.P., J.L. Luxon, and the DIII–D Group, "DIII–D: A Status Report," in *Fusion Tech.* **19** No. 3 (1991) 1247; General Atomics Report GA-A20299 (1990).

Cummings, J.W., P.A. Thurgood, "Software Upgrade for the DIII–D Neutral Beam Control Systems," in Proc. 14th Symp. on Fusion Engineering, IEEE, San Diego, California, September 30–October 3, 1991; General Atomics Report GA-A20590 (1991).

de Haas, J.C.M., T.C. Luce, C.C. Petty, W.H. Meyer, "Modulated ECH Experiments at DIII–D," in Bull. 33rd Annual American Physical Society Meeting, November 4-8, 1991, Tampa, Florida (Abstract), **36** (1991) 2476.

DeBoo, J.C., G.L. Jackson, T. Luce, D.P. Schissel, C.M. Greenfield, T. Osborne, C.C. Petty, T.S. Taylor, R.E. Waltz, J. Winter, "An Overview of Energy Confinement and Transport Studies in DIII–D," in Bull. 33rd Annual American Physical Society Meeting, November 4-8, 1991, Tampa, Florida (Abstract), **36** (1991) 2323.

DeBoo, J.C., R.E. Waltz, T. Osborne, "Comparison of Dimensionally Similar Discharges with Similar Heat Deposition Profiles," in Proc. 18th EPS Conf. on Controlled Fusion and Plasma Physics, June 3-7, 1991, Berlin, Germany; General Atomics Report GA-A20466 (1991).

The DIII–D Team, "Recent Results from DIII–D and Future Plans," in Proc. 14th Symp. on Fusion Engineering, IEEE, San Diego, California, September 30–October 3, 1991; General Atomics Report GA-A20711 (1992).

The DIII–D Team, "VH–Mode: A Very High Confinement Regime in the Boronized DIII–D Tokamak," in Proc. 18th EPS Conf. on Controlled Fusion and Plasma Physics, June 3-7, 1991, Berlin, Germany; General Atomics Report GA-A20552 (1991).

Doyle, E.J., R.J. Groebner, K.H. Burrell, P. Gohil, T. Lehecka, N.C. Luhmann, Jr., H. Matsumoto, T.H. Osborne, W.A. Peebles, R. Philipona, "Modifications in Turbulence and Edge Electric Fields at the L-H Transition in DIII–D," special issue of *Physics of Fluids B* **3** (1991) 2300; General Atomics Report GA-A20366 (1991).

Duong, H.H., W.W. Heidbrink, R.I. Pinsker, E.J. Strait, P.L. Taylor, "Confinement of Fast Ions During TAE Instabilities," in Bull. 33rd Annual American Physical Society Meeting, November 4-8, 1991, Tampa, Florida (Abstract), **36** (1991) 2477.

Evans, T.E., "Statistical Properties of Intrinsic Topological Noise in Tokamaks," in Proc. 18th EPS Conf. on Controlled Fusion and Plasma Physics, June 3-7, 1991, Berlin, Germany; General Atomics Report GA-A20448 (1991).

Evans, T.E., and The ASDEX Team, "Measurements of Poloidal and Toroidal Energy Deposition Asymmetries in the ASDEX Divertors," Max-Planck-Institut für Plasmaphysik Report IPP III/154 (1991).

Evans, T.E., J. Neuhaser, F. Leuterer, E.R. Müller, and The ASDEX Team, "Characteristics of Toroidal Energy Deposition Asymmetries in ASDEX," in *J. Nucl. Mater.* **176/177** (1990) 202-207; General Atomics Report GA-A20076 (1990).

Evans, T.E., M. Goniche, C. DeMichelis, D. Guilhem, W. Hess, M. Mattioli, P. Monier-Garbet, J-C. Vallet, and the L–H Group, "First Results from Combined Ergodic Boundary Layer and LHCD Experiments in Tore Supra," in Bull. 33rd Annual American Physical Society Meeting, November 4-8, 1991, Tampa, Florida (Abstract), **36** (1991) 2367.

Ferron, J.R., M.S. Chu, J. DeBoo, L. Lao, K. Matsuda, D. Schissel, E.J. Strait, T.S. Taylor, "The Effect of Current Profile Changes on Confinement in the DIII–D Tokamak," in Bull. 33rd Annual American Physical Society Meeting, November 4-8, 1991, Tampa, Florida (Abstract), **36** (1991) 2324.

Ferron, J.R., A. Kellman, E. McKee, T. Osborne, P. Petrach, T.S. Taylor, J. Wight, E. Lazarus, "An Advanced Plasma Control System for the DIII–D Tokamak," in Proc. 14th Symp. on Fusion Engineering, IEEE, San Diego, California, September 30–October 3, 1991; General Atomics Report GA-A20641 (1991).

Gohil, P., K.H. Burrell, E.J. Doyle, R.J. Groebner, J. Kim, R. Philipona, R.P. Seraydarian, "Study of the Edge Electric Field at the L–H Transition and ELMs in DIII–D," in Bull. 33rd Annual American Physical Society Meeting, November 4-8, 1991, Tampa, Florida (Abstract), **36** (1991) 2323.

Gohil, P., K.H. Burrell, E.J. Doyle, R.J. Groebner, N.C. Luhmann, Jr., W.A. Peebles, R. Philipona, R.P. Seraydarian, "Study of Edge Electric Field and Edge Microturbulence at the L–H Transition in DIII–D," in Proc. 18th EPS Conf. on Controlled Fusion and Plasma Physics, June 3-7, 1991, Berlin, Germany; General Atomics Report GA-A20481 (1991).

Gohil, P., K.H. Burrell, R.J. Groebner, J. Kim, W.C. Martin, E.L. McKee, R.P. Seraydarian, "The Charge Exchange Recombination Diagnostic System on the DIII–D Tokamak," in Proc. 14th Symp. on Fusion Engineering, IEEE, San Diego, California, September 30–October 3, 1991; General Atomics Report GA-A20652 (1991).

Gohil, P., K.H. Burrell, R.J. Groebner, R.P. Seraydarian, "High Spatial and Temporal Resolution Visible Spectroscopy of the Plasma Edge in DIII–D," in *Rev. Sci. Instru.* **61** No. 10 (1990) 2949; General Atomics Report GA-A20105 (1990).

Greene, K.L., "Displaying DIII–D Plasma Data Using DEC's X Window System," in Proc. 14th Symp. on Fusion Engineering, IEEE, San Diego, California, September 30–October 3, 1991; General Atomics Report GA-A20610 (1991).

Greenfield, C.M., K.H. Burrell, J.C. DeBoo, R.J. Groebner, G.L. Jackson, L.L. Lao, D.P. Schissel, T.S. Taylor, J. Winter, "Transport Analysis of VH–Mode Discharges in DIII–D," in Bull. 33rd Annual American Physical Society Meeting, November 4-8, 1991, Tampa, Florida (Abstract), **36** (1991) 2475.

Greenfield, C.M., G.L. Campbell, T.N. Carlstrom, J.C. DeBoo, C.-L. Hsieh, R.T. Snider, P.K. Trost, "A Real-Time Digital Control, Data Acquisition and Analysis System for the DIII–D Multipulse Thomson Scattering Diagnostic," in *Rev. Sci. Instru.* **61** (1990) 3286; General Atomics Report GA-A20097 (1990).

Groebner, R.J., K.H. Burrell, P. Gohil, R.P. Seraydarian, "Spectroscopic Study of Edge Poloidal Rotation and Radial Electronic Fields in the DIII–D Tokamaks," in *Rev. Sci. Instru.* **61** (1990) 2920; General Atomics Report GA-A20100 (1990).

Groebner, R.J., K.H. Burrell, P. Gohil, R.P. Seraydarian, J. Kim, T.C. Carlstrom, R.R. Dominguez, G.M. Staebler, E. Doyle, R. Philipona, C. Rettig, "Edge Ion Dynamics Before and After L–H Transition in DIII–D," in Bull. 33rd Annual American Physical Society Meeting, November 4-8, 1991, Tampa, Florida (Abstract), **36** (1991) 2474.

Harris, T.E., "Active Heater Control and Regulation for the Varian VGT-8011 Gyrotron," in Proc. 14th Symp. on Fusion Engineering, IEEE, San Diego, California, September 30–October 3, 1991; General Atomics Report GA-A20645 (1991).

Harvey, R.W., S.C. Chiu, M.G. McCoy, G.D. Smith, K.T. Mau, "3D Fokker-Planck Calculation of Combined Fast Wave and Electron Cyclotron Current Drive in a Tokamak Reactor," in Bull. 33rd Annual American Physical Society Meeting, November 4-8, 1991, Tampa, Florida (Abstract), **36** (1991) 2340.

Heidbrink, W.W., in collaboration with M.S. Chu, L.L. Lao, E.J. Strait, A.D. Turnbull, E.J. Doyle, C. Rettig, H. Duong, "TAE Modes in DIII–D," in Bull. 33rd Annual American Physical Society Meeting, November 4-8, 1991, Tampa, Florida (Abstract), **36** (1991) 2402.

Heidbrink, W.W., E.J. Strait, E.J. Doyle, G. Sager, R. Snider, "An Investigation of Beam-Driven Alfvén Instabilities in the DIII–D Tokamak," in *Nucl. Fusion* **31** (1991) 1635; General Atomics Report GA-A20254 (1991).

Hill, D.N., D. Buchenauer, R. Doerner, A. Futch, C.C. Klepper, R. Lehmer, B. Leikind, S. Lippmann, M.A. Mahdavi, M. Menon, J. Salmonson, M. Schaffer, L. Schmitz, J. Smith, J. Watkins, "Plasma Diagnostics for the DIII–D Divertor Upgrade," in *Rev. Sci. Instru.* **61** (1990) 3308; General Atomics Report GA-A20099 (1990).

Hill, D.N., D. Buchenaur, C.C. Klepper, A.W. Leonard, R. Moyer, T.W. Petrie, M.E. Rensink, J. Watkins, "Divertor-Plasma Characterization in DIII–D Plasmas," in Bull. 33rd Annual American Physical Society Meeting, November 4-8, 1991, Tampa, Florida (Abstract), **36** (1991) 2325.

Hodapp, T.R., G.L. Jackson, J. Phillips, K.L. Holtrop, P.I. Petersen, J. Winter, "A System to Deposit Boron Films (Boronization) in the DIII–D Tokamak," in Proc. 14th Symp. on Fusion Engineering, IEEE, San Diego, California, September 30–October 3, 1991; General Atomics Report GA-A20624 (1991).

Hogan, J., C. Klepper, L. Owen, P.K. Mioduszewski, E.A. Lazarus, R. Mangi, B. Braams, T. Taylor, R. Groebner, A. Mahdavi, M. Schaffer, D. Hill, "Plasma Modeling of Baffle Pressure Scaling Studies in the DIII–D Advanced Divertor Experiment," in Bull. 33rd Annual American Physical Society Meeting, November 4-8, 1991, Tampa, Florida (Abstract), **36** (1991) 2503.

Holtrop, K.L., G.L. Jackson, K.M. Schaubel, A.G. Kellman, "Glow Discharge Initiation with Electron Gun Assist," in Proc. 14th Symp. on Fusion Engineering, IEEE, San Diego, California, September 30–October 3, 1991; General Atomics Report GA-A20617 (1991).

Holtrop, K., A.G. Kellman, R.L. Lee, P.L. Taylor, "Behavior of Plasma Current During DIII–D Disruptions," in Bull. 33rd Annual American Physical Society Meeting, November 4-8, 1991, Tampa, Florida (Abstract), **36** (1991) 2478.

Hong, R., J. Phillips, J. Wight, "Effects of Filament Temperature on the Arc Discharge and Beam Operation of the DIII–D Neutral Beam Ion Sources," in Bull. 33rd Annual American Physical Society Meeting, November 4-8, 1991, Tampa, Florida (Abstract), **36** (1991) 2424.

Howl, W., A.D. Turnbull, T.S. Taylor, L.L. Lao, F.J. Helton, J.R. Ferron, and E.J. Strait, "Sensitivity of the Kink Instability of the Pressure Profile," General Atomics Report GA-A19953 (1991); submitted to *Physics of Fluids B.*

Hsieh, C., T. Carlstrom, M. Chu, J. DeBoo, C. Greenfield, R. Snider, R. Stockdale, T. Taylor, "Electron Temperature and Density Profiles in Tokamaks," in Bull. 33rd Annual American Physical Society Meeting, November 4-8, 1991, Tampa, Florida (Abstract), **36** (1991) 2477.

Jackson, G.L., T.S. Taylor, P.L. Taylor, "Particle Control in DIII–D with Helium Glow Discharge Conditioning," in *Nucl. Fusion* **30** (1990) 2305; General Atomics Report GA-A19891 (1990).

Jackson, G.L., J. Winter, T.S. Taylor, K.H. Burrell, J.C. DeBoo, C.M. Greenfield, R.J. Groebner, T. Hodapp, K. Holtrop, E.A. Lazarus, L.L. Lao, S.I. Lippmann, T.H. Osborne, T.W. Petrie, J. Phillips, D.P. Schissel, E.J. Strait, A.D. Turnbull, The DIII–D Team, "Regime of Very High Confinement in the Boronized DIII–D Tokamak," in *Phys. Rev. Lett.* **67** (1991) 3098; General Atomics Report GA-A20567 (1991).

James, R.A., R.F. Ellis, R. Harvey, J. Lohr, T. Luce, C. Petty, R. Pinsker, R. Prater, "Second Harmonic Electron Cyclotron Current Drive Experiments in DIII-D Using 60 GHz Inside Launched ECH," in Bull. 33rd Annual American Physical Society Meeting, November 4-8, 1991, Tampa, Florida (Abstract), **36** (1991) 2471.

James, R.A., G. Giruzzi, A. Fyakhretdinov, B. de Gentile, Yu. Gorelov, R. Harvey, S. Janz, J. Lohr, T.C. Luce, K. Matsuda, C.P. Moeller, R. Prater, L. Rodriguez, R. Snider, V. Trukhin, "Electron Cyclotron Current Drive Experiments in the DIII-D Tokamak," General Atomics Report GA-A20429 (1991); submitted to *Phys. Rev. A.*

Jensen, T.H., J.M. Greene, P.A. Politzer, "Large Anomaly of the Perpendicular Resistivity of a Tokamak," in Bull. 33rd Annual American Physical Society Meeting, November 4-8, 1991, Tampa, Florida (Abstract), **36** (1991) 2412; General Atomics Report GA-A20557 (1991); submitted to *Phys. Fluids B.*

Jensen, T.H., A.W. Leonard, R.J. La Haye, M.S. Chu, "Effects of Plasma Flow on Error Field Islands," in *Physics of Fluids B* **3** (1991) 1650; General Atomics Report GA-A20091 (1990).

Jensen, T.H., D.G. Skinner, "Support of the Model for 'Vertical Displacement Episodes' from Numerical Simulation of Episodes Observed in the DIII-D Tokamak," in *Physics of Fluids B* **2** (1990) 2358; General Atomics Report GA-A19882 (1990).

Khayrutdinov, R.R., E.A. Azizov, A.G. Kellman, "Numerical Study of Plasma Behavior During Disruptions in DIII-D," in Bull. 33rd Annual American Physical Society Meeting, November 4-8, 1991, Tampa, Florida (Abstract), **36** (1991) 2478.

Kim, J., R.J. Groebner, K.H. Burrell, P. Gohil, R.P. Seraydarian, "Comparison of Experimental Values of Impurity Poloidal and Toroidal Flow Velocities with Predictions of Neoclassical Theory," in Bull. 33rd Annual American Physical Society Meeting, November 4-8, 1991, Tampa, Florida (Abstract), **36** (1991) 2474.

Klepper, C.C., J.T. Hogan, N.H. Brooks, D. Buchenauer, A.H. Futch, S. Tugarinov, W.P. West, "Spectral Profiles of Neutral Particles in the DIII-D Divertor," in Bull. 33rd Annual American Physical Society Meeting, November 4-8, 1991, Tampa, Florida (Abstract), **36** (1991) 2504.

Klepper, C.C., J.T. Hogan, M.A. Mahdavi, M.J. Schaffer, D. Buchenauer, G. Haas, D.N. Hill, R. Maingi, P.K. Mioduszewski, L.W. Owen, R. Stambaugh, "Divertor Neutral Pressure Enhancement with a Baffle in DIII–D," in Bull. 33rd Annual American Physical Society Meeting, November 4-8, 1991, Tampa, Florida (Abstract), **36** (1991) 2325.

Kurki-Suonio, T., R.J. Groebner, K.H. Burrell, "Changes in Local Confinement After an L–H Transition in DIII–D," General Atomics Report GA-A20450 (1991); submitted to *Nucl. Fusion.*

Kurki-Suonio, T., R.J. Groebner, R. Philipona, C. Rettig, E. Doyle, K.H. Burrell, W.A. Peebles, "Comparison of Reduction in Fluctuations and Transport on DIII–D," in Bull. 33rd Annual American Physical Society Meeting, November 4-8, 1991, Tampa, Florida (Abstract), **36** (1991) 2475.

La Haye, R.J., "Calculation of the Effects of Field Errors on Diverted Magnetic Field Lines in the DIII–D Tokamak," in *Nucl. Fus.* **31** (1991) 1550; General Atomics Report GA-A20327 (1991).

La Haye, R.J., "Critical Error Fields for Locked Mode Instability in Tokamaks," General Atomics Report GA-A20709 (1991); submitted to special issue of *Phys. Fluids B.*

La Haye, R.J., "Error Field Considerations for BPX," in Proc. 14th Symp. on Fusion Engineering, IEEE, San Diego, California, September 30–October 3, 1991; General Atomics Report GA-A20579 (1991).

La Haye, R.J., J.T. Scoville, "A Method to Measure Poloidal Field Coil Irregularities in Toroidal Plasma Devices," in *Rev. Sci. Instru.* **62** (1991) 2146; General Atomics Report GA-A20356 (1991).

La Haye, R.J., J.T. Scoville, "Non-Linear Instability of DIII–D to Error Fields," in Proc. IAEA Technical Committee Mtg., September 10-12, 1991, Culham Laboratory, Abingdon, UK; General Atomics Report GA-A20653 (1991).

Lao, L.L., "Effects of Current Profile on the Ideal Ballooning Mode," in *Physics of Fluids B* **4** (1992) 232; General Atomics Report GA-A20593 (1991).

Lao, L.L., J.R. Ferron, T.S. Taylor, E.J. Strait, V.S. Chan, M.S. Chu, E.A. Lazarus, K. Matsuda, H. St. John, A.D. Turnbull, "Dependence of Plasma Stability and Confinement on the Current Density Profile," in Bull. 33rd Annual American Physical Society Meeting, November 4-8, 1991, Tampa, Florida (Abstract), **36** (1991) 2477.

Lao, L.L., T.H. Jensen, "Magnetohydrodynamic Equilibria in Elongated Tokamaks After Loss of Vertical Stability," in *Nucl. Fusion* **31** (1991) 1909; General Atomics Report GA-A20101 (1991).

Lao, L.L., T.S. Taylor, M.S. Chu, A.D. Turnbull, E.J. Strait, J.R. Ferron, E.A. Lazarus, "Effects of Current Profiles on MHD Stability," in Proc. 18th EPS Conf. on Controlled Fusion and Plasma Physics, June 3-7, 1991, Berlin, Germany; General Atomics Report GA-A20479 (1991).

Lazarus, E.A., M.S. Chu, J.R. Ferron, F.J. Helton, J.T. Hogan, A.G. Kellman, L.L. Lao, J.B. Lister, T.H. Osborne, R. Snider, E.J. Strait, T.S. Taylor, A.D. Turnbull, "Higher Beta at Higher Elongation in the DIII–D Tokamak," in a special issue of *Physics of Fluids* **3** No. 8 (1991) 2220; General Atomics Report GA-A20352 (1991).

Lazarus, E.A., L.L. Lao, M.S. Osborne, A.D. Chu, A.D. Turnbull, E.J. Strait, T.S. Taylor, "Second Stable Core Plasma in DIII–D," in Bull. 33rd Annual American Physical Society Meeting, November 4-8, 1991, Tampa, Florida (Abstract), **36** (1991) 2324.

Lazarus, E.A., L.L. Lao, T.H. Osborne, T.S. Taylor, A.D. Turnbull, M.S. Chu, A.G. Kellman, E.J. Strait, J.R. Ferron, R.J. Groebner, W.W. Heidbrink, T. Carlstrom, F.J. Helton, C.L. Hsieh, S. Lippmann, D.P. Schissel, R. Snider, D. Wroblewski, "An Optimization of Beta in the DIII–D Tokamak," General Atomics Report GA-A20571 (1991); submitted to *Physics of Fluids*.

Lee, R.L., K. Holtrop, A. Kellman, M. Menon, P. Petersen, J.T. Scoville, E.J. Strait, P. Taylor, "Development of a Database for Operations and Disruptions Physics," in Bull. 33rd Annual American Physical Society Meeting, November 4-8, 1991, Tampa, Florida (Abstract), **36** (1991) 2478.

Leonard, A.W., A.M. Howald, A.W. Hyatt, T. Shoji, T. Fujita, M. Miura, N. Suzuki, S. Tsuji, The JFT–2M Group, "The Effects of Applied Error Fields on the H–mode Power Threshold of JFT–2M," in *Nucl. Fusion* **31** (1991) 1511; General Atomics Report GA-A20315 (1991).

Leonard, A.W., A.W. Hyatt, T. Shoji, S. Tsuji, Y. Miura, M. Mori, N. Suzuki, N. Ohyabu, "The New JFT–2M Ergodic Magnetic Limiter," in Bull. 33rd Annual American Physical Society Meeting, November 4-8, 1991, Tampa, Florida (Abstract), **36** (1991) 2368.

Lippmann, S.I., "Radially Resolved Measurement of Intrinsic Impurities on DIII–D," in Bull. 33rd Annual American Physical Society Meeting, November 4-8, 1991, Tampa, Florida (Abstract), **36** (1991) 2473.

Lister, J.B., E.A. Lazarus, A.G. Kellman, J.-M. Moret, J.R. Ferron, F.J. Helton, L.L. Lao, J.A. Leuer, E.J. Strait, T.S. Taylor, and A.D. Turnbull, "Experimental Study of the Vertical Stability of High Decay Index Plasmas in the DIII–D Tokamak," in *Nucl. Fusion* **30** (1990) 2349; General Atomics Report GA-A19843 (1990).

Lloyd, B., G.L. Jackson, T.S. Taylor, E.A. Lazarus, T.C. Luce, R. Prater, "Voltage Ohmic- and ECH-Assisted Startup in DIII–D," in *Nucl. Fusion* **31** (1991) 2031; General Atomics Report GA-A20453 (1991).

Lohr, John, R.W. Harvey, R.A. James, T.C. Luce, C.C. Petty, V.V. Alikaev, A.A. Bagdasarov, A.A. Borshchegovsky, Yu.V. Gorelov, A.B. Pimenov, K.A. Razumova, I.N. Roi, V.M. Trukhin, and N.L. Vasin, "Analysis of Non-Inductive Current Drive from ECCD and Bootstrap on T–10," in Proc. 9th Topical Conf. on Radio Frequency, August 19-21, 1991, Charleston, South Carolina; General Atomics Report GA-A20647 (1991).

Luce, T.C., S.C. Chiu, R.W. Harvey, M.J. Mayberry, C.C. Petty, R.I. Pinsker, R. Prater, S.I. Tsunoda, "Modeling of Fast Wave Current Drive Experiments on DIII–D," in Proc. 9th Topical Conf. on Radio Frequency, August 19-21, 1991, Charleston, South Carolina; General Atomics Report GA-A20691 (1991).

Luce, T., C. Petty, D. Schissel, T. Osborne, J. DeBoo, "Inward Energy Transport During Off-Axis Heating," in Bull. 33rd Annual American Physical Society Meeting, November 4-8, 1991, Tampa, Florida (Abstract), **36** (1991) 2349.

Luce, T.C., C.C. Petty, J.C.M. de Haas, "Inward Transport of Energy in Tokamak Plasmas," in *Phys. Rev. Lett.* **68** (1992) 62; General Atomics Report GA-A20541 (1991).

Mahdavi, M.A., R.J. Groebner, D.N. Hill, A. Hyatt, A. Leonard, T. Osborne, M.S. Schaffer, G. Staebler, R. Stambaugh, E.J. Strait, "Effects of Edge Currents and Electric Fields on the H–mode Transition," in Bull. 33rd Annual American Physical Society Meeting, November 4-8, 1991, Tampa, Florida (Abstract), **36** (1991) 2324.

Mahdavi, M. Ali, M. Schaffer, P. Anderson, C. Baxi, J.N. Brooks, D. Buchenauer, R. Doerner, A. Futch, G. Haas, D.N. Hill, J. Hogan, W.L. Hsu, G.L. Jackson, T. Jarboe, A.G. Kellman, C.C. Klepper, E. Lazarus, B. Leikind, S. Lippmann, J. Luxon, G.F. Matthews, M. Menon, P. Mioduszewski, B. Mills, R. Moyer, T. Osborne, L. Owen, P. Petersen, G. Porter, E. Reis, M.E. Rensink, L. Schmitz, J.T. Scoville, J. Smith, G.M. Staebler, R. Stambaugh, P. Taylor, J. Watkins, and C. Wong, "Divertor Baffling and Biasing Experiments on DIII–D," in Proc. 13th Int. Conf. on Plasma Physics and Controlled Nuclear Fusion Research, October 1-6, 1990, Washington, D.C., Vol. 3, IAEA, Vienna (1991) 335; General Atomics Report GA-A20317 (1991).

Matsumoto, H., K.H. Burrell, T.N. Carlstrom, E.J. Doyle, P. Gohil, R.J. Groebner, T. Lehecka, N.C. Luhmann, Jr., M.A. Mahdavi, T.H. Osborne, W.A. Peebles, R. Philipona, "Suppression of the Edge Turbulence at the L to H Transition in DIII–D," General Atomics Report GA-A20383 (1991); submitted to *Plasma Physics and Controlled Fusion.*

Matsumoto, H., R.E. Stockdale, J. de Haas, D. Hill, K.H. Burrell, "Perturbative Particle Transport Study of DIII–D H–mode Plasmas," in Bull. 33rd Annual American Physical Society Meeting, November 4-8, 1991, Tampa, Florida (Abstract), **36** (1991) 2476.

Matthews, G., D.N. Buchenauer, D.N. Hill, M.A. Mahdavi, M. Rensink, P.C. Stangeby, "Impurity Transport at the DIII–D Divertor Strike Points," in Proc. 18th EPS Conf. on Controlled Fusion and Plasma Physics, June 3-7, 1991, Berlin, Germany; General Atomics Report GA-A20472 (1991).

Matthews, G.F., D.N. Hill, M.A. Mahdavi, "The Angular Dependence of Power in the DIII–D Divertor," in *Nucl. Fusion* **31** No. 7 (1991) 1383; General Atomics Report GA-A20308 (1990).

Mayberry, M.J., R.I. Pinsker, S.C. Chiu, G.L. Jackson, S.I. Lippmann, M. Porkolab, R. Prater, F.W. Baity, R.H. Goulding, D.J. Hoffman, "Fast Wave Current Drive Antenna Performance on DIII–D," in Proc. 9th Topical Conf. on Radio Frequency, August 19-21, 1991, Charleston, South Carolina; General Atomics Report GA-A20694 (1991).

McHarg, Jr., B.B., "The Use of a VAX Cluster for the DIII–D Data Acquisition System," in Proc. 14th Symp. on Fusion Engineering, IEEE, San Diego, California, September 30–October 3, 1991; General Atomics Report GA-A20584 (1991).

Moeller, C., R. Callis, W. DeHope, J. Doane, R. Freeman, R. Prater, D. Remsen, L. Sevier, "110 GHz ECH System for DIII–D," in Proc. 18th EPS Conf. on Controlled Fusion and Plasma Physics, June 3-7, 1991, Berlin, Germany; General Atomics Report GA-A20471 (1991).

Moeller, C.P., J.L. Doane, "A Coaxial Converter for Transforming a Whispering Gallery Mode to the He_{11} Mode," in Proc. 9th Topical Conf. on Radio Frequency, August 19-21, 1991, Charleston, South Carolina; General Atomics Report GA-A20628 (1991).

Moyer, R.A., J.G. Watkins, K. Burrell, R.W. Conn, R. Doerner, D. Hill, R. Lehmer, M.A. Mahdavi, L. Schmitz, G. Tynan, "Initial Characterization of Fluctuations in the DIII–D Edge Plasma with the SNL/UCLA Fast Reciprocating Langmuir Probe," in Bull. 33rd Annual American Physical Society Meeting, November 4-8, 1991, Tampa, Florida (Abstract), **36** (1991) 2472.

Osborne, T., D. Bhadra, R. Waltz, "H–Mode Confinement at High Aspect Ratio," in Bull. 33rd Annual American Physical Society Meeting, November 4-8, 1991, Tampa, Florida (Abstract), **36** (1991) 2477.

Osborne, T., N. Brooks, K.H. Burrell, T. Carlstrom, R. Groebner, D. Hill, W. Howl, A. Kellman, L. Lao, N. Ohyabu, M. Perry, T. Taylor, "Observation of H–mode in Ohmically Heated Divertor Discharges on DIII–D," in *Nucl. Fusion* **30** (1990) 2023; General Atomics Report GA-A19362 (1990).

Ozeki, T., M.S. Chu, L.L. Lao, T.S. Taylor, M.S. Chance, S. Kinoshita, K.H. Burrell, "Plasma Shaping, Edge Ballooning Stability, and the Occurrence of Giant ELMs in DIII–D," in *Nucl. Fusion* **30** (1990) 1425; General Atomics Report GA-A19495 (1989).

Parks, P.A., "Electric Field and Current Distributions Near the Ablation Cloud of a Pellet Injected into a Tokamak Magnetic Field," in Bull. 33rd Annual American Physical Society Meeting, November 4-8, 1991, Tampa, Florida (Abstract), **36** (1991) 2497.

Petersen, P.I., S.M. Miller, "The DIII–D Tokamak Trouble Report Database," in Proc. 14th Symp. on Fusion Engineering, IEEE, San Diego, California, September 30–October 3, 1991; General Atomics Report GA-A20612 (1991).

Petrie, T.W., D.N. Hill, J. Baptista, M. Brown, "Infrared Thermography System on DIII–D," in *Rev. Sci. Instru.* **61** (1990) 3557; General Atomics Report GA-A20112 (1990).

Petrie, T.W., D.N. Hill, D. Buchenauer, A. Futch, K. Holtrop, C. Klepper, "Radiative Experiments in ELMing H–mode Plasmas in DIII–D," in Bull. 33rd Annual American Physical Society Meeting, November 4-8, 1991, Tampa, Florida (Abstract), **36** (1991) 2471.

Petrie, T.W., D.N. Hill, D. Buchenauer, A. Futch, C. Klepper, S. Lippmann, M.A. Mahdavi, "Recent Gaseous Divertor Experiments in DIII–D," in Proc. 18th EPS Conf. on Controlled Fusion and Plasma Physics, June 3-7, 1991, Berlin, Germany; General Atomics Report GA-A20478 (1991).

Petty, C.C., T.C. Luce, J.C.M. de Haas, R.A. James, John Lohr, K. Matsuda, R. Prater, R. Stockdale, "Non-Diffusive Heat Transport During Electron Cyclotron Heating on the DIII–D Tokamak," in Proc. 18th EPS Conf. on Controlled Fusion and Plasma Physics, June 3-7, 1991, Berlin, Germany; General Atomics Report GA-A20465 (1991).

Petty, C.C., R.I. Pinsker, M.J. Mayberry, S.C. Chiu, T. Luce, T. Osborne, R. Prater, R. James, M. Porkolab, F.W. Baity, R.H. Goulding, D.J. Hoffman, "Direct Electron Absorption of 60 MHz Fast Waves on DIII–D," in Bull. 33rd Annual American Physical Society Meeting, November 4-8, 1991, Tampa, Florida (Abstract), **36** (1991) 2470.

Petty, C.C., R.I. Pinsker, M.J. Mayberry, S.C. Chiu, M. Porkolab, T.C. Luce, R. Prater, P.T. Bonoli, J.C.M. de Haas, R.A. James, F.W. Baity, R.H. Goulding, D.J. Hoffman, "Direct Electron Heating by 60 MHz Fast Waves on DIII–D," in Proc. 9th Topical Conf. on Radio Frequency, August 19-21, 1991, Charleston, South Carolina; General Atomics Report GA-A20688 (1991).

Petty, C.C., R.I. Pinsker, M.J. Mayberry, M. Porkolab, P.T. Bonoli, R. Prater, F.W. Baity, R.H. Goulding, D.J. Hoffman, "Fundamental and Second Harmonic Hydrogen Fast-Wave Heating on DIII-D," in Proc. 9th Topical Conf. on Radio Frequency, August 19-21, 1991, Charleston, South Carolina; General Atomics Report GA-A20693 (1991).

Philipona, R., R.J. Groebner, K.H. Burrell, E.J. Doyle, P. Gohil, N.C. Luhmann, Jr., H. Matsumoto, W.A. Peebles, C.L. Rettig, R.D. Stambaugh, "Two-Stage Turbulence Suppression and E × B Plasma Flow Measured at the L–H Transition," General Atomics Report GA-A20516 (1991); submitted to *Phys. Rev. Lett.*

Pinsker, R.I., M.J. Mayberry, C.C. Petty, W.P. Cary, J. Pusl, D. Remsen, F.W. Baity, R.H. Goulding, D.J. Hofmann, "30-60 MHz FWCD System on DIII-D: Power Division, Phase Control, and Tuning for a Four-Element Antenna Array," in Proc. 14th Symp. on Fusion Engineering, IEEE, San Diego, California, September 30–October 3, 1991; General Atomics Report GA-A20619 (1991).

Pinsker, R.I., M.J. Mayberry, C.C. Petty, M. Porkolab, S.C. Chiu, R. Prater, F.W. Baity, R.H. Goulding, D.J. Hoffman, "ICRF Heating Experiments on DIII-D," in Proc. 9th Topical Conf. on Radio Frequency, August 19-21, 1991, Charleston, South Carolina; General Atomics Report GA-A20697 (1991).

Pinsker, R.I., C.C. Petty, M.J. Mayberry, S.C. Chiu, R. Harvey, T.C. Luce, T. Osborne, M. Porkolab, R. Prater, T. Taylor, R.A. James, F.W. Baity, R.H. Goulding, D.J. Hoffman, the DIII-D Group, "Initial Results from the DIII-D Fast Wave Current Drive Experiment," in Bull. 33rd Annual American Physical Society Meeting, November 4-8, 1991, Tampa, Florida (Abstract), **36** (1991) 2470.

Politzer, P.A., G.D. Porter, "Power Threshold for Neutral Beam Current Drive," in *Nucl. Fusion* **30** (1990) 1605; General Atomics Report GA-A19869 (1990).

Prater, R., F.W. Baity, S.C. Chiu, D. Ehst, R. Freeman, R.H. Gouldings, R. Harvey, D.J. Hoffman, R. James, H. Kawashima, J. Lohr, T. Luce, T.K. Mau, M. Mayberry, C. Petty, R. Pinsker, M. Porkolab, "Initial Fast Wave Current Drive Experiments on DIII-D," in Bull. 33rd Annual American Physical Society Meeting, November 4-8, 1991, Tampa, Florida (Abstract), **36** (1991) 2324.

Prater, R., T.J. Mayberry, C.C. Petty, R.I. Pinsker, S.C. Chiu, R.W. Harvey, T.C. Luce, M. Porkolab, F.W. Baity, R.H. Goulding, D.J. Hoffman, R.A. James, H. Kawashima, A. Becoulet, D. Moreau, V. Trukhin, "Initial Fast Wave Heating and Current Drive Experiments on the DIII-D Tokamak," in Proc. IAEA Tech. Committee Mtg. on Fast Wave Current Drive, Arles, France, September 23-25, 1991; General Atomics Report GA-A20784.

Project Staff, "DIII-D Research Operations Annual Report to the U.S. Department of Energy," T. Simonen (ed.), General Atomics Report GA-A20361 (1991).

Reis, E., R.D. Blevins, T.H. Jensen, J.L. Luxon, P.I. Petersen, E.J. Strait, "Modeling and Measurement of the Motion of the DIII-D Vacuum Vessel During Vertical Instabilities," in Proc. 14th Symp. on Fusion Engineering, IEEE, San Diego, California, September 30–October 3, 1991; General Atomics Report GA-A20636 (1991).

Rensink, M.E., J.L. Milovich, T.D. Rognlien, A.H. Futch, R.A. Jong, G.D. Porter, D.N. Hill, T.W. Petrie, D. Buchenauer, C. Klepper, A.W. Leonard, R. Moyer, J. Watkins, M.A. Mahdavi, "Modeling of DIII-D Divertor Plasmas at ITER-like Power Levels," in Bull. 33rd Annual American Physical Society Meeting, November 4-8, 1991, Tampa, Florida (Abstract), **36** (1991) 2472.

Schaffer, M.J., D. Buchenauer, D.N. Hill, C.C. Klepper, M.A. Mahdavi, T. Osborne, T.W. Petrie, R.D. Stambaugh, "Advanced Divertor Experiments on DIII-D," in Proc. 18th EPS Conf. on Controlled Fusion and Plasma Physics, June 3-7, 1991, Berlin, Germany, Vol. 15C, Part III (1991) 241; General Atomics Report GA-A20480 (1991).

Schaffer, M.J., D.N. Hill, N. Brooks, A. Hyatt, C. Klepper, L.L. Lao, S. Lippmann, M.A. Mahdavi, T. Osborne, T. Petrie, G. Porter, J. Smith, R. Stambaugh, G. Staebler, "Biased Divertor Experiments on DIII-D," in Bull. 33rd Annual American Physical Society Meeting, November 4-8, 1991, Tampa, Florida (Abstract), **36** (1991) 2325.

Schaffer, M.J., B.J. Leikind, "Observation of Electric Currents in Diverted Tokamak Scrape-Off Layers," in *Nucl. Fusion Lett.* **31** (1991) 1750; General Atomics Report GA-A20128 (1991).

Schaffer, M.J., S.I. Lippmann, M.A. Mahdavi, T.W. Petrie, R.D. Stambaugh, J. Hogan, C.C. Klepper, P. Mioduszewski, L. Owen, D.N. Hill, M. Rensink, D. Buchenauer, "Particle Control in the DIII–D Advanced Divertor," in Proc. 14th Symp. on Fusion Engineering, IEEE, San Diego, California, September 30–October 3, 1991; General Atomics Report GA-A20631 (1991).

Schaffer, M.J., M.A. Mahdavi, C.C. Klepper, D.N. Hill, M.E. Rensink, "Effect of Divertor Bias on Plasma Flow in the Tokamak Scrape-off Layer," General Atomics Report GA-A20474 (1991); submitted to *Nucl. Fusion.*

Schaubel, K.M., C.B. Baxi, G.L. Campbell, A.M. Gootgeld, A.R. Langhorn, G.J. Laughon, J.P. Smith, P.M. Anderson, M.M. Menon, "Design of the Advanced Divertor Pump Cryogenic System for DIII–D," in Proc. 14th Symp. on Fusion Engineering, IEEE, San Diego, California, September 30–October 3, 1991; General Atomics Report GA-A20607 (1991).

Schissel, D.P., J.C. DeBoo, K.H. Burrell, J.R. Ferron, R.J. Groebner, H. St. John, R.D. Stambaugh, the DIII–D Research Team, B.J.D. Tubbing, K. Thomsen, J.G. Cordey, M. Keilhacker, D. Stork, P.E. Stott, A. Tanga, and the JET Team, "H–Mode Energy Confinement Scaling from the DIII–D and JET Tokamaks," in *Nucl. Fusion* **31** (1991) 73; General Atomics Report GA-A19925 (1990); JET Report JET-P(90)16.

Schissel, D.P., J.C. DeBoo, R. Ryter, O. Gruber, O. Kardaun, F. Wagner, "H–Mode Energy Confinement Scaling from the ASDEX, DIII–D, and JET Tokamaks," in Proc. 18th EPS Conf. on Controlled Fusion and Plasma Physics, June 3-7, 1991, Berlin, Germany; General Atomics Report GA-A20548 (1991).

Schissel, D.P., A.G. Kellman, R.T. Snider, R.D. Stambaugh, K.H. Burrell, J.C. DeBoo, T.H. Osborne, J.D. Callen, Z. Chang. "An Examination of DIII–D Energy Confinement at Small Values of the Plasma Safety Factor," in *Nucl. Fusion* **32** (1991) 107; General Atomics Report GA-A20438 (1991).

Schissel, D.P., T.H. Osborne, J.C. DeBoo, J.R. Ferron, E.A. Lazarus, T.S. Taylor, "An Examination of Heat Transport During Off Axis Neutral Beam Injection in DIII–D," General Atomics Report GA-A20696 (1991); submitted to *Nucl. Fusion.*

Schissel, D.P., T. Osborne, J.C. DeBoo, R.E. Waltz, T.C. Luce, C.C. Petty, "Non-Diffusive Heat Transport During Off-Axis NBI in DIII–D," in Bull. 33rd Annual American Physical Society Meeting, November 4-8, 1991, Tampa, Florida (Abstract), **36** (1991) 2323.

Scoville, J.T., R.J. La Haye, "Design of a Coil to Correct Magnetic Field Errors on the DIII–D Tokamak," in Proc. 14th Symp. on Fusion Engineering, IEEE, San Diego, California, September 30–October 3, 1991; General Atomics Report GA-A20577 (1991).

Scoville, J.T., R.J. La Haye, "Measurement and Correction of Error Fields on the DIII–D Tokamak," in Bull. 33rd Annual American Physical Society Meeting, November 4-8, 1991, Tampa, Florida (Abstract), **36** (1991) 2478.

Scoville, J.T., R.J. La Haye, A.G. Kellman, T.H. Osborne, "Locked Modes in DIII–D and a Method for Prevention of the Low Density Mode," in *Nucl. Fusion* **31** (1991) 875-890; General Atomics Report GA-A19983 (1990).

Scoville, J.T., P.I. Petersen, "A Low-Cost Multiple Hall Probe Current Transducer," in *Rev. Sci. Instru.* **62** No. 3 (1991) 755-760.

Seraydarian, R.P., K.H. Burrell, R.J. Groebner, "A Global Fitting Code for Multichordal Neutral Beam Spectroscopic Data," in Bull. 33rd Annual American Physical Society Meeting, November 4-8, 1991, Tampa, Florida (Abstract), **36** (1991) 2474.

Simonen, T.C., "Overview of the 1990's DIII–D Research Program," presented at the Fusion Power Associates Annual Meeting and Symposium, June 25-26, 1991, Princeton, New Jersey; General Atomics Report GA-A20569 (1991).

Simonen, T.C., D. Brower, P. Efthimion, J.C.M. DeHaas, E. Fredrickson, K.W. Gentle, E.B. Hooper, E. Marmar, R. Stambaugh, "Plasma Transport Studies Using Transient Techniques," in *Comments on Plasma Phys. in Contr. Fusion* **14** (1991) 57; General Atomics Report GA-A20053 (1991).

Smith, J.P., C.B. Baxi, E. Reis, M.J. Schaffer, K.M. Schaubel, M.M. Menon, "The Design and Fabrication of a Toroidally Continuous Cryocondensation Pump for the DIII–D Advanced Divertor," in Proc. 14th Symp. on Fusion Engineering, IEEE, San Diego, California, September 30–October 3, 1991; General Atomics Report GA-A20672 (1991).

Smith, J.P., M.J. Schaffer, A.W. Hyatt, "The Electrical Insulation of the DIII–D Advanced Divertor Electrode," in Proc. 14th Symp. on Fusion Engineering, IEEE, San Diego, California, September 30–October 3, 1991; General Atomics Report GA-A20623 (1991).

Snider, R., "Sawtooth Crashes in JET," JET Report JET-IR(91) 08 (1991).

Snider, R.T., "Scaling of the Sawtooth Inversion Radius and Mixing Radius on DIII–D," in *Nucl. Fusion* **30** (1990) 2400; General Atomics Report GA-A19610 (1990).

Snider, R., and the DIII–D Team, "The DIII–D Tokamak and Energy Confinement at Low q," in Proc. 18th Annual Conf. on Plasma Physics, July 3-5, 1991, Colchester, England; General Atomics Report GA-A20556 (1991).

St. John, H., K.H. Burrell, R.J. Groebner, "Automated Analysis of Ion Temperature from the CER Diagnostic," in Bull. 33rd Annual American Physical Society Meeting, November 4-8, 1991, Tampa, Florida (Abstract), **36** (1991) 2473.

Staebler, G.M., "Transport Modeling of Divertor Bias Experiments," in *Nucl. Fusion* **31** (1991) 729; General Atomics Report GA-A20185 (1990).

Stambaugh, R.D., "On the Use of Positrons to Probe Magnetic Versus Electrostatic Turbulence," in *Rev. Sci. Instru.* **61** (1990) 3043; General Atomics Report GA-A20096 (1990).

Stambaugh, R.D., and the DIII–D Team, "DIII–D Research Program Progress," in Proc. 13th Int. Conf. on Plasma Physics and Controlled Nuclear Fusion Research, October 1-6, 1990, Washington, D.C.; General Atomics Report GA-A20273 (1990).

Stambaugh, R.D., L.L. Lao, "On the Relation of Vertical Stability and Aspect Ratio in Tokamaks," General Atomics Report GA-A20603 (1991); submitted to *Nucl. Fusion.*

Strait, E.J., M.S. Chu, J.R. Ferron, L.L. Lao, E.A. Lazarus, T.H. Osborne, T.S. Taylor, A.D. Turnbull, "Dependence of the DIII–D Beta Limit on the Current Profile," in Proc. 18th EPS Conf. on Controlled Fusion and Plasma Physics, June 3-7, 1991, Berlin, Germany (Abstract) **15C**, Part II (1991) 105; General Atomics Report GA-A20477 (1991).

Strait, E.J., L.L. Lao, J.L. Luxon, E.E. Reis, "Observation of Poloidal Current Flow to the Vacuum Vessel Wall During a Tokamak Vertical Instability," in *Nucl. Fusion* **31** (1991) 527; General Atomics Report GA-A20036 (1990).

Strait, E.J., W.W. Heidbrink, M.S. Chu, L.L. Lao, T.S. Taylor, A.D. Turnbull, "Stability of TAE Modes in DIII–D," in Bull. 33rd Annual American Physical Society Meeting, November 4-8, 1991, Tampa, Florida (Abstract), **36** (1991) 2324.

Taylor, P.L., "DIII–D Radiation Shielding Procedures and Experiences," in Proc. 14th Symp. on Fusion Engineering, IEEE, San Diego, California, September 30–October 3, 1991; General Atomics Report GA-A20570 (1991).

Taylor, P.L., "Initial Operational Experience After Installation of the DIII–D Radiation Shield," General Atomics Report GA-A20558 (1991).

Taylor, T.S., E.A. Lazarus, M.S. Chu, J.R. Ferron, F.J. Helton, W. Howl, G.L. Jackson, T.H. Jensen, Y. Kamada, A.G. Kellman, L.L. Lao, R.J. La Haye, J.A. Leuer, J.B. Lister, T.H. Osborne, R. Snider, R.D. Stambaugh, E.J. Strait, A.D. Turnbull, "Profile Optimization and High Beta Discharges and Stability of High Elongation Plasmas in the DIII–D Tokamak," in Proc. 13th Int. Conf. on Plasma Physics and Controlled Nuclear Fusion Research, October 1-6, 1990, Washington, D.C.; General Atomics Report GA-A20283 (1991).

Thomas, M.P., T.N. Carlstrom, J.C. DeBoo, J. Evans, C.M. Greenfield, C.L. Hsieh, R.E. Stockdale, "The DIII–D Multipulse Thomson Scattering Diagnostic," in Bull. 33rd Annual American Physical Society Meeting, November 4-8, 1991, Tampa, Florida (Abstract), **36** (1991) 2473.

Trost, P.K., T.N. Carlstrom, J.C. DeBoo, C.M. Greenfield, C.L. Hsieh, R.T. Snider, "A Multi-Laser System for a Fast Sampling Thomson Scattering Diagnostic," in *Rev. Sci. Instru.* **61** (1990) 2864; General Atomics Report GA-A20095 (1990).

Waltz, R.E., J.C. DeBoo, M.N. Rosenbluth, "Magnetic Field Scaling of Dimensionally Similar Tokamak Discharges," in *Physics of Fluids B* **2** (1990) 2118; General Atomics Report GA-A20172 (1990).

West, W.P., N.H. Brooks, S. Lippmann, C.C. Klepper, G.L. Jackson, J.M. McChesney, J. Winters, "Impurities in DIII–D After Boronization and During VH–Mode," in Bull. 33rd Annual American Physical Society Meeting, November 4-8, 1991, Tampa, Florida (Abstract), **36** (1991) 2476.

Wight, J., "A Network-Based Macintosh Serial Host Interface Program," in Proc. 37th ISA Int. Instrum. Symp., May 5-9, 1991, San Diego, California; General Atomics Report GA-A20440 (1991).

Wight, J., R.M. Hong, J. Phillips, "Recent DIII–D Neutral Beam Calibration Results," in Proc. 14th Symp. on Fusion Engineering, IEEE, San Diego, California, September 30–October 3, 1991; General Atomics Report GA-A20650 (1991).

Wroblewski, D., "Multichannel Current Profile Diagnostic for DIII–D," in Bull. 33rd Annual American Physical Society Meeting, November 4-8, 1991, Tampa, Florida (Abstract), **36** (1991) 2473.

Wroblewski, D., L.L. Lao, "Determination of the Safety Factor in Sawtoothing Discharges in DIII–D," in *Physics of Fluids B* **3** (1991) 2877; General Atomics Report GA-A20402 (1991).

END

DATE FILMED

4/27/92